UNIVERSITY OF NOTTINGHAM

DEPARTMENT OF PRODUCTION ENGINEERING

AND PRODUCTION MANAGEMENT

A COMPTUTER PACKAGE FOR SIMULATION AND ANALYSIS OF ROTARY FORGING

by

Saeed Mansour. B.Sc., M.Phil.

Thesis submitted to the University of Nottingham

for the degree of Doctor of Philosophy.

April 1988

CONTENTS

CHAPTER SIX

CALCULATION OF THE AREA OF CONTACT AND VOLUME OF MATERIAL REMOVED (FOR A PLAIN CONIC TOOL)

LIST OF TABLES

LIST OF FIGURES

NOMENCLATURE

α	Conic die base angle.
D	Workpiece diameter.
H	Billet aspect ratio.
N	Nutation-axial feed per revolution.
$\Delta N, \Delta N1, \Delta Nn$	Instantaneous nutation axial feed in the 1st and intermediate revolutions respectively.
ψ	Spin angle.
$\dot{\psi}$	Rate of change of spin angle/unit time (second).
φ	Precession angle.
$\dot{\varphi}$	Rate of change precession angle/unit time (second).
r	Conic tool radius.
R	Workpiece radius.
S, Sn	Axial feed per revolution, in nth revolution.
$\Delta S1, \Delta Sn, \Delta Sf$	Instantaneous axial feed in first, intermediate and last revolutions respectively.
$\dot{S}$	Die closure rate.
θ	Nutation angle.
$\dot{\theta}$	Rate of change of nutation angle/unit time (second).
t	Time.
x,y,z	Co-ordinates of a point, on a rigid body, before any rotation.
X,Y,Z	Co-ordinates of a point, on a rigid body, after rotation.

LIST OF ABBREVIATION

CAD - Computer Aided Design

FEM - Finite Element Method

FROGS - Forging Rotational Graphical Simulator

ICA - Instantaneous Area of Contact

MGM - Mathematical/geometrical Model

ACKNOWLEDGEMENTS

I have been fortunate to receive extensive help and constructive suggestions from experts in different areas. I acknowledge my indebtedness to Dr. P.M. Standring, my supervisor. His critical comments throughout the course of my research were always stimulating and inspiring.

I am also grateful to Dr. R.J. Barson, the system manager, Interactive Computer Facility, Department of Production Engineering and Production Management, University of Nottingham. His advice were always constructive and helpful.

I wish to thank my colleagues, past and present, for their valuable assistance.

I am grateful to Mrs. D. Dennis for her efforts in typing parts of this thesis.

To My Parents

ABSTRACT

This thesis presents the development of a software package to simulate and graphically represent the tool/workpiece kinematics in rotary forging. A hypothetical workpiece of non-constant volume is always used. Shape changes are achieved by a process of material removal, analogous to metal cutting. Using a quantitative approach, the software is shown to be capable of calculating the tool/workpiece instantaneous contact zone and the volume of material being removed. The software has been developed and used to produce an analysis of radially configurated conic tools. This is believed to be a unique approach to the simulation of the rotary forging process.

Various types of rotary forging machines can be identified by the motion of the conic tool and the hypothetical workpiece. A mathematical/geometrical model is developed which can be used to simulate all possible rotary forging die motions. The model is used to determine the position in space of any point on the die, regardless of its motion and geometry. The software development has been used to graphically simulate the loci of points on a die, during movement of the die.

The mathematical model is used to simulate a non-constant volume workpiece consisting of a large number of concentric cylinders of specified height and radius, with infinitesimal thickness.

The interaction between tool and workpiece is achieved by using a method of geometric comparison. This allows an assessment of changes in the shape of the workpiece.

Extension of the program, using a generated mesh, results in a numerical analysis of the rotary forging process. The data generated from the simulation phase, incorporating some previously developed software, is used to calculate the instantaneous area of contact and the volume of material being removed.

Radially configurated tooling is achieved by the introduction of a database, into the software package. Guidelines are established for the practical design of radially configurated tools. The ability of the program to interact radially configurated tools with non-constant volume workpieces, is graphically/numerically investigated.

The developed program could offer many potential applications in areas such as: the calculation of forming loads and stresses, pressure distribution, etc.. Further, the program can establish some basic boundary conditions; which are essential information for the development of any finite element package for predicting metal flow in rotary forging.

CHAPTER ONE

CHAPTER ONE

1.1. INTRODUCTION

For the purpose of completeness a brief description of the differences between rotary forging and other conventional forging is given below.

In simple upsetting the forces required to achieve deformation, for a given workpiece material, are dependent on the area of work contacted by the tooling. Where the tooling is larger than the workpiece, the cross-sectional area of contact between die and workpiece will increase as deformation takes place. The consequent increase in area of contact will result in a higher applied force in order to continue that deformation.

Rotary forging is an incremental deformation process in which the deforming force is limited by applying it to a partial area of contact, with respect to the total cross-sectional area of the workpiece. The applied force causes a localised plastically deformed zone; which is cyclically swept around the upper contact region of the workpiece, until the desired deformation is achieved.

A reduced area of contact between die and workpiece is achieved by using a shallow conic die arrangement such that its axis is inclined to the workpiece axis, as illustrated in fig. 1.1.

Movement of the contact zone around the workpiece is caused by the motion of conic die axis in relation to the workpiece axis. This gives rise to the cyclic nature of the process.

1.2. THE CLASSIFICATION OF THE TOOL MOTION

A feature common to all rotary forging systems (irrespective of the employed tooling) is the existence of a pivot point; normally the vertex of a conic die; about which all motion of the die axis takes place. Since translation of the dies along a common axis to produce the 'die closure', is a normal function of any forging press; this function has not been considered in terms of rotary forging machine classification. Hence, the only other motions of which the die is capable are those of rotation about the pivot point in cartesian form about the X, Y and Z axes respectively. As the conic die is a solid of revolution, the above mentioned rotations could be described in terms of three Eulerian angles of Nutation, Precession and Spin.

Nutation (θ)

Nutation is defined as the rotation of the die axis about its pivot point in a vertical plane (See fig. 1.2.a).

Precession (φ)

Precession is defined as the rotation of the die axis about the vertical axis of the workpiece in space (See fig. 1.2.b).

Spin (ψ)

Spin is defined as the rotation of the die about its own axis in space (See fig. 1.2.c). It should be noted that in order to achieve kinematic compatability, the workpiece must also spin about its own axis at some appropriate angular speed.

A tool motion classification system based on the Eulerian motion has been proposed [1]. The system classifies the rotary forging process, by a family of seven different types of machines according to the motion of the conic tool; which is either Nutation, Precession or Spin or a combination of these three basic rotations. The classification system associated with the Eulerian angles and the translational motion of the lower die will be used throughout this work.

Earlier independent systems for the classification of rotary forging machines have been produced, based on rotational kinematic motions. These yielded three types of machine [2, 3]:

Type 1 machine [2], operated with both top and bottom dies having their axes fixed and being capable of only rotational motion (Spin). Similarly to other machines, one die has additional translational motion to effect die closure. In this

system where only one die is power driven and the other is a follower, the forge is type 1A. If both dies are driven, the process is designated type 1B.

In type 2, the top die has orbital (Precession) and rotational (Spin) motion, while the lower die is translational only.

In type 3, the die axis is only capable of orbital motion while the lower die is translational only.

1.3. HISTORICAL DEVELOPMENT OF ROTARY FORGING MACHINES

The historical development of rotary forging machines with particular attention to features such as machine design, forging capacities, operating principles, etc., is given in more detail elsewhere [4]. A short review of historical development of rotary forging machines with emphasis attached to tool motion is presented below.

The pioneering work is attributed to E.E. Slick [5], who at the beginning of this century designed and developed the Slick Mill. This was a horizontal machine with two dies spinning about their own axes. In order to achieve incremental deformation between the conical tool and the workpiece, the former was inclined at 10 2/3 degrees with respect to horizontal axis of the latter. Die closure was achieved by axial movement of non-inclined die.

In 1929, H.F. Massey, of B. and S. Massey Ltd, U.K., was granted a patent for a vertically operated oscillating die forging press [6], which appears to have never been built. From tool motion consideration, it seems the design was similar to the Slick Mill but with a fundamental difference; that the conic tool was constrained from rotation about its own axis, i.e. Precession motion only. B.S. Massey renewed their interest in 1969 by taking two patents [7, 8] which were incorporated into the Rotaform prototype machine. Following trials on Rotaform, machine design was further developed, and resulted in 1972 in the construction of the first production machine, equivalent to a 1300-2000 kN conventional forging press.

A U.K. patent by Marciniak in 1970 [9] introduced some novel features into Precession (rocking-die) vertical axis forging presses. The motion of the conic tool on the Marciniak press was available in four basic modes as shown in fig. 1.3. The inclination angle could vary from zero to +2 or -2 degrees, hence the machine could be classified as Nutation or Nutation/Precession machine. Once the mode was selected the tool motion pattern was fixed. Variability of tool motion was limited to axial die feed.

In recent years the Heinrich Schmid of Switzerland has adopted the Marciniak rocking head design in the manufacture of their rocking die forging presses. Two types of machine with capacity of 2000 kN and 6000 kN are currently being manufactured . A 2000 kN press is capable of cold forging parts with maximum

diameter and height of 180 and 120 mm respectively.

In 1964 a model experimental rotary forging press, which was quite similar to the B.S. Massey machine, was constructed and commissioned at the University of Manchester Institute of Science and Technology. The upper die angle of inclination could be varied between zero and ten degrees. One feature of this design was the ability to rotate the upper die about its own axis as well as its Precession motion; although practice showed this to be of no obvious advantage. A second UMIST machine was completed in 1972, with the angle of inclination limited to eight degrees and with no rotation of the conic die about its axis. The first academic paper published in the U.K.; which described the first UMIST machine, was published in 1970 [10].

A 300 kN rotary forging machine was commissioned at the University of Nottingham in 1976; which consist of many features present in the second UMIST design with regard to the rocking head and hydraulics; though with gearbox, clutch and motor mechanism turned through 90 degrees. The oscillation speed of the upper die was variable between 45-400 revolutions per minute and the angle of inclination of the rocking head could be set between zero and ten degrees.

A patent by Ulrych [11], applied for in 1968, concerned a vertical axis machine, the operation of which was similar to that of the Slick Mill. Both dies were capable of rotation about their own axes. The parameters affecting the tool motion

were confined to die axial feed and the selection and fixing of the angular speeds of spin for the two co-acting dies.

Wagner Dortmund of West Germany, a manufacturer of machine tools with many years of experience, has developed a new forging machine for hot forming purposes. The machine is referred to as a 'Closed-Die Axial Rolling Mill' (AGW) [12]. The largest machine sold so far has a rolling force of 4000 kN and is capable of rolling parts up to 1100 mm in diameter; while the smallest machine with 500 kN rolling force can roll parts up to 150 mm in diameter. The tool motion design is similar to Slick Mill, i.e. two rotary units, the lower one is fixed, while the upper one can be moved vertically with respect to axis of the lower rotary unit. The upper unit is inclined to the axis of lower die by an angle between 3 and 12 degrees; however, it cannot be changed during the forging operation.

Rotary forging machines have been classified according to the motions which they have been designed to produce (see table 1). The developed machines are mostly the Precession (P) type. Other developed machines are the Spin (S), Nutation (N), Precession-Spin (PS) and Nutation-Precession (NP) types. The Nutation-Precession-Spin (NPS) type press, with its tool undergoing the most complex motion, has not been developed as yet.

As table 1 reveals, there are a number of rotary forging presses which have been designed and developed; with their conic tool

nutating in a vertical plane. In the main such machines are mechanically constrained, to operate with fixed or very limited conic die axis movements; two to four degrees axis inclination from the workpiece axis being typical. Recently, a unique machine of 500 kN capacity and capable of extending the range of inclination continuously between zero and 45 degrees has been designed and built at Nottingham [13]. The machine, which combines the capability of producing two die axis rotation simultaneously is computer controlled, and can provide a complex deformation program tailored to suit a particular forming operation.

From the above, it will be appreciated that the motions and geometries of rotary forging tooling are very complex. It would therefore seem essential to further progress in the area, that a mathematical model be developed which is capable of describing both the motion and position in space of the surface of a rotary forging die. It is the objective of this research to define and create such a first step on the ladder of process simulation.

CHAPTER TWO

CHAPTER TWO

LITERATURE REVIEW

2.1. INTRODUCTION

During the last fifteen years, Computer Aided Design, Engineering and Manufacturing (CAD/CAE/CAM) have been used increasingly in the metal forming industry. The practical application of CAD/CAE/CAM has the potential of cost reduction, quality improvement and the reduction of the dependence of skilled tool and die makers. There are basically two types of applications of the computer in metal forming technology:

(a) Drafting and numerical (NC) machining.

(b) Analysis of forming processes, i.e. prediction of stresses, metal flow, temperatures and forming load and energy.

The latter application and its development by various research groups around the world, has been reviewed in this chapter.

An accurate determination of the effects of various parameters

on metal flow is a prime requirement for proper control of any metal forming process. Without the knowledge of the influence of such variables as friction conditions, material properties and workpiece geometry on the process mechanics, it would not be possible to design the dies and equipment adequately and thus remove the expensive practice of trial and error, or to predict and prevent the occurrence of defects. Hence, a rigorous analysis of the process is essential. Furthermore, since it is difficult to separate the influence of an individual parameter experimentally, it is necessary to resort to mathematical modelling of the process and it's relevant theoretical analysis.

There are some classical methods for analysing metal forming problems, namely: the slab method, slip line field theory and the upper bound method. These methods carry certain assumptions and provide approximate solutions, and as it is shown in this chapter, they are capable of providing useful information. However, recent development of more elaborate types of numerical methods, in particular the Finite Element Method (FEM), and advancement in computing technology and reduction in its cost, has offered a more realistic simulation of metal forming processes.

2.2. BULK METAL FORMING PROCESSES

2.2.1. Finite Element Method (FEM)

The major advantage of FEM is its ability to generalise. That is, the method can be applied to a wide class of boundary value problems with little restriction on workpiece geometry. This is achieved by the proper discretisation procedure used in FEM.

EPFEP3

The elastic-plastic finite-element program for three-dimensional non-linear deformation problems (EPFEP3) was developed at Department of Mechanical engineering, University of Birmingham. The original programs were two-dimensional, small displacement formulations. Since 1980, research has been concentrated on the development of elastic-plastic three-dimensional finite-element formulations, to study bulk metalforming problems. A brief description of its approach, theory and applications is given in this section.

It is argued [14] that in the early stages of deformation, when the workpiece is in the process of yielding, elastic regions predominate. Also, since the unloading of a previously-deformed workpiece is a purely elastic phenomenon, accurate prediction of the residual stress distribution is only possible if the analysis takes the elastic behaviour of the body into account, hence an elastic-plastic approach was adopted.

The workpiece is partitioned into a finite number of regions, or elements, inter-connected at the nodes. EPFEP3 uses

'brick-type' elements, each element contains eight nodes. The accuracy of analysis and its computing time, depend on the number of elements to be considered.

Metalforming processes involve situations where the geometry of the body, the boundary conditions and material properties are changing in a non-linear manner. Hence the simulation is reduced to a series of incremental linear steps, say 1% of the total deformation, which approximates to the real behaviour. During each increment, the stiffness relationship between the applied force and resulting displacement is determined at the mid-point of the increment [15]. A more analytical approach to the finite increment expressions and solutions to the stiffness matrix are given elsewhere [16, 17].

The Von Mises' criterion is assumed and the strain divided into its elastic (recoverable) and plastic (irrecoverable) parts. Hence, Prandtl-Reuss flow rate was obeyed.

The package is capable of calculating the stress and heat generated by plastic deformation, and the effects of strain rate and temperature on the yield stress and strain hardening modulus.

When the width of the plate or slab is much greater than its height, there is no lateral spread, i.e. plane-strain deformation, hence analytical methods, such as slip-line field could be used to predict deformation. But, if the height is of

the same order as the width, then a three-dimensional model is required for proper analysis. EPFEP3 has been used to simulate metal flow [15] and the results have shown close agreement with the experimental work.

The finite-element technique has been used to model the unlubricated upsetting of rectangular blocks of commercially pure aluminium [17]. The resulting deformation patterns and the distributions of material hardness and die-interface pressure are generally in good agreement with experimental observations.

Although, non-symmetric three dimensional forgings forms a small portion of all forged components, it is these that cause the majority of problems. EPFEP3 was used to simulate metal flow during the most complex stage of the cold forging of a model of an aluminium connecting rod [18]. The analysis predicts the deformation patterns and hardness distributions which have been checked by selected experiments and showed to be in close agreement.

The mentioned finite-element programs for metal flow simulation have been combined with die-design programs in an intelligent knowledge-based system (IKBS) [19]. The die-design programs incorporated in 'IKBS', are: 'CIRCON' (design and manufacture die for axi-symmetric forgings), 'INTERACTIVE MODCON' (consists of modules for solid modelling, finishing and preform die design, die block layout and data calculation for the forging machines), 'UPSETDIE' (design of operational sequences and dies

for upset forging).

Other researchers around the world, have been involved in developing finite-element packages, for analysis of metal flow in forming processes. Lee and Kobayashi [20] have developed a rigid-plastic FEM program which is suited for problems involving large plastic deformation. The approach is also applicable to steady state and non-steady state problems. The method has successfully been applied to analysis of various problems, such as cylinder compression and flange drawing [20], ring-compression [21], sheet bending [22] and bar extrusion and drawing [23]. The results were in excellent agreement with the experimental observations.

Kobayashi extended his work to develop a three-dimensional finite-element package which is based on a rigid-viscoplastic formulation [24]. The rigid-viscoplastic material is an idealisation of an actual one, by neglecting the elastic response. The material shows the dependence of flow stress on strain rate in addition to the total strain and temperature. The rigid-viscoplastic material simplifies the solution process and reduces the required computation. The method is applicable to problems where deformation is plane-strain or axi-symmetric and elastic behaviour can be neglected. The package is used for simulation of compression of rectangular blocks under two different friction conditions. The computational scheme was further implemented to take into account the presence of a neutral zone and the occurrence of folding and lifting. The

approach was applied to analyse the compression of a wedge-shaped block between two flat parallel dies. The results were compared with experimental results and showed close agreement.

The collaboration between S.Kobayashi and Battelle-Columbus Laboratories, resulted in the formulation of the early version of a well known finite-element package, 'ALPID', which is applicable to forging processes.

ALPID

Analysis of Large Plastic Incremental Deformation (ALPID) is a computer code for the analysis and simulation of metal flow in forming processes. It is based on the finite-element method and uses (a) higher order elements (b) a greater and automated description of the die and boundary conditions, and (c) an automated initial guess generation [25]. In its early days, 'ALPID' was a two-dimensional package based on a rigid-plastic finite-element method. However, the 'ALPID' code was revised to simulate material of rigid-viscoplastic behaviour.

Some of the simple forming operations simulated during the early development of 'ALPID' are : flashless forging of a gear blank [25]; cylinder disk forging [26]; backward extrusion [27] and axi-symmetric spike forging [24, 27, 28].

The development of three-dimensional 'ALPID' has been initiated, starting with relatively simple deformation geometries, such as upsetting of a rectangular block and wedge-shaped block [25, 29]. It can predict the geometry (contours, bulge) of a forged part as well as local strains, strain rates and stresses. However, the typical computation time (CPU time) of 2300 seconds, on a CDC 7600 mainframe, for total deformation of 60% reduction in height is considered high in terms of computational cost.

There are number of computer packages, based on the finite element method, being developed for different processes. A simulation package has been developed [30] for hot radial forging processes, in which an elasto-plastic or elasto-viscoplastic material coupled with heat transfer is assumed. Another available program [31] is based on rigid-plastic behaviour and is used for simulation of axi-symmetric component with plane-strain flow.

2.2.2. Upper Bound Elemental Technique (UBET)

The upper bound technique is commonly used to predict over-estimate values of load in metal forming. In it, the plastically deforming body is divided into simple zones, usually triangular, which remain rigid and is separated from their neighbours by lines of velocity discontinuity [32].

In 1960, Kudo [33], utilised this method, for plane-strain forging, by dividing the deformed region into rectangular regions (elemental rings), linked together through shear surfaces. The material is assumed non-work-hardening and rigid plastic and follow the Von Mises' yield criterion. Hence, the best values of forging loads were obtained from calculating the minimum energy dissipation within the deformed zone by considering a plastically-kinematically admissible velocity field. The approach, referred to as 'UBET', was mathematically involved. However, other researchers across the world, have utilised the technique, for various metal forming processes.

In U.K, research using 'UBET' has been carried out by Bramley and his co-workers for the past fifteen years [34]. In the early works [35], the cross-section of the workpiece was divided into rectangular, triangular and circular cross-sectional rings. The elemental division was preformed manually, and each element had its pre-calculated velocity components. The boundary of deforming billet could only be precisely defined at the die-closure, hence calculating the maximum load only. The analysis was satisfactory in predicting load and flash geometry. The automatic element generation, through software, was achieved by inputing the critical co-ordinate points [36], where each point was indicative of a change of surface direction. This technique of element generation led to rings of rectangular and triangular sections. They also suggested, 'generalized elements', which allow flow of any magnitude and direction on all the boundaries. The velocity calculations which resulted in a matrix of element

boundary condition, are based on constancy of volume of the workpiece, and quite frequently, some velocities are not uniquely defined, hence, an optimisation method was adopted [36].

The 'UBET' approach has been developed for prediction of metal flow in the die-cavity, in forging and extrusion processes [37]. The analysis was based on the assumption that material tends to flow in the direction which requires minimum power and least resistance. Hence, starting from the original billet or preform, and based on the energy minimisation principle, the rates of movement of various parts of workpiece were determined at various increments of deformation. The technique has been applied to forging preform design, through 'reverse solution' [38]. This entails starting from the final forging shape and arriving at the initial billet, while the component height increases at the rate equal to the die velocity.

The attractiveness of the approach lies in its relatively short analysis time, 53 seconds CPU time, in predicting final load, in a closed die forging operation [34]. This makes it an interactive tool, suitable for industrial use [39].

In France, research on 'UBET' is being undertaken by Oudin et.al. at the University of Valenciennes. In their approach, the cross section of the workpiece is divided into several rectangular and/or trapezoidial regions [40]. The material was idealised by rigid-plastic behaviour, obeying Von Mises' yield

criterion. There are limitations to the flow direction in each region [40], which resulted in 34 rectangular regions and 16 trapezoidial ones [41]. The subdivision of the workpiece was carried out manually. The dimensions of each region, direction of the flow and friction conditions, are conveyed to software written in Fortran, which runs on a S.E.M.S. T1600 mini-computer. The software calculates the velocity at each boundary, during each step of forming process and determines the internal energy dissipation and the forming loads.

A second program was connected to the first one, which was capable of calculating the shifts of specific points during the simulation of the forging process [41]. At the start, the workpiece cross section was divided into a square grid of equally spaced points. Inside each region, the component of velocity was calculated and the trajectories were deduced. If the point crosses a discontinuity when it was shifted, then the new component of velocity was calculated. The increment at which calculations were carried out, was defined by the movement of the tool from one position to the next. It is claimed [41], the average time needed for the analysis of one trajectory increment of the moving tool during a non-steady state process was less than 60 seconds (CPU time). The technique was used to calculate the mean pressure on the die during forging and extrusion [40]. Also, the technique was used to plot grid deformation in forging, extrusion and compression of square bars [41].

In Japan, Kiuchi has developed the 'UBET' for predicting loads and material flow in single and compound axi-symmetric metal forming processes. The workpiece cross section was divided into number of elements, having either rectangular or triangular geometry [42]. The kinematically admissible velocity field for each element was calculated. The generated elements were connected together through boundaries of velocity discontinuity, where only the continuity of the normal component of velocity across the boundary is ensured. The total power of deformation was calculated by summing up the internal powers, shear losses and friction losses in every element and on their boundaries. Total power of deformation was minimised through an optimisation process. Also, a computer program was introduced which simulated the deformation in an incremental manner.

The technique was used to simulate a closed die forging process and the calculated load and billet height reduction correlated with experimental results [42]. They also calculated the pressure distribution on the contact surface, through 'UBET' by introducing the concept of an 'imaginary element'. The results obtained through this new concept, in a simple upsetting process and backward extrusion, showed very good agreement with results obtained by the slab method [42].

2.2.3. Slab Method

This method, considers the stresses on a plane perpendicular to

the metal flow direction. A slab of infinitesimal thickness is selected in this plane at any arbitrary point in the deformed metal. The forces on the slab are balanced and this resulted in a differential equation of static equilibrium. Through analytical or numerical integration and the introduction of boundary conditions, it is possible to determine the forming forces but not the redundant work of the deformation.

This method lends itself to an easy discretisation, and therefore computer aided implementation, and the solution can be rapidly calculated. The stresses acting on a gear tooth cross section, in the forging of bevel gears, were estimated using slab and finite element methods [43]. The results obtained practically indicated the accuracy of the slab methods analysis.

Another classical method of analysis of metal working problems, is the slip line method. The slip line field theory has been around for many years and been applied to forging, drawing and extrusion [32]. However, the procedure is tedious and time consuming and although it has been developed using computer techniques [44], it has not been found suitable for implementation in CAD/CAM packages.

2.3. ROTARY FORGING PROCESS

Little research and development has been directed towards the simulation or prediction of metal flow in rotary forging. This

could be attributed to the mechanism of deformation which is non-plane strain and inhomogeneous under non-steady state conditions. Also, problems associated with specifying the boundary conditions are considerable. This, as mentioned in the previous chapter, is due to multiplicity and complexity of tool/workpiece motions and their effect on material flow in the deforming zone. The author is not aware of the existence of any computer package, capable of predicting the material deformation that occurs in the workpiece during the rotary forging process.

In China, work carried out at the Beijing Engineering Research Institute led to a comprehensive analysis of rotary forging force, torque, energy and mechanism of deformation [45]. Plane-strain flow was assumed and the upper bound method was used to determine the energy dissipation.

In France, Oudin used model materials, as an inexpensive method of generating visioplasticity information for analysis in rotary forging [46]. He also theoretically analysed the torque, forging force and workpiece final dimensions and showed good agreement with experimental results [47]. An upper bound solution was adopted for materials following Von Mises' criterion. The theoretical analysis was capable of calculating strain rate in radial, tangential and vertical directions (non-plane strain). A precession type machine was used and it was suggested the billet cross section consists of six specific zones; a principal deformed zone, two rigid zones, a principal plastic hinge and two secondary plastic hinges. Hence, the

total dissipated power, is the sum of, internal power dissipated in the principal deformed zone, friction power, power dissipated in the discontinuity and power dissipated in the hinges. It was suggested for a 2 degree upper die, the evolution of the ring geometry during an oscillation of the upper die, could be represented by three indentations. The dimensions of the billet at the end of each oscillation was determined, through calculation of the velocity fields. The calculations of forging force, the torque and final dimensions were carried out on a 32k micro-computer. The running time of about 300 seconds C.P.U was required to simulate a 40% reduction in height. However, for upper values of reduction, a non-symmetric folding was observed, indicative of change in the real velocity, hence the flow predictions were not as good as those at the earliest stages of the process.

In U.S.A, Drexel University and Dyna East Corporation, have developed a computer code that simulates the metal flow in the workpiece during the rotary forging process. The Dyna East Finite Element Lagrangian code (DEFEL), uses an elastic-plastic model. The code was successfully used to simulate metal flow in cylinder upsetting and indicated the workpiece experiencing barrelling and lift-up at 10% reduction in height [48]. This seems to be the only work which utilises FEM and is dedicated to rotary forging. Unfortunately, little information appears to have been published regarding further development of the 'DEFEL' model.

2.4. CONCLUSION

A literature review of the methods and the available computer packages, to simulate and predict metal flow in forming processes has been conducted. As might be expected, this has revealed that most research and development has been directed towards the bulk metal forming processes. Due to rapid advancement of computer technology, the Finite Element Method has received most attention and many systems which use the technique, are commercially available.

Other computer packages, based on the Upper Bound Elemental Technique, require less processing time and could be applied interactively using personal computers and stand alone work stations. This approach has provided accurate results and in many cases, the predicted metal flow, was close to experimental observations.

For a general forming problem, it is not possible to obtain a complete solution without the introduction of some simplification and approximation of the deformation mechanism. This is due to the fact that the boundary conditions necessary for a solution can not be clearly defined. In the majority of software packages, it is assumed that the metal behaves in a rigid-plastic or as in 'ALPID', a rigid-viscoplastic manner. Only EPFEP3, emphasises the importance of elastic behaviour of the material. As far as rotary forging is concerned, it would appear that given the cyclic loading and unloading of the metal

during its incremental deformation, the elastic response can not be ignored. Hence, an elastic-plastic model of material which could incorporate both the elastic recovery and strain hardening found in cold forging, would appear to be the most suitable for use in this process.

Also, in most of the above mentioned packages, plane-strain flow is assumed, only 'ALPID' and EPFEP3 have tackled 3-dimensional flow problems. However, any system, suitable for prediction of metal flow in rotary forging, should be capable of simulating plastic flow in radial, tangential and vertical direction.

In rotary forging, as in any other forming process, the deformation takes place in the contact zone, and its size changes due to flow of material in the radial direction. However, the other factor which influence the size of the contact zone, is the tool motion. As will be shown in the following chapters, the tool/workpiece contact area varies if the tool motion involves any nutation component. Hence, the plastically deformed zone is affected not only by material flow, but primarily by the tool motion which causes it. For this reason it follows that a comprehensive rotary forging simulation package would have to incorporate the two factors. It is the purpose of this work to consider the problems of complex tool motion in rotary forging and as a first stage to provide the analysis required to establish some basic boundary conditions for the process.

CHAPTER THREE

THE DEVELOPMENT OF A MATHEMATICAL/GEOMETRICAL MODEL

3.1. INTRODUCTION

Recognising the complexity involved in a complete analysis of rotary forging tool motion, it was considered necessary to reduce the problem to suitable component tasks. These, shown in fig. 3.1, cover the development and analysis of a computer based study of the problem. Elements of the work are presented later, but to provide an overall appreciation, are briefly mentioned below.

Referring to fig. 3.1:

Mathematical/Geometrical Model (MGM)

This concerns the development of a set of expressions, capable of describing the geometry and the position in space, of any point on a rotary forging die in a cartesian co-ordinate system.

Software development

A computer program was developed which utilises the derived MGM.

The software was developed using an iterative approach. It was capable of generating sufficient data to determine the path of any point on the die as it moves through space. The further development of the software in order to incorporate interactive graphics facilities, allowed the graphical simulation of:

(a)- Tool motion

The loci of any point on a conic tool, as it rotates through space about a pivot point, was graphically represented. The motion of plain and configurated cones (with radial features) were simulated.

(b)- The workpiece

As an initial approach; in order to avoid the introduction of the complex nature of plasticity; a hypothetical non-constant volume workpiece was simulated.

Interaction between tool and the workpiece

Software development was carried out to allow the determination of instantaneous contact area between the surface of the workpiece and the interpenetrating conic tool.

Simulation of the interaction

Further software development was undertaken to produce wire-frame and solid presentations of the surface topography resulting from tool/workpiece interaction.

The Finite Element Analysis approach

The program was extended to incorporate a FEM approach. A numerical method was adopted, in order to calculate the area of instantaneous contact and the volume of material being removed at any stage of deformation.

3.2. DEVELOPMENT OF MGM

In real rotary forging machine systems, the mechanically produced interaction between tool and workpiece is extremely complex. It is advantageous to have a mathematical model, that can be used to describe the die motion from first principles. Such an adaptation can be used to analyse a system free from physical constraints

The motion in space of a rigid body (such as satellite, gyroscope, spinning top or upper die of a rotary forging machine) is an established area of classical dynamics. As mentioned in the chapter 1, the rotation of the die is fully

described by the three Eulerian angles. Hence this area of rigid dynamics was studied in greater depth, in order to achieve the desired model.

When a rigid body rotates in space, it has six degrees of freedom: three of which are rotational and may be described by the three Eulerian angles of Nutation, Precession and Spin; while the others are translational motion in three mutually perpendicular directions (See Fig. 3.2). With reference to fig. 1.1, the pivot point O , about which the rotation of the axis of conic die takes place, is in fact the origin of the Eulerian system. Whilst translation of the point may occur along a common axis with the workpiece, its position in space is immaterial in analysis of subsequent tool motion.

It is often convenient to express the motion of a rigid body in space, with respect to either a fixed or a moving set of axes. If a point has co-ordinates X,Y,Z with respect to a axis of invariable direction (reference axis), and also x,y,z with respect to a moving set of axes; there exists a directional cosine relation which conforms to the matrix form of equation (3.1):

$$\begin{pmatrix} X \\ Y \\ Z \end{pmatrix} = \begin{pmatrix} l1 & m1 & n1 \\ l2 & m2 & n2 \\ l3 & m3 & n3 \end{pmatrix} \begin{pmatrix} x \\ y \\ z \end{pmatrix} \qquad (3.1)$$

Where for example m_3 relates the direction cosine of OZ to Oy .

If the co-ordinates of a point with respect to a set of variable axes are known; it is possible to obtain its co-ordinates with respect to a fixed set of axes from equation (3.2); which is the matrix multiplication of equation (3.1).

$$\begin{aligned} X &= l_1 x + m_1 y + n_1 z \\ Y &= l_2 x + m_2 y + n_2 z \\ Z &= l_3 x + m_3 y + n_3 z \end{aligned} \qquad (3.2)$$

Consider two orthogonal right handed triads: the triad (x,y,z) is fixed in the rigid body (upper die) and the triad (X,Y,Z) is fixed in the frame of reference (machine axes). Table 2 [49], which is the table of scalar products, represents the direction cosine of the vectors (x,y,z) relative to (X,Y,Z) or vice versa. (For full proof see Appendix A) [50].

If a point on the rigid body, prior to any rotation is described by co-ordinates x,y,z , with respect to the fixed axis; it is possible to obtain its new position X,Y,Z , with respect to the same axis, after the rigid body has turned through various angles of precession, nutation and spin (See fig. 3.3). Introducing the matrix elements of table 2, in equation (3.2),

produces the basic equations of the mathematical model presented in this work, as equation (3.3):

$$
\begin{aligned}
X = {} & x\,(-\operatorname{Sin}\varphi \operatorname{Sin}\psi + \operatorname{Cos}\theta \operatorname{Cos}\varphi \operatorname{Cos}\psi) \\
& + y\,(-\operatorname{Sin}\varphi \operatorname{Cos}\psi - \operatorname{Cos}\theta \operatorname{Cos}\varphi \operatorname{Sin}\psi) \\
& + z\,(\operatorname{Sin}\theta \operatorname{Cos}\varphi)
\end{aligned}
$$

$$
\begin{aligned}
Y = {} & x\,(\operatorname{Cos}\varphi \operatorname{Sin}\psi + \operatorname{Cos}\theta \operatorname{Sin}\varphi \operatorname{Cos}\psi) \\
& + y\,(\operatorname{Cos}\varphi \operatorname{Cos}\psi - \operatorname{Cos}\theta \operatorname{Sin}\varphi \operatorname{Sin}\psi) \qquad (3.3) \\
& + z\,(\operatorname{Sin}\theta \operatorname{Sin}\varphi)
\end{aligned}
$$

$$
\begin{aligned}
Z = {} & x\,(-\operatorname{Sin}\theta \operatorname{Cos}\psi) \\
& + y\,(\operatorname{Sin}\theta \operatorname{Sin}\psi) \\
& + z\,(\operatorname{Cos}\theta)
\end{aligned}
$$

During rotation of the upper die, there are, three controllable variables, namely rate of change of nutation, precession and spin.

$$\dot{\theta} = \alpha$$
$$\dot{\varphi} = \beta$$
$$\dot{\psi} = \gamma$$

Where α , β and γ are all constant. By integrating (with respect to time) the above equalities, the value of θ , φ and ψ could be obtained at any interval of time hence:

$$\begin{aligned} \theta(t) &= \alpha t + \theta(0) \\ \varphi(t) &= \beta t + \varphi(0) \\ \psi(t) &= \gamma t + \psi(0) \end{aligned} \qquad (3.4)$$

where $\theta(0)$, $\varphi(0)$ and $\psi(0)$ are the values of Eulerian angles at time $t = 0$.

Substitution of equation (3.4) into (3.3), produces set of equations (3.5); which can be used to calculate the position of any point, on the conic tool, with respect to the reference axis at any instant of time, in a cartesian co-ordinate system.

$$X = x\,(-\sin(\beta t + \phi(o))\sin(\gamma t + \psi(o)) + \cos(\alpha t + \theta(o))\cos(\beta t + \phi(o))\cos(\gamma t + \psi(o)))$$
$$+ y\,(-\sin(\beta t + \phi(o))\cos(\gamma t + \psi(o)) - \cos(\alpha t + \theta(o))\cos(\beta t + \phi(o))\sin(\gamma t + \psi(o)))$$
$$+ z\,(\sin(\alpha t + \theta(o))\cos(\beta t + \phi(o)))$$

$$Y = x\,(\cos(\beta t + \phi(o))\sin(\gamma t + \psi(o)) + \cos(\alpha t + \theta(o))\sin(\beta t + \phi(o))\cos(\gamma t + \psi(o))) \qquad (3.5)$$
$$+ y\,(\cos(\beta t + \phi(o))\cos(\gamma t + \psi(o)) - \cos(\alpha t + \theta(o))\sin(\beta t + \phi(o))\sin(\gamma t + \psi(o)))$$
$$+ z\,(\sin(\alpha t + \theta(o))\sin(\beta t + \phi(o)))$$

$$Z = x(-\sin(\alpha t + \theta(o))\cos(\gamma t + \psi(o))) + y\,(\sin(\alpha t + \theta(o))\sin(\gamma t + \psi(o))) + z\,(\cos(\alpha t + \theta(o)))$$

Where the upper die axis is coincident with the machine axis, at time $t = 0$, the following will result:

$$\theta(0) = \varphi(0) = \psi(0) = 0$$

However, at time $t = 0$, the initial values of Eulerian angles, do not necessarily have to be zero, and could take up any value.

There are a number of points which should be taken in to consideration, when the derived MGM is being employed for the simulation.

3.2.1. Range of Eulerian angles

As shown in fig. 3.3, the angles of precession and spin, could take up any value between zero and 360 degrees, i.e. $0 \leqslant \varphi \leqslant 2\pi$ and similarly $0 \leqslant \psi \leqslant 2\pi$. Theoretically, the nutation angle can fall anywhere within the same range as the other two Eulerian angles. However, due to the general requirement to produce workpieces having horizontal surfaces; values of $\theta = \alpha$ are rarely departed from. (Where α and θ are the cone and inclination angles respectively.)

3.2.2. Direction of rotation

The convention of rotational movement adopted in this work is indicated in fig. 3.3. For angles of precession and spin, the direction is considered positive, if by observing the rotation from the origin along the axis of OZ* and Oz* respectively, the rotation is clockwise. The vertical plane of Z-X , fig. 3.3, is the natural plane of nutation, and the direction is positive if a clockwise rotation is observed along the OY* axis from the origin.

For initial Eulerian angles of zero degree at time $t = 0$, nutation starts in the direction towards the X axis in the Z-X plane; while an initial precession angle of 90 degrees, would give a path with nutation towards the Y axis in the Z-Y plane.

3.2.3. Finite and infinitesimal rotation

At this stage, the distinction between finite and infinitesimal displacement and their effect on the motion of a rigid body (such as conic die in a rotary forging operation) should be appreciated.

If a rigid body undergoes a series of finite displacements; the order in which the displacement are applied is important and the law of commutative addition does not hold (i.e. in finite

rotation analysis , vector addition can not be applied. See Appendix B) [51]. On the other hand, if a rigid body undergoes a number of small rotations about a point, the resultant displacement is the vector sum of those rotations (i.e. the order in which those infinitesimal displacement are applied , does not effect the final displacement. See Appendix B).

As it is shown in Appendix A; in order to rotate a rigid body about a fixed point, for example to evaluate the set of equations (3.3), which describe its position after rotation; three successive finite rotations should be applied. The body should rotate through angles of precession (φ), nutation (θ) and spin (ψ) respectively. However, in a rotary forging operation, the upper die rotates through an infinitesimal angle during a short time interval and hence, it could be assumed that the three rotations are being applied instantaneously. Having established this important criterion, the sets of equations (3.3) and (3.5), could be employed for analysis, without any consideration for the order in which the Eulerian angles are being applied.

3.3. VALIDITY OF THE PROPOSED MGM

The validity of the proposed MGM could easily be investigated by considering two points on a plain cone. Point 'A' is on the die axis, while 'B' is a point on the surface of the cone (See fig. 3.4.a). The co-ordinates (0, 0, 1) and (0, 1, 1), describe

the positions of points 'A' and 'B' in the cartesian reference system of X Y Z .

If the solid cone was allowed to rotate by $\pi/4$ radians, about Y axis, in the Z-X plane, the points 'A' and 'B' would be rotated to new positions of 'A1' and 'B1' respectively. The new set of co-ordinates of $(1/\sqrt{2},\ 0,\ 1/\sqrt{2})$ and $(1/\sqrt{2},\ 1,\ 1/\sqrt{2})$; with respect to the same reference axis; could easily be attained, due to the simple geometrical relation, which exists between the two set of points, as is shown in figs. 3.4.a and 3.4.b.

Now the set of equation (3.3), which is the basis of the proposed MGM; could be employed in order to calculate the co-ordinates of 'A1' and 'B1'. The values of x, y, z , i.e. the co-ordinates before any rotation; are as above and the Eulerian angle of precession, nutation and spin are zero, 45 and zero degrees respectively. Hence, by substituting these values into equation (3.3), the points 'A' and 'B', after rotation of $\pi/4$ radians, would be described by co-ordinates $(1/\sqrt{2},\ 0,\ 1/\sqrt{2})$ and $(1/\sqrt{2},\ 1,\ 1/\sqrt{2})$ respectively.

The above example was chosen for its simplicity and it clearly indicates that the results obtained; from both a simple intuitive approach and from this adaptation of the MGM, are exactly the same. This emphasises the validity of the proposed MGM.

3.4. CONCLUSIONS

The layout of the work in hand and the tasks to be accomplished at each stage of research, has been established.

The relationship between two sets of axes, one with and the other without variable direction; has been thoroughly investigated. A set of expressions; in terms of the three Eulerian angles of Nutation, Precession and Spin, has been established which provide the basis of the mathematical/geometrical model, being used in this research. The direction of each rotation and the irrelevancy of the order of rotations has been clarified. It has been proved that if the cartesian co-ordinates of a point, with respect to the reference axis, are known; the proposed MGM would calculate the new co-ordinates, with respect to the same axis, after any number of rotations.

By introducing three controllable variables; i.e. rate of change nutation, precession and spin, the MGM has been shown to be capable of calculating the position of any point on the tool, at any instant.

CHAPTER FOUR

CHAPTER FOUR

SIMULATION OF THE TOOL, TOOL MOTIONS AND THE WORKPIECE

4.1. INTRODUCTION

Given, the position of a point on a rotary forging die, the subsequent movement of the die axis will allow the new position of that point to be calculated. If the motion of the die axis is designed to simulate the die motion of a rotary forging operation; the path of any point on the die as it moves through space could be determined. Such an analysis, indicates the requirement for software development and interactive graphics facilities.

The software development of the MGM, should generate sufficient spatial co-ordinates; such that it is possible to simulate any die geometry, configuration and angle of inclination. The data representing the tool, should always be available for future analysis.

The software should be capable of simulating the path of any number of points, on a solid tool, as it undergoes various rotations. The further development of the software should result in simulation of a cylindrical workpiece of non-constant volume.

4.2. SOFTWARE DEVELOPMENT

The developed software package; which in future will be referred to as FROGS (Forging ROtational Graphical Simulator); was written in FORTRAN 77 and run on a PRIME 9650, with the relevant support facilities. FROGS may be divided into four interrelated sections (shown as a block diagram in fig. 4.1). FROGS has been further developed to incorporate a graphics package; so that the data generated through an iterative approach, could be represented graphically. The graphics simulation was achieved, through an 'in-house' developed package, with some GINO-F (Graphic INput Output-Fortran)[52] compatible routines.

4.3. SIMULATION OF A CONIC TOOL

The software was written such that it can simulate any die geometry, and the resultant data could graphically be represented. The reason for such simulation; as will be shown later; is to interact a solid tool with the surface of a simulated workpiece. As shown in fig. 4.1, there are two stages to this simulation.

4.3.1. Assessment of the die geometry

To establish the die geometry, FROGS enquires regarding the following parameters :(See fig. 4.12)

(a)-The value of cone angle (α).

(b)-The value of die axis inclination angle (θ).

(c)-The value of conic tool radius (r), normally defined as unity.

From the above information, it is possible to determine the shape of a plain conic tool.

It should be noted that the majority of rotary forging machines manufactured in industry, have conic tools of very small α values, ranging from 2 to 10 degrees. However, manufacturing components of complex configurations, necessitates the conic tool to be inclined at a large angle. Hence, the need for using conic tools of large α values, perhaps in excess of 30 degrees. Therefore, in this work, conic tools of 30 degrees base angle, have frequently been simulated.

4.3.2. Data generation for a plain conic tool

The above information, establishes a point on a generator at radius r . For the sake of simplicity, a point, A , is assumed to lie on the vertical plane Z-Y , in the cartesian co-ordinate system, as shown in fig. 4.2.b. The FROGS software, divides the distance between A and origin, into number of equal segments, and determines the corresponding Y-component of each segment. The resultant data simulates the only generator, which lies on a Z-Y plane; of a plain conic tool with zero inclination angle. The number of segments, which should be conveyed to FROGS and determines the number of circumferential lines, depends on the required accuracy of the simulation.

In order to simulate a plain conic tool, the developed MGM was used to rotate the above mentioned generator, about the vertical axis, through 360 degrees. Using an iterative approach, the co-ordinates of those points on the generator are calculated at equal time intervals and stored in the form of a matrix. Each element of the matrix represents X, Y and Z co-ordinates of a point on the surface of a plain conic tool, with respect to the machine axis. The time interval, at which the motion of the generator, is being interrogated, will influence the number of radial lines (See fig. 4.2.a), and consequently the accuracy of the simulation.

The generated data can graphically represent a conic tool with its axis, normal to the horizontal plane. The simulated tool can be placed at any position in space. For example, it is possible to place the lowest generator on the horizontal axis.

This could be achieved by rotation of generated data points through the inclination angle ($\theta = \alpha$), about the X-axis. If the co-ordinates of a point on the cone before any rotation, are (x,y,z); then its co-ordinates (X,Y,Z) after a rotation of (θ) degrees, about X-axis, are given by set of equations (4.1) [53]:

$$\begin{aligned} X &= x \\ Y &= y\mathrm{Cos}(-\theta) + (-\mathrm{Sin}(-\theta)z) \\ Z &= y\mathrm{Sin}(-\theta) + (\ \mathrm{Cos}(-\theta)z) \end{aligned} \qquad (4.1)$$

Once again, a right handed co-ordinate system is adopted, whereby, the rotation is negative if it is anti-clockwise, by looking from origin along the axis of rotation. As the rotation is taking place in a vertical plane, there is no change in the X-component.

4.3.3. Data generation for a configurated tool

Any configurated die could be simulated, by introducing radial and circumferential features, into the surface of a plain conic tool. In this work, configuration is accomplished by the introduction of radial features into the generator; which is in the vertical plane, whilst, the tool axis is at 90 degrees to the horizontal plane. The MGM was employed as before, to

generate sufficient data for simulation of a configurated tool.

The data to simulate the above mentioned generator, is extracted from a database; which has been previously tailored to incorporate the desired radial features. This clearly limits the range of configuration which may be introduced , to the number of DATAFILEs that may be accommodated in advance of any simulation. However, this limitation could be removed by, either improvisation of an extensive database, or employment of a interactive graphics input facility. The disadvantages associated with the former are: the amount of computer memory which is required to accommodate such an extensive database; and the tedious task of its construction. Also, no matter how extensive the database is, it can only simulate a small number of configurated tools.

However, in this research, the database approach was adopted and; as is shown later; four simple radial configurations are simulated.

4.3.4. Graphical presentation of conic tools

The geometric presentation of the conic tool can be produced by using the graphics package to join the generated spatial points together, in a specified fashion. This could be an attractive facility for tool design purposes.

The hard copy presentation of all simulations, in this work, was obtained through TEKTRONIX 4692 hard copier; which is connected on-line, to a TEKTRONIX 4111 colour graphics terminal. The reproduction is not as accurate as a drawing produced on a plotter; but in this research, the pattern of the drawing is of prime concern. Hence, a hard copier with its screen dumping feature, was selected, because of its speed and ease of operation.

One of the options available on the MAINMENU of FROGS, enables the operator to view the solid cone in plan and elevations. Upon the selection of one of four available views, two subroutines are executed, which draw the radial and circumferential lines respectively. A wire-frame representation of a solid cone is achieved, using the above mentioned routines; by drawing straight lines between the generated data points. Thus, the greater the number of co-ordinates used, the greater the accuracy of the simulations. A separate menu provides an isometric view of the conic tool; by enabling the operator to input the necessary angles of rotation through the X, Y and Z axes .

A conic tool with a 30 degree base angle, is shown in plan, elevations and isometric views in figs. 4.3 and 4.4 respectively; while fig. 4.5 represents a tool with a base angle of 10 degrees . No attempt is made to remove the hidden lines. It is also possible to represent simulated cones as solid objects. This is achieved by developing the software such

that, the conic tool surface is considered to consist of large number of polygons; which all are drawn in a certain colour; hence, resembling a solid object, (figs. 4.6 and 4.7 show the above mentioned tools as solid objects).

Only a small database was created to represent the four simple radial configurations simulated by FROGS. These are shown in fig. 4.8. Figs. 4.9 and 4.10, showing respectively three orthogonal and isometric views.

4.4. SIMULATION OF TOOL MOTION

The tool motion variations which can be simulated by FROGS, are based on table 1. Hence, prior to any simulation, the type of conic tool motion should be selected. The developed MGM is capable of tracing the loci of any number of points on the tool, as it goes through its rotation. It is believed, that this is a unique approach for analysis of the tool motion in rotary forging. Moreover, the MGM can simulate the most complex motions, where all three Eulerian angles are present.

4.4.1. Assessment of tool motion

This section succeeds the conic tool simulation, where the geometry of the tool has already been established. The routines which calculate the co-ordinates of one, or any number of points

on the lowest generator, prior to any die motion, are similar to section 4.3.2. However, further information is needed, in order to simulate the tool motion. Depending on which type of rotary forging machine classification is to be simulated, FROGS enquires about rate of change of nutation ($\dot{\theta}$), precession ($\dot{\varphi}$) or spin ($\dot{\psi}$) per second, or 2π radians rotation of the lower die.

4.4.2. Data generation and graphics presentation

After establishing the co-ordinate geometry of a point on the lowest generator and inputting various parameters which influence the motion; the set of equations (3.5) is used to calculate the new co-ordinates of the point; with an equal size time interval; as it goes through its specific motion. The time interval and the number of points to be simulated, which depends on the accuracy of the simulation, should be conveyed to FROGS.

As before, the generated data is stored in a specified format, so that the drawing routines mentioned in previous sections, are employed to trace the loci of any number of points on the die surface as the die axis moves about the pivot point. A comprehensive approach; which results in the graphical simulation of all types of tool motions; according to the classification of table 1, is given below. In all simulations, a plain conic tool with a 30 degree base angle, is assumed. As

mentioned in chapter 3, one of the six degrees of freedom associated with die motion, is translational motion in vertical plane; which is referred to as die closure rate, or axial feed rate. This could be simulated, by reducing the vertical component (Z-co-ordinate) of each and every calculated point, by a constant value which is determined by the axial feed rate. An illustration of the effect of simulating die closure on various machine types, is presented below.

(a)-Spin (S):

The locus of an arbitrary point on the lowest generator of a conic tool, as it rotates about its own axis, at the rate of 2π radians per second, is shown in fig. 4.11.a. The effect of introducing a constant axial feed rate into the die motion, is shown in fig. 4.11.b. (The point on the vertex is also simulated).

(b)-Precession (P):

As shown in chapter one, precession is rotation of the axis of an inclined conic tool about the Z-axis (fig. 1.2.b). However, in order to trace the loci of a point on such cone, the following should be considered.

Fig. 4.12 which represents the tool/workpiece geometry,

illustrates that the radius of the workpiece (R) is greater than the radius of an equivalent position on the cone (r). Therefore, for any conic tool, there is an inherent discrepancy distance for a pure rolling motion, which is simply the circumferential distance difference due to $R > r$, i.e. $2\pi(R-r)$. This will result in the tool not returning to its initial position on completion of 2π radians precession. However, if the upper die is radially configurated, it would be necessary for a point on the die to interact with the same point on the workpiece on each successive precession cycle. To ensure this occurs, constraining mechanisms have been designed to introduce a rotation of the die about its own axis [1].

In the proposed MGM, the constraining mechanism is simulated by also rotating the conic tool about its own axis, through an angle, equal but opposite in direction to the, precession angle. This results in a more kinematically complex motion for any machine classification involving precessional rotation.

The loci of one point on the tool, undergoing 2π radians precession is shown in fig. 4.13.a. It shows a tear drop shape representation and demonstrates that the point has the same spatial co-ordinates at the end of its motion. The introduction of an axial feed rate and its effect on the tool motion is shown in fig. 4.13.b.

(c)-Nutation-Precession (NP):

A point on a 30 degree conic tool with an initial angle of zero inclination, has been traced as it nutates and precesses at the rate of 15 and 360 degrees per second respectively. Fig. 4.14.a shows such a tool motion in plan and elevations. Fig. 4.14.b shows a similar tool motion, whilst a constant axial feed rate being employed.

(d)-Nutation-Spin (NS):

In this motion, the conic tool, once again is initially in a vertical position and nutates towards the pivot plane at the 30 degrees/second, while rotating about its own axis. The tool motion is simulated as it rotates in space for a period of one second; and the locus of a point on the tool is shown in fig. 4.15.a. FROGS could simulate the above tool, to move down through the horizontal pivot plane. As shown in fig. 4.15.b, the point ends up somewhere, below the Y-axis, depending on the magnitude of the axial feed rate.

(e)-Precession-Spin (PS):

The trace of a point in PS system is shown in fig. 4.16.a. In this figure, simulation has resulted from the precession and simultaneous spin of a 30 degrees cone, with its axis inclined at $\theta = \alpha$. The simulation of such a tool motion, with axial feed, is shown in fig. 4.16.b.

(f)-Nutation-Precession-Spin (NPS):

Due to its complexity, this type of machine system has not yet been built. However, using FROGS, such a tool motion can be simulated. In fig. 4.17.a, the conic tool inclined at 15 degrees to the vertical, is caused simultaneously to nutate, precess and spin at rates of 15, 90 and 360 degrees/second respectively. The loci of a point on the base of the cone, initially in Z-Y plane, is shown at the end of a one second interval. The introduction of a constant axial feed, will produce the tool motion shown in fig. 4.17.b.

The above mentioned examples and their resultant loci, clearly indicate that any small variation in parameters such as rate of change of Eulerian angles, axial feed rate, tool geometry, angle of inclination etc., will yield different tool motions. Therefore, due to infinity of possibilities, only a limited number of tool motion simulations are represented in this work. Their significance however, serves to highlight the importance of a computer package such as FROGS; which can accommodate any small variation in different parameters and translate them into the resultant simulations.

4.5. SIMULATION OF THE WORKPIECE

As shown in block 'C' of fig. 4.1, FROGS is used to generate data for simulation of a workpiece; which as is shown in the next chapter, can be interacted with the conic tool, to provide the resultant deformation. In all simulations, a cylindrical workpiece of specified radius and height is assumed. However, at this stage of research, and to concentrate on establishing the principles, the workpiece is assumed to be of non-constant volume. As a hypothetical situation is considered, only the material removal in the vertical plane is simulated; with no consideration being given to the problems of deformation in radial directions.

This is best resembled by a rotary cutting operation; in which a conic tool with number of cutting edges, penetrates into the workpiece and cuts the material away, resulting in a reduction in height of the billet, while its radius is always kept constant.

4.5.1. Data generation and presentation

Once again, the developed MGM was employed to generate sufficient spatial co-ordinates to simulate a workpiece of cylindrical shape, with a specified radius. In all cases, the primary objective is the simulation of the top surface of the workpiece, in contact with the tool.

After establishing the cartesian co-ordinates of a point on the

Y-axis (where in all simulations which are free from nutation, the point is assumed to have similar co-ordinates to a point on the base of the lowest generator of a inclined conic tool), it is allowed to rotate about the machine axis. The MGM is used to calculate the co-ordinates of the point at a different angular distance from the Y-axis, during 2π radians rotation about the vertical component of the reference axis. The number of radial lines; which determine at what angular distance the co-ordinates of the point should be calculated; is equal to number of radial lines used in the simulation of the solid tool. Also, the radial lines joining the vertex to the point on the Y-axis, are divided into a number of equal segments. Then, a point on each segment is also rotated for 2π radians. The resultant simulation is shown in fig. 4.18. A thorough investigation of figs. 4.2.a and 4.18.a, reveals, that they consist of equal number of radial and circumferential lines. This ensures that there are an equal number of data points in the arrays representing both the tool and the workpiece. The importance of this criterion will be made clear in the next chapter.

4.5.2. Membrane model

Representation of the workpiece by a number of concentric cylinders (fig. 4.18.b.), is in close agreement with the membrane model proposal [13]. Using the membrane model, a solid billet may be considered to consist of an infinitely large

number of concentric cylindrical membranes, each having a different radius and specified height, but with an infinitesimal thickness, and the axis passing through the vertex of the conic tool and perpendicular to the pivot plane.

Such a model is considered particularly useful when investigating the process parameters of bite size, instantaneous contact area between tool and workpiece, billet geometric shape changes and material volume removal (for a non-constant volume workpiece).

The interpenetration and relative rotation of the conic tool into a workpiece produces a helical surface. A developed cylindrical membrane; for situations where there is no nutation motion involved and the axial pitch is constant, is shown in fig. 4.19.a [13]. The broken lines represent the generated spiral with the base length $2\pi R$ representing the circumference of the developed membrane. The position on the membrane of lowest generator of the conic die, was used to determine the instantaneous bite at different spin angles.
It can be seen in the figure, that the instantaneous value of $\Delta S1$ increases with spin (to a maximum value of Sn) during the first revolution. Subsequent bites ΔSn are equal for intermediate revolutions. In the last revolution, the ΔSf reduces to zero height from a maximum bite of Sn.

Also, in any machine classification involving nutation, the simultaneous nutation and spin of the tool will reduce the

height of the cylindrical membrane; and for one revolution of the bottom die, such a motion would generate a spiral on the membrane. As before, a cylindrical membrane is shown in fig. 4.19.b [13], where N represents the axial pitch for different revolutions of the lower die. It can be seen that the instantaneous bite in the first revolution $\Delta N1$, increases with spin and nutation, while subsequent instantaneous bites ΔNn (n=2,3,....) diminish progressively. Hence:

$$N1 > N2 > ..... N_{n-1} > Nn > N_{n+1} > ..... > Nf$$

In order to investigate this characteristic associated with nutation, FROGS was employed to simulate a 30 degree conic tool which nutates towards the horizontal plane at rate of 1 degree/second. At the end of each revolution, the nutation axial pitch, which is defined as the lead of the helix described by the lowest generator of the conic die in one revolution of the bottom die measured at a fixed radius, was calculated. The tool was allowed to nutate till its lowest generator reached the horizontal plane. The graph of fig. 4.20 shows the nutation axial pitch, measured at various angles of inclination, for 30, 15 and 5 degrees conic tool. The importance of work in [13] and fig. 4.20, is that the nutation rate has a significant influence on the rate of die closure.

4.5.3. Simulation of a helical surface

In order to simulate a spiral surface, it is assumed that an inclined conic tool $\theta = \alpha$, with its lowest generator acting as a cutting edge, is rotating about the vertical axis of machine co-ordinate system, and at the same time is penetrating into the surface of an imaginary billet, at a preselected axial feed. After a 360 degree rotation, the resultant surface resembles a spiral, with the distance between the lowest and highest points on the spiral representing the axial feed per revolution.

The algorithm which simulates the surface of the billet (given in fig. 4.18) was employed; while the Z-component of the calculated data was corrected according to equation (4.2).

$$Znm = Znm + (\psi 1/2\pi)Sn \qquad (4.2)$$

where,

n = 1,2,3,.....number of radial lines.

m = 1,2,3,.....number of circumferential lines.

Sn is axial pitch for intermediate revolutions.

$\psi 1$ is the angular position from the Y-axis.

Fig. 4.21.a represents, in plan and elevation, the locus of a

point on the workpiece. The simulation model may show numerous cylindrical membranes; which in total produce a solid workpiece; as illustrated in isometric view of fig. 4.21.b.

In any conic tool, with its axis of inclination ranging from θ=0 to α degrees, nutation alone cannot cause workpiece deformation. Hence, in any machine classification involving nutation (namely N, NP, NS, and NPS); uni-axial axi-symmetric compression is considered to be a prerequisite for any subsequent deformation [13]. Axial compression is used in a preforming role and combined with a single N, NP, NS or NPS rotary forging cycle.

In this work, axi-symmetric compression is assumed, by interpenetration of a 30 degrees conic tool (α = 30, θ = 0), into a cylindrical workpiece. As shown in fig. 4.22, the tool circumference is in total contact with the billet membranes. However, as a non-constant volume workpiece is assumed, there can be no lateral flow of material.

Once again, the MGM was used to simulate a membrane; which is penetrated (after the initial compression stage) by a 30 degree conic tool, as it nutates (towards the pivot plane) and rotates (about the Z component of machine axis) at the rate of 30 and 360 degrees/second respectively. Fig. 4.23.a shows the resultant simulation, and as the plan view indicates, the radius of the membrane gradually increases as the angles of precession and nutation approaches 360 and 30 degrees

respectively. This could be attributed to the characteristics of the nutation, which has radial and axial components of displacement. The radial displacement causes the resultant simulated membrane, to contradict the proposed membrane theory, which considers the workpiece to consist of large number of concentric cylinders.

In order to overcome this undesirable radial component, a dedicated algorithm was introduced into FROGS, which ensures a simulated membrane with constant radius. To do so, FROGS was allowed to calculate the same set of data points which represent the single membrane of fig. 4.23.a. The co-ordinates of each point were modified according to a simple geometric relation (given in Appendix C), so that each point on the membrane has a constant radius. Fig. 4.23.b, shows a modified simulated membrane of fig. 4.23.a.

4.6. CONCLUSIONS

It has been established, that due to the complexity of tool motion in rotary forging, it is essential that a mathematical geometrical model is introduced, which can simulate the motion of a point on a conic tool as it undergoes various rotations. Also, the importance of a computer power and computer graphics for simulation of number of points, on a solid tool has been highlighted. The structure of the developed software package, for this research indicates, there are three interrelated

sections to each simulation.

The FROGS package can simulate a conic die of any configuration (simple or complex), geometry and inclination. Four tool configurations have been employed in the database.

The variation in tool motion, is confined to the three Eulerian angles of nutation, precession and spin. Applying the three rotations individually or in different combinations, gives seven types of tool motions simulation. The developed MGM was modified to accommodate the mechanical constraint that is incorporated into tool motion involving precession. The loci of one or number of points on a plain conic tool were simulated and graphically represented. FROGS is capable of simulating the most complex motion, namely NPS; which has not yet been designed and developed. The translation of the conic tool in the vertical plane and its impact on tool motion, has also been investigated.

The resultant simulation of some motions, is similar to those which may be obtained through either an intuitive or a theoretical approach.

FROGS is a unique approach to simulation of tool motion in rotary forging. The ability and ease with which it accommodates any variation in tool geometry or motion parameters, is also quite significant.

The membrane model proposal was adopted to simulate a cylindrical workpiece of a fixed height. At this initial stage of development a hypothetical (non-constant volume) workpiece has been assumed. This has allowed programme development without introducing the enormous complexity of attempting to model a workpiece of constant volume, subject to plastic deformation. Also, a spiral surface, generated by penetration of conic tool into the workpiece, has been graphically simulated. The parameters, of instantaneous bite, axial feed and nutation axial pitch (and its relation with angle of inclination) have been investigated.

CHAPTER FIVE

CHAPTER FIVE

SIMULATION OF WORKPIECE DEFORMATION

5.1. INTRODUCTION

This chapter deals with the simulation/development of a non-constant volume workpiece, as it is being deformed by a plain conic tool.

The interaction between the tool and the workpiece, with a predefined constant axial feed, will result in a series of continuous instantaneous positions of contact. This method allows the simulation of deformation at any stage of the process, to be evaluated.

The investigations presented in chapter four, demonstrated that the FROGS system is capable of analysing the tool motion associated with the whole range of rotary forging machine tool classification. Application of FROGS to determine instantaneous contact areas, has been limited in this work to the following cases.

(a) Spin.

(b) Precession.

(c) Nutation-Spin.

This restriction is for convenience only, evaluating the more appropriate machine systems available to the local researchers. However, the same approach can be used, when required, to apply FROGS to analysis of contact zones generated by any of the machine systems.

In this chapter the effect of process variables; i.e. conic die geometry, the motion of its axis and the rate of translation of the workpiece in vertical plane; are investigated with respect to contact zone produced [54].

For clarity, the same graphical presentations, i.e. wire-frame and solid modelling, have been continued.

5.2. INTERACTION BETWEEN TOOL AND WORKPIECE

It has been shown that FROGS is capable of generating two data files: one a solid tool of specified geometry and configuration; the other a spiral surface, which is generated due the relative motion of the tool into a hypothetical workpiece. The data representing each file, is generated by the proposed MGM and stored in two separate arrays, with the size depending on the accuracy of the simulation (the greater the accuracy, the larger the size of each array).

The helical surfaces (shown in figs. 5.1 and 5.2) are unrealistic representations of interpenetration of the tool into workpiece; since there could not be a discontinuity (fig. 5.2) on any circumferential line which makes up such a surface. However, this will be removed by interacting the surface with the tool and replacing those parts which are in contact, with the impression of the cone. This approach yields an interface between tool and workpiece which is referred to as the 'Instantaneous Contact Area' (ICA) or 'foot print',see fig. 5.3. The resultant ICA, represents a parabola, confirming the geometry identified by other workers in the area [45, 63, 64].

The fig. 5.2 shows two graphics simulations: one a spiral workpiece surface with its unrealistic discontinuity (the distance between the highest and lowest points , 02 and 01 , is equivalent to axial feed per revolution S); the other a solid cone with its lowest generator on the horizontal plane. In order to extract the ICA; the superposition of a conic tool on the workpiece surface, is always assumed. However, certain conditions should be met; in order that a point on the helix surface can be contacted by the tool.

5.3. CONDITIONS TO EXTRACT THE ICA

In order to locate those points which constitute the ICA, a number of requirements should be met and checks made.

The first requirement, is that the two graphical simulations should have a common datum line (i.e. equal X,Y and Z components). Therefore for example, in the case where a plain conic tool is spinning or precessing, the line representing the lowest generator of the conic tool (where $\theta = \alpha$), should coincide with the radial component of the workpiece surface; which lies on the horizontal plane. The radial line 01 (in fig. 5.2, where 0 is the pivot point) is considered to be the datum line.

Also, as mentioned in the previous chapter, the two simulations should have an equal number of circumferential and radial lines. This means that in each of the two arrays representing the tool and the un-interacted workpiece surface; there are equal numbers of data points. This ensures that the two corresponding points; which have common radial and circumferential components; on each set of data are being compared. For example, a point which is on the lowest generator (i.e. the Y-axis of fig. 5.2) is never compared against a point which has its X and Y components at π radians from the datum line.

Having fulfilled the above mentioned requirements, a further check is made. This check compares the Z- components of the two corresponding points. The outcome of this test, determines whether a point on the tool is in contact with the workpiece or not. FROGS investigates the three possible outcomes of such comparisons.

(1)-If the vertical component of the tool is greater than the vertical component of the corresponding point on the workpiece, then the tool does not intersect the workpiece at that point.

(2)-If the two vertical components are equal, then the tool and workpiece are in contact at that point.

(3)-If the vertical component of the workpiece is greater than the vertical co-ordinate of the corresponding point on the tool, it means the tool has penetrated into the workpiece.

(The vertical components are measured with respect to horizontal pivot plane.)

5.4. SNAP SHOT PRESENTATION OF THE PROCESS

Fig. 5.4 shows the flow chart diagram of the subroutine in the FROGS which locates and isolates the ICA. It indicates a new data array of (nx3) being created, with the first and second columns being equal to the X and Y-components of data; which represent the spiral surface. However, the elements representing the Z co-ordinates, depend on the outcome of the test. If the point is on the ICA then the Z co-ordinate, is the height of the conic tool at that point; otherwise it is the

height of the spiral surface. The generated data, which represents the workpiece surface for one complete revolution; consists of two distinct surface elements: one the area which has already been in contact with the tool; the other, the zone of instantaneous contact.

Such a surface is graphically simulated in fig. 5.3, which is equivalent to the interpenetration of an inclined solid cone into cross section of a cylindrical workpiece (see fig. 5.5). This method allows a snap shot of the resulting deformation produced at any stage of the process.

5.5. THE DYNAMIC vs STATIC APPROACH

The ultimate objective of any simulation or CAD package, is to undertake a dynamic approach to the task in hand. For example, a car door panel which has been designed using a CAD package, might incorporate a degree of stress analysis due to some load. Such a load would cause a strain on the door hinges. A dynamic representation, of the door as it moves about the hinges, would be of considerable use to the designer of the door/hinge. This reasoning could also be applied to the deformation of a hypothetical workpiece as it is being interacted by a conic tool. The best analysis could be achieved by animating the material removal as the process took place.

However, as mentioned earlier, in this work, two sets of data

points, each of a large magnitude, ((1800,3) being a typical array size) are calculated and compared against each other, in order to locate the ICA. The animation of the process, requires the above analysis to be repeated a number of times in a short space of time. Hence, this indicates the need for a fast processor; which in the interests of speed, should be solely for this analysis. The problem can be further highlighted if other requirements, for example, the calculation of the volume of material being removed, are requested.

As an extension of the analysis, it was decided to simulate the process either at different revolutions or for various stages of one revolution, hence extracting the changes which occur at each stage of the process. Although the technique is a static approach; thus requiring less processing and drawing time than that produced dynamically; it represents the historical development of a hypothetical workpiece during a rotary forging process.

5.6. DEFORMATION IN A SPIN TYPE TOOL MOTION

As mentioned earlier, in all simulations a cylindrical workpiece is assumed and its deformation at various stages of the process is represented. For the convenience, the tool is considered to be a conic section with a 30 degree base angle and radius of 1 unit. In simulations represented in the rest of this section, 1 unit = 90 mm, the choice being simply a function of the size of

the screen being used. The radius of the workpiece is $r/\mathrm{Cos}\,\alpha$, with axial pitch S given the arbitrary value of 0.2 of one unit per revolution of the lower die. The lowest generator is on the Y-axis ($\theta=\alpha$) and the pure rolling condition is always assumed.

For achieving a reasonable accuracy, the workpiece is sectioned by 90 equally spaced radial lines and 20 equally spaced cylindrical membranes. Hence, arrays of (90x20,3) are calculated. Assuming as a first step, a constant value axial feed rate, three distinctly different elements of deformation would be observed. These can be identified as the deformation due to the first revolution, deformation due to intermediate revolutions and deformation due to the last revolution.

5.6.1. The first revolution (Spin)

As indicated in the section 4.2 of the previous chapter, in the first revolution of the lower die, the $\Delta S1$ increases from zero, to a maximum value of S1 at the end of 2π radians rotation. This results in a variation in size and geometry of the ICA. In order to investigate this, the snap shot of the process was simulated at 120-degree intervals, resulting in four graphical representations during each revolution. Figs. 5.6.a, 5.7.a and 5.8.a show such analysis in plan, elevation and isometric view. The instantaneous views should be considered from left to right and top to bottom.

As fig. 5.6.a indicates, there is a line contact between the inclined tool and the workpiece at zero degree rotation. As the $\Delta S1$ increases, the ICA (shown in magenta) becomes more prominent, reaching its maximum at the end of first revolution. Figs. 5.7.a and 5.8.a, also indicate the rate of material reduction for a non-constant volume billet. At the start of the process, the billet is at its maximum height, while as it is being moved in the vertical plane and penetrated by the conic tool, its height is reduced by the factor of $(\psi 1/2\pi)S$ (See equation 4.2).

FROGS can be applied to simulate the first revolution of deformation produced by a plain cone, deforming any workpiece under any variation of the parameters involved.

5.6.2. The intermediate revolutions (Spin)

During this stage of the process, ΔSn is considered constant for 2π radians rotation of the lower die, and is equal to the axial pitch. This means that the ICA is unaffected by the rotation of the lower die as long as the S value is constant.

In the same way as for the first revolution, figs. 5.6.b, 5.7.b and 5.8.c show a non-constant volume workpiece, being deformed by a conic tool during one of a number of intermediate revolutions. Fig. 5.6.b shows a plan view of the workpiece at 4 stages of the process, and as expected, does not indicate any

change in contact zone. However, figs. 5.7.b and 5.8.b clearly indicate the height of the workpiece being reduced by the conic tool during a single revolution. The axial feed remains constant as in the first revolution, and the instantaneous views shown in figures, represent the height reduction at 0, 120,240 and 360 degrees respectively. Hence, the height difference between the top-left and bottom-right billets, is equal to axial feed. It should be noted the bottom right presentation of fig. 5.7.a, is the same as that of fig. 5.7.b; illustrating the end of the first revolution and start of intermediate revolutions.

It should be emphasised that the bulk of deformation is achieved during the intermediate revolutions and much attention should be directed towards this stage of the process. But, as a workpiece of non-constant volume with fixed axial feed is simulated, it means the only change possible during the intermediate revolutions, is the reduction in height of the billet. So, it was decided, for the sake of simplicity, to simulate an unrealistic situation, in which, only one intermediate revolution is adequate to achieve the necessary deformation. However, FROGS is capable of simulating any number of intermediate revolutions.

5.6.3. The final revolution (Spin)

The start of this revolution is with termination of axial feed

This leaves an instantaneous bite Δsf , less than the value of axial feed/revolution S , which must be subsequentially rolled out during the final revolution [13].

Figs. 5.6.c, 5.7.c and 5.8.c represent the last revolution of this simulation and demonstrate the result of an imaginary multi blade conic cutter interacting, whilst the workpiece is rotating in anti-clockwise direction. The simulation sequence indicates that the ICA to the left of the lowest generator is being reduced till only line contact along the Y-axis remains.

5.7. DEFORMATION IN A PRECESSION TYPE TOOL MOTION

Using a similar approach to that of 5.6; in this simulation a cylindrical workpiece is translated along the vertical axis, at a rate of 0.2 of a unit per second, while a plain conic tool of $\theta = \alpha = 30$ degrees, is precessing for 360 degrees during the same time interval. Once again a pure rolling situation is assumed and the same number of data points, as for the previous section (i.e.(90x20,3)), is being calculated each time.

5.7.1. The first revolution (Precession)

In this revolution, the $\Delta S1$ varied from zero to a maximum value of S as the conic tool precess for a period of 2π radians. In the precession system and for a given

tool/workpiece geometry, S is the sole factor which determines the bite size.

The deformation of the workpiece during the first revolution contacted by a precessing tool, is shown in figs. 5.9.a and 5.10.a. The figures show an initial line of contact expanding and rotating around the workpiece surface, during 2π radian rotation. The size and the position of the ICA can be compared with those previously generated for spin, in fig. 5.6.a. The comparison can be made because the parametric values used for workpiece, tool and axial feed were the same. This comparison illustrates the kinematic comparability between the two cases of spin and precession, although achieved by different mechanical systems.

5.7.2. The intermediate revolutions (Precession)

As in the case of spin, during this phase of the process, the ΔSn is constant for a 360 degrees precession of the tool. This means that, if there is no change in axial feed the resulting size of the ICA is constant during any number of intermediate revolutions, but its position around the axis of the billet will change.

Figs. 5.9.b and 5.10.b show a non-constant volume workpiece, being deformed during one intermediate revolution. The rate of instantaneous height reduction is calculated from equation

(4.2).

5.7.3. The final revolution (Precession)

As in the case of spin, the final revolution begins immediately after the axial feed is terminated. The subsequent 2π revolution of the tool, reduces the spiral surface to a horizontal plane passing through the pivot.

Figs. 5.9.c and 5.10.c show a graphical representation of the final revolution. The size of ICA is maximum, identical to that produced during intermediate revolution. However, as the tool rotates about the Z-axis, it removes the trailing edge, while it is only in contact with the leading edge. The Z-component of the leading edge continues to be reduced (as there is no axial feed), and hence the ICA diminishes until there is only a line of contact between the tool and the workpiece.

5.8. DEFORMATION IN A 'N-S' TYPE TOOL MOTION

As mentioned in the previous chapter, an initial uni-axial axi-symmetric compression is considered to be a prerequisite to any deformation of a cylindrical billet, on a nutation-spin press. Hence, for such a simulation, a plain conic tool is fully interpenetrated in a non-constant volume workpiece.

Fig. 5.11 shows an instantaneous view of a cylindrical workpiece, which has been uni-axially compressed by a co-axial (θ=0) plain conic tool. From the figure, it can be seen that the tool has penetrated the workpiece sufficiently that the outer membrane of the workpiece is contacted by the tool. In such circumstances, when using a non-constant volume workpiece, material will be removed and not displaced to appear elsewhere.

In order to simulate a nutation/spin system, the die is nutated from the Z-axis to the Y-axis, in the vertical plane (Z-Y). The arbitrary value chosen to represent a nutation phase is 4 degrees. The nutation of the conic tool is continued until a lowest generator on its surface reaches the Y-axis, when $\theta=\alpha$. Using a nutation rate of 4 degrees per 2π radians rotation, a complete nutation cycle will be achieved after $8x2\pi$ radians.

Graphical representation of a nutation/spin phase is shown in figs. 5.12.a and b. It should be noted that this simulation does not include a component of axial feed, i.e. S=0 . The surface element (shown in magenta) in the top left-hand representation of fig. 5.12.a shows the ICA after the tool has nutated 4 degrees. The ICA is represented by a segment of a circle, with its size being reduced as the die nutates towards the Y-axis. The bottom left-hand picture of fig. 5.12.b, represents the billet surface after the lowest generator has achieved the Y-axis. Fig. 5.13 shows the same process in an isometric view, and it clearly indicates the cylinder being

opened up and its height reduced as the tool nutates towards the Y-axis while the workpiece rotates about its own axis. The rate at which the billet height is reduced during nutation, is dependent on the nutation axial feed pitch, which is known to vary during each revolution of the bottom die (see fig. 4.20).

Fig. 5.14 shows the same simulation as considered in fig. 5.12, but with additional component of constant rate axial feed S . Fig. 5.14 reveals a much greater area of billet surface is in contact with the tool at any instant, compared to that shown in fig. 5.12. This is due to large axial bite per revolution, which is defined as the lead of a helix described by the lowest generator of the conic die in one complete revolution of the lower die and measured at a fixed radius. This axial feed pitch consists of two components: one due to nutation and the other due to workpiece translation in a vertical plane. FROGS recognises that the two components are moving in opposite directions and that therefore the resultant axial bite will be the sum of the two components. Figs. 5.15.a and b, show a billet deformation produced by combined nutation and axial feed.

The final revolution can only commence when nutation and axial feed rates are zero. If either one of these two components achieves a zero condition before the other; then the final revolution cannot take place until the other components have also achieved a zero condition. In the final revolution, the deformation produced, would depends on tool/workpiece geometry, axial feed rate and nutation/axial feed rate in the penultimate

final revolution, and is the same as that shown in fig. 5.9.c.

5.9. WIRE-FRAME AND SOLID PRESENTATION

In general, there are three types of geometric model to represent a physical object (such as cylindrical workpiece or a conic die) in CAD systems. These are wire-frame, surface and solid models. In this work only wire-frame and surface modelling has been used.

5.9.1. Wire-frame modelling

Wire-frame models are the simplest method of modelling; although they are less pleasing visually, but they are considerably faster, easier and simpler to create. They require relatively little computer time and memory, and even inexpensive computers can cope with the processing needed. However, wire-frame modelling becomes less attractive in the 3-dimensional analysis; as there is no attempt to simulate the way opaque objects make certain surfaces invisible. This problem is highlighted through the simulations which have been graphically presented in this chapter, as each image could be interpreted in many different ways.

Hidden-line removal will result in an outline drawing which shows only the outline of the visible surfaces, and the lines of

intersection between the surfaces. There are algorithms [55] which can be used to achieve hidden-line removal; thus eliminating such ambiguities associated with wire-frame images. It should be noted that hidden line removal involves considerable computing time; thus increasing the time required for interactive graphics.

Wire-frame modelling was considered suitable for this work, since it offers the ability to interact rapidly with the data, as it is being generated through various stages of deformation.

5.9.2. Surface modelling

A higher level of sophistication in geometric modelling, is the surface modeller, which can overcome many of the ambiguities of wire-frame models. A surface model can be built by defining the surfaces on the wire-frame model. The procedure for constructing a surface model is analogous to stretching a thin film of material over a framework.

In order to create a surface model of the deformed workpiece shell, the FROGS software divides the billet into a large number of polygons. The edges of the polygons are straight lines and their vertices are described by the X, Y and Z co-ordinates of the data generated through the MGM. FROGS was further developed to present each polygon as a solid surface, by the selective colouring of specific polygons. However, to achieve a realistic image of a cylinder, a large number of such polygons have to be

simulated. The problem of increased processing and drawing time was reduced by the decision to remove those polygons (surfaces) which were invisible. Whilst the computing time for hidden-surface removal remains considerable; the number of surfaces to be plotted, was reduced. Hence, a trade off between increased drawing and decreased processing time, was established.

The geometric method for hidden-surface removal consists of three major steps. First, the software applies a visibility test to each polygon to quickly eliminate those surfaces which are totally hidden. Second, a series of tests are applied to the scene to determine the relationships between polygons, which determines if any two or more surfaces overlap. Third, a depth test is applied to any pairs of overlapping polygons to determine which of the two would be visible.

As the workpiece is a plain solid cylinder and free from any surface protuberances or recesses; there cannot be any line of sight where two polygons can overlap. For this reason, only the visibility test was considered necessary to evaluate the surfaces.

The visibility test is designed to identify faces which are hidden by the volume of the solid object to which they belong. The test involves a comparison between a line of sight drawn from the eye position to a point on the polygon and the surface normal vector at that point. A surface normal vector is

defined, as an outward-pointing vector perpendicular to the plane containing the polygon (See fig. 5.16). When the angle between the two lines is greater than 90 degrees, the polygon is invisible.

Software within FROGS, was developed; which calculates the above angle for all polygons constituting the workpiece shell.If the polygon is visible it was filled and drawn in yellow. Otherwise, it was eliminated from the set of surfaces which make up the displayed cylinder (See fig. 5.5).

As stated previously, the upper surface of a workpiece is considered to consist of two elements: i.e. the spiral surface and the ICA. The two elements are illustrated by identifying the boundaries of each element and then by colouring their surfaces differently. Clearly, the regularity of the polygon boundaries will be affected by the number of data points generated through the system.

The two polygons are drawn as long as the boundaries are visible. Since the topography of the deformed workpiece is the main modelling objective; the two polygons are always present. However, the presentation of any object through one or any number of surfaces will provide a two dimensional image. In order to obtain a more realistic image, depth should be introduced into the object. A 3-dimensional scene could be produced from a successful simulation of shading effects; which takes into account the light source, surface characteristics and

the position and orientation of the surfaces and sources. A more detailed analysis of this effect is given elsewhere [53, 56, 57]. It is sufficient to emphasise that the introduction of such a tool, involves more sophisticated and dedicated software. Although beyond the scope of the work contained in this thesis; the matter is discussed in suggestions, for future work.

In the rest of this chapter, the version of FROGS which, produces a solid presentation of the graphics simulation, has been employed. Fig. 5.17 shows in plan, a billet as it is being deformed by an inclined precessing conic tool, during an intermediate revolution. This should be compared with fig. 5.9.b. However, a much greater number of data points (180x90,3) must be calculated each time. The same billet is shown in isometric view in fig. 5.18; while fig. 5.19 shows a cylindrical workpiece being interacted by an inclined plain conic tool, rotating about its own axis.

5.9.3. Solid modelling

Most commercially available solid modelling systems, that are believed to be the most efficient for geometric modelling; use one or two common approaches to construct solid models. One approach is to use simple geometric shapes; referred to as primitives; such as cubes, spheres and cylinders etc.. The idea is, to combine a number of such primitives to create

complex solid models. Primitives can be combined to construct a solid model by Boolean or logical operations. With this approach, the modeller must ensure that the primitives are in the proper place, then invoke the required logical operator to obtain the desired shape. This approach works best on parts that do not have sculptured and complex surfaces. However, it is believed [58]; that the four primitives of plane, cylinder, cone and sphere; are adequate to model most engineering parts. A commercially available 3-dimensional solid modeller called BOXER [59], uses 5 primitives of block, cylinder, sphere, cone and torus to construct a component.

It is suggested [58], that the most complex shapes can be modelled much more easily and efficiently by boundary or perimeter modelling. The principle behind this approach is that part geometry is different from part topology, and they can be defined separately, in other words, two parts might have identical topology, but different geometry. In this system, once a particular topology has been defined, many different operations can be performed on the part to adjust geometry without changing basic topology.

A more comprehensive analysis of the above solid modellers is given elsewhere [58]. It should be emphasised that various modelling approachs could be employed for more efficient presentation of the workpiece under investigation. However, the production of more realistic images in this work, was not of the prime concern; but may prove useful in some later

investigation.

5.10. PARAMETERS INFLUENCING DEFORMATION

As mentioned earlier, the topology of a workpiece; being deformed by a rotary forging press, reveals two elements. One, is the instantaneous zone of tool/workpiece contact, and the other, the formed surface geometry resulting from the contact. The ratio between these two surface elements, which determines the geometry of the billet deformation, is greatly influenced by two parameters.

5.10.1. Tool geometry

FROGS is capable of simulating a conic tool of any shape and configuration. The results of variation in tool geometry, on the workpiece deformation, are simulated. The only parameter, which is considered to affect tool geometry, without changing its radius, is the cone base angle α .

Three simulations are considered for a rotary forging press; with its inclined conic tool spinning about its own axis, while the axial feed per revolution S , is constant. Fig. 5.20.a, b and fig. 5.3 show in plan, an instantaneous view of a billet deformation, during an intermediate revolution, where α =10, 20 and 30 degrees respectively. These indicate that the

shallower the cone angle, the larger is the area of instantaneous contact. Hence, through simulation, it becomes possible to predict the rate of material deformation, through variation in tool geometry.

5.10.2. Axial feed per revolution

As stated in section 5.8, there are two components which can influence axial feed. One is due to vertical movement of the workpiece towards the conic die; and the other is produced by nutation of the conic die axis. Figs. 5.12, 13 and 14 demonstrate the effect of simulating a nutation/spin rotary forging machine motion. It will be recognised that, given a range of process variables; for example, tool and workpiece geometry, spin/precession rates, axial feed rates, there exists an infinity of possibilities for simulation within a forging cycle.

The following simulation to demonstrate the effects of axial feed rate, have been carried out only to demonstrate the FROGS package and to give an appreciation of the resulting ICA. Clearly the software is capable of extending this range of simulations to suit any required set of parameters.

Fig. 5.21.a, shows in plan view, a cylindrical workpiece which has been deformed by a 30 degree conic tool. The value of S is 1/10th of the conic tool radius. If the value of S is

increased by a factor of 5; the resultant simulation is as shown in fig. 5.21.b. It clearly indicates, that a greater portion of the hypothetical workpiece is being removed as the axial feed pitch is increased.

5.11. CONCLUSIONS

The interaction between a plain conic tool and non-constant volume workpiece has been investigated.

Software has been developed; which can generate sets of data to simulate conic tools and spiral surfaces. Methods of interrogation for the corresponding co-ordinate geometry of each set of data, have been developed, and used to identify the geometry of the workpiece/tool interface.

A technique has been developed to represent the ICA produced during a simulated rotary forging cycle. Three distinct stages of deformation have been identified and simulated: relating to first, intermediate and final revolution respectively. A hypothetical non-constant volume workpiece has been subjected to simulated rotary forging deformation, using the motions of spin, precession and nutation/spin. Variations in the surface geometry produced, have been investigated.

The FROGS software has been extended to incorporate a technique for hidden surface removal. Deformation boundaries have been

identified and surface representation enhanced using a method of differential colouring.

A surface modelling approach has been applied to a preliminary investigation, to demonstrate the effects of tool geometry and axial feed on a workpiece deformation.

CHAPTER SIX

CHAPTER SIX

CALCULATION OF THE AREA OF CONTACT AND VOLUME OF MATERIAL REMOVED (FOR A PLAIN CONIC TOOL)

6.1. INTRODUCTION

The mesh generation provided by FROGS was used as the basis of a numerical analysis to calculate the area of instantaneous contact between a plain conic tool and workpiece produced during a simulated rotary forging operation. The approach was extended and the software was further developed to calculate the volume of material removed/displaced between any two stages in the process.

The effect of variation in tool geometry and axial feed rate, on the calculated actual area of tool/workpiece contact and the rate of material removal, has been investigated.

This is believed to be a unique approach to the calculation of contact zone area in rotary forging.

6.2. FINITE ELEMENT METHOD

The advent of the finite element method analysis, combined with

the rapid development of the digital computer, has provided the engineer with a very powerful and versatile method for the analysis of complex continuous domains in many fields of engineering. Although, initially developed in the field of structural mechanics, the method is receiving increased interest in the fields of heat transfer, electromagnetics, fluid mechanics and as mentioned earlier, for metal flow simulation in metal forming processes.

It is not the aim of this research to consider the finite element method in any depth, as it is a well established numerical technique with extensive research being carried out [58, 60]. However, a brief description, with respect to mesh generation techniques, seems appropriate.

The basis of the finite element method is to divide the continuum into discrete segments called finite elements. In two dimensional analysis, the continuum is separated by imaginary lines and in three dimensions, by imaginary surfaces. The nodal points are then defined by the intersection of these lines and surfaces and the finite elements are then divided by these nodal points. The topography and geometry of the finite elements, together with the associated boundary loading conditions, can be input to a finite element package and a numerical solution obtained.

Thus, any finite element analysis can be divided into three stages:

1- The division of a continuum into finite elements and the generation of associated data.

2- Finite element analysis.

3- Presentation and evaluation of the results.

6.3. MESH GENERATION TECHNIQUES

From the point of view of mesh generation, finite element models of objects may be classified in ascending order of complexity. At the simplest level are two dimensional and axi-symmetric objects, above these are three dimensional surfaces (contact zone calculation) and at highest level three dimensional solids (volume removal calculation).

A problem common to all three classes of models, is to provide a mathematical representation of the model itself, such that a finite element mesh may be generated within it. The three dimensional approach requires a mathematical definition of a region, or set of mathematical expressions defining the boundaries of the region, then a mesh is produced, usually by some interpolation and mapping technique. There are a number of

algorithms available for mesh generation [61], with some capable of introducing a weighting factor into mesh density [62].

It is quite feasible to define the boundaries of a cylindrical workpiece in terms of a mathematical expression and to divide the continuum domain into a finite number of elements. This could be achieved, for 2- and 3-dimensional analysis, through implementation of various and readily available mesh generation techniques. However, the data generated through FROGS, simulating the formed billet during any stage of the process, could be used to define the nodal points of an element (primitive) of defined geometry. A collection of such elements, constitutes a solid workpiece. The number of elements is always constant and predefined (depending on the number of radial and circumferential lines), and mesh density is evenly distributed throughout the workpiece.

It should be emphasised that no finite element package, for predicting the material flow, or calculating stress, strain, pressure, etc. has been used in this research. Therefore, the only similarity, between FROGS and other FEM packages lies in the areas of mesh generation technique and calculation of volume of material removed/displaced and tool/workpiece contact zone. However, as it is shown in the rest of this chapter, each time the tool is interacted with a hypothetical billet, the nodal points on each element are updated and could be utilised by a future finite element package for wider range of analysis.

6.4. MESH GENERATION FOR AREA CALCULATION

A subroutine of FROGS was developed which divided the surface into number of macro-blocks. These were used to calculate the instantaneous area of contact at the tool/workpiece interface. The macro-blocks were of two types, namely trilateral and quadrilateral elements.

Fig. 6.1, shows the plan view of an interrogated workpiece surface. The interrogation technique seeks to identify the ICA, evaluating nodal points, small to large in a clock-wise direction. Adjacent nodal points are interrogated to determine whether they lie inside or outside the ICA. When points outside the boundary are identified, for example (4,5) in fig. 6.1, the boundary is drawn between points (3,5) and (4,4). Hence, a trilateral area, (3,4)-(3,5)-(4,4), can be evaluated as indeed can all those which form quadrilateral elements. The flow chart diagram of the developed subroutine is given in fig. 6.2.

If the interrogation of a data array, by the above mentioned subroutine, established a trilateral macro-block, then sufficient data co-ordinates are extracted in order to calculate the area of such an element. The area of a trilateral element is the half of the vector (cross) product of two of its sides (see Appendix D). Hence, the data shown in fig. 6.3.a is transferred to another subroutine which calculates the area.

However, if the data interrogation, established a quadrilateral

macro-block, once again, there are sufficient data co-ordinates for surface area calculation.

For calculating the area of a quadrilateral surface, which is enclosed by four boundaries, it has to be represented by a function p(s,t), which is made of four boundaries and the co-ordinates of the four corners. Fig. 6.3.b, shows such an element on the surface of the contact zone of fig. 6.1. The area of such element is given by equation (6.1).

$$\text{AREA} = \int_{-1}^{1}\int_{-1}^{1} (\delta p/\delta s)x(\delta p/\delta t)\, dsdt \qquad (6.1)$$

Where

$$-1 \leqslant t \leqslant 1$$

$$-1 \leqslant s \leqslant 1$$

Software previously developed [62], was incorporated in to the FROGS package, and applying numerical integration, was capable of calculating the area of each quadrilateral macro-block (see Appendix E).

Hence, the actual area of contact, is the sum of the areas of all elements in X,Y and Z, which make up the contact zone. In order to obtain an accurate surface area, a large number of

macro-elements should be calculated. Clearly, it is the number of radial and circumferential lines which determine the accuracy of the calculated area of contact. The increased number of macro-elements, will result in simulating a polynomial/cylindrical workpiece.

It was considered of paramount importance to divide the workpiece into a certain number of elements, in order to simulate a cylindrical object. To assess the accuracy of this approach, a circular object of unit radius and negligible thickness was simulated for different combination of radial and circumferential lines. It was assumed, in all cases, that the complete flat circular surface lies in the contact zone, hence, the calculated area should be close to π . The outcome of the investigation is given in table 3. It shows that the accuracy of the calculation is increased as the number of radial and circumferential lines increases.

In order to reduce processing time, the number of radial and circumferential lines used throughout this chapter were 360 and 10 respectively.

6.5. CALCULATION OF TOOL/WORKPIECE CONTACT ZONE

6.5.1. Spin type tool motion

As shown in chapter five, for a given axial feed, the shallower the conic tool, the greater would be the ICA or tool footprint. It was also shown, that for a given tool geometry, any increase in axial feed rate, would result in an enlarged tool/workpiece contact zone. Such analysis, as described earlier, was based on geometrical comparisons of graphical figures. The numerical analysis carried out by FROGS will enable an engineer to monitor the influence of the parameters involved in rotary forging.

Fig. 6.4.a, shows the variation in calculated area of instantaneous contact, for different tool geometries as the axial feed rate increases ($\theta = \alpha$). Table 4 shows the ICA as a function of axial feed for a number of plain conic tools of various geometries. Fig. 6.4.b, shows the graph of ICA against various cone angles for six pre-set axial feed rates. From these graphs, it can be deduced that:

(a)- the actual ICA does not increase linearly with axial feed rate. Although for shallow conic tools (for example α = 2.5, 5 or 7.5 degrees) it could approximated by a linear relation, but this would not be true for large α values.

(b)- for a given axial feed rate, the change in the size of actual ICA is relatively insignificant for large cone angles in comparison with shallow cones.

These graphs would provide the machine operator or tool designer with valuable information. For instance, if fig. 6.4.a is extended such that it covers a wide range of conic angles, then an operator is capable of assessing the resultant ICA for any tool geometry and axial feed rate. Also, he is able to achieve a certain contact zone by either varying the axial feed rate or choosing a different tool geometry.

FROGS was used to investigate and compare the area of contact calculations proposed by other researchers. Marciniak [63] and Kubo [64] have established theoretical expressions for area of contact through geometrical analysis of the intersection of the helical and conical sections. Kubo has investigated the theoretical relationship between the coefficient λ (which is the ICA divided by the total cross section of the workpiece) and the axial feed S per revolution for a 2 degree plain conic tool. Fig. 6.5.a, shows Kubo's results for different workpiece diameters, against results obtained using FROGS. They were found to be in close agreement.

In his work, Kubo [64] stated that the shape of the theoretical area of contact depends on the relationship of the dimension $2R\tan\alpha$ (where R and α are workpiece radius and conic tool angle respectively) and the spiral lead S. He investigated the theoretical relationship between λ and relative spiral feed SO, where $SO=S/2R\tan\alpha$, and established

an expression relating the two, for conic angles ranging between zero and 10 degrees. Fig. 6.5.b, shows the above mentioned relationship, for α =2.5, 5 and 10 degrees, obtained through a numerical analysis by the FROGS software. It indicates a variation between 17% to 5% in the calculated λ for SO ranging from 0 to 1 . Hence, FROGS shows some disagreement with theoretical values calculated by Kubo.

The theoretical relationship between $2R\tan\alpha$ and λ , for a 2 degree conic tool, was investigated by Marciniak [63]. He introduced a coefficient a/R , which is the ratio of the length of the arc of contact, over the circumferential distance of the billet outer surface. Figs. 6.6.a and b shows results obtained by Marciniak alongside the results obtained through FROGS numerical analysis. Although Marciniak results were obtained by determining data points from a previously published figure, however, the two sets of values showed close agreement. The expression derived by Marciniak, representing λ in terms of $2R\tan\alpha$ is similar to the expression used by FROGS. As expected figs. 6.6.a and b indicate that any increase in axial feed, or decrease in the value of cone angle, would result in a greater portion of the workpiece in contact with the tool.

6.5.2. Nutation-spin type tool motion

The introduction of a nutation motion into a spin type rotary forging system, means that the size of tool footprint is

influenced by tool geometry and two tool motions, i.e. nutation/spin and axial feed/spin.

In all work carried out in this section, the simulation was started with a uni-axial axi-symmetric compression with the inclination angle $\theta = 0$ degrees. Under such circumstances the actual area of contact for a given indentation of a workpiece would be a maximum. Also, the end of simulation was reached when the lowest generator achieved the horizontal plane, i.e. $\theta = \alpha$. In all cases the axial feed and nutation rates were kept constant during each simulation.

Figs. 6.7.a and b, represent the variation in actual ICA at various angles of inclination for two different tool geometries. In each case, there was no axial feed, but the nutation rate was varied.

The effect of axial feed rate on the ICA was investigated, by allowing a 5 degree cone angle to nutate at a constant rate, while the axial feed rate was increased from zero to .075 unit/rev, in a equal intervals. The result of such analysis is shown in fig. 6.8.a. As mentioned previously, the bite size is the sum of nutation and axial feeds, and for a given axial feed rate and small angles of inclination, its value is large. However, as the the tool reaches the horizontal plane, the axial feed due to nutation is reduced, resulting in a much reduced contact zone.

Fig. 6.8.b, represents the graph of ICA against various axial feed rates, for five different angles of inclination. The relationship between the two functions, could be approximated linearly for the largest inclination angle, where the nutation axial feed is minimum. Information of this type could be useful to an operator in controlling the bite size during the nutation/spin tool motion.

Also, the graphs presented in this section indicate that irrespective of nutation rate and for a given axial feed rate, at position '$\theta = \alpha$', the large cone angle tools, produce a greater zone of contact.

6.6. MESH GENERATION FOR VOLUME CALCULATION

In order to analyse the relative effectiveness of a given set of parameters during the simulated rotary forging operation, it was decided to modify FROGS to allow a determination of the volume of the material removed/displaced at any stage during the process.

A subroutine within the FROGS software was developed to divide the hypothetical cylinder of length H , into a number of macro-blocks. There are two types of such elements, prismatic-pentahedron and hexahedron with 5 and 6 sides, respectively.

Fig. 6.9 shows a cylindrical workpiece of radius R and height H . The billet is made up of number of elements, two of which are shown in the figure. The position of any point on the solid cylinder is measured from a datum plane parallel to the bottom end surface of the cylinder. The data array simulating the billet is interrogated by the subroutine. The subroutine is relatively simple, as it considers those elements within the inner cylindrical membrane as prismatic-pentahedrons, while those elements within any other membranes considered as hexahedrons. Each time the tool is interacted with the billet, the above subroutine is called upon, to calculate a new mesh.

If the interrogation of the data array, by this subroutine, establishes a prismatic-pentahedron, fig. 6.10.a, then 6 nodal points are required for representing its geometry. However, to represent a hexahedron, fig. 6.10.b, eight nodal points are needed. The only difference between the data co-ordinates representing nodal points 1 and 4 , in fig. 6.10.a, or points 1 and 5 in fig. 6.10.b, lies in their vertical components. The data points extracted from such analysis, is transferred to another subroutine for volume calculations.

For calculating the volume of a macro-element, which is enclosed by either 5 or 6 surfaces, it will have to be represented by a function p(s,t,u), which is made of 5 or 6 surfaces and the co-ordinates of 6 or 8 corners. The volume of such element is given by equation (6.2).

$$\text{VOLUME} = \int_{-1}^{1}\int_{-1}^{1}\int_{-1}^{1} (((\delta p/\delta s) x (\delta p/\delta t)) \cdot \delta p/\delta u) ds dt du \quad (6.2)$$

Where

$$-1 \leqslant t \leqslant 1$$

$$-1 \leqslant s \leqslant 1$$

$$-1 \leqslant u \leqslant 1$$

Software previously developed [62] was incorporated in the FROGS system. Applying numerical integration, the extended package was capable of calculating the volume of elements of the above mentioned geometry.

It follows that the volume of the cylindrical billet, during any stage of the simulation, is the sum of the elements which makes up the solid object. The total number of elements, is given by $m \times n$, where m and n represent the radial and circumferential lines respectively. Hence, the greater the values of m and n, the greater the accuracy of the resultant volume of the solid. To reduce computation time, the values of m and n chosen to demonstrate the technique, were considered to be 360 and 10 respectively.

6.6.1. Spin type tool motion

In spin type tool motion, the rate of reduction in volume of a hypothetical workpiece, of a fixed height and radius, is dependent on the bite size per revolution of the conic tool. Where the axial feed rate is constant, the reduction during intermediate revolutions, will be steady state. In this analysis, the reduction in workpiece volume is determined as a percentage of the original volume.

The parameters which affect bite size, and hence the volume of the material removed per revolution, namely tool geometry and axial feed rate are examined here.

The variation in axial feed rate and its resultant effect on the volume of the material being removed for H/D ratio of 2 and 1 are shown in figs. 6.11.a and b respectively. As a non-constant volume workpiece is being simulated, an increase in axial feed rate, will increase the volume of material being removed. Clearly, using the percentage displace material as a measure of volume removed, it follows that the larger the workpiece aspect ratio, i.e. H/D , the smaller the volume displaced for a given cone angle and axial feed rate (figs. 6.11.a and b). For constant feed rate, volume removed is directly proportional to axial feed.

6.6.2. Nutation-spin type tool motion

The volume of material removed is due to two tool motions, i.e.

nutation/spin and axial feed/spin. Therefore, the effects of two parameters of nutation rate and axial feed rate have been investigated.

In all simulations presented in this section, the height of the billet was chosen to be twice that of the diameter and an initial uni-axial compression has always been assumed. This means that, when nutation begins a volume of material has already been displaced. Also, it should be noted that in this situation, nutation always increases the angle of inclination of conic tool with respect to vertical axis. The reverse nutation is possible using FROGS, by reversing the sign.

Fig. 6.12 shows the reduction in volume of a cylindrical workpiece, as the axial feed rate varies, while the tool geometry and nutation rate remain unchanged. The figure shows the reduction in volume as the axial feed rate increases from zero to 0.3 'unit/rev', in six equal intervals. If the reduction in volume due to nutation/spin, for a given inclination angle, is deduced from each set of data given in fig. 6.12, and re-ploted, it produces a number of straight lines with their gradients increasing by equal amounts, as the axial feed rate increases at a steady rate, therefore indicating removal of equal volume of material.

This is in close agreement with the findings of other researchers [13] resulting in the conclusion that the theoretically removed volume after any number of revolutions is

due to two components of individual tool motions, viz. nutation/spin and axial feed/spin. In this analysis, the former is kept constant and the latter is increased linearly and the volume of material removed accordingly.

The variation in nutation rate, while other parameters, namely tool geometry and axial feed rate, are kept constant, influences the speed of forging cycle. The greater the nutation rate, the faster the rotary forging process.

Through a limited number of simulations presented here, it is clear that the smallest variation in any of the above mentioned process parameters, results in different product deformation. FROGS is capable of simulating any variation in tool geometry, axial feed rate, nutation rate, height to diameter ratio and conic tool motion. It is feasible to generate a whole series of information. The stored data could be extracted by the operator for selecting the most suitable parameters, in order to achieve the desired deformation.

6.7. CONCLUSIONS

The generated data points, through the simulation, were used to calculate the area of contact zone and the percentage reduction in the volume of the material being removed.

A basic concept of the finite element analysis was introduced.

The importance of dividing the cylindrical workpiece, into finite number of elements of specific geometry, was emphasised. It was decided to use the generated data points, which are in the cartesian co-ordinate system, as the representation of the nodal points of the macro-elements. A subroutine was developed which divided the billet surface into a number of trilateral or quadrilateral macro-elements. A further subroutine was developed within the FROGS software, which divided the billet workpiece of certain height (measured from the pivot plane), into a number of macro-blocks. Those elements which were on the most inner cylindrical membrane, were represented by prismatic-pentahedrons, while the rest were represented by hexahedrons. The two mesh generation routines could be applied during any stage of the deformation.

In order to calculate the area of a trilateral or quadrilateral element, a previously developed software was employed, which, through a numerical integration, calculated the area of each individual element within the generated mesh. The sum of the areas of all calculated elements, resulted in the area of tool/workpiece contact zone. Two types of tool motion were simulated, spin and nutation-spin and the resultant surface areas were examined. The effects of parameters, such as axial feed rate, nutation rate and tool geometry on the shape of the ICA were investigated. The resultant information, was found to be in good agreement with other geometrical analysis carried out in chapter five.

The simulation of a non-constant volume workpiece enabled FROGS to calculate the volume of the billet during any stage of the deformation. Previously developed software, which is available on most FEM packages, was introduced into FROGS, which through numerical integration, was capable of calculating the volume of the macro-block within the generated mesh. The sum of volumes of all elements, yield the deformed workpiece volume and hence the reduction in volume at any stage of the process. The effect of parameters, such as axial feed and nutation axial feed were also investigated.

This kind of analysis and the derived information could be used as a tool by a machine operator to set various process parameters, in order to achieve a certain product geometry

CHAPTER SEVEN

CHAPTER SEVEN

INVESTIGATION INTO FROGS CAPABILITY FOR SIMULATING CONFIGURATED CONIC TOOLS

7.1. INTRODUCTION

A software package, capable of graphically simulating the deformation of a non-constant volume workpiece by a plain conic tool, has been developed. However, many of the components manufactured in industry, are of complex shape, with various degrees of complexity. A rotary forged product with certain features could be produced using a conic tool of the required geometry and inclination angle. This chapter deals with the incorporation of configurated tooling into the FROGS software and its analysis.

The types of features which could be super-imposed onto a plain conic tool, are radial, circumferential or a combination of the two. This aspect is determined by the geometry of the top surface of the final product. The author carried out a survey on the rotary forged components manufactured in the west. This concluded that as much as 95% of manufactured configurated components, mainly in the car industry, have radial features on them. However, for manufacturing components of circumferential features, the required configuration was incorporated in the lower die. Hence, it seemed appropriate, at this stage of

research, to simulate tools with radial features only. However, FROGS could be developed to accommodate the simulation of circumferentially configurated tools. In order to obtain a radially configurated component, the required tool is simulated through implementation of a datafile which represents the desired features.

The loci for a number of points, on the configurated tool are graphically represented as it undergoes various motions. A cylindrical workpiece, consisting of a number of cylindrical membranes is simulated and its interaction with a configurated conic tool, either with spin, or with spin-nutation, is considered.

As the features on a conic tool become more varied and its motion more complex, the deformation of the workpiece under investigation becomes more complicated. However, the developed software for calculation of the workpiece/tool contact zone could be used to assess the state of billet deformation during any stage of the process.

7.2. SIMULATION OF A RADIALLY CONFIGURATED TOOL

Any radially configurated workpiece, could be obtained by super-imposition of the desired configuration onto a plain conic tool. FROGS achieves this by extracting a datafile representing, on the horizontal plane, the lowest generator of

such a configuration. The resultant simulation is shown in fig. 7.1.a.

The next step in simulating a radially configurated tool, is to rotate the data points representing the above mentioned lowest generator, by an amount equal to θ , in the Y-Z plane about the pivot point (see fig. 7.1.b.). The FROGS software, through the set of equations (4.1), is capable of generating a data matrix, with each element representing the X, Y and Z co-ordinate of a point on the surface of the radially configurated conic tool. The magnitude of the rotation of the lowest generator , away from the Y-axis, is sufficient to cause the tool axis to be co-axial with the vertical component of the machine axis.(i.e. $\theta = \alpha$).

The data which represents a lowest generator of a specific configuration , was extracted from a database which has been previously tailored to incorporate the desired radial features. Obviously, any variation in configuration is limited by the number of datafiles which have already been accommodated in advance of any simulation. Alternatively, an interactive graphics input facility, could be used to input a set of data which can simulate any die geometry.

Any radial configuration could be expressed in terms of deviation, in the vertical plane, of the lowest generator of a plain cone at $\theta = \alpha$ position. Hence, in theory, any radial configuration could be achieved by introducing a feature which

is inclined at some angle ω to the lowest generator or a line parallel to it . The range of such angle, in an anti-clockwise direction, could vary from 0 to 360 degrees, see fig. 7.2.

It might be assumed that the die designer could achieve any radial configuration on a rotary forged component, by reproducing a mirror image of a such a configuration on to the surface of a plain conic tool. However, in reality, due to the tool motion , there are limitations to the practical workpiece geometry which could be obtained, using certain radially configurated tools. For example, a radially configurated tool, with its lowest generator shown in fig. 7.3.a, will not produce a component with its features being the mirror image of the tool. As the tool spins or precesses, it would cause the twisting of the material trapped within the segments 'a' and 'b', hence the resultant feature on the tool would be different.

Such limitations could be explained in terms of the various radial configurations of fig. 7.3.b, which represent a conic tool, with $\theta = \alpha = 30$ degrees. Each tool profile can be made up from a number of points, which increase with the complexity of the radial configuration. The projection of these points into, plan or side elevation, yields interesting results. Consideration of any two points which constitute an element of the tool profile, for example '0' and '1', or '1' and '2', reveals that monotonically increasing points have equal or greater radial distance than those of their respective starting points. Therefore, if the point '2' has a radial distance less

than that of point '1', the interaction of such a tool with the workpiece would result in a different configuration than that of the tool profile. This limitation could also be explained in terms of vector analysis. That is, the magnitude of the vector passing through the origin and the starting point of a segment, should always be less than the magnitude of the vector which passes through the origin and the end point.

These limitations, should be translated to the FROGS software, to ensure such a situation does not arise. The FROGS software interrogates the data co-ordinates representing any radial configuration, extracted from a database, or, through a graphics input device. If a situation has occurred , in which the end point of a tool segment has greater Y-component than its starting point, then it makes sure the two, have at least, equal radial distance. This would cause some modification of the conic tool design.

To demonstrate the application of FROGS to simulate a radially configurated cone, four case study examples have been used. The four configurated lowest generators, shown in fig. 7.4, represent cases ranging from simplest to most difficult, with the intermediate range covering realistic cases of rotary forged components. In future, the four configurations, as shown in fig. 7.4, will be referred to, as CONF1, CONF2, CONF3 and CONF4 respectively.

7.3. SIMULATION OF TOOL MOTION

In rotary forging, as previously shown in fig. 4.1 and table 1, the type of tool motion must be specified prior to any simulation. Depending on which type of machine classification is to be simulated, the information should be conveyed to FROGS, regarding the rate of change of Nutation ($\dot{\theta}$), Precession ($\dot{\psi}$) or Spin ($\dot{\varphi}$) per second or per 2π radians rotation of the lower die.

Having established the co-ordinates of those points which describe the lowest generator, FROGS is capable of tracing the loci of all points on one such generator, as the configurated tool undergoes its respective motion. The number of data points incorporated into a datafile and the time interval at which calculations should be carried out, will influence the accuracy of the simulation.

The generated data points are stored in a specified format, as described in the earlier chapters. The drawing routines are called to trace the loci of any number of points on the conic tool surface, irrespective of its configuration, as its axis moves about the pivot point. Only a few tool motions are simulated here and in each case a 30 degree conic tool is considered. The choice of tool configuration is purely arbitrary and is selected for the purpose of demonstration. As with previous simulations, a pure rolling situation at the tool/workpiece interface is specified.

(a)-Spin:

The trace of the lowest generator, represented by CONF4 is simulated as the tool rotates about its own axis for 2π radians. The graphical representation, consisting of three orthogonal views and an isometric view, is similar to those shown in figs. 4.9 and 10 respectively ($\theta = \alpha$).

(b)-Precession:

If a configurated conic tool, with its lowest generator represented by CONF3, undergoes 2π radians precessional rotation, the loci of the lowest generator after an elapse of one second, are simulated graphically in figs. 7.5.a and b respectively ($\theta = \alpha$).

(c)-Nutation-Spin

A radially configurated tool, with its lowest generator on the horizontal plane is shown by CONF1. The tool axis is assumed to be co-axial with the machine axis at t = 0. Then it nutates towards the pivot plane at the rate of 20 degrees per second, while spinning about its own axis at the rate of 2π radians per second. The trace of the lowest generator of a tool

undergoing such a motion, is shown in the orthogonal and isometric views of figs. 7.6.a and b, respectively. It should be noted that the large nutation rate was selected to provide a clear graphical presentation of the tool motion.

(d)-Nutation-Precession-Spin:

The conic tool, with a similar configuration to the previous case, is allowed to precess, spin and nutate towards the Y-axis at rates of 15, 90 and 360 degrees per second, respectively. The trace of such motion is shown in the isometric view of fig. 7.7.

The geometry of the workpiece surface, being deformed by a rotary forging tool, is determined by the tool geometry, its angle of inclination, and the motion which it undergoes. In the simulation, the lowest generator of the tool acts as a formed cutter on the billet surface and produces a spiral surface. In such cases, where the cone is plain and its axis free from nutation, the surface could be predicted and simulated with relative ease and confidence. However, the importance of tool motion simulation will be appreciated as the tool motion becomes more complex (for example nutation-precession-spin) and its geometry more varied (for example with radial and circumferential features).

7.4. SIMULATION OF THE WORKPIECE

As before, the workpiece is assumed to be a membrane model of non-constant volume, and hence any deformation would result in reduction in height, without any consideration of material flow.

If the tool axis is free from any nutational motion, the data points representing the lowest generator at $\theta = \alpha$, are allowed to rotate about the vertical axis, for 360 degrees. The MGM (Mathematical/Geometrical Model) was used to calculate the co-ordinates of the points at different angular positions from the Y-axis. The number of radial and circumferential lines, at which the calculation should be carried out, is equal to the number of lines used for simulating a configurated conic tool. This ensures that there are equal numbers of data points in the arrays representing the workpiece and configurated tool.

7.5. INTERACTION BETWEEN TOOL AND WORKPIECE

To simulate the interaction between tool and the workpiece, two sets of data have been obtained. One represents a solid of specified geometry and radial configuration, the other, a spiral surface generated due to the relative motion of the tool and hypothetical workpiece moving in a vertical plane. The interaction between the two, results in a surface which represents the tool impression on the billet. As in previous cases, the deformed surface consists of two parts, one being the

area of instantaneous contact (ICA), and the other being the surface which has previously been contacted by the tool.

The first requirement for locating the ICA, is that the two graphical simulations should have a common datum line. Therefore, the line, representing the lowest generator at $\theta = \alpha$, was chosen to coincide with the radial component of the workpiece surface which lies on the Y-axis. In addition, the two simulations should have equal numbers of radial and circumferential points to ensure direct comparison between two corresponding points. After fulfilling the above requirements, the vertical components of each set of corresponding points are compared. The outcome of such investigation, determines if a point on the simulated helical surface is on the ICA or not. This is similar to analysis described in the earlier chapters. The approach allows an instantaneous view of the resulting deformation at any stage of process.

7.6. SPIN TYPE TOOL MOTION

7.6.1. Simulation of workpiece deformation

Fig. 7.8.a shows four instantaneous views of a cylindrical workpiece during 360 degrees rotation of the bottom die. The radially configurated conic tool has a fixed angle of inclination, $\theta = \alpha = 30$ degrees, and its lowest generator is

represented by CONF1. The axial feed rate per revolution is constant, S = 0.2 Unit.

For a conic tool, with its lowest generator on the horizontal and represented by CONF3, the instantaneous view of deformation of an intermediate revolution is shown in fig. 7.8.b. In this analysis, the axial feed rate is as in the previous simulation, while $\theta = \alpha = 5$ degrees. It indicates, as expected, an increased tool/workpiece contact zone. It also emphasises the need for much improved graphics presentation, which could be achieved through techniques such as hidden line removal or solid modelling.

7.6.2. Calculation of ICA and volume reduction

It is possible to calculate the configurated tool/workpiece contact zone and the volume of the billet, as it is being penetrated by the tool. In doing so, the same mesh generation techniques and algorithm, used in the previous chapter for area and volume calculations, were employed.

A quantitative approach enables the design engineer and machine operator to assess the workpiece and its geometry at different stages of the process. The calculated ICA, in conjunction with the calculated volume of the workpiece, give an exact account of the geometry of deformation at any instant of time. This could be investigated through a few simple examples. Figs. 7.9.a and

b, show in plan and isometric view, a radial segment of a cylindrical workpiece. For ease of analysis, it is assumed each segment is made up of only three elements, 'a', 'b' and 'c' and that the billet is interacted with a radially configurated tool with it's lowest generator represented by fig. 7.9.c. The conic tool is at angle of inclination of $\theta = \alpha = 30$ degrees and is spinning about its own axis, whilst the workpiece is moving in the vertical plane at a constant rate.

The effect of variation in vertical segment of the tool profile, i.e. H , on the actual ICA for one radial segment is shown in fig. 7.10. This indicates that the variation in actual ICA, due to segment 'b', is directly proportional to changes in H , whilst its width is kept constant. However, if H increases at a similar rate, but in the opposite direction (see fig. 7.9.d), the calculated ICA for the three segments would be the same as in the previous case. In order to distinguish between the two cases, the calculated volume of each element is investigated. If the volume due to segment 'a' is greater than that in 'c', the tool profile would be as in the condition shown in fig. 7.9.c, i.e. negative H . Where the converse is true, the configuration would be as represented in fig. 7.9.d.

This analysis, could be extended to all elements constituting the workpiece and hence, an accurate picture of workpiece deformation could be obtained. Apart from tool configuration, other parameters which influence the contact zone geometry and volume of material being removed, namely axial feed rate and

conic angle, were investigated. These were found to yield similar results to those of a plain conic tool. Hence there is no need to reproduce them in this chapter.

7.6.3. Importance of a numerical approach

The significance of calculating the tool/workpiece contact zone, or volume of the material being removed, lies in its ability to provide engineers and tool designers with a quantitative method of assessing the workpiece deformation. FROGS is capable of graphically representing the various stages of the deformation, but doing so requires generating a large amount of pictorial information, which is both a tedious and time-consuming task. Also, as the tool motion becomes more complex and its configuration more varied, its analysis necessitates the use of more advanced graphics software and hardware. This in turn would add to the time and cost required to provide such information.

However, similar information could be extracted through constructing a database, which could accommodate the surface area of the workpiece and its volume. This numerical information could be extended, to be used to assess the state of deformation during the process. Furthermore, the tool designer could use such a quantitative approach, as a method of comparison to investigate the effect of parameters such as feed rate, nutation rate, tool geometry, etc..

The further advantage of numerical analysis, is in its applications in estimating forming stresses, average pressure, total forming load, and the calculation the centre of loading, etc.. Furthermore, the investigation of such physical conditions, for example, the effect of material properties on the deformation of a workpiece would be impossible using a graphics only approach.

7.7. NUTATION - SPIN TYPE TOOL MOTION

7.7.1. Simulation of workpiece deformation

In this section a conic tool of similar configuration to those shown in fig. 7.4, has been simulated and used with nutation and/or spin, to profile the upper surface of a workpiece. In all simulations a conic tool of 30 degrees base cone angle was used with an initial uni-axial compression to provide full tool penetration into the workpiece, similar to that shown in fig. 5.11.

Fig. 7.11.a shows the lowest generator of a conic tool having a similar radial configuration to CONF1, and its axis co-axial with the machine axis. A similar method of assessment has been used to that of the previous section. From this figure it is apparent that the Y-component of points '1', '2' and '3', which are the end points of tool segments 'a', 'b' and 'c', are

greater than those of their respective starting points, i.e. '0', '1' and '2'. Representations I , II and III show the lowest generator at three inclination angles of 0, 15 and 30 degrees respectively. Fig. 7.11.b, represents the same approach applied to a second cone with its profile similar to that of CONF2.

Fig. 7.12.a shows a lowest generator of similar configuration to CONF3. The representation I (with parts in broken line) shows such a generator when the tool axis is co-axial with the machine axis. It is clear that in free upsetting deformation, material will not flow into the region enclosed by the two segments of the tool shown in broken lines. Also the examination of the Y-components of points '0' to '5' would support such an assertion. This is because the end point of segment 'd', i.e. point '4' has a greater Y-component than point '3'. Hence, the tool has to be modified in order to avoid such situations. It was also suggested that for each segment, the end point should have Y-components greater or equal to its starting point. Hence, in accordance with this proposal, the tool profile was modified and is represented in solid line. therefore, the angle subtended by segments 'c' and 'd', should be increased by ι which it would have the minimum value of α degrees. The representations II and III show similar analysis where the angle of inclination is equal to 15 and 30 degrees respectively.

It could be concluded that a radially configurated conic tool which is nutating towards the Y-axis, can not produce components

with features similar to CONF3. However the closest match to such a configuration, could be obtained by re-designing the tool in accordance with some simple rules. The modified die design and its impression on the component, is shown in fig. 7.12.a.

Fig. 7.12.b shows a similar approach to a conic tool with a radial configuration, shown by CONF4.

The FROGS software, as mentioned earlier, would accommodate any modification of the tool, if it was required.

To obtain the interaction between the tool and the workpiece, the method of geometrical comparison was applied to two sets of data points. One set represents a radially configurated conic tool, which has already been through the test for assessing the Y components of constituting points and modified where necessary. The other set represent a spiral surface produced through penetration of a nutating/spinning tool into the workpiece. The same algorithm and procedure, which was mentioned in section 4.5.3, was used for obtaining the helical surface.

Figs. 7.13.a and b show the penetration of a radially configurated conic tool (α = 32 degrees) into a billet of fixed height which is moving in the vertical plane at a constant rate. Uni-axial axi-symmetric compression is assumed, and the figure represents the instantaneous view of such a simulation at angles of inclination of 8, 16, 24 and 32 degrees respectively. The

profile achieved on the workpiece is similar to CONF1.

In a second case, FROGS was employed to simulate the interaction of a radially configurated tool with a cylindrical workpiece, such that at $\theta = \alpha$, a workpiece profile similar to CONF3 is achieved. A conic tool of $\alpha = 32$ degrees is simulated which is nutating towards the Y axis and spinning at the rate of 8 and 360 degrees per second respectively. From the previous section, it is obvious that the tool profile has to be modified. Figs. 7.14.a, b and c show such simulation at $\theta = 8$, 16, 24 and 32 degrees. As shown in fig. 7.14.a, the ICA (shown in magenta) is reduced as the tool reaches the Y axis. Fig. 7.14.b, where only the workpiece surface is shown for the sake of clarity, indicates the resultant configuration is slightly different from CONF3, which is due to the necessary modification of the tool profile.

As stated at the beginning of this chapter, it is the tool geometry and its position in space which together determine the profile of the upper workpiece surface. Where the interaction of the tool and workpiece leads to unsatisfactory conditions during forming, for example in the case of CONF3 and nutation, then tooling geometries would have to be revised along the lines shown in fig. 7.12.a.

In order to produce a workpiece with a final upper surface geometry similar to CONF3, a shallower conic tool , of say α=4 degrees, should be introduced. Figs. 7.15.a and b show

the resultant interaction between such a conic tool and a cylindrical billet. In the simulation, the tool nutates at the rate of 1 degree per revolution of the lower die. The resultant simulation of the workpiece geometry, at $\theta = \alpha$ is very similar to CONF3. The importance of a simulation package to explore these interactions is self evident.

7.8. CONCLUSION

The importance of configurated tooling, in industry, for forging components of various configurations and geometry was emphasised. Also highlighted was the significance of a computer package, for simulation of tool motion and prediction of the workpiece geometry, as the tool features become varied and its motion more complex.

A radially configurated tool was achieved by super-imposition of the desired features onto a plain conic tool. The required data, for simulating such a tool, was extracted from a datafile, and the necessary steps for constructing the required data matrix were mentioned. Four different radially configurated tools were introduced and investigated.

It was shown, that due to tool motion, there are limitation ,to the practical workpiece geometry which could be obtained, using a certain radially configurated tool. Certain guidelines were introduced which, by their implementation during the design

stage, would remove such limitations.

FROGS was used to graphically simulate the tool motion,using four available radially configurated tools. The significance of the tool motion simulation has been emphasised. This is particularly important where the tool motion becomes more complex (for example Nutation=-Precession-Spin) and its geometry more varied.

The interaction between a radially configurated tool, which was either spinning, or nutating and spinning, and a cylindrical workpiece, was investigated and graphically represented. Due to practical limitations, and in accordance with the established guidelines, the tool design had to be modified. The FROGS software was shown to be able to simulate the redesigned conic tool and its resultant interaction with the workpiece.

The FROGS package was capable of quantitatively assessing the workpiece geometry at any stage of the deformation. The numerical analysis enables the die designer or machine operator to detect minute variations in the calculated ICA, or the volume of material being removed, hence investigating the parameters which cause such variation. In addition, the quantitative approach could be applied to provide estimations of the forging loads and their instantaneous positions on the workpiece surface.

CHAPTER EIGHT

CHAPTER EIGHT

CONCLUSIONS AND SUGGESTIONS FOR FURTHER WORK

8.1. CONCLUSIONS

A computer package, capable of graphically simulating the tool motions of various types of rotary forging machines has been developed and extended to include the interaction of a conic tool into a non-constant volume cylindrical workpiece. The package was extended to explore the generated data for the purpose of numerical analysis. The software package, which is referred to as FROGS (Forging Rotational Graphical Simulator), was written in FORTRAN 77 and was run on a PRIME 9650 mini-computer.

A research programme was followed to achieve objectives listed below:

(1)- The development of a mathematical/geometrical model for rotary forging.

(2)- The graphical simulation of tool motion of a complete family of rotary forging machine systems.

(3)- The simulation of tool/workpiece and their interaction during a rotary forging operation.

(4)- A numerical analysis of the simulated data produced in 1 to 4.

(5)- The initiation of a computer aided design package for the design of rotary forging conic tools.

(6)- The simulation of radially configurated tooling used in rotary forging.

8.1.1. Development of a Mathematical/Geometrical Model (MGM) for rotary forging

(a)- A set of equations based on the three Eulerian angles of rotation has been developed as the basis of a mathematical model for rotary forging.

(b)- It has been shown that the MGM is capable of calculating the position (using a cartesian co-ordinate system), of any point on the tool, at any given instant of tool motion.

(c)- This has been achieved through the introduction into the MGM, of the three controllable variables, namely the rates of change of nutation, precession and spin.

(d)-The MGM has been extended to incorporate normal die closure motion seen by a workpiece. The system has been used to identify the path, rate and direction of any tool/workpiece interface, during a simulated rotary forging cycle.

8.1.2. Graphical simulation of tool motion in rotary forging

(a)- A software package has been developed capable of graphically simulating the data generated using the MGM.

(b)- It has been shown that all seven types of rotary forging tool motions can be simulated.

(c)- A system has been developed which can graphically simulate the loci of any point, on a conic tool during a rotary forging motion.

(d)- It has been claimed that the simulation of rotary forging tool motion is a necessary requirement in determining the boundary conditions which are essential for any future finite element package designed to predict metal flow.

8.1.3. Simulation of tool/workpiece and their interaction during rotary forging

(a)- It has been shown that a conic tool of any geometry and inclination angle can be simulated and graphically represented, using the proposed MGM and the relevant software.

(b)- The membrane model proposal has been adopted and the software was developed to graphically simulate a solid billet by incorporating a finite number of membranes in a sigle workpiece.

(c)- The FROGS software package has been shown to be able to represent tool and workpiece, either as a wire-frame, or a surface, geometric model.

(d)- FROGS was shown to be capable of graphically simulating the workpiece surface contacted by a conic tool. The resultant surface was shown to consists of two elements, the Instantaneous Contact Area (ICA) and that resulting from previous contact.

(e)- It has been shown that irrespective of tool geometry and

configuration, two ICA geometries can be produced. The first one is a parabola, associated with spin or precession only. The rate of reduction in the height of the workpiece has been shown to be dependent on two componenets. One due to workpiece translation in the vertical plane and the other due to nutation. The second ICA geometry is represented by the segment of a circle which is the product of nutation only.

(f)- The ICA due to axial feed of the workpiece will produce an area of constant contact around the vertex of the tool. Its magnitude is dependent on the bite size at that instant. The same is not true for axial feed due to nutation only since the vertex of the tool does not penetrate the workpiece.

(g)- For a given tool/workpiece geometry and axial feed rate, the presence of nutation with either spin or precession will reduce or increase the actual bite size depending on the direction of the nutating axis towards or away from the billet and the rate of workpiece translation in the vertical plane.

(h)- It has been shown that where nutation is introduced, the die closure rate is not a linear fuction. Therefore, a steady state area of contact could only be achieved by variation of the workpiece translation in the vertical plane. These investigations have indicated that for a Marciniak/Schmid press,

axial feed due to main ram motion is not the die closure rate seen by the workpiece.

8.1.4. Numerical analysis of rotary forging using FROGS

(a)- The FROGS package has been extended to allow numerical analysis of the instantaneous area of contact and the volume of material removed/displaced. The investigations have shown that in a spin/or precession type tool motion:

(I)- The ICA does not increase linearly with axial feed rate, but there is a power relationship between the two. This is particularly true for conic tools of large base angle. The estimated instantaneous area of contacts have been compared directly with those values produced by other researchers and good agreement has been shown between all the techniques.

(II)- For a given axial feed rate, the change in the ICA is relatively insignificant for large cone angles in comparison with shallow cones.

(III)- The rate of reduction in volume of a hypothetical workpiece is dependent on the bite size per revolution.

Also, investigations have shown that for a nutation-spin type tool motion:

(I)- Where there is zero axial feed rate, the variation in the ICA is directly related to variation in nutation-axial pitch. This is proved to be true for any tool/workpiece geometries.

(II)- The ICA results from two components of axial feed due to nutation and die closure. Analysis has shown that the ICA can be controlled by the variation of either components with respect to the other. This variation would clearly affect the displaced volume of material and therefore, the deformation process can be force or displacement controlled.

(b)- The generated data points were used as nodal points of macro-elements; which are essential information in any analysis of this nature. It has been demonstrated that an accurate analysis is achieved, using a mesh of (360x10) elements.

(c)- It has been demonstrated that the FROGS software for numerical analysis, has many potential applications in the areas of estimation of forming stresses, pressure distribution, forming loads, etc.. This could offer particular advantages in the long term, for die designers and process engineers.

8.1.5. Simulation of radially configurated tools used in rotary forging

(a)- Typical, radially configurated tools, used in rotary forging have been successfully simulated by FROGS software.

(b)- A database has been constructed which uses four initial elementary radial tool profiles to model rotary forging conic dies.

(c)- Limiting conditions for radially configurated conic tool geometries have been determined.

(d)- Guidelines have been established for the practical design of radially configurated conic tools for rotary forging.

(e)- Guidelines for the design of radially configurated rotary forging tools have been incorporated into the FROGS software and a first generation CAD system produced.

(f)- The enhanced FROGS package has been shown to be capable of designing, checking for feasibility, simulating and graphically representing the interaction of radially configurated tools and workpieces.

(g)- The approach used in FROGS is believed to be unique in the development of rotary forging technology.

(h)- The interactive design/simulation package has been used and comparisons of different forging tools have been made using the technique of numerical analysis, developed by this work. This further highlights the significance of such a software package.

8.2. SUGGESTIONS FOR FURTHER WORK

8.2.1. Software improvement

The FROGS could be developed to be more user friendly. This could be achieved by calling different menus and being able to reproduce a certain instant of deformation without having to

regenerate all stages of the process. This could be achieved through implementation of a datafile, which could store the data representing the billet at a certain stage of the process. A large number of such files would provide a database, describing the workpiece deformation from start to finish.

Another area of improvement, could be in the method of locating the ICA. Using the existing system, an equal number of data points are generated for the tool and workpiece, and the two corresponding points are always compared. A more comprehensive method of search, might enable each point on the workpiece, to be investigated against every point on the tool. However, this would naturally increase the computing time.

8.2.2. Graphics input device

A graphical digitising input device, namely a tablet, with incorporation of relevant software, could be used to input interactively, a set of data which could simulate any die geometry and configuration. Various tablets, operating using different principles, are being marketed [56]. Basically these provide a flat drawing area, with a number of lines parallel to the X and Y axes respectively, each individual line carrying a unique digitally coded signal which can be picked up by the cursor. Inside the cursor, a sensitive amplifier detects the pulses from the lines, amplifies and delivers them to decoding logic, which in turn deposits binary integer co-ordinates in the

host processor. It is possible, through specially dedicated software for the origin of the tablet to be compatible with the vertex of a conic tool. Hence, it would be possible to trace, using the tablet, the line of any configuration, so the delivered co-ordinates, simulate the generator, in the vertical plane, of a conic tool with its axis at 90 degrees to the horizontal.

The above improvements could be accomplished in matter of weeks, and some are currently under development.

8.2.3. Graphics presentation

The wire-frame presentation could be greatly improved by the inclusion within the FROGS software, of hidden line removal routines. A more realistic solid representation of the workpiece could be obtained, by introducing depth into the object. A 3-dimensional picture could be produced from a successful simulation of shading effects. It would be particularly useful for the presentation of workpieces being deformed by configurated tools undergoing complex motions. However, this requires a more sophisticated and dedicated software and hardware.

8.2.4. Introduction of constant volume workpiece

In this research, the ability of FROGS to simulate the workpiece deformation and its relevant numerical analysis, was confined to processes such as rotary cutting and powder metal compaction. In other words, simulating the deformation of a hypothetical billet with its volume always reducing during a forging cycle. It seems the most important phase of improvement and extension, at this stage, would be to develop FROGS to incorporate the deformation of a constant volume material. This phase or module, would produce a state of the art package capable of predicting the material flow in rotary forging, and would be of great value to the die/product designer.

However, it should be emphasised that the development of a constant volume module would not be possible without the ability to define and simulate the tool/workpiece motion, their interaction and the boundary conditions necessary for any finite element plasticity software. In effect, the work described in this thesis.

APPENDICES

Appendix A

The Eulerian Angles

In order to describe the position of a rigid body (which is free to rotate about a fixed point) after being rotated and producing a table of scaler products, which represent the cosine relation which exists between the two sets of vectors, consider the following arguments (50).

Fig A shows two unit orthogonal right-handed triads $(\underset{\sim}{i}, \underset{\sim}{j}, \underset{\sim}{k})$ and $(\underset{\sim}{I}, \underset{\sim}{J}, \underset{\sim}{K})$ at the point O. The triad $(\underset{\sim}{i}, \underset{\sim}{j}, \underset{\sim}{k})$ is fixed in a rigid body which turns about O, and the triad $(\underset{\sim}{I}, \underset{\sim}{J}, \underset{\sim}{K})$ is fixed in the frame of reference.

The first Eulerian angle, θ is the angle between k and K. The second angle ϕ is the angle between the plan (k - K) and the plane (K-I). The third angle ψ is the angle between the plane (k-i) and the plane (K-k). The angle θ and ϕ fix $\underset{\sim}{k}$ and ψ is the angle rotation about $\underset{\sim}{k}$. It is evident that θ, ϕ, ψ determine the position of $(\underset{\sim}{i}, \underset{\sim}{j}, \underset{\sim}{k})$ and hence the position of the whole body.

The above description does not make it clear when ϕ and ψ are to be counted positive and when negative. This vagueness is removed by the following description of the angles in terms of finite rotation. Let us take an initial position in which $(\underset{\sim}{i}, \underset{\sim}{j}, \underset{\sim}{k})$ coincide with $(\underset{\sim}{I}, \underset{\sim}{J}, \underset{\sim}{K})$. We can bring the body to the general position shown in fig. A.1 by applying "in the order", of the following finite rotations.

i) A rotation ϕ K; this bring the movable triad $(\underset{\sim}{i}, \underset{\sim}{j}, \underset{\sim}{k})$ into coincidence with $(\underset{\sim}{I}', \underset{\sim}{J}', \underset{\sim}{k})$. Hence

$$\underset{\sim}{I}' = \text{Cos}\,\phi\,\underset{\sim}{I} + \text{Sin}\,\phi\,\underset{\sim}{J}$$

$$\underset{\sim}{J}' = -\text{Sin}\,\phi\,\underset{\sim}{I} + \text{Cos}\,\phi\,\underset{\sim}{J}$$

$$K' = K$$

(† is an example to clarify the above conclusion)

† Consider a set of co-ordinate (I, J)with unit vectors (i, j). After the transformation of the axes, it could be said, the vector $\underset{\sim}{i}$ consist of two components.

$$\underset{\sim}{i} = \text{Cos } \theta \ \underset{\sim}{I} + \text{Sin } \theta \ \underset{\sim}{J}$$

similarly

$$\underset{\sim}{j} = -\text{Cos } (\pi/_2 - \theta)\ I + \text{Sin } (\pi/_2 - \theta)\ \underset{\sim}{J}$$

$$= -(\text{Cos } \pi/_2 \text{ Cos } \theta + \text{Sin } \pi/_2 \text{ Sin } \theta)\ \underset{\sim}{I}$$

$$+(\text{Sin } \pi/_2 \text{ Cos } \theta - \text{Cos } \pi/_2 \text{ Sin } \theta)\ \underset{\sim}{J}$$

$$\therefore \quad \underset{\sim}{j} = -\text{Sin } \theta \ \underset{\sim}{I} + \text{Cos } \theta \ \underset{\sim}{J}$$

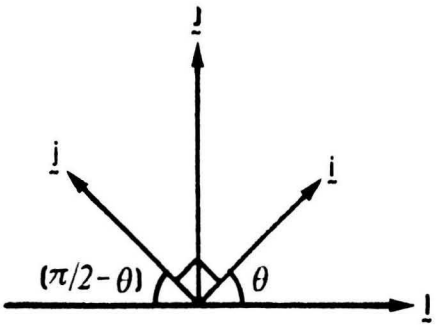

---

ii) Rotation θJ', brings (I', J', K) into coincidence with (I",J',k,

$$I'' = -\text{Cos } (\pi/_2 - \theta)\ \underset{\sim}{K} + \text{Sin } (\pi/_2 - \theta)\ I'$$

$$= -\text{Sin } \theta \ \underset{\sim}{K} + \text{Cos } \theta \ \underset{\sim}{I}'$$

Now by substituting I' from section (i)

$$I'' = -\text{Sin } \theta \ \underset{\sim}{K} + \text{Cos } \theta \ (\text{Cos } \phi \ \underset{\sim}{I} + \text{Sin } \phi \ \underset{\sim}{J})$$

$$I'' = \text{Cos } \theta \text{ Cos } \phi \ \underset{\sim}{I} + \text{Sin } \phi \ \underset{\sim}{J} - \text{Sin } \theta \ \underset{\sim}{K}$$

$$J' = J' = -\text{Sin } \varphi \ I + \text{Cos } \varphi \ J$$

$$k = \text{Cos } \theta \ K + \text{Sin } \theta \ \underset{\sim}{I}'$$

once again by substituting I' from section (i)

$$\therefore \quad \underset{\sim}{k} = \text{Sin } \theta \ \text{Cos } \varphi \ \underset{\sim}{I} + \text{Sin } \theta \ \text{Sin } \varphi \ \underset{\sim}{J} + \text{Cos } \theta \ \underset{\sim}{K}$$

iii) Rotation ψ k, brings ($\underset{\sim}{I}$", $\underset{\sim}{J}$', $\underset{\sim}{k}$) to the required final position, i.e.($\underset{\sim}{i}$, $\underset{\sim}{j}$, $\underset{\sim}{k}$)

$$\underset{\sim}{i} = \text{Cos } \psi \ \underset{\sim}{I}'' + \text{Sin } \psi \ \underset{\sim}{J}'$$

by substituting $\underset{\sim}{I}$" and $\underset{\sim}{J}$' from sections (i) and (ii), hence:

$$\underset{\sim}{i} = (\text{Cos } \theta \text{ Cos } \phi \text{ Cos } \psi - \text{Sin } \phi \text{ Sin } \psi)\ \underset{\sim}{I} + (\text{Cos } \theta \text{ Sin } \varphi \text{ Cos } \varphi + \text{Cos } \phi \text{ Sin } \psi)$$

$$\underset{\sim}{J} - \text{Sin } \theta \text{ Cos } \psi \ \underset{\sim}{K}$$

Also

$$\underset{\sim}{j} = -\text{Sin } \psi \ \underset{\sim}{I}'' + \text{Cos } \psi \ \underset{\sim}{J}'$$

once again by substituting $\underset{\sim}{I}''$ and $\underset{\sim}{J}'$ from sections (i) and (ii) , it could be said

$$\underset{\sim}{j} = (-\text{Cos } \theta\text{Cos } \phi\text{Sin } \psi - \text{Sin } \phi\text{Cos}\psi \ )\underset{\sim}{I} + (\text{Cos } \phi\text{Cos } \psi - \text{Cos}\theta \ \text{Sin}\phi \ \text{Sin}\psi \ ) \ \underset{\sim}{J}$$
$$+ \text{Sin } \theta \ \text{Sin } \psi \ \underset{\sim}{K}$$

and as the previous section

$$\underset{\sim}{k} = \text{Sin } \theta \ \text{Cos } \phi \ \underset{\sim}{I} + \text{Sin } \theta \ \text{Sin } \phi \ \underset{\sim}{J} + \text{Cos } \theta \ \underset{\sim}{K}$$

The last three expressions for unit vectors $\underset{\sim}{i}$, $\underset{\sim}{j}$ and $\underset{\sim}{k}$ could be rearranged to produce a table of scaler products (exactly the same as table 2),which relates the direction cosines of a set of unit vectors (in a right-handed cartisian co-ordinator) to another set of unit vectors.

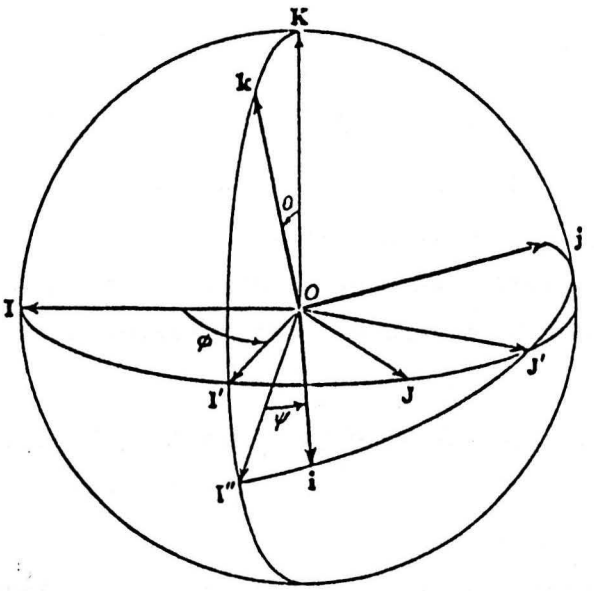

Fig. A

Appendix B

Finite and Infinitesimal Rotation

1. Finite Rotation: In order to prove that the final rotation is effected by the order in which the individual rotation are applied, consider the following illustrated example (51).

Let A_x represent a rotation of a body (such as rectangular parallelepiped) about the x-axis while A_y represents a rotation about the y-axis. We assume such rotations takes place in a positive or anticlockwise direction according to the right hand rule.

Fig. B.1.a. shows the parallelepiped in its original position, while fig. B.1.b shows the body after the rotation A_x about x-axis is performed. Finally fig. B.1.C shows the parallelepiped after being rotated through y-axis. Thus fig. B.1.C is the result of the rotation Ax + Ay on fig. B.1.a.

As shown in fig. B.2.a, the parallepiped is in the same original position as the previous case, but this time the rotation Ay through y axis is performed first (fig. B.2.b) and then rotation Ax about x axis is indicated in fig. B.2.C. Thus fig. B.2.C is the result of rotation $A_y + A_x$ on fig. B.2.a.

Since the final position of the parallelepiped of fig.B.1.C is not the same as that of fig. B.2.C. it could be concluded that the operation $A_x + A_y$ is not the same as $A_y + A_x$. Thus the commutative law is not satisfied, so that A_x and A_y can not possibly be represented by vectors.

2. Infinitisemal Rotation: In order to prove that the order of rotation does not effect the final displacement, in an infinitisimal rotation, consider the following:

In a given displacement of a rigid body, the vector displacement of a particle with position vector $\underset{\sim}{r}$ is a vector function of $\underset{\sim}{r}$, say $A(\underset{\sim}{r})$. For another displacement, it will be a different vector function say $B(\underset{\sim}{r})$. Consider now the application of the two displacement in succession.
The position vectors of a particle are as follows:

i) $\underset{\sim}{r}$, before displacement
ii) $\underset{\sim}{r} + A(\underset{\sim}{r})$, after the first displacement
iii) $\underset{\sim}{r} + A(\underset{\sim}{r}) + B(\underset{\sim}{r} + A(\underset{\sim}{r}))$, after the second displacement.

(The symbol $B(\underset{\sim}{r} + A(\underset{\sim}{r}))$ means the vector displacement of the particle which is at $\underset{\sim}{r} + A(\underset{\sim}{r})$ before the displacement B is applied.)

Now, if the displacements are infinitesimal, $\underset{\sim}{r} + A(\underset{\sim}{r})$ and $\underset{\sim}{r}$ differe only by a small vector quantity of the first order. Hence commit only an error of the second order if we write.

$$B(\underset{\sim}{r} + A(\underset{\sim}{r})) = B(\underset{\sim}{r})$$

Thus, to the first order of small quantities, the resultant displacement of the particle is:

$$A(\underset{\sim}{r}) + B(\underset{\sim}{r})$$

If the displacements are applied in the opposite order, the resultant displacement of the particle is:

$$B(\underset{\sim}{r}) + A(\underset{\sim}{r})$$

Hence the order in which infinitesimal displacements are applied to a rigid body does not effect the final displacement.

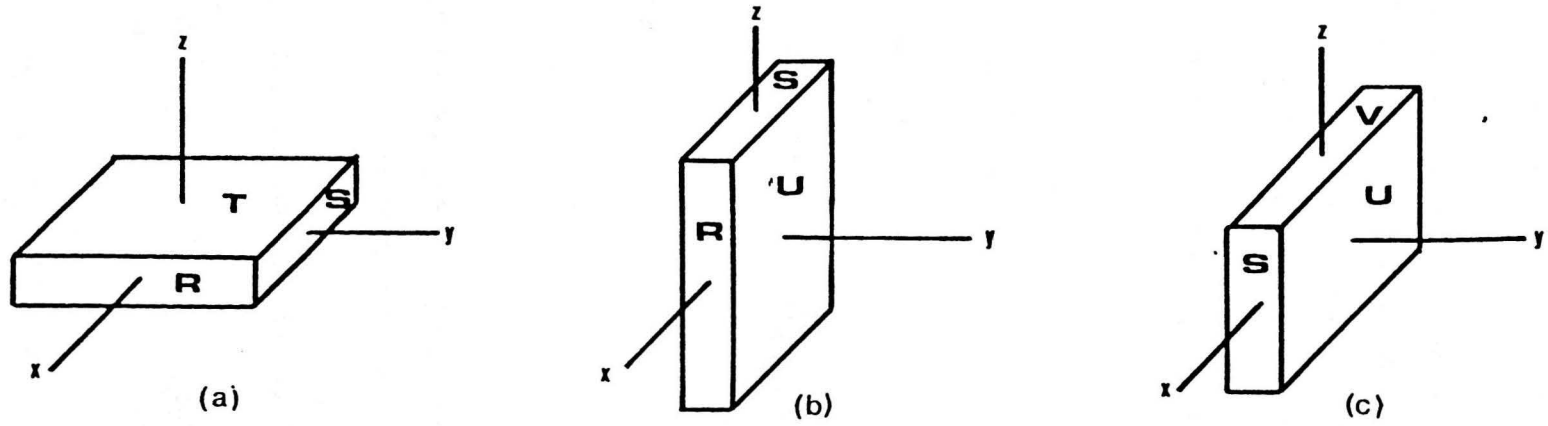

Fig. B-1

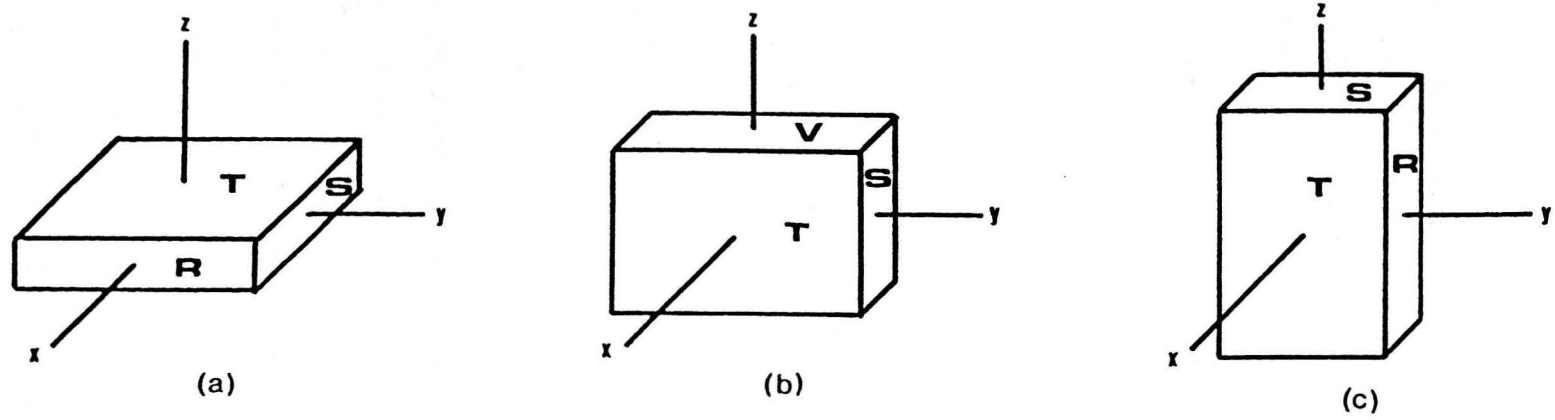

Fig·B· 2

Appendix C

Workpiece membrane of constant radius:

To obtain a cylindrical membrane of constant radius as it is being penetrated by a nutating conic tool, consider fig. C.a. The aim is to calculate the co-ordinates of an ideal point 'A', from the co-ordinates of point 'B' resulted from unmodified simulation.

From two similar triangles, shown in plan view (fig. C.a) it can be deduced:

$$\frac{XB}{RB} = \frac{XA}{RA} \qquad X_A = \frac{XB \times RA}{RB}$$

and similarly

$$\frac{YB}{RB} = \frac{YA}{RA} \qquad Y_A = \frac{YB \times RA}{RB}$$

where:

$$RB = X_B^2 + Y_B^2$$

and RA is the radius of the workpiece membrane which is calculated for any cylindrical membrane at beginning of the simulation.

Also, from the two similar triangles of fig. C.b, it can be deduced:

$$\frac{ZB}{RB} = \frac{ZA}{RA} \qquad Z_A = \frac{ZB \times RA}{RB}$$

Hence, X_A, Y_A, Z_A substitute X_B, Y_B and Z_B respectively in the data array.

Fig·C

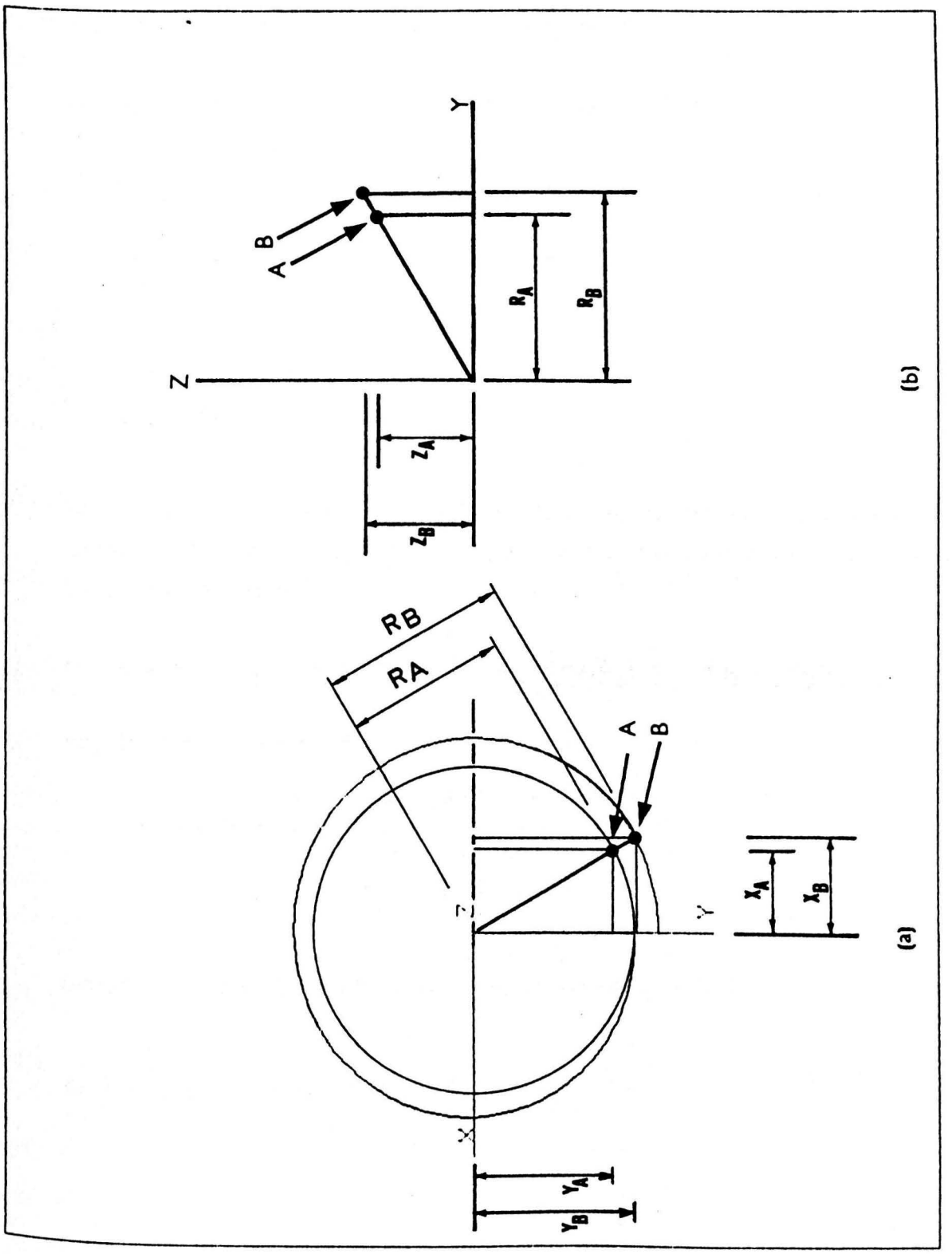

Appendix D

Area Calculation for a Trilateral macro-block

If two sides of trilateral element is represented by two vector a and b.

where

$$a = (x_2 - x_1)\ \underset{\sim}{i} + (y_2-y_1)\ \underset{\sim}{j} + (z_2-z_1)\ \underset{\sim}{k}$$
$$b = (x_3 - x_2)\ \underset{\sim}{i} + (y_3-y_2)\ \underset{\sim}{j} + (z_3-z_2)\ \underset{\sim}{k}$$

or

$$a = a_1\ \underset{\sim}{i} + a_2\ \underset{\sim}{j} + a_3\ \underset{\sim}{k}$$
$$b = b_1\ \underset{\sim}{i} + b_2\ \underset{\sim}{j} + b_3\ \underset{\sim}{k}$$

The area of a trilateral is half of the vector product of the two sides. The vector or cross product of two vectors a and b is given by vector c, where

$$c = a \times b = (a_2\ b_3 - a_3\ b_2)\ \underset{\sim}{i} + (a_3\ b_1-a_1 b_3)\ \underset{\sim}{j} + (a_1\ b_2-a_2 b_1)\ \underset{\sim}{k}$$

or, in a determinant form.

$$a \times b = \begin{vmatrix} \underset{\sim}{i} & \underset{\sim}{d} & \underset{\sim}{k} \\ a_1 & a_2 & a_3 \\ b_1 & b_2 & b_3 \end{vmatrix}$$

hence, the area is half of the magnitude of vector C.

$$\text{Area} = \tfrac{1}{2}\ (\ (a_2\ b_3-a_3\ b_2)^2 + (a_3\ b_1-a_1 b_3)^2 + (a_1\ b_2-a_2 b_1)^2\ )^{.5}$$

Appendix E

The quadrature presented by 4 straight boundaries, is represented by the function (62):

$$P(S,t) = \tfrac{1}{4}(1-S)(1-t)P_1 + \tfrac{1}{4}(1-S)(1+t)P_2 + \tfrac{1}{4}(1+S)(1+t)P_3 + \frac{1}{4}(1+S)(1+t)P_4$$

the derivatives w.r.t. S and t are

$$\frac{\delta P}{\delta S} = \tfrac{1}{4}((1-t)(P_2-P_1) + (1+t)(P_4-P_2))$$

$$\frac{\delta p}{\delta t} = \tfrac{1}{4}((1-S)(P_3-P_1) + (1+S)(P_4-P_2))$$

Also

$$dPt = \frac{\delta P}{\delta S}\, dS; \quad dPS = \frac{\delta P}{\delta t}\, dt$$

hence the vector of cross product, is given by

$$V_{S,t} = \frac{\delta P}{\delta S}\, ds \times \frac{\delta P}{\delta t}\, dt = \left(\frac{\delta P}{\delta S} \times \frac{\delta P}{\delta t}\right) dsdt$$

in vector representation

$$V_{S,t} = \left(\frac{\delta x}{\delta S}\underset{\sim}{i} + \frac{\delta y}{\delta S}\underset{\sim}{j} + \frac{\delta z}{\delta S}\underset{\sim}{k}\right) \times \left(\frac{\delta x}{\delta t}\underset{\sim}{i} + \frac{\delta y}{\delta t}\underset{\sim}{j} + \frac{\delta z}{\delta t}\underset{\sim}{k}\right) dsdt$$

in determinant form

$$V_{S,t} = \begin{vmatrix} \underset{\sim}{i} & \underset{\sim}{j} & \underset{\sim}{k} \\ \frac{\delta x}{\delta S} & \frac{\delta y}{\delta S} & \frac{\delta z}{\delta S} \\ \frac{\delta x}{\delta t} & \frac{\delta y}{\delta t} & \frac{\delta z}{\delta t} \end{vmatrix} dsdt$$

$$V_{S,t} = \underset{\sim}{i}\left|\left(\frac{\delta y}{\delta S}\cdot\frac{\delta z}{\delta t} - \frac{\delta y}{\delta t}\cdot\frac{\delta z}{\delta S}\right)\right| dsdt + \underset{\sim}{j}\left|\left(\frac{\delta x}{\delta t}\cdot\frac{\delta z}{\delta S} - \frac{\delta x}{\delta S}\cdot\frac{\delta z}{\delta t}\right)\right| dsdt + \underset{\sim}{k}\left|\left(\frac{\delta x}{\delta S}\cdot\frac{\delta y}{\delta t} - \frac{\delta x}{\delta t}\cdot\frac{\delta y}{\delta S}\right)\right| dsdt$$

where

$$\frac{\delta x}{\delta S} = \tfrac{1}{4}\left((1-t)\ (x_2-x_1) + (1+t)\ (x_4-x_3)\right)$$

$$\frac{\delta y}{\delta S} = \tfrac{1}{4}\left((1-t)\ (y_2-y_1) + (1+t)\ (y_4-y_3)\right)$$

$$\frac{\delta z}{\delta S} = \tfrac{1}{4}\left((1-t)\ (z_2-z_1) + (1+t)\ (z_4-z_3)\right)$$

$$\frac{\delta x}{\delta t} = \tfrac{1}{4}\left((1-S)\ (x_3-x_1) + (1+S)\ (x_4-x_2)\right)$$

$$\frac{\delta y}{\delta t} = \tfrac{1}{4}\left((1-S)\ (y_3-y_1) + (1+S)\ (y_4-y_2)\right)$$

$$\frac{\delta z}{\delta t} = \tfrac{1}{4}\left((1-S)\ (z_3-z_1) + (1+S)\ (z_4-z_2)\right)$$

Therefore area $= \int_{-1}^{1}\int_{-1}^{1} |\ V_{s,t}\ |\ dsdt \quad (1)$

Gauss Quadrature

It is possible to form a definite integral of a function such as f (x) from a data given by a set of values given in Gaussian quadrature formula (60) hence

$$\int_{-1}^{1} f\ (x)\ dx = \sum_{j=i}^{n} Hi\ \ f(aj)$$

where H and a are obtained from Gauss Quadrature table

The integration of quadrature could be applied to equation (1)

$$\int_{-1}^{1}\int_{-1}^{1} |V(s,t|dsdt = \sum_{i=1}^{n}\sum_{j=1}^{n} Hi\ \ Hj\ \ V\ \ (S_j,\ t_i)$$

where H_i, H_j S_j and t_i is found from Gauss Quadrature Table.

REFERENCES

[1] - Standring.P.M. "Investigation into Rotary Forging". Ph.D. Thesis. University of Nottingham. 1982.

[2] - Standring.P.M. and Appleton.E. "The Kinematic Relationship between Angled die and Workpiece in Rotary Forging". The 1st Int. Conf. on Rotary Metal Working Processes. London. U.K. Nov. 1979. pp.275-288.

[3] - Chou.P.C. and Sivpuri.R. "The Design and Construction of a Precision Rotary Forging Machine". Proc. 3rd. Int. Conf.on Rotary Metal working Processes. Japan. Sept.1984. pp43-59.

[4] - Standring.P.M. and Appleton.E. "The Development of Rotary Forging Machine Design". Chartered Mechanical Engineer. vol. 26. no:4. April. 1979. pp.44-50.

[5] - Slick.E.E. U.S.A. Patent no:965035. Manufacture of wheels. Filed in June 1907.

[6] - U.K. Patent Specification Number 319065. Massey Ltd. Improvement in Forging and Upesetting Machines. Sept. 1929.

[7] - U.K. Patent Specification Number 1224259. B and S.Massey Ltd. Filed July. 1969. Published. March 1971.

[8] - U.K. Patent Specification Number 1224260. B and S.Massey Ltd. Filed July. 1969. Published. March 1971.

[9] - U.K. Patent Specification Number 1205171. Politechnika Warzawska. Filed January 1968. Published. Sep. 1970.

[10] - Slater.R.A.C., Barooah.N.K., Appleton.E. and Johnson.W. "The Rotary Forging Concept and Initial Work with an Experimental Machine". Proc. Inst. Mechanical Engineers. vol. 184. part I. no:32. 1969-1970. pp.577-586.

[11] - Ulrich.O. U.S.A. Patent no: 3611771. Method for Rolling Disks and a Disk Rolling Mill for the Practice of the Method. Filed in June.1969.

[12] - Thyssen Maschinenbau (Wagner Dortmund). "Axial Closed Die Rolling of Forming Process for the Manufacture of Axially Symmetrical Forging". Metallurgia. Feb. 1987. pp.59-62.

[13] - Mwenda.H.M. "Design, Construction and Evaluation of a Nutation-Spin Forging Press". Ph.D. Thesis. University of Nottingham. 1986.

[14] - Pillinger.I, Hartley.P, Sturgess.C.E.N and Rowe.G.W. "Elastic-Plastic Three Dimensional Finite-Element Analysis of Bulk Metalforming Process". 1st International workshop on Simulation of Forming Processes by the Finite-Element Method (SIMOP-I). Stuttgart 1985. Proceedings Springer-Verlag 1986.

pp.91-124.

[15] - Liu.c., Hartley.p., Sturgess.C.E.N. and Rowe.G.W. "Finite-Element Modelling of Deformation and Spread in Slab Rolling". Int. J. of Mechanical Sciences. vol 29.no:4. 1987. pp.271-283.

[16] - Pillinger.I, Hartley.P, Sturgess.C.E.N and Rowe.G.W. "A new Linearized Expression for Strain Increment in Finite-Element Analysis of Deformation involving Finite Rotation". Int. J. of Mechanical Sciences. vol.28. no:5. 1986. pp.253-262.

[17] - Pillinger.I, Hartley.P, Sturgess.C.E.N and Rowe.G.W. "An Elastic-Plastic Three-Dimensional Finite-Element Analysis of the Upsetting of Rectangular Blocks and Experimental Comparison". Int. J. of Machine Tool Design and Research.vol.25. no:3. 1985. pp.229-243.

[18] - Pillinger.I, Hartley.P, Sturgess.C.E.N and Rowe.G.W. "A Three-Dimensional Finite-Element analysis of the Cold Forging of a Model Aluminium Connecting Rod". Proc. of Int. Mechanical Engineering. vol.199. no:c4. 1985. pp.319-324.

[19] - Hartley.P, Sturgess.C.E.N, Dean.T.A and Rowe.G.W. "Forging Die Design and Flow Simulation : their Integration in Intelligent Knowledge-Based System". Int. J. Mechanical Working Technology. vol.15. 1987. pp.1-13.

[20] - Lee.C.H and Kobayashi.S. "New solutions to Rigid-Plastic deformation problems using a Matrix Method". Trans. ASME. J. of Engineering for Industry. vol.95. August 1973. pp.865-873.

[21] - Matsumoto.H., Oh.S.I. and Kobayashi.S. "A note on the Matrix Method for Rigid-Plastic Analysis of Ring Compression". Proc. of 18th Int. Machine Tool Design and research Conf. London. Sep.1974. pp.3.

[22] - Oh.S.I and Kobayashi.S. "Finite-Element Analysis of Plane-Strain sheet bending". Int. J. of Mechanical Sciences. vol.22. 1980. pp.583-594.

[23] - Chen.C.C, Oh.S.I and Kobayashi.S. "Ductile Fracture in Axi-symmetric Extrusion and Drawing. Part 1. Deformation Mechanics of Extrusion and Drawing". Trans.ASME. J. of Engineering for Industry. vol.101. 1979. pp.23-35.

[24] - Oh.S.I. "Finite Element Analysis of Metal Forming Processes with Arbitrary Shaped Dies". Int. J. of Mechanical Sciences. vol.24. no:8. 1982. pp.479-493.

[25] - Altan.T and Oh.S.I. "CAD/CAM of Tooling and Process for Plastic Working". Keynote paper, Advanced Technology of Plasticity. vol.1, 1984. pp.531-544.

[26] - Oh.S.I, Park.J.J, Kobayashi.S and Altan.T. "Application of FEM Modelling to Simulate Metal Flow in Forging a Titanium

Alloy Engine Disk". Trans.ASME. J. of Engineering for Industry. vol.105. Nov.1983. pp.252-258.

[27] - Altan.T. "Computer Aided Design and Manufacturing (CAD/CAM) of Hot Forging Dies". J. of Applied Metalworking. vol.2. no:2. January 1982.

[28] - Oh.S.I, Malas.J, Gegel.H and Altan.T. "Practical experience and Future Developments in Computer Applications in Forging". Advanced Manufacturing Processes. 1(2). 1986. pp.195-221.

[29] - Park.J.J. and Kobayashi.S. "Three-Dimensional Finite Element Analysis of Block Compression". Int. J. of Mechanical Sciences. vol.26. no:3. 1984. pp.165-176.

[30] - Rodic.T. and Owen.D.R.J. "The computer Simulation of Radial Forging Processes". Auto Tech 87. Congress and Exhibition. New Approach to Forging Technology. Paper no:2. Birmingham. U.K. Dec.1987.

[31] - Osakada.K and Nakano.J. "Finite Element Method for Rigid-Plastic Analysis of Metal Forming-Formulation for Finite Deformation". Int. J. of Mechanical Sciences. vol.24. no:8. 1982. pp.459-468.

[32] - Rowe.C.W. "Elements of Metalworking Theory". Edward Arnold. (Publishers)Ltd. London. 1979. pp.78.

[33] - Kudo.H. "An Upper-Bound Approach to Plane-Strain Forging and Extrusion-I". Int. J. of Mechanical Sciences. vol.1. 1960. pp.57-83.

[34] - Bramley.A.N. "Computer Aided Forging Design". Annals of the CIRP. vol.36. 1987. pp.135-138.

[35] - McDermot.R.P and Bramley.A.N. "An Elemental Upper-Bound Technique for General use in Forging Analysis". Proc. of the 15th. Int. Conf. Machine Tool Design and Research. Birmingham. U.K. 1974.pp.437-443.

[36] - Cramphorn.A. and Bramley.A.N. "Computer Aided Forging Design with UBET". Proc. of 18th. Int. Conf. Machine Tool Design and Research. London.U.K. 1977. pp.717-724.

[37] - Osman.F.H and Bramley.A.N. "Metal Flow prediction in Forging and Extrusion using UBET". Proc. of the 20th. Int. Conf. Machine Tool Design and Research. Birmingham. U.K. 1979. pp.51-59.

[38] - Osman.F.H and Bramley.A.N. "Forging and Preform Design using UBET". Advanced Technology of Plasticity. Vol.I. 1984. pp.563-568.

[39] - Bramley.A.N. "Simulation of Forging Processes". Auto Tech 87. Congress and Exhibition. New Approach to Forging Technology. Birmingham. U.K. Dec.1987.

[40] - Oudin.J and Ravalard.Y. "A General Method for Computing Plane-Strain Plastic Flow". Proc. of the 20th. Int.Machine Tool Design and Research. Birmingham. U.K. 1979. pp.211-216.

[41] - Oudin.J and Ravalard.Y. "An Upper Bound Method for Computing Loads and Flow Patterns in Plane-Strain Forging". Int. J. of Machine Tool Design and Research. vol.21. no:3/4. 1981. pp.237-250.

[42] - Kiuchi.M and Murate.Y. "Simulation of Contact Pressure Distribution on Tool Surface by UBET". Proc. of the 20th. Int. Machine Tool Design and Research Conf. Swansea. U.K. 1980. pp.13-20.

[43] - Sabroff.A.M, Douglas.J.R, Badawy.A and Altan.T. "Application of CAD/CAM Techniques to Close Tolerance Forging of Spiral Bevel Gears". Annals of CIRP. vol.31/1. 1982. pp.141.

[44] - Sonmez.A.I. "Application of Computer Solutions to Slip-Line Field Problems of Metalworking Operations". Ph.D. Thesis. The University of Nottingham. 1979.

[45] - Meng.Z. "Calculating Force and Energy during Rotary Forging". Proc. 3rd. Int. Conf. on Rotary Metalworking Processes. Japan.Sept.1984. pp.115-124.

[46] - Oudin.J and Ravalard.Y. "Simulation of the Rotary Forging of Ring Shaped Billets with Plasticine".

Proc. 2nd. Int. Conf.on Rotary Metalworking Processes. U.K. Oct.1982. pp.125-133.

[47] - Oudin.J, Ravalard.Y, Verwaerde.G and Gelin.J.C. "Force, Torque and Plastic Flow Analysis in Rotary Forging Upsetting of Ring Shaped Billets". Int. J. Mechanical Sciences. vol.27. no:11/12. 1985. pp.761-780.

[48] - Chou.A and Labriola.M. "Rotary Forging- A Precision Process". J. of Mechanical Engineering. March.1985. pp.73-77.

[49] - Arnold.R.N. "Gyrodynamics and its Engineering Applications". Academic Press. 1961.

[50] - Synge.J.L. and Grifith.B.A. "Principles of Mechanics". McGraw Hill. 1959.

[51] - Spiegel.M.R. "Theory and Problems of Theoretical Mechanics". Schaum' Series. McGraw Hill. 1980.

[52] - GINO-F User's Manual (2.6). CADC. Cambridge.

[53] - Newman.W.M, Sprowll.R. "Principles of Interactive Computer Graphics". McGraw-Hill. 2nd.Edition. 1984. pp.335.

[54] - Mansour, S., Standring, P.M. "The Graphical Simulation

of Tool-Workpiece Kinematics and Deformation in Rotary Forging." Second National Conference of Production Research. Edinburgh. September.1986.pp. 386-405.

[55] - Foley.J.D., Van Dam.A. "Foundamentals of Interactive Computer Graphics." Addison-Wesley System Programming series. 1983.

[56] - Scott.J.E. " Introduction to Interactive Computer Graphics." John Wiley and Son. Inc. 1982.

[57] - Harrington.S. " Computer Graphics, a programming approach." Second Edition. McGraw-Hill Book Company. 1987.

[58] - Besant.C.B., Lui.C.W.K. " Computer-Aided Design and Manufacture." Ellis Horwood Series in Engineering Science. Third Edition. 1986.

[59] - BOXER Manual. PAFEC Ltd. Strelley Hall. Nottingham.

[60] - Zienkiewicz.O.C. " The Finite Element Method". Third Edition . McGraw-Hill Book Company. 1977.

[61] - Ghassemi.F. " Data Presentation for Finite Element Analysis." Ph.D. Thesis. University of London. 1978.

[62] - Barson.R.J. " Computer-Aided Mesh Generation for Finite Element Analysis". Ph.D. Thesis. University of Leicester. 1982.

[63] - Marciniak.Z." A Rocking-die Technique for Cold-Forming Operation". Machinery and Producting. November 1970.

[64] - Kubo.K., Hiraai.Y., Ogiso.s. and Ito.S. "Preliminary Work of Rotary Forging Processes with a Experimental Press". J. of Japan Society for Technology of Plasticity. Vol.14, no: 151. Aug. 1973. pp.648-655.

TABLES

Table 1 Rotary Forging Machine development.
(After Standring)

DESIGNER	COUNTRY	DATE	KINEMATIC TYPE						
			N	P	S	PN	NS	PS	NPS
Slick	U.S.A.	1906		*	*				
Slick	U.S.A.	1907			*				
Slick	U.S.A.	1907		*					
Slick	U.S.A.	1910			*				
Slick	U.S.A.	1911		*					
Brindley	U.K.	1914					(*)		
Slick	U.S.A.	1918						*	
Massey (H.F.)	U.K.	1928		*					
Silichev	U.S.S.R.	1962		*					
Silichev	U.S.S.R.	1962		*					
Silichev	U.S.S.R.	1964		*					
Sci & Res Inst of A'mobl Ind. Tech.	U.S.S.R.	1964			*				
Marciniak	Poland	1967	*	*		*			
Massey (B & S)	U.K.	1969		*					
UMIST	U.K.	1969			*			*	
Ulrych	W. Germany	1971		*					
Silichev	U.S.S.R.	1971		*					
Silichev	U.S.S.R.	1972		*					
Kubo	Japan	1972		*					
Kubo	Japan	1972		*					
Silichev	U.S.S.R.	1973	*						
Silichev	U.S.S.R.	1974	*						
Silichev	U.S.S.R.	1974		*					
Silichev	U.S.S.R.	1974	*						
UMIST	U.K.	1975		*					
Silichev	U.S.S.R.	1976	*						
Nottingham Uni	U.K.	1979		*					
Harbin I.T.	P.R.China	1979		*					
Wagner Dortmund	W.Germany	1980			*				
Aisin Seiki	Japan	1980		*					
Nitto Seiko	Japan	1980		*					
Kyodo	Japan	1980		*					
Shanghai Inst. of Res. Mach. Tool Bldg Tech	P.R China	1981			*				
City Uni	U.K.	1981			*				
Grzeskowiak	Poland	1981	*						
Dyna East	U.S.A.	1983			*				
Nottingham Uni	U.K.	1984					*		

N - Nutation, P - Precession, S - Spin

Table 2 Direction Cosine relation between two sets of axes

	X	Y	Z
x	$-\sin\phi\sin\psi + \cos\theta\cos\phi\cos\psi$	$\cos\phi\sin\psi + \cos\theta\sin\phi\cos\psi$	$-\sin\theta\cos\psi$
y	$-\sin\phi\cos\psi - \cos\theta\cos\phi\sin\psi$	$\cos\phi\cos\psi - \cos\theta\sin\phi\sin\psi$	$\sin\theta\sin\psi$
z	$\sin\theta\cos\phi$	$\sin\theta\sin\phi$	$\cos\theta$

Table 3. The calculated surface area, through FROGS, for various combinations of radial and circumferential lines.

$\pi = 3.141592$		
Number of radial lines	Number of circumferential lines	Calculate surface area of contact (Unit) ^{2}
180	40	3.140928
360	10	3.141453
360	20	3.141568
720	10	3.141738

Table 4. Instantaneous area of contact, expressed in terms of axial feed rate, for various Tool Geometry.

Cone Angle	Instantaneous Area of Contact in terms of Axial Feed Rate
45	$1.51 \quad (S)^{.600}$
30	$1.8302 \quad (S)^{.600}$
27.5	$1.9046 \quad (S)^{.605}$
25.	$2.00 \quad (S)^{.605}$
22.5	$2.0945 \quad (S)^{.605}$
20.	$2.2035 \quad (S)^{.610}$
17.5	$2.5308 \quad (S)^{.620}$
15.	$2.8020 \quad (S)^{.6204}$
12.5	$3.10590 \quad (S)^{.625}$
10	$3.666 \quad (S)^{.633}$
7.5	$4.400 \quad (S)^{.640}$
5.	$8.72 \quad (S)^{.660}$
2.5	$9.2310 \quad (S)^{.660}$

FIGURES

Fig. 1.1. Basic die-workpiece arrangement in rotary forging

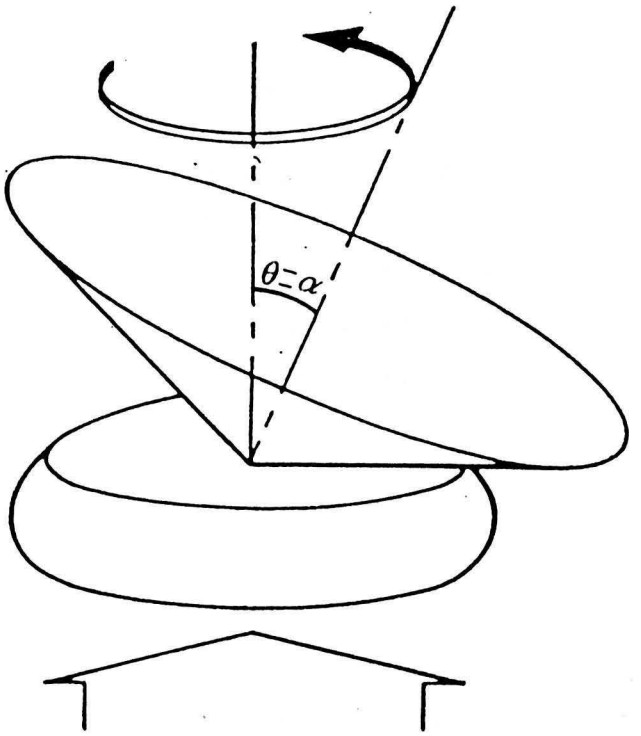

relationship between upper die & workpiece

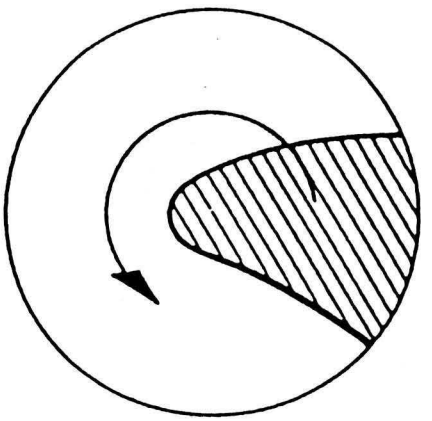

plan view of 'footprint' formed by contact between upper die & workpiece

Fig. 1.2. Illustration of tool/workpiece arrangement representing three Eulerian angles of:

1.2.a. Nutation

1.2.b. Precession

1.2.c. Spin

(The sequence of presentation is from right to left, top to bottom)

FIG. 1.2.a

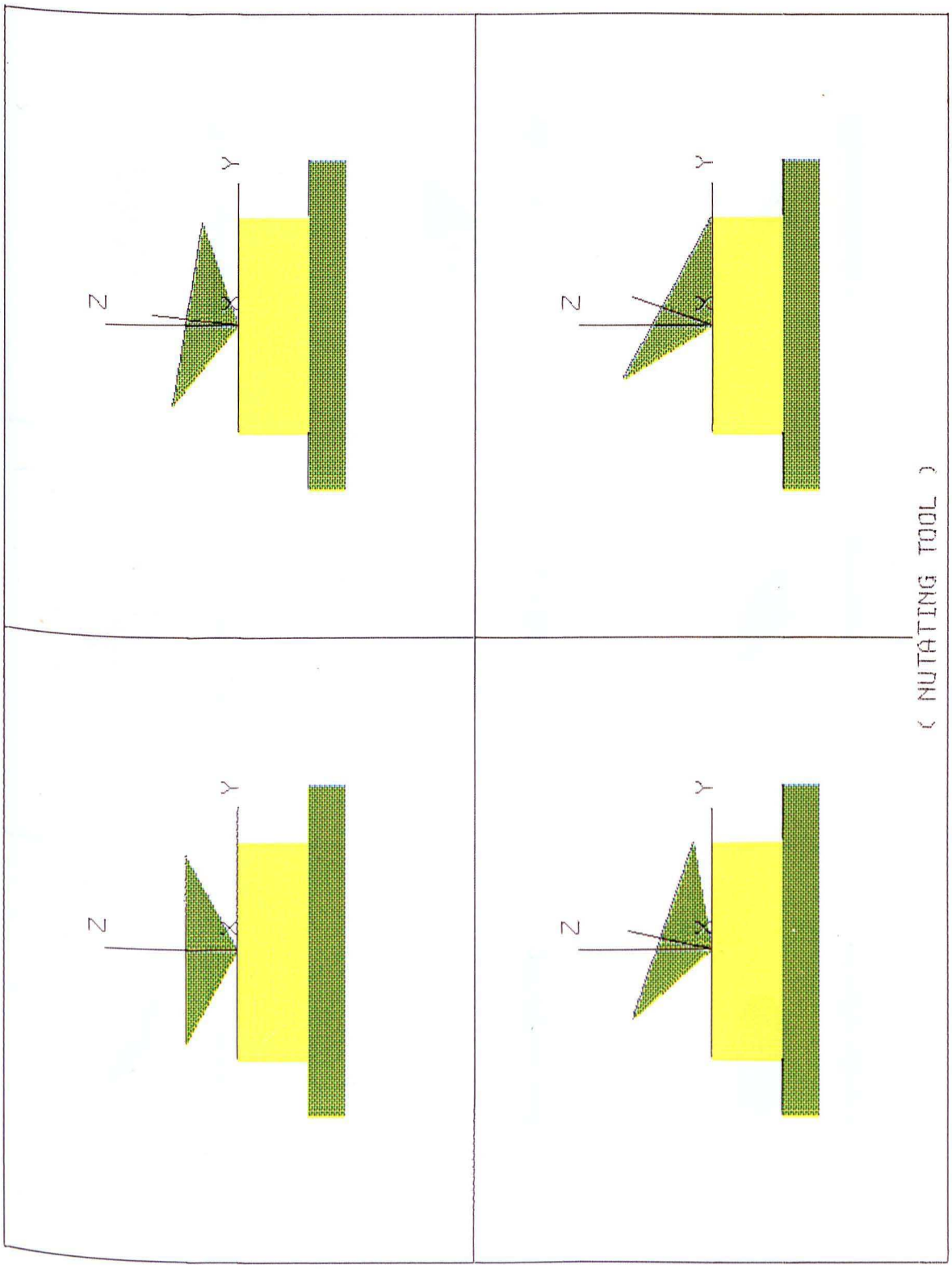

FIG. 1.2.b

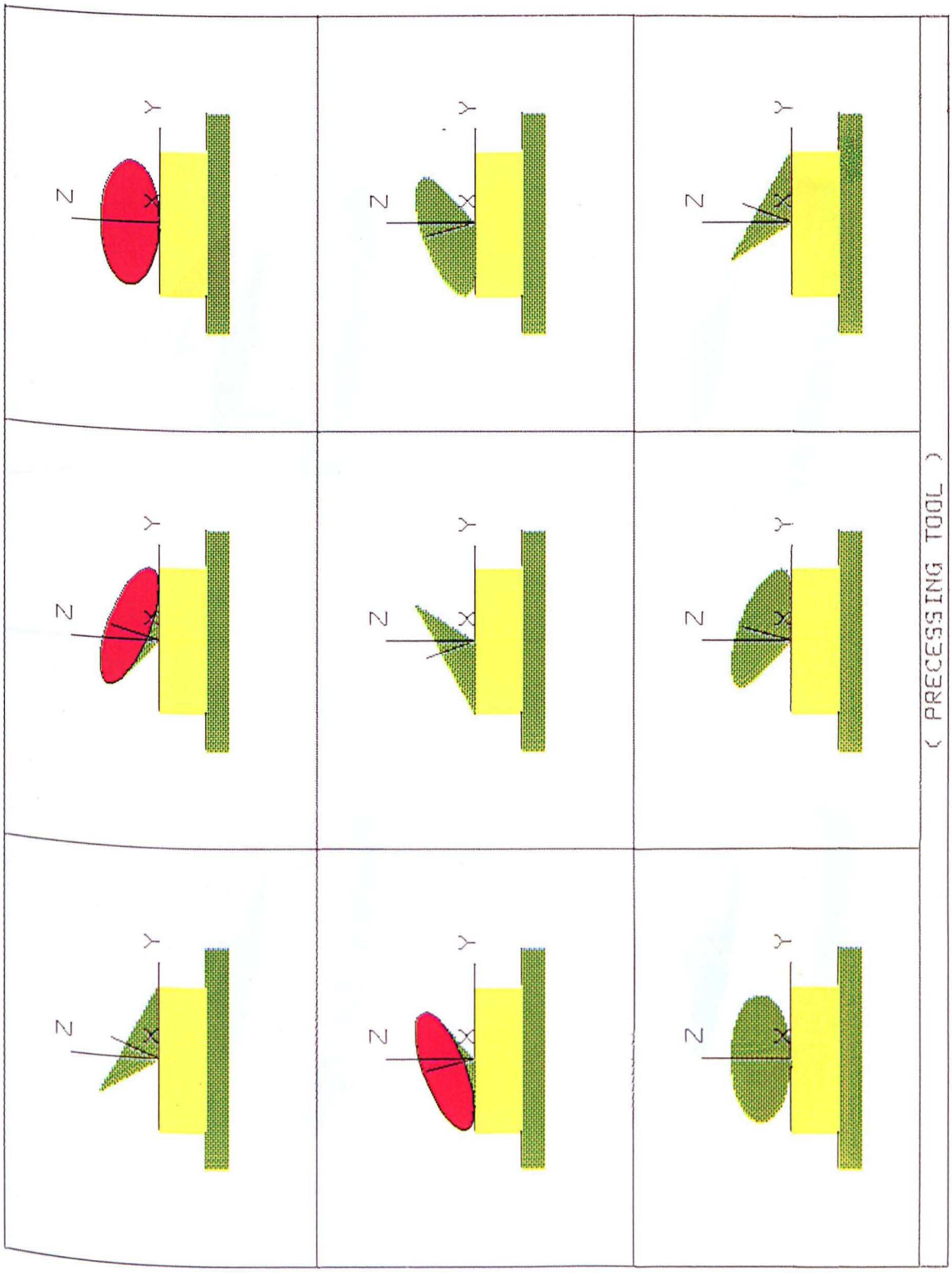

FIG.1.2.c

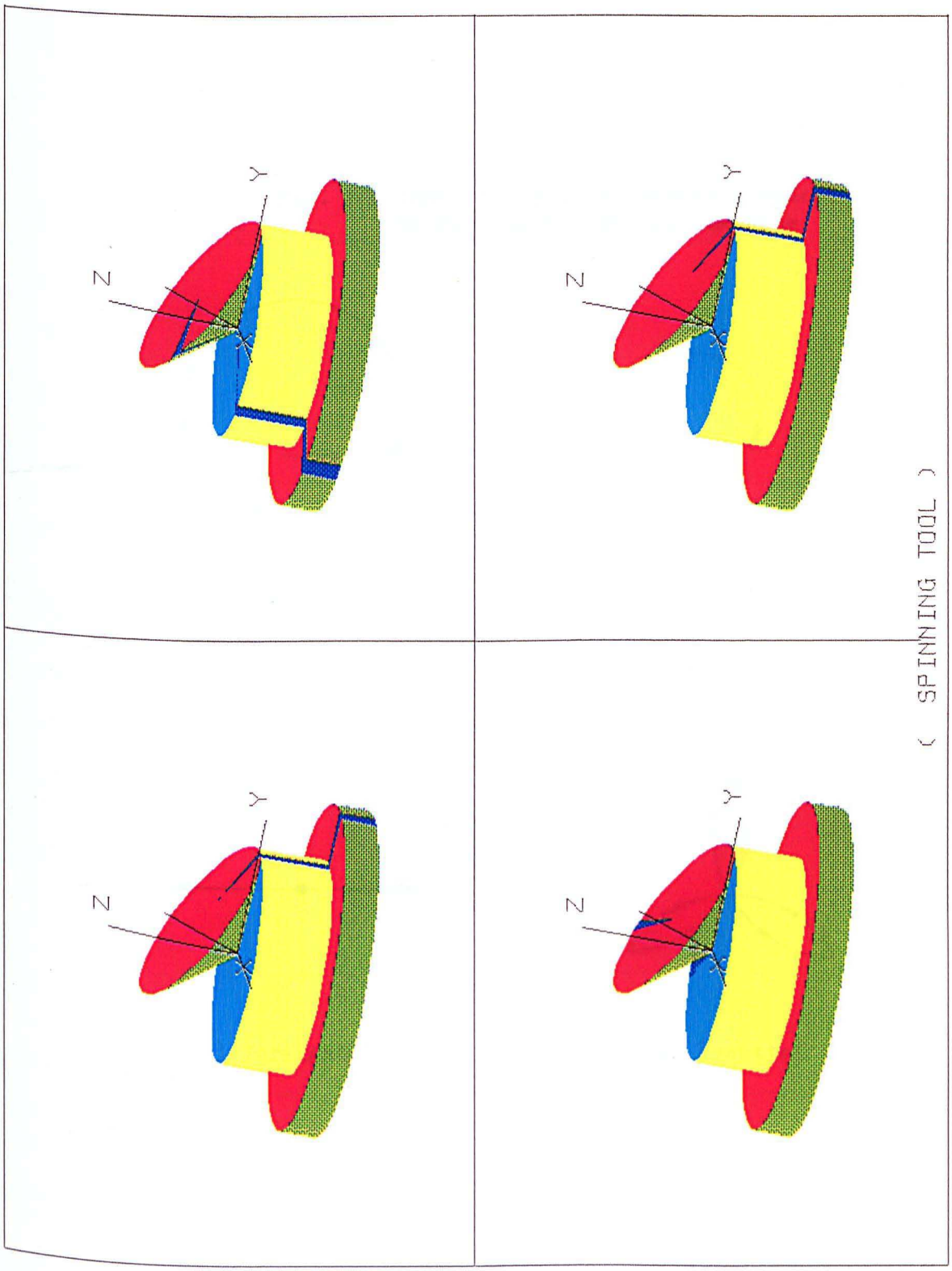

Fig. 1.3 Conic die axis movements produced by Marciniak's NP type machine

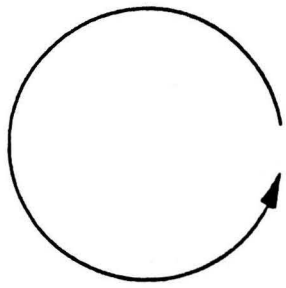

(a) Precession

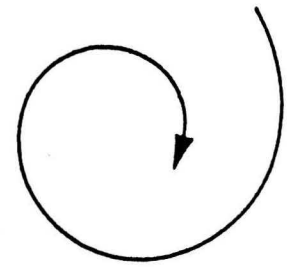

(b) Spiral

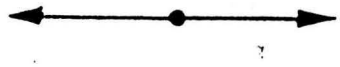

(c) Straight line

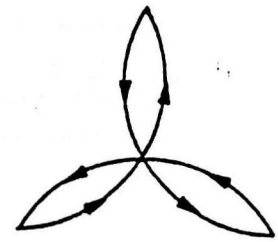

(d) Rosette

Fig. 3.1. The software development structure

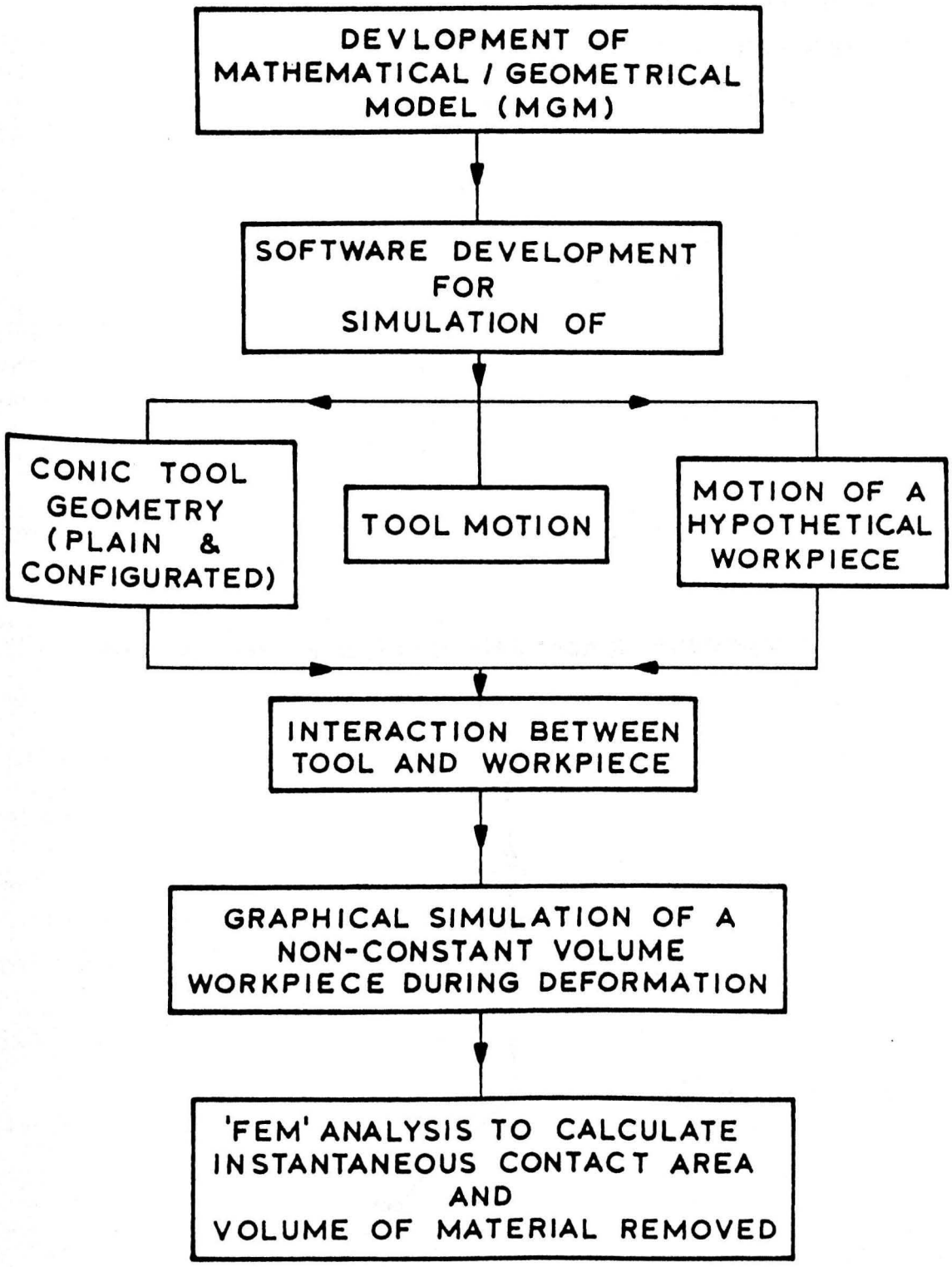

Fig. 3.2. The six degrees of freedom define the motion of a rigid body in space

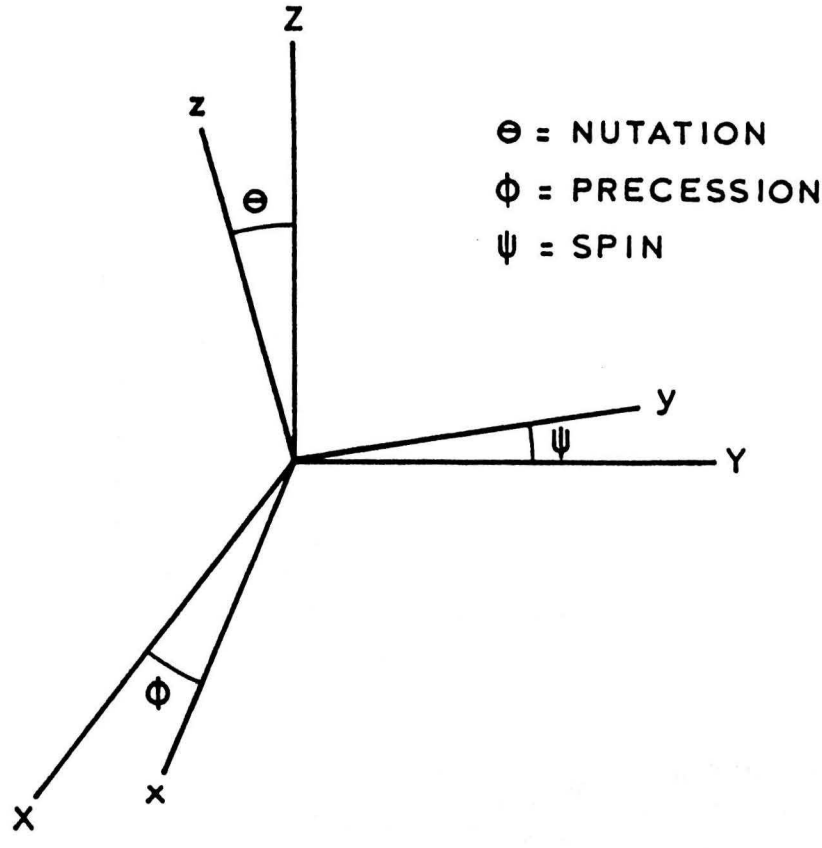

(a) Three rotational degrees of freedom

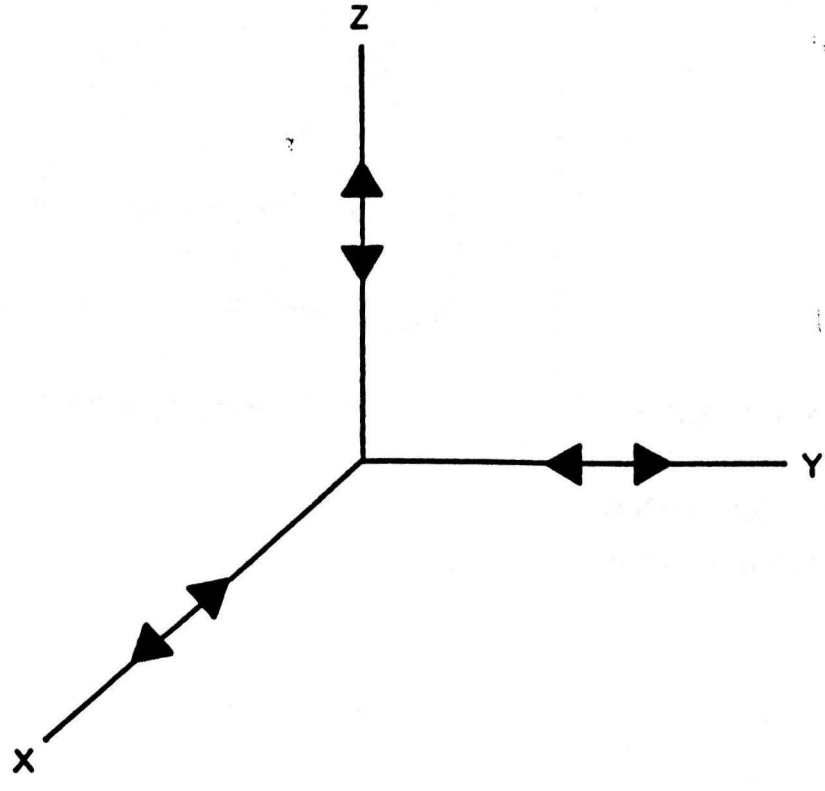

(b) Three transational degrees of freedom

Fig. 3.3. The movement of a rigid body due to rotation of the axis through the angles of nutation, precession and spin

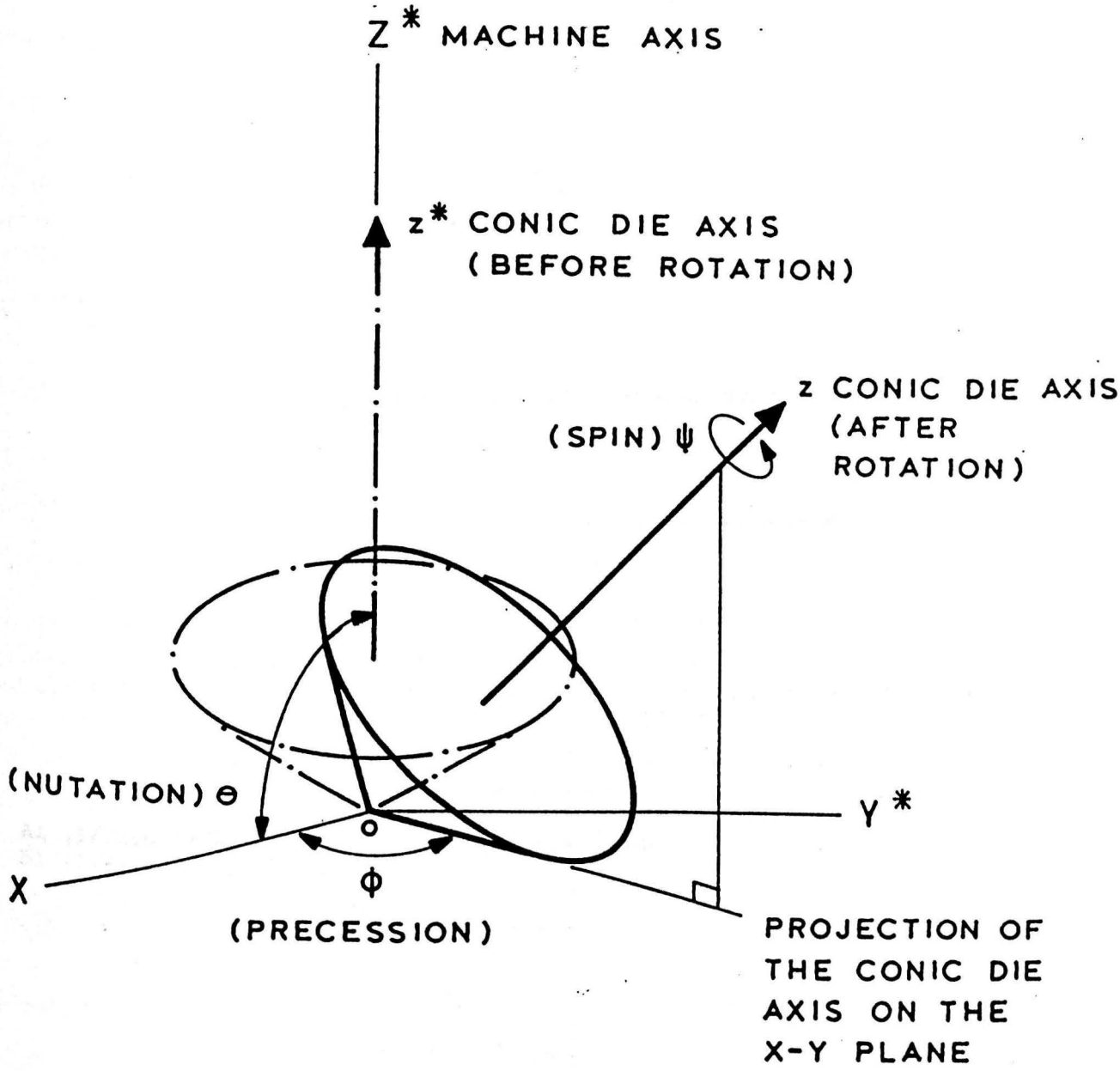

Fig. 3.4. Representation of two points on a solid cone

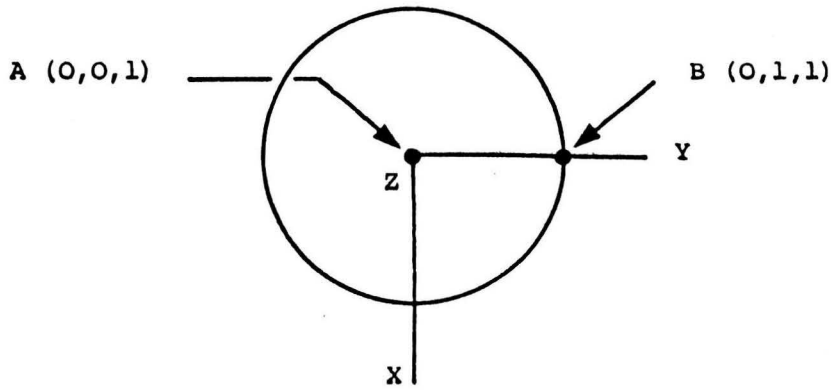

Plan View

Front Elevation

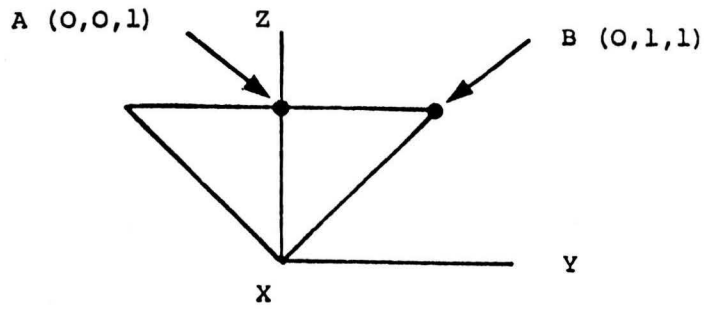

a. Before rotation of $\pi/4$ radians

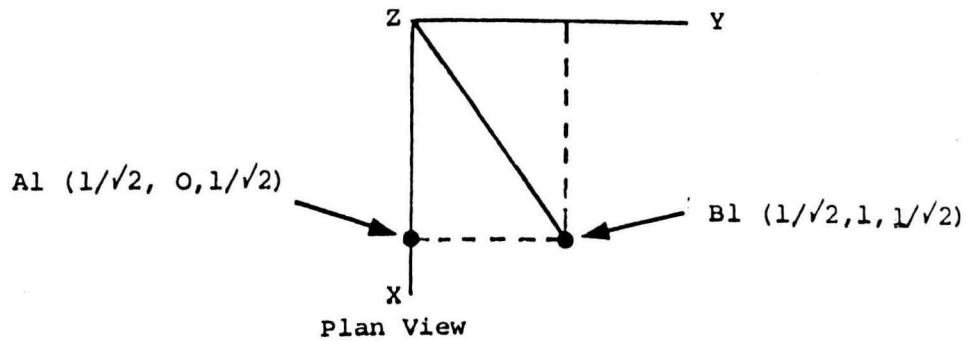

Plan View

Side Elevation

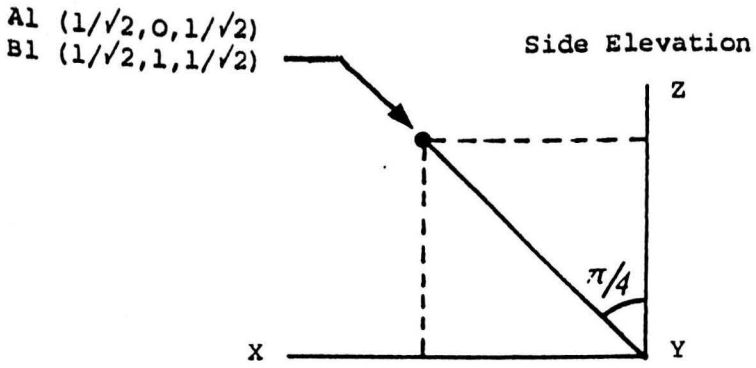

b. After rotation of $\pi/4$ radians

Fig. 4.1. The interrelated structure of FROGS

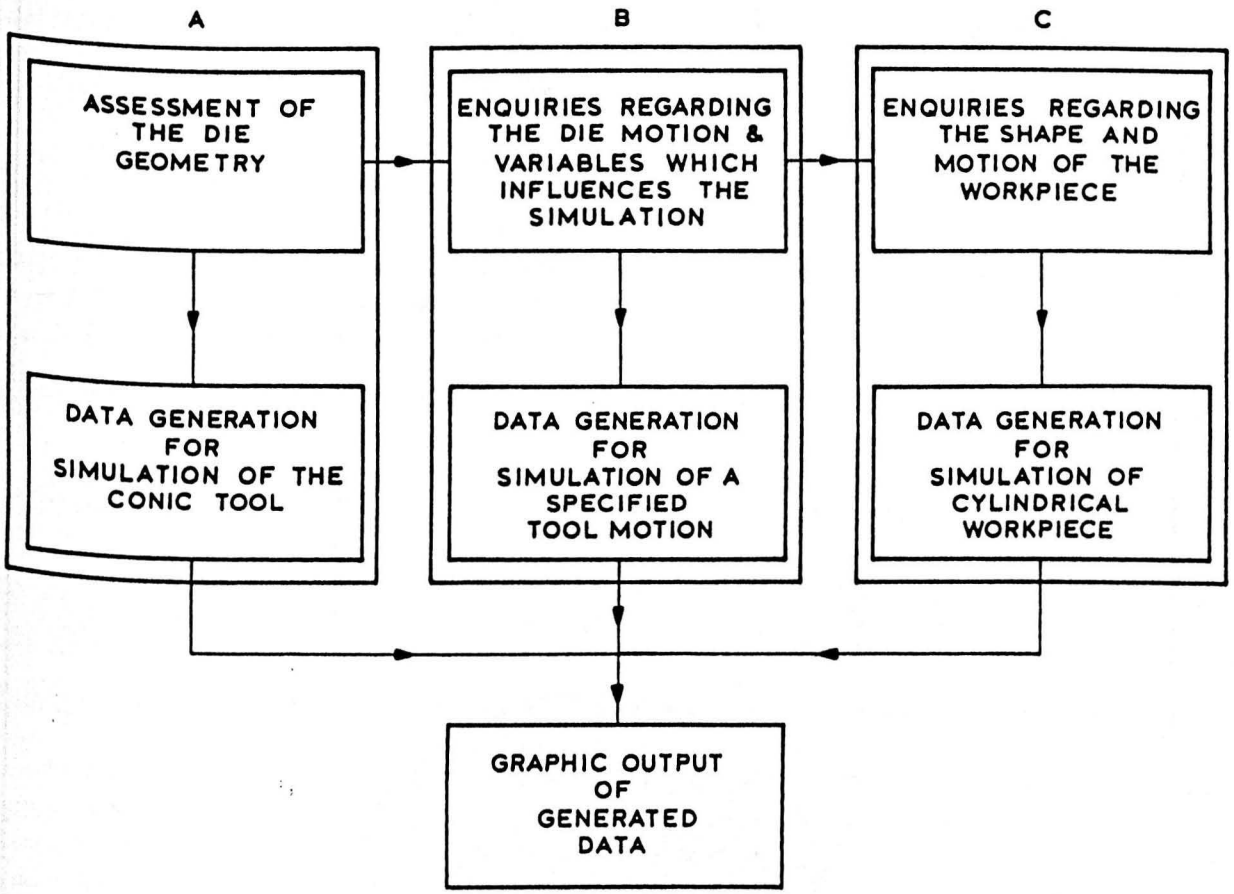

Fig. 4.2. A plain conic tool with zero angle of inclination
α = 30 (Deg), θ = 0

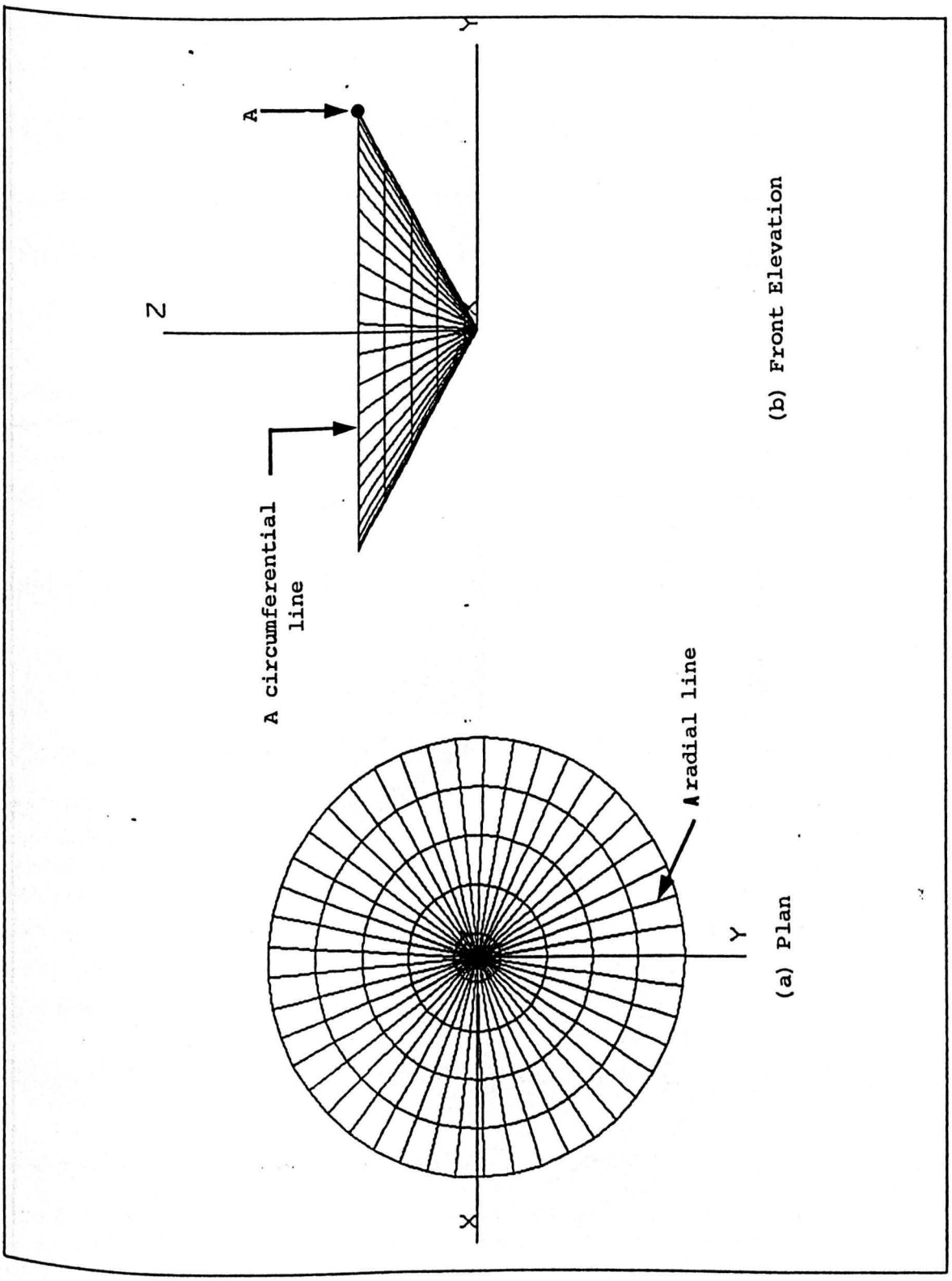

Fig. 4.3. A plain conic tool with vertical inclination equal to the cone angle $\theta = \alpha = 30$ (Deg)

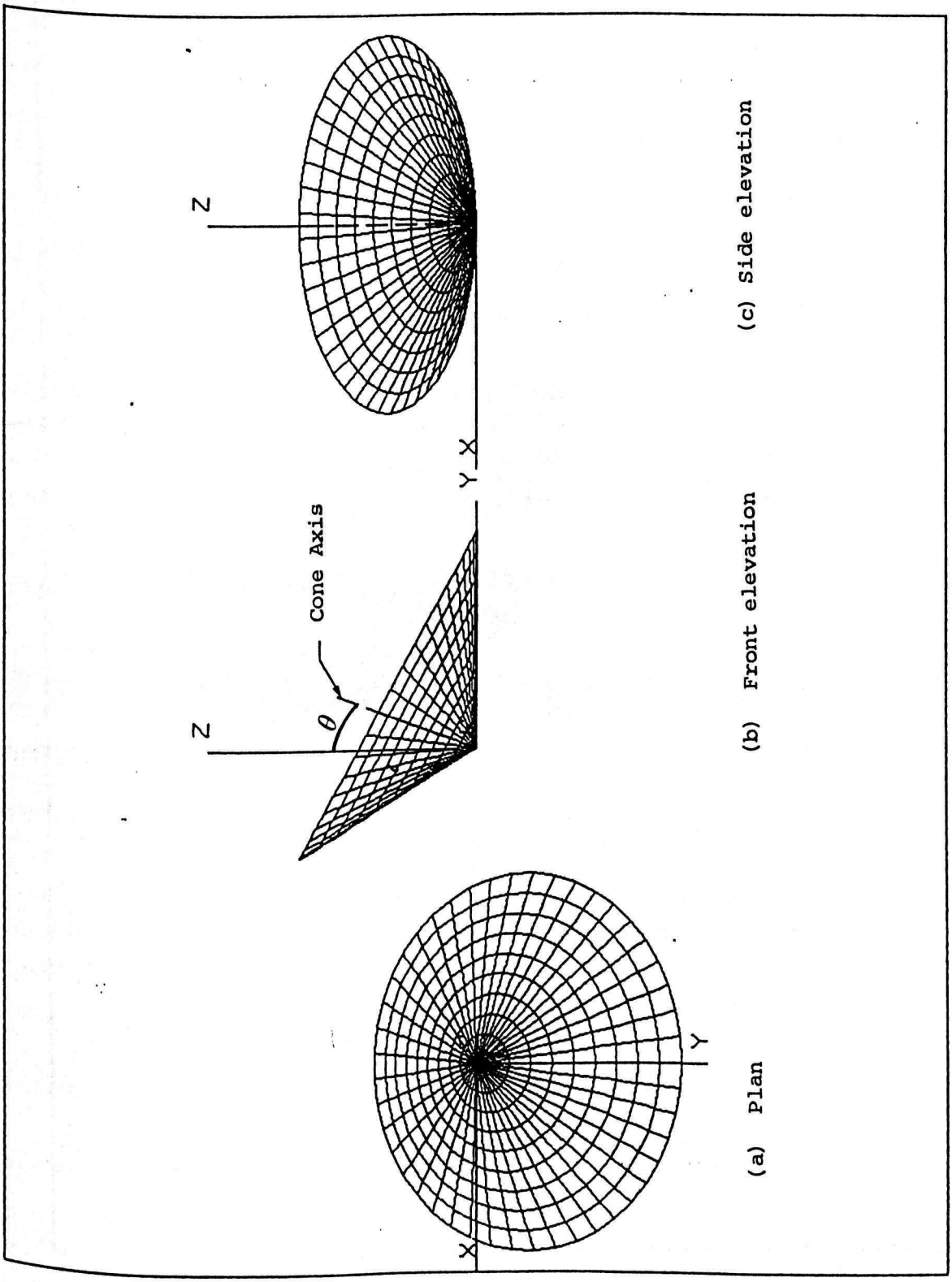

Fig. 4.4. An isometric view of an inclined conic tool (wire-frame representation)
$\theta = \alpha = 30$ (Deg)

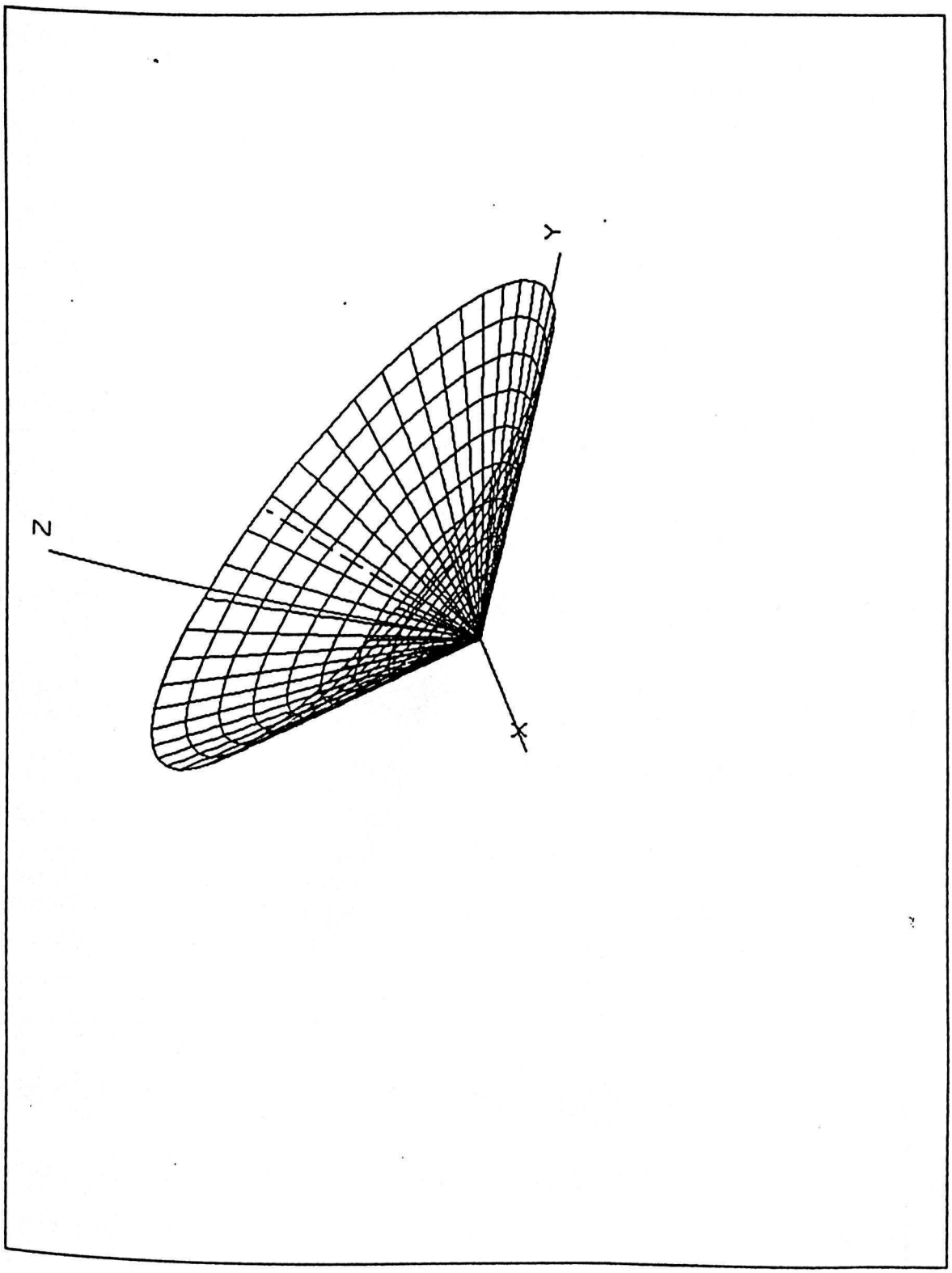

Fig. 4.5. An isometric view of an inclined plain conic tool (wire-frame representation) $\theta = \alpha = 10$ (Deg)

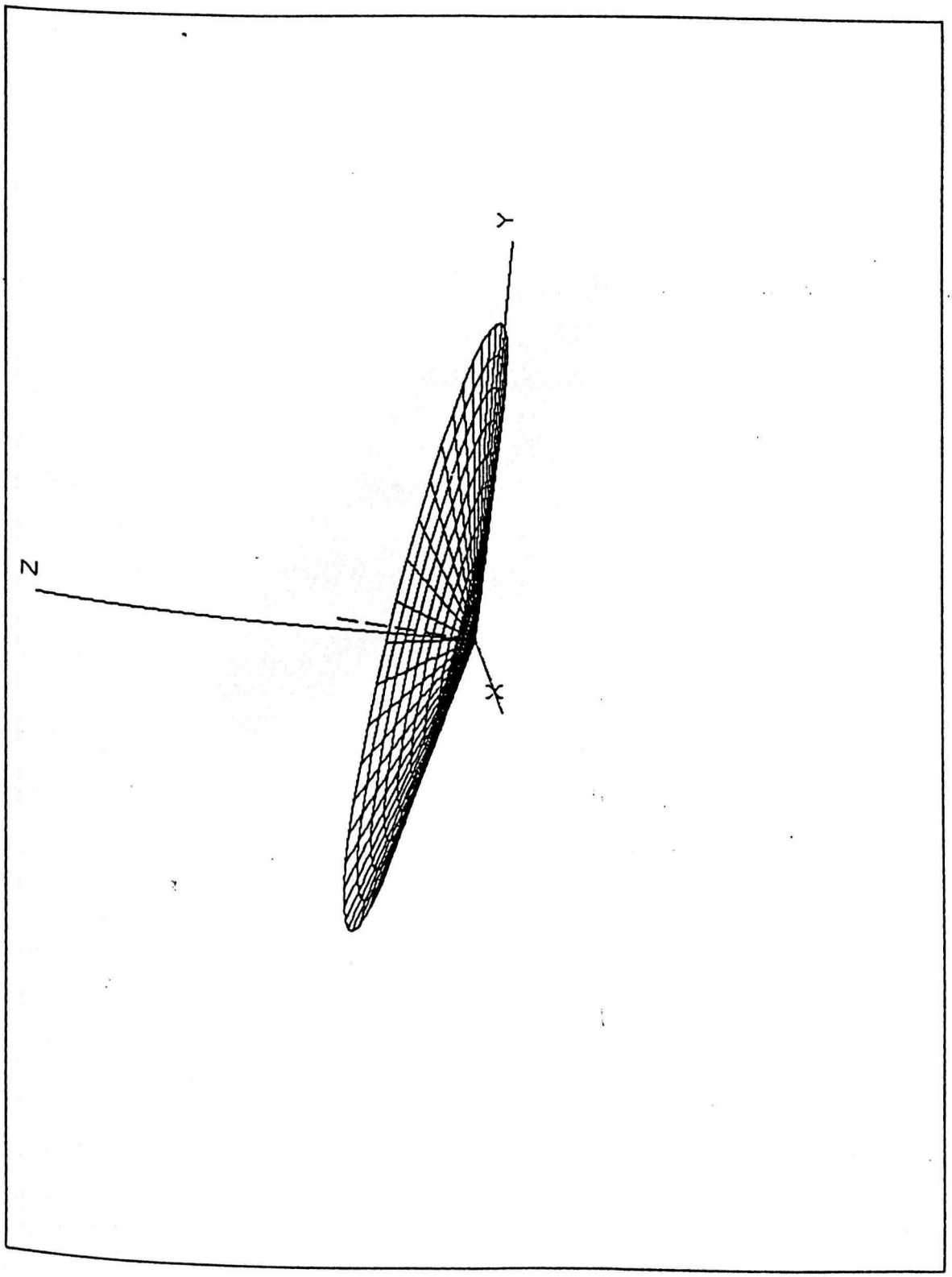

Fig. 4.6. Isometric view of an inclined conic tool (solid representation)
$\theta = \alpha = 30$ (Deg)

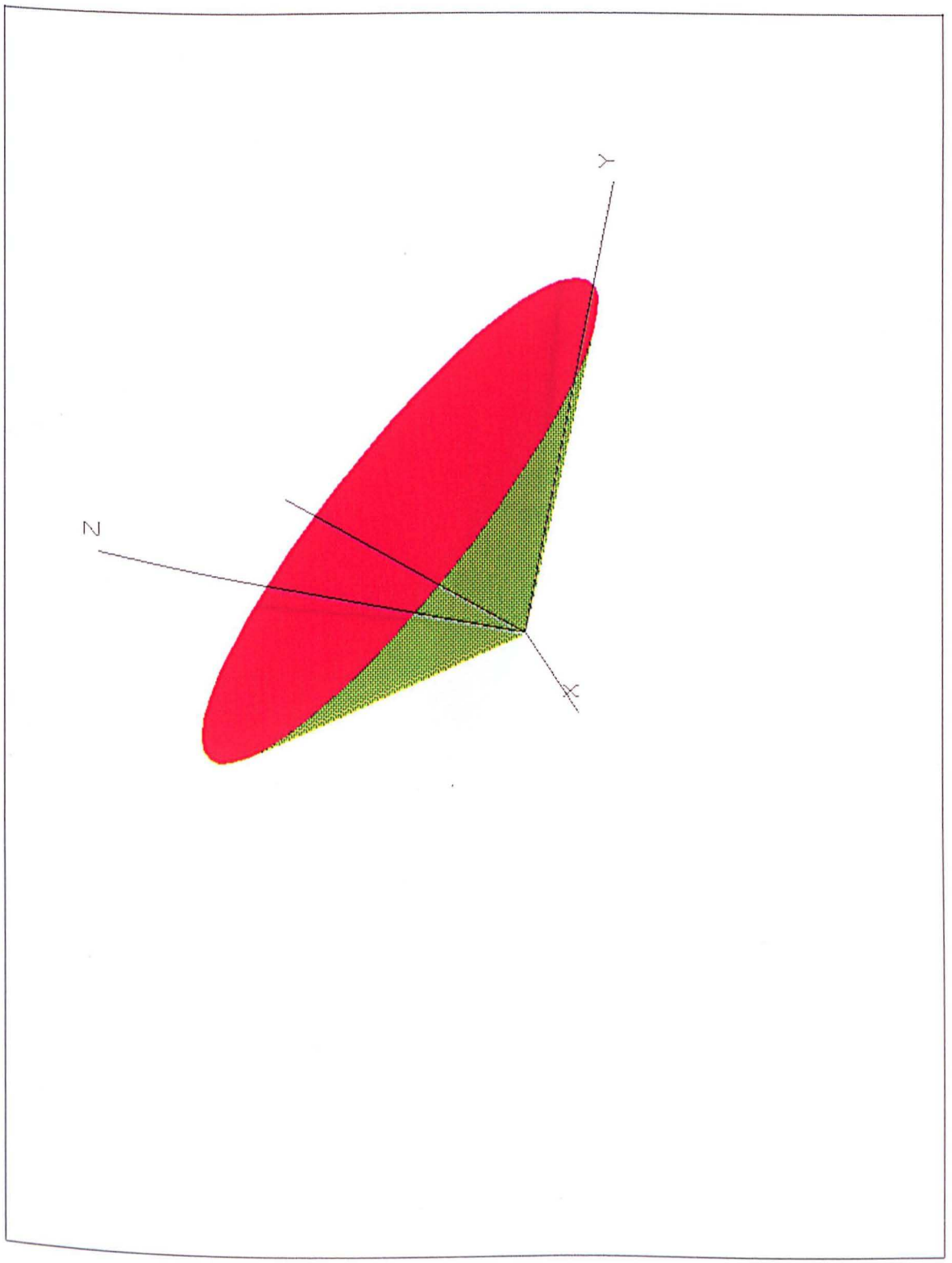

Fig. 4.7. Isometric view of an inclined conic tool (solid representation)
$\theta = \alpha = 10$ (Deg)

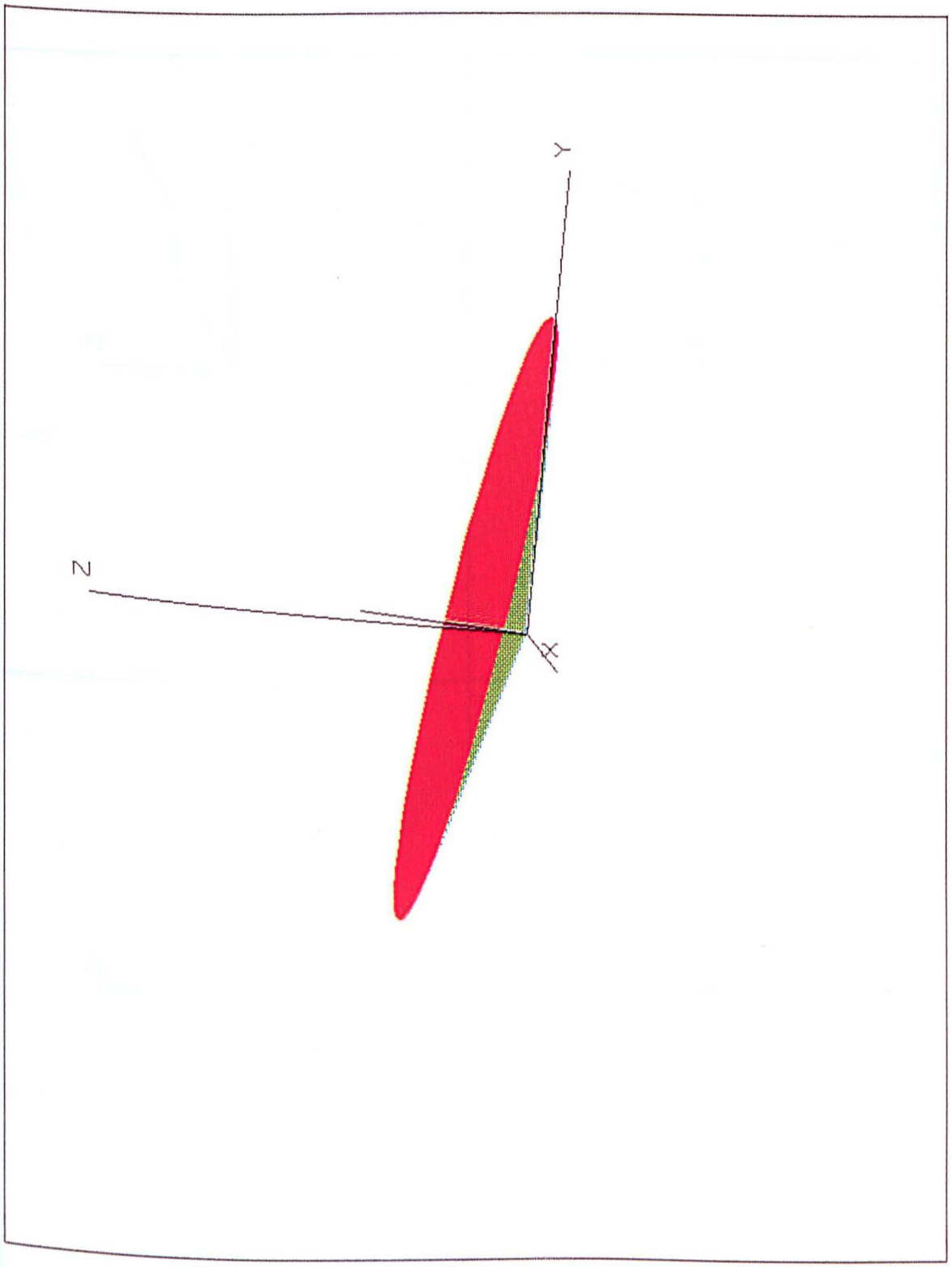

Fig. 4.8. Four simple tool configurations generated using FROGS

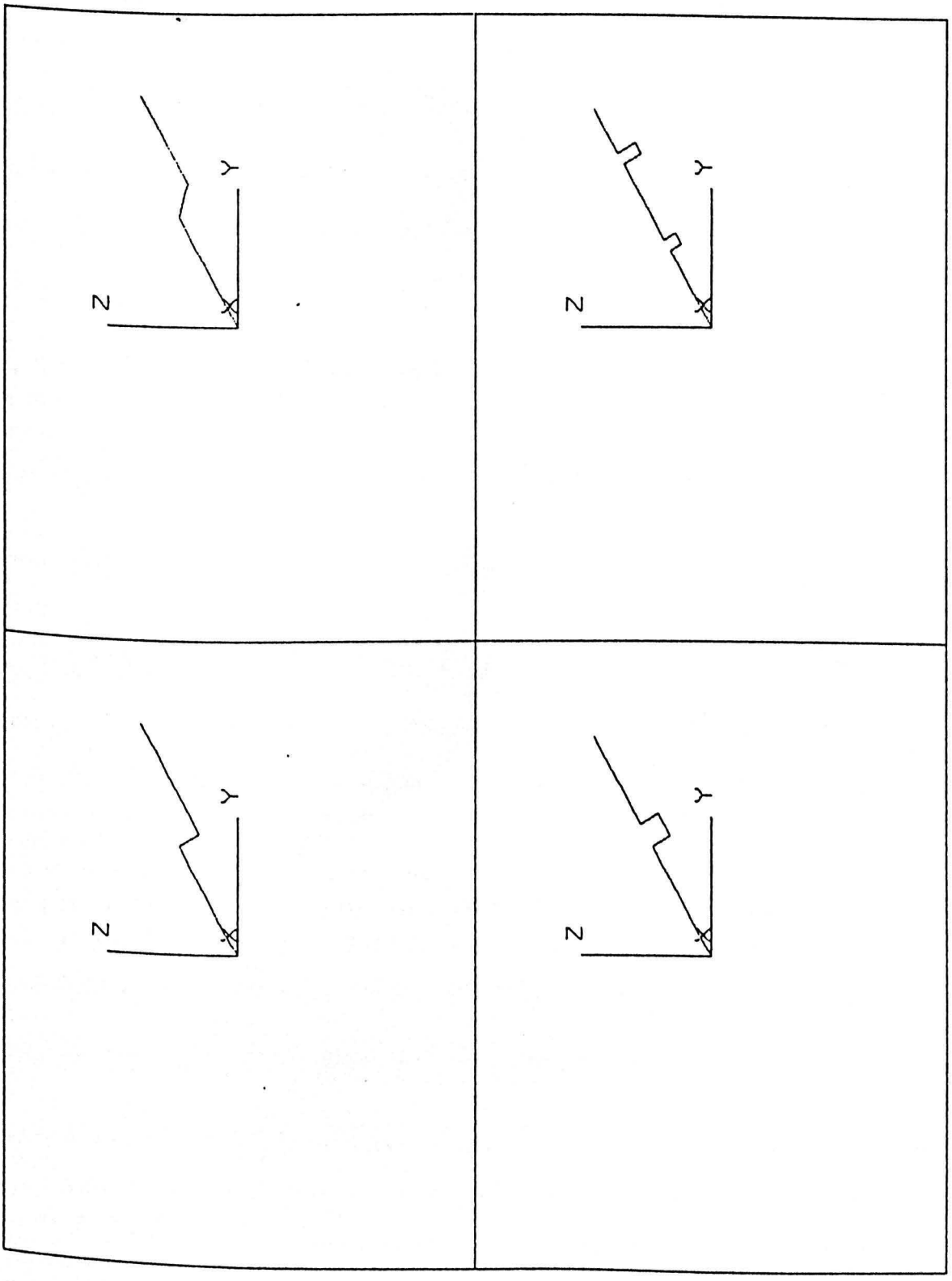

Fig. 4.9. Three orthogonal views of a radially configurated conic tool

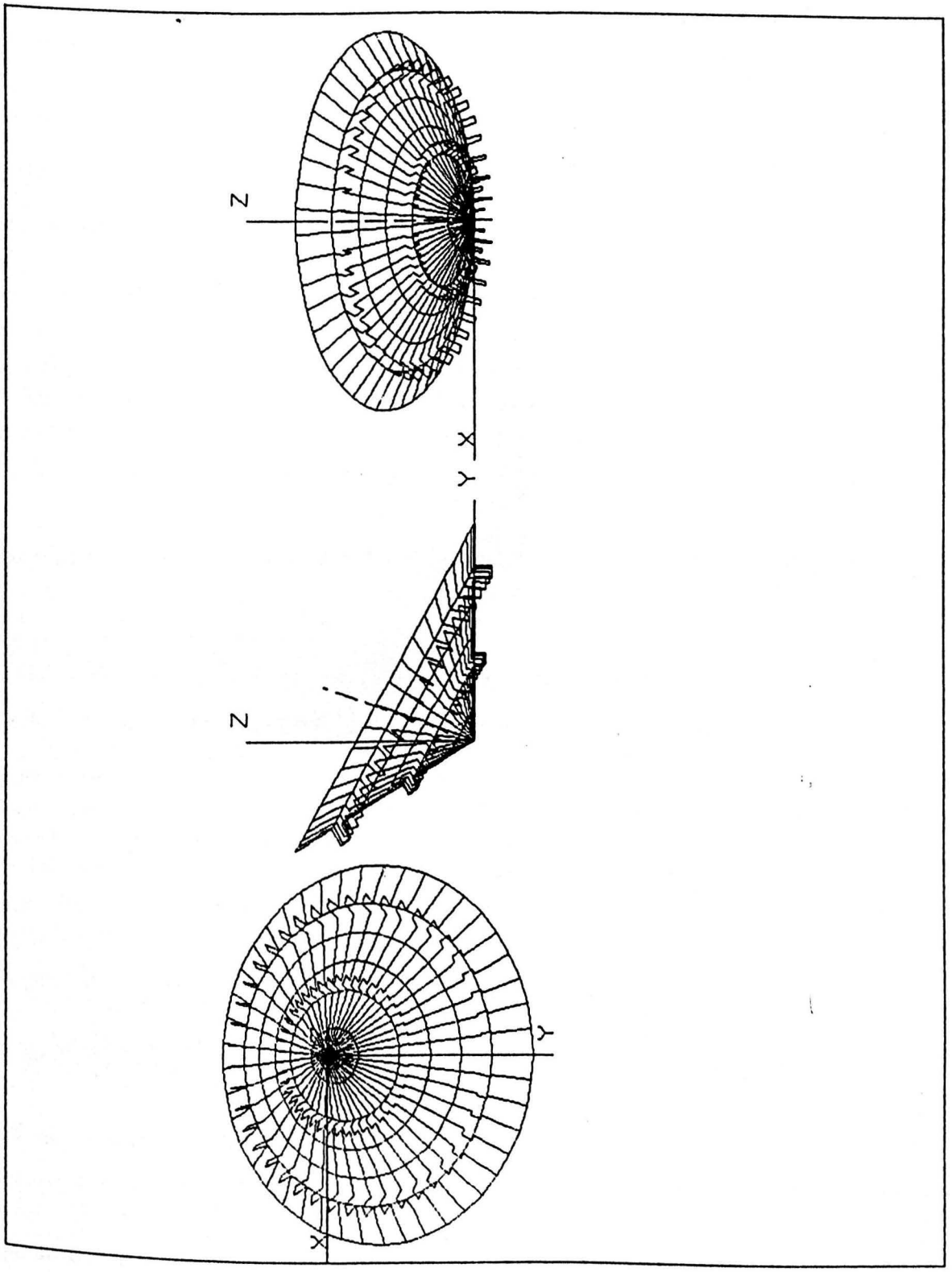

Fig. 4.10. An isometric view of a radially configurated conic tool

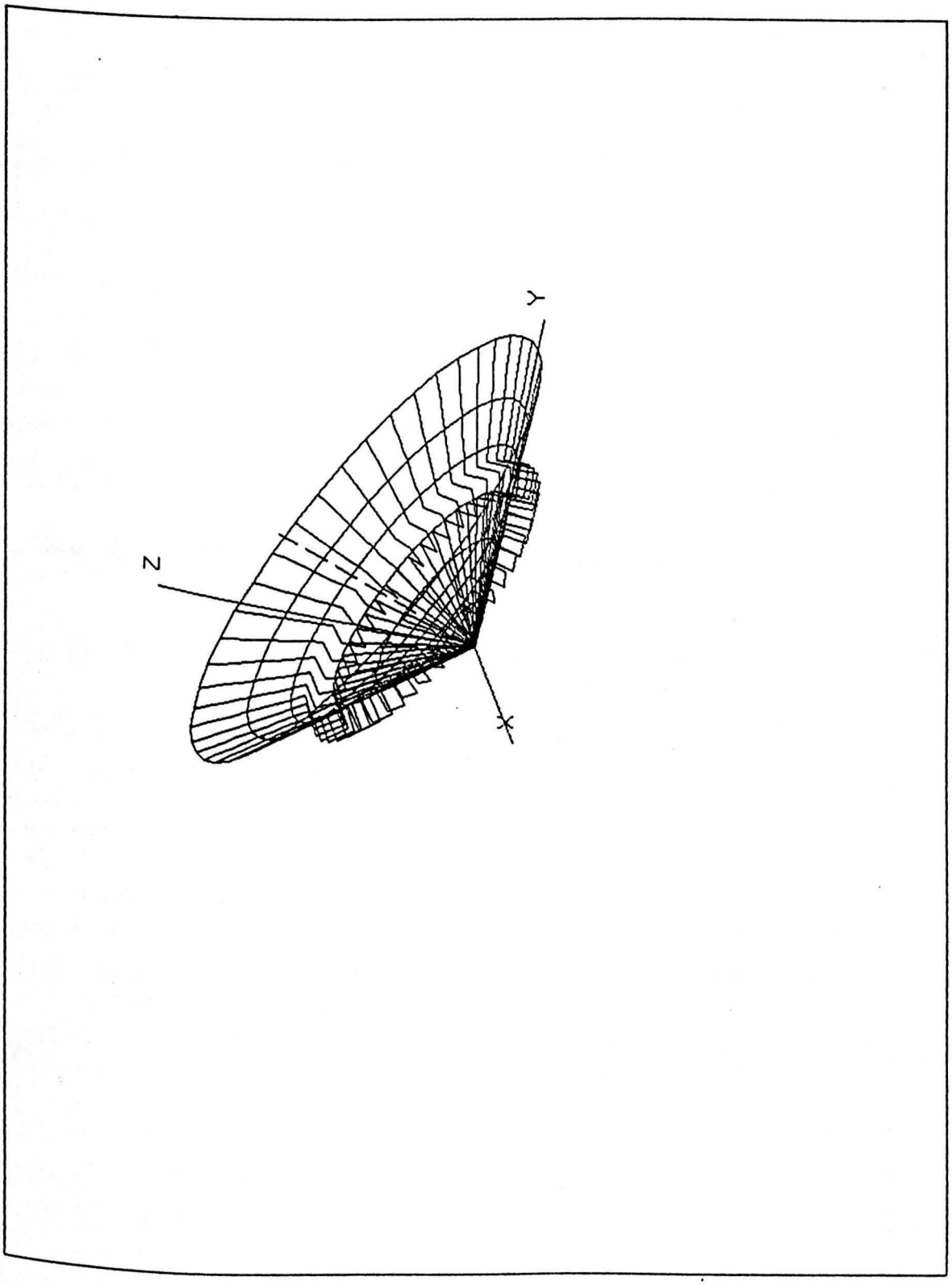

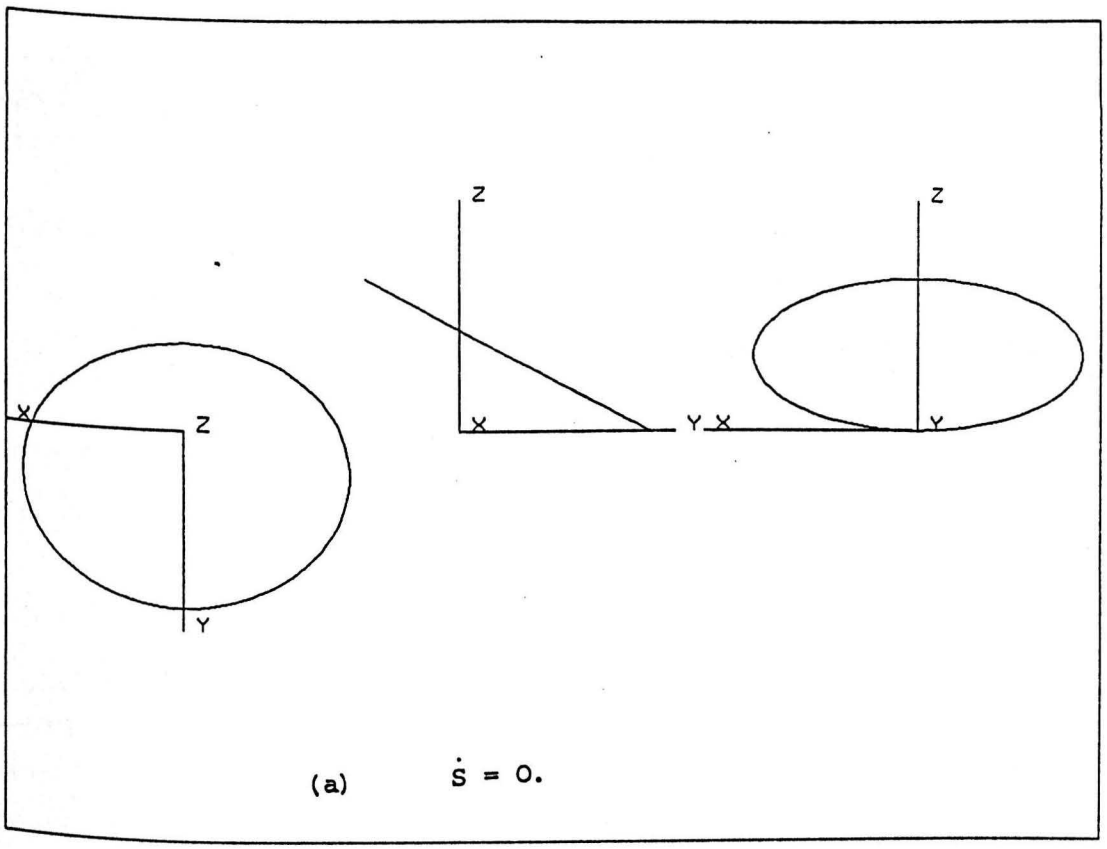

(a) $\dot{S} = 0.$

Fig. 4.11. The locus of a point on a Conic Tool

Tool motion: Spin

$\theta = \alpha = 30$ (Deg)

$\dot{\theta} = 0,\ \dot{\phi} = 0,\ \dot{\psi} = 360$ (Deg/sec).

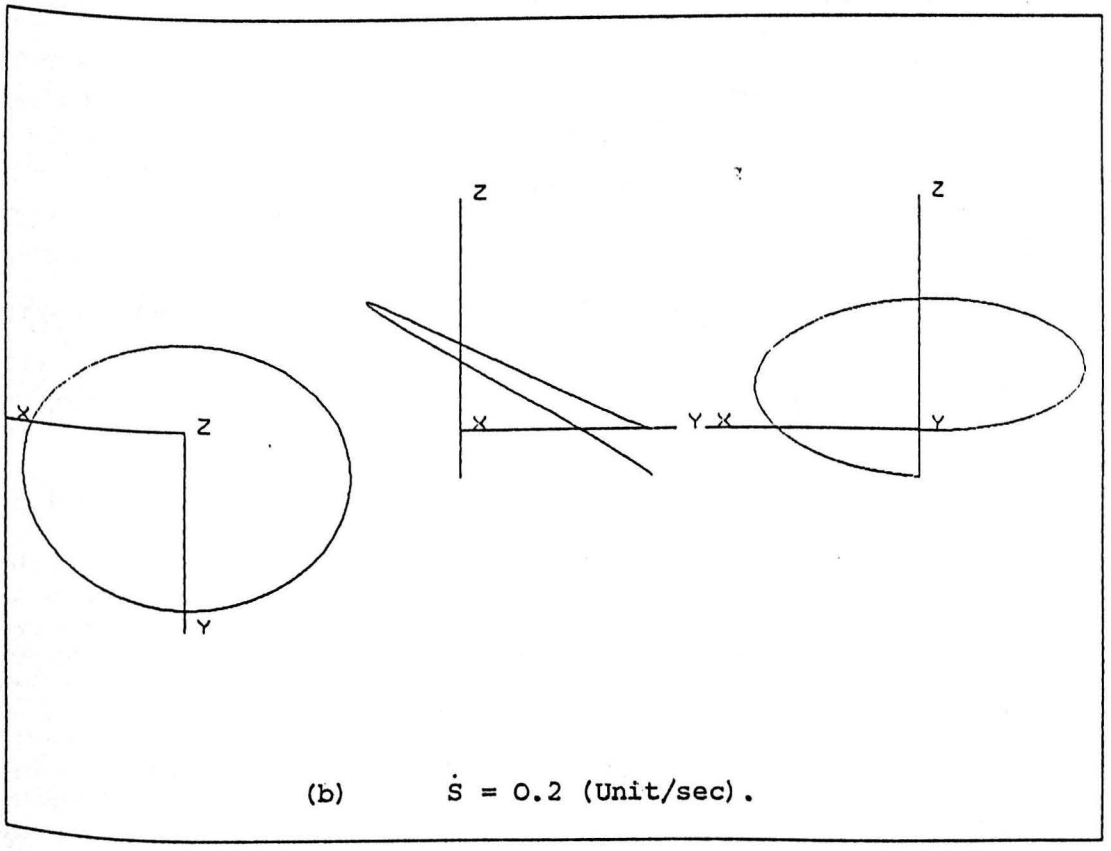

(b) $\dot{S} = 0.2$ (Unit/sec).

Fig. 4.12. Tool/workpiece arrangement in a precession type machine

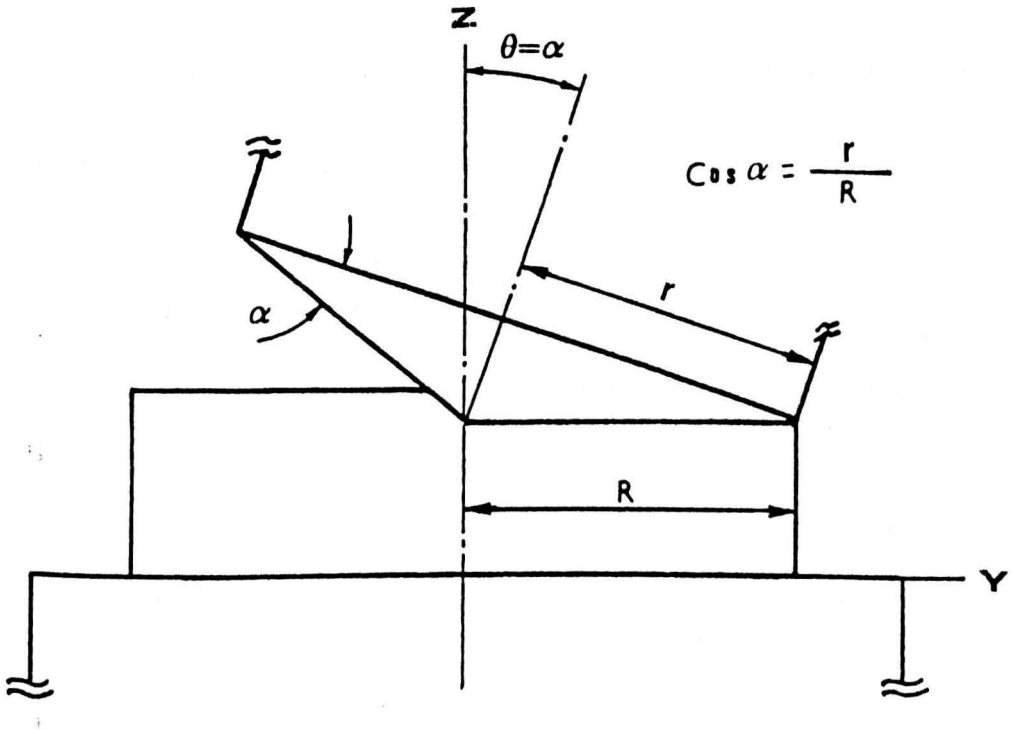

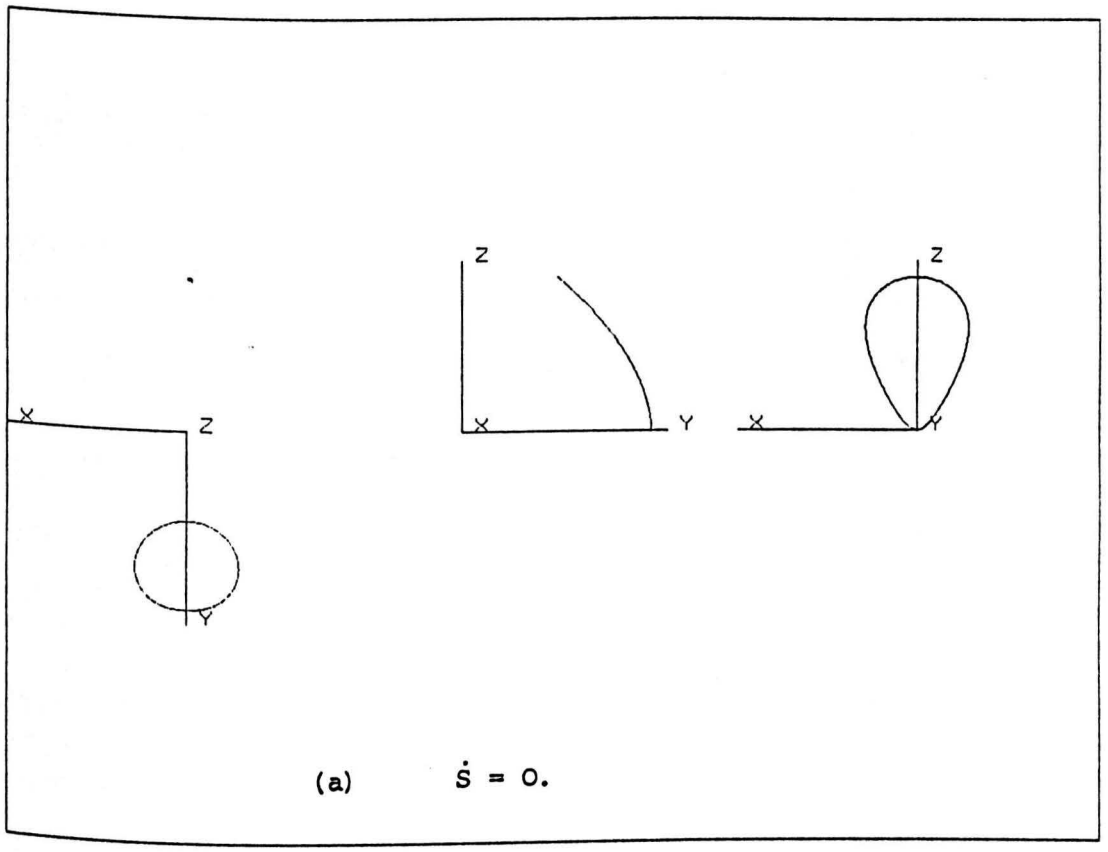

(a) $\dot{S} = 0.$

Fig. 4.13. The locus of a point on a Conic Tool

Tool motion: Precession

$\theta = \alpha = 30$ (Deg)

$\dot{\theta} = 0$, $\dot{\phi} = 360$ (Deg/sec), $\dot{\psi} = 0.$

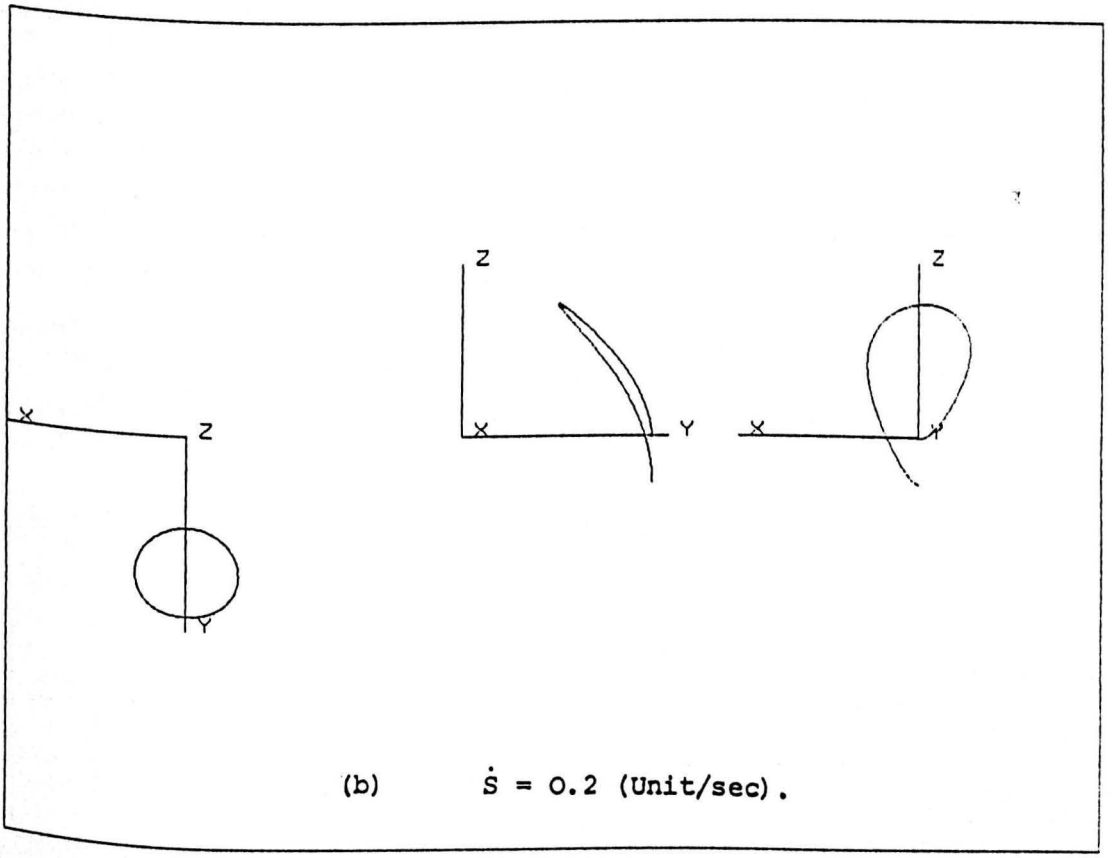

(b) $\dot{S} = 0.2$ (Unit/sec).

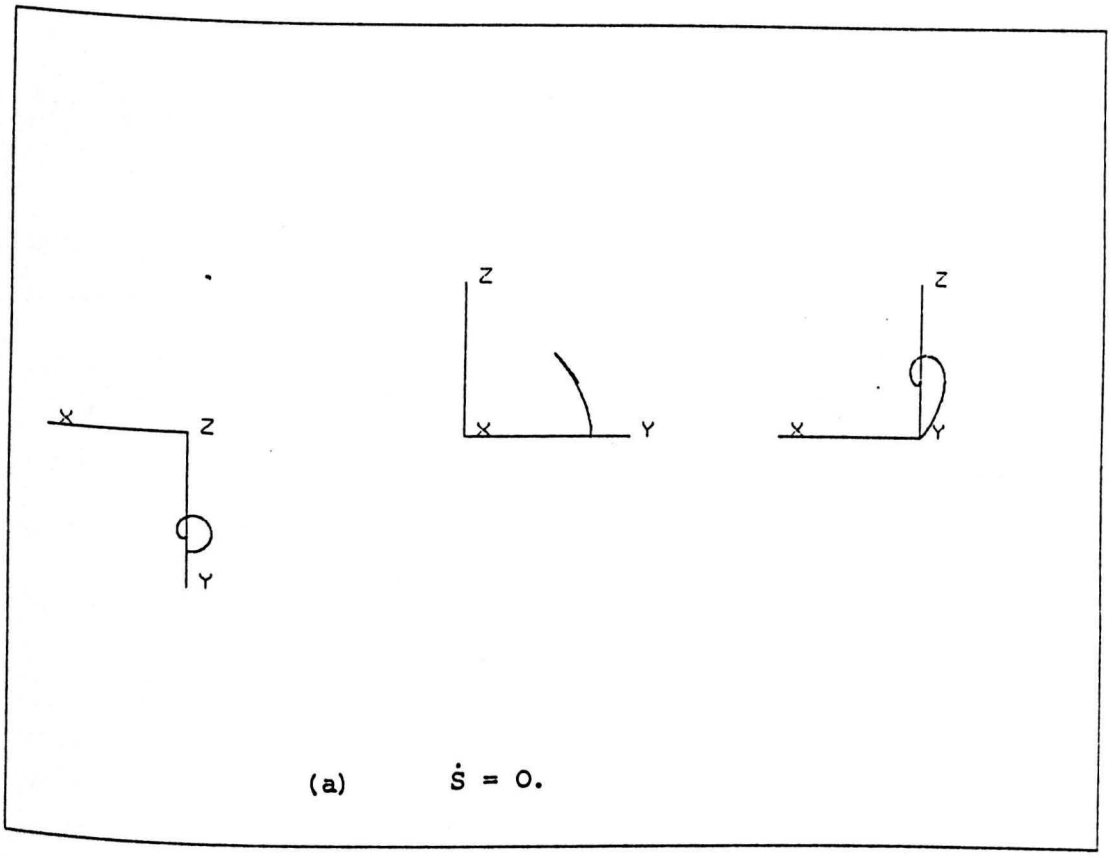

(a) $\dot{S} = 0.$

Fig. 4.14. The locus of a point on a Conic Tool
Tool motion: Nutation - Precession
$\alpha = 30$ (Deg), $\theta = 0.$
$\dot{\theta} = 30$ (Deg/sec), $\dot{\phi} = 360$ (Deg/sec), $\dot{\psi} = 0.$

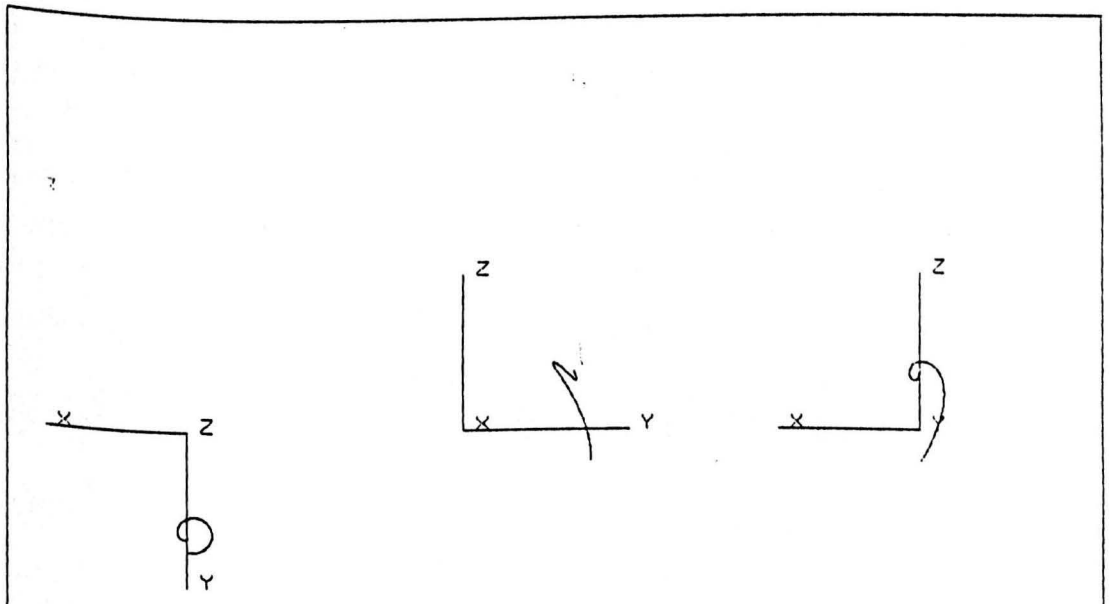

(b) $\dot{S} = 0.2$ (Unit/sec).

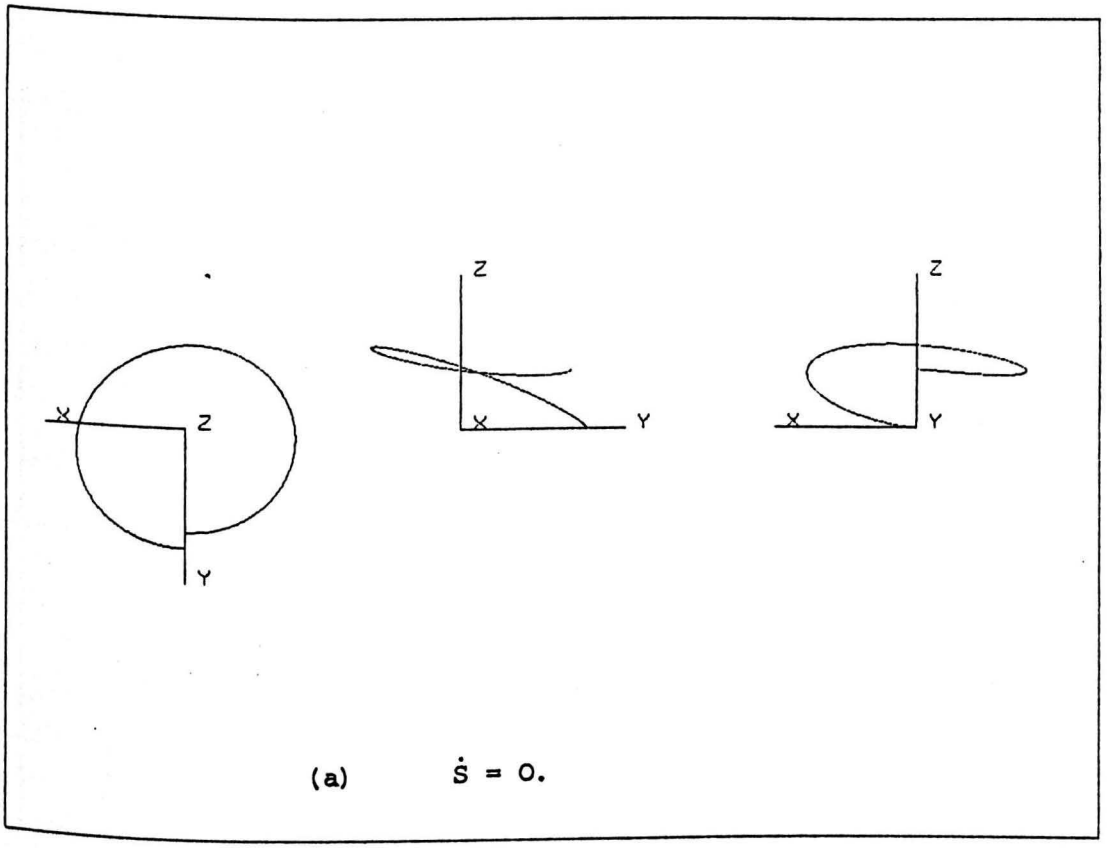

(a) $\dot{S} = 0.$

Fig. 4.15. The locus of a point on a Conic Tool
Tool motion: Nutation - Spin
$\alpha = 30$ (Deg), $\theta = 0$
$\dot{\theta} = 30$ (Deg/sec), $\dot{\phi} = 0$, $\dot{\psi} = 360$ (Deg/sec).

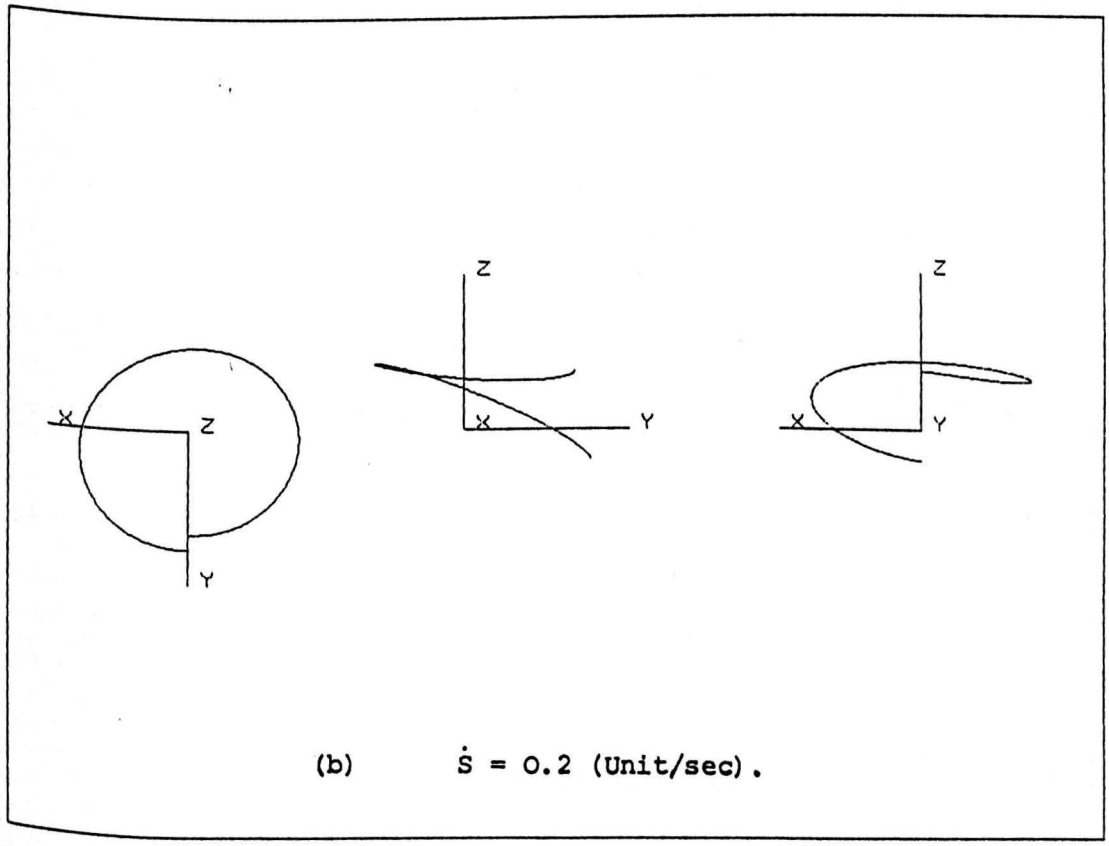

(b) $\dot{S} = 0.2$ (Unit/sec).

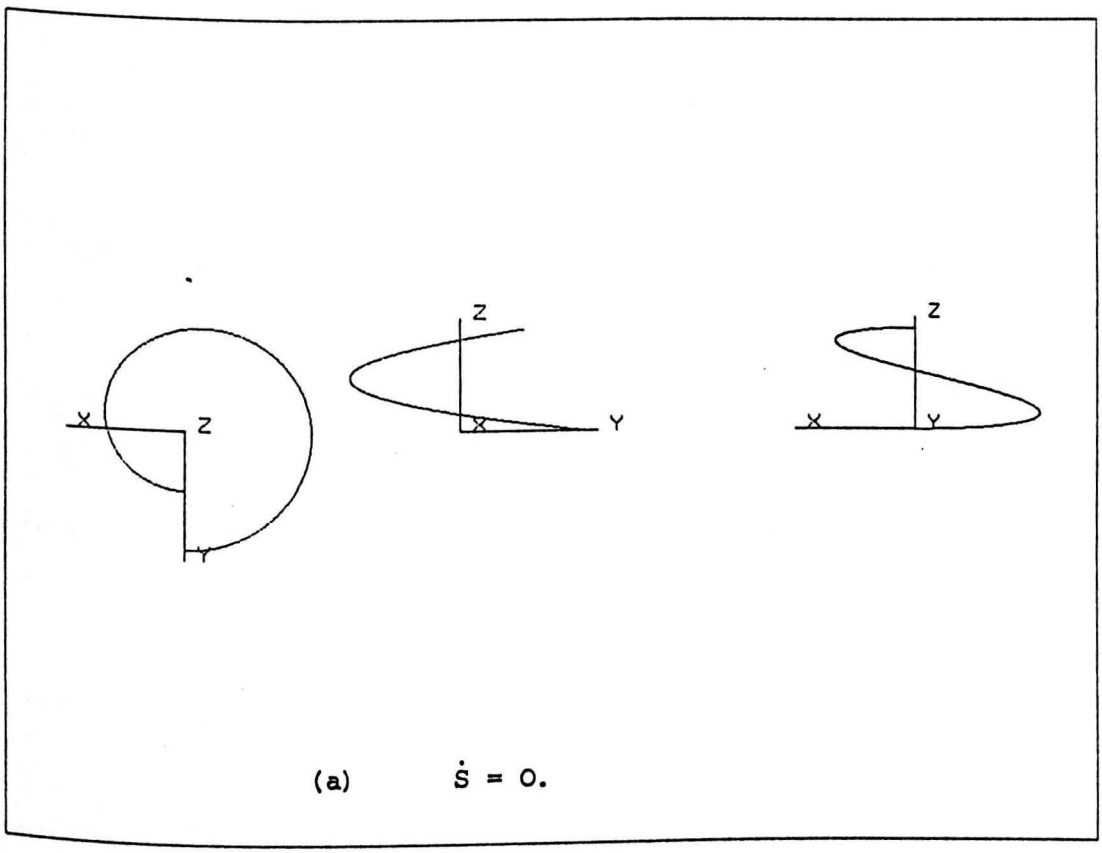

(a) $\dot{S} = 0.$

Fig. 4.16. The locus of a point on a Conic Tool

Tool motion: Precession - Spin

$\theta = \alpha = 30$ (Deg)

$\dot{\theta} = 0, \dot{\phi} = 180$ (Deg/sec), $\dot{\psi} = 360$ (Deg/sec).

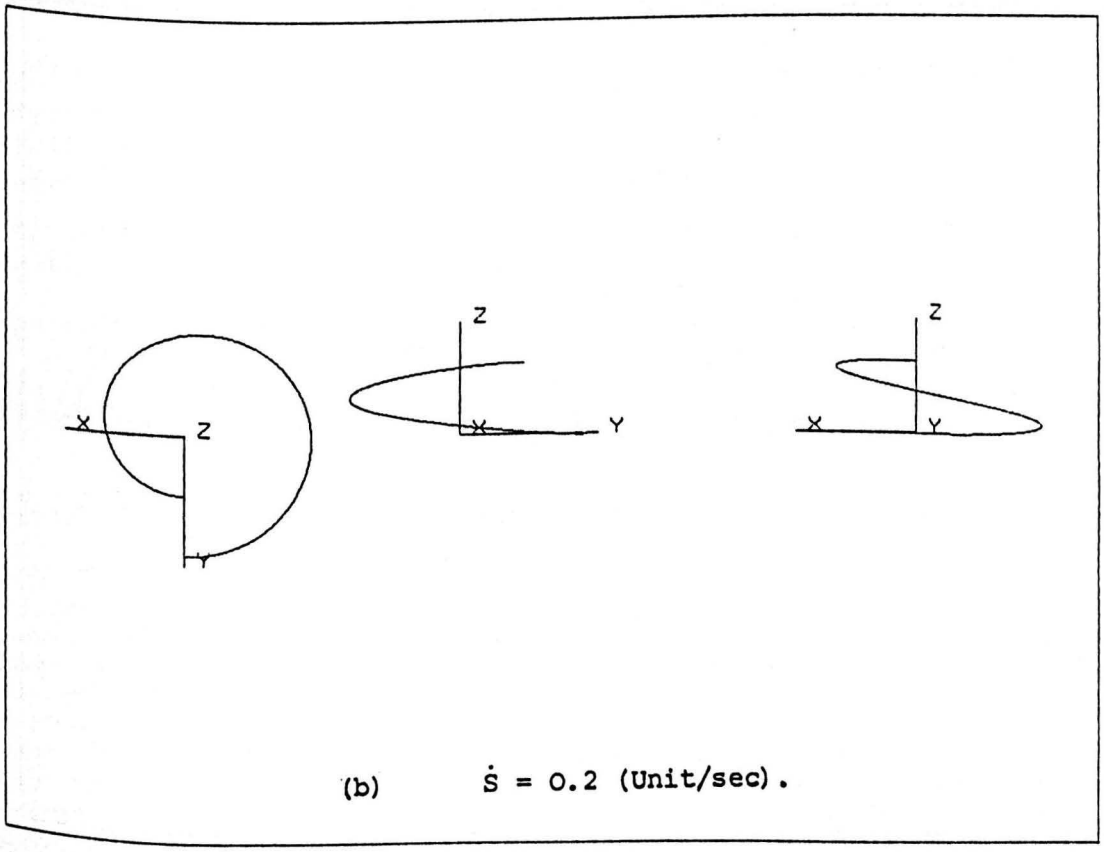

(b) $\dot{S} = 0.2$ (Unit/sec).

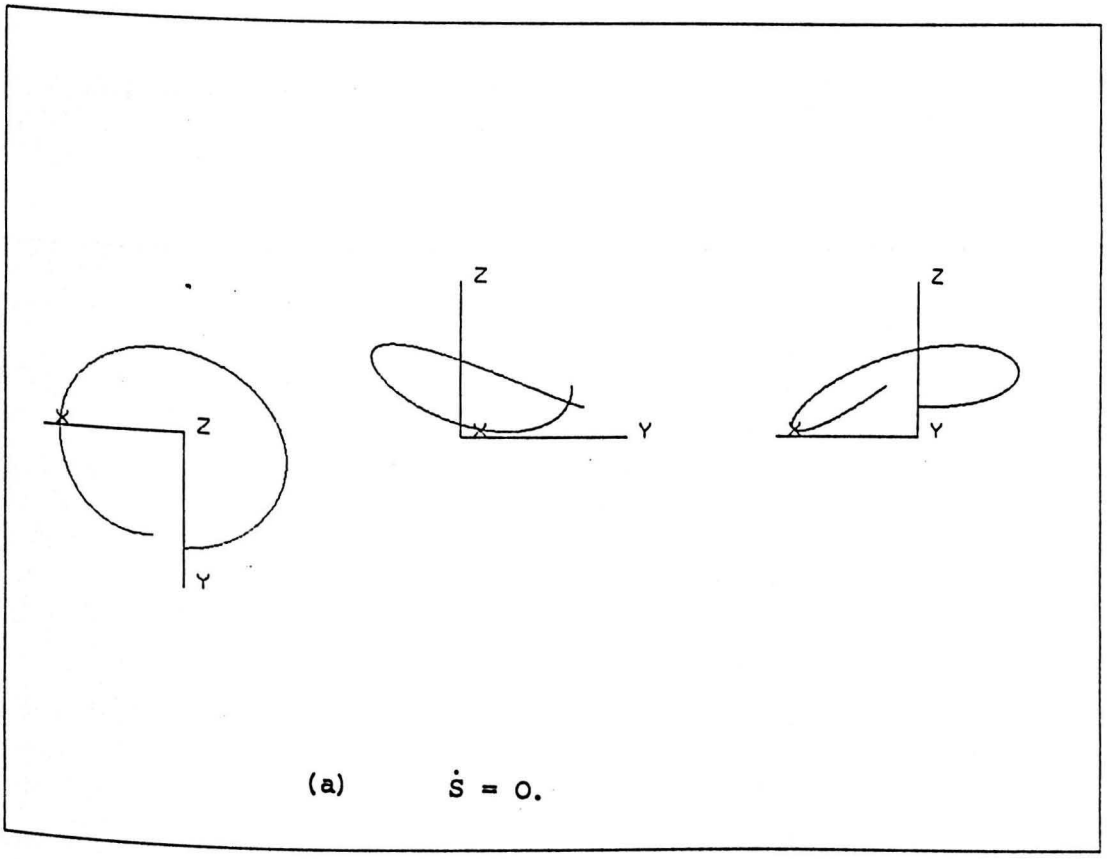

(a) $\dot{S} = 0.$

Fig. 4.17. The locus of a point on a Conic Tool
Tool motion: Nutation - Precession - Spin
$\alpha = 30$ (Deg), $\theta = 15$ (Deg)
$\dot{\theta} = 15$ (Deg/sec), $\dot{\phi} = 90$ (Deg/sec), $\dot{\psi} = 360$ (Deg/sec).

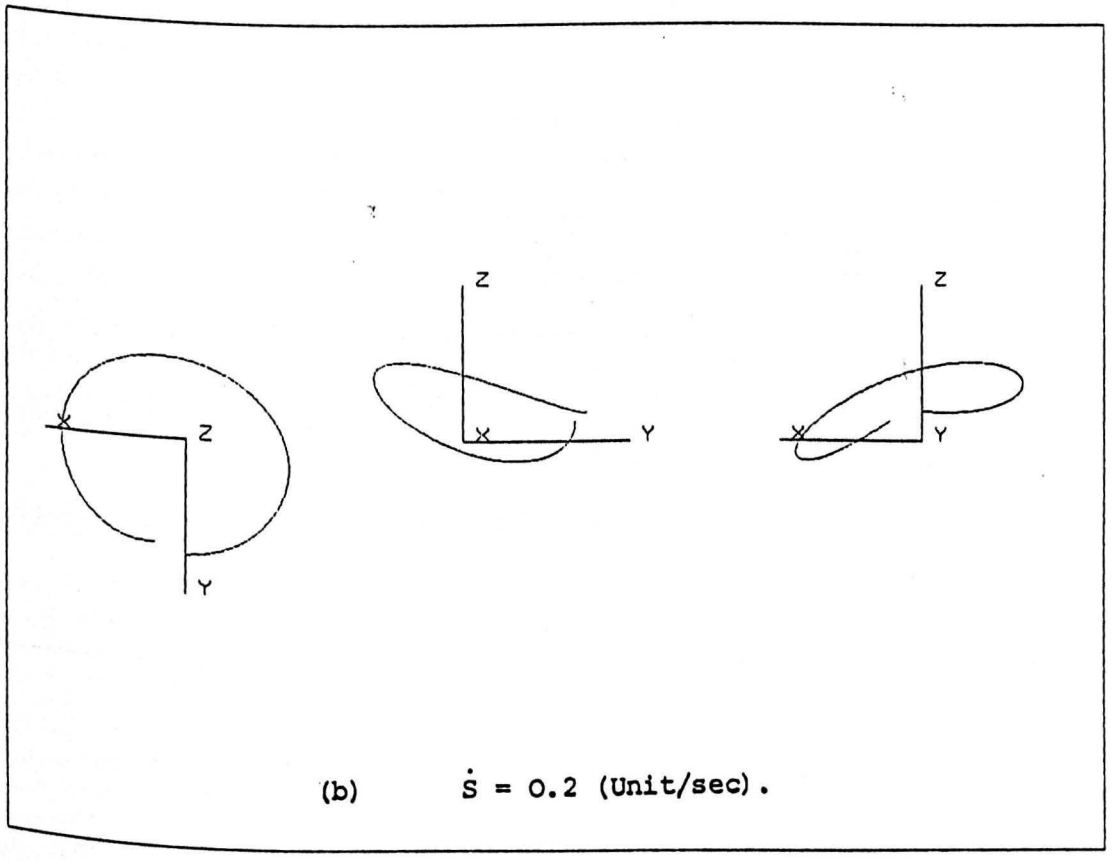

(b) $\dot{S} = 0.2$ (Unit/sec).

Fig. 4.18. Wire-frame representation of a simulated workpiece, which consists of a number of concentric cylinders

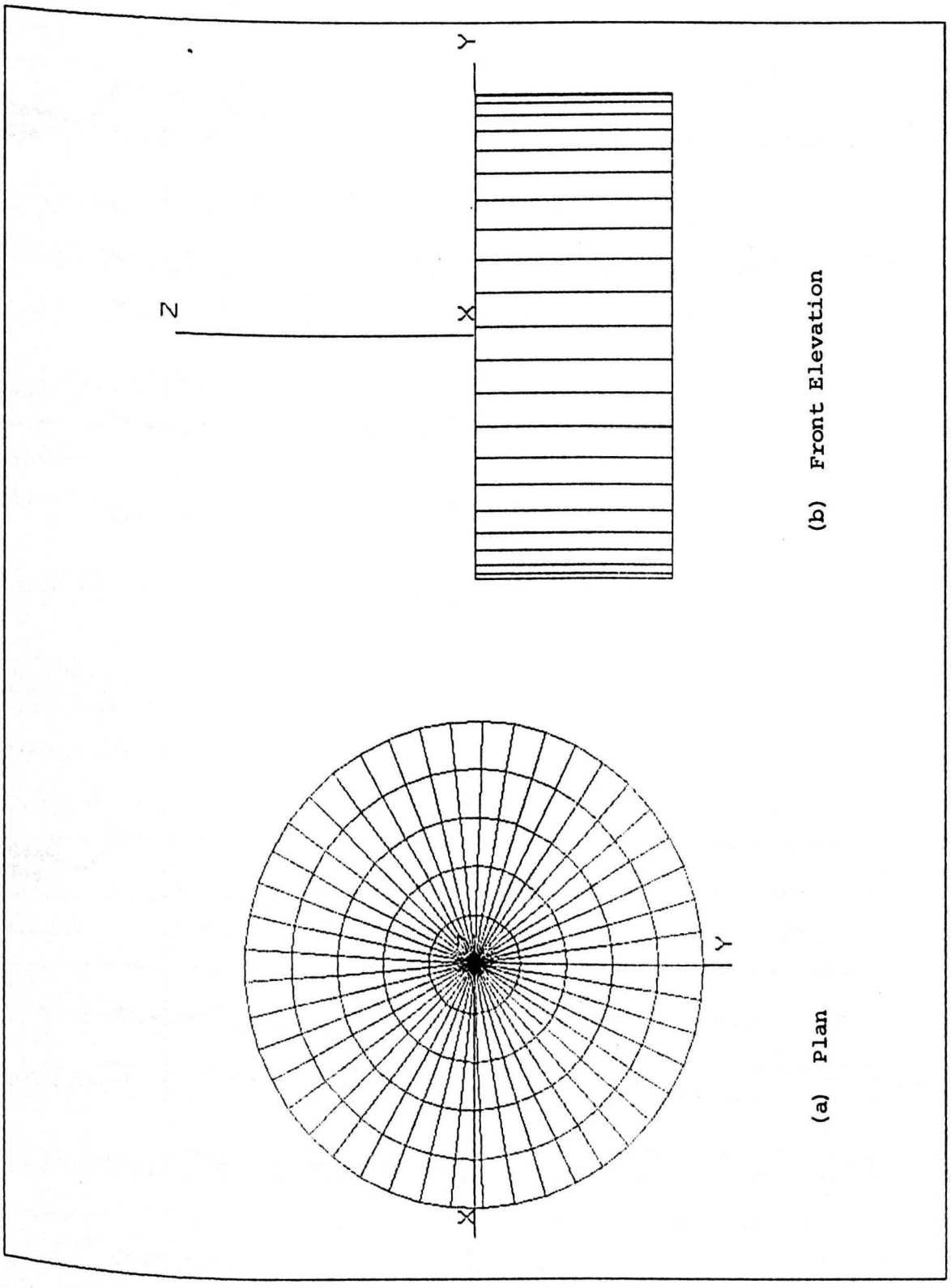

Fig. 4.19. - A developed membrane

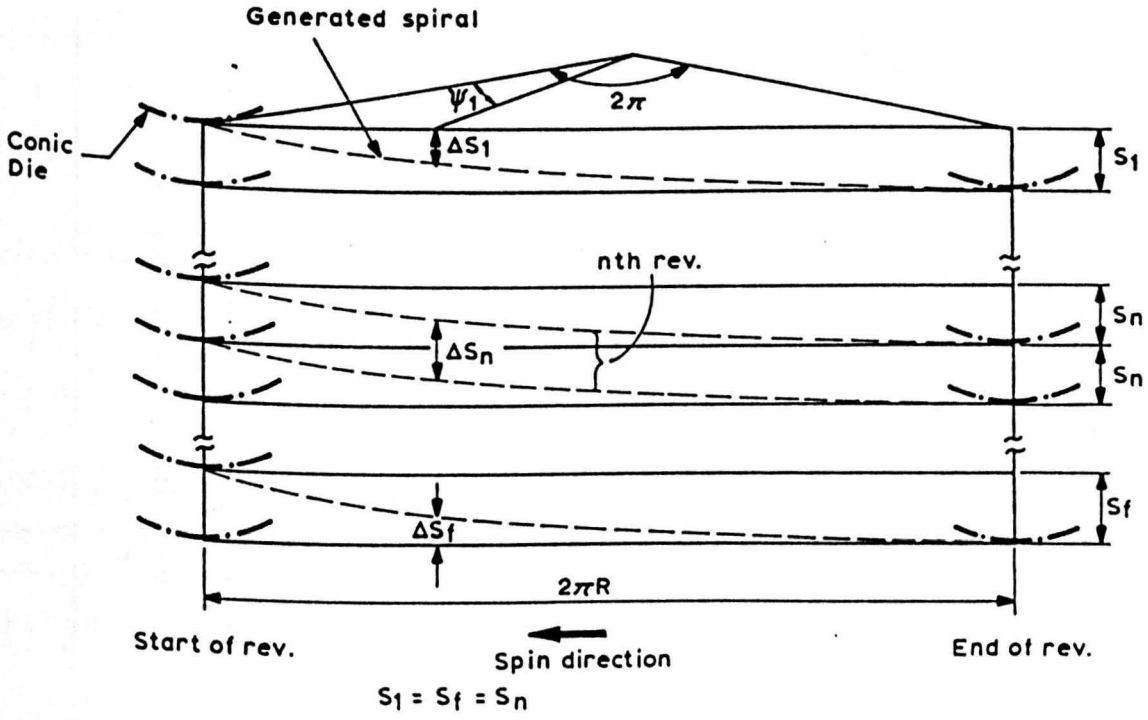

$S_1 = S_f = S_n$

a. Tool motion: Spin or Precession

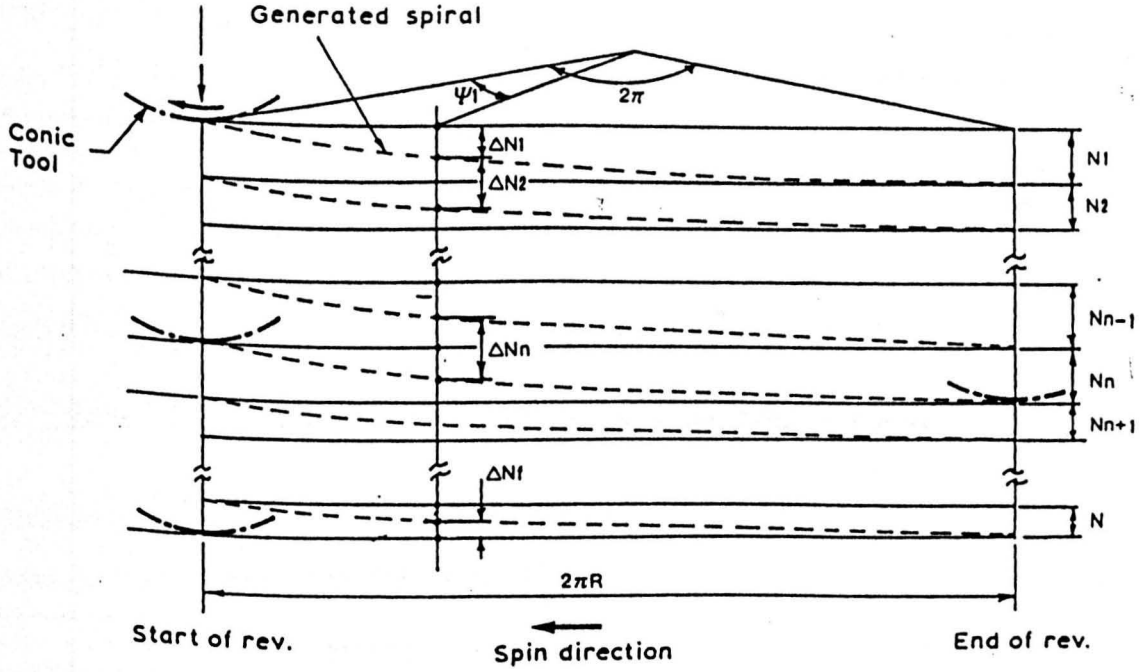

b. Tool motion: Nutation/Spin

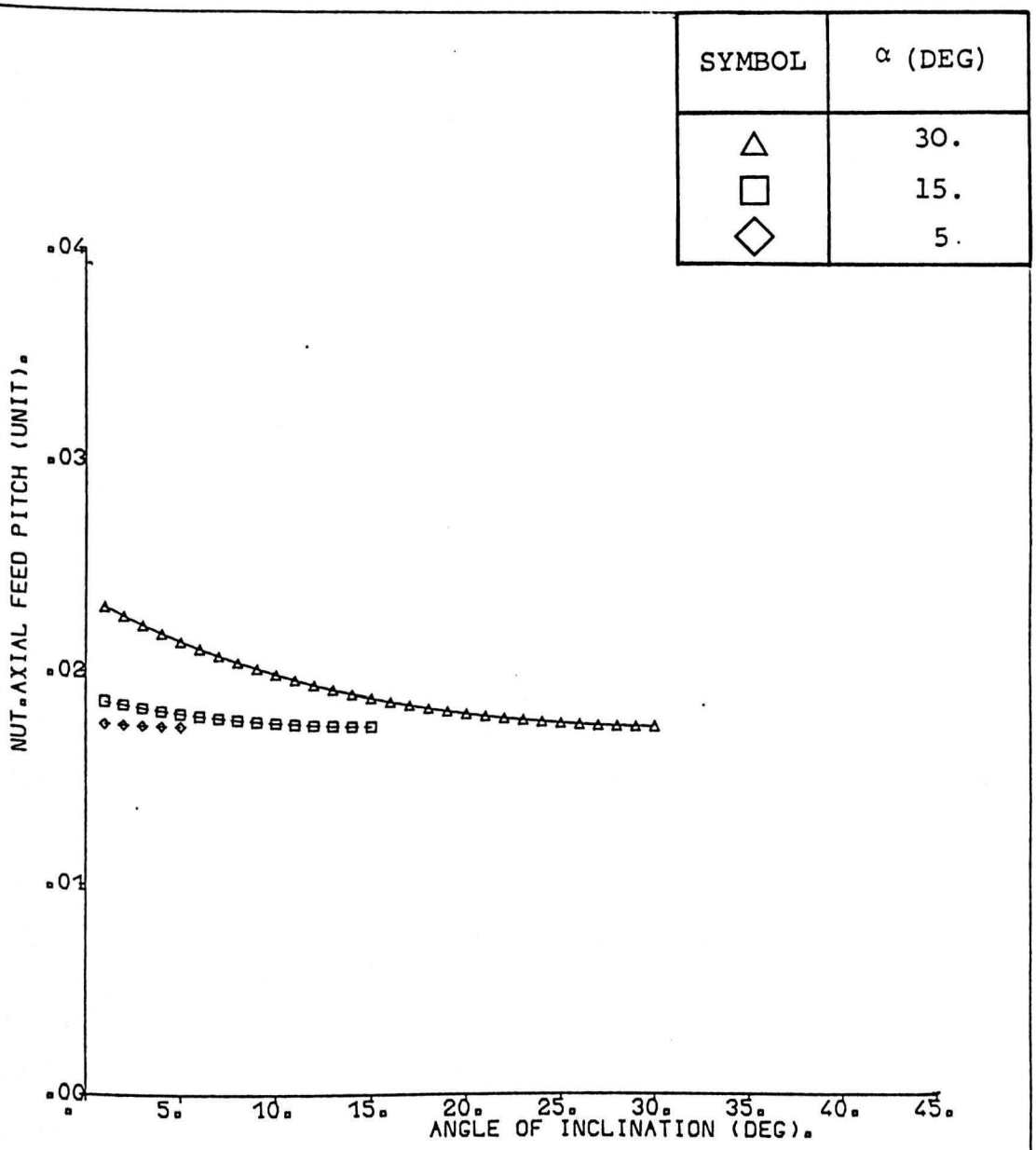

FIG.4.20.GRAPH OF NUTATION AXIAL FEED PITCH VS ANGLE OF INCLINATION.

NUTATION RATE = 1 (DEG/SEC).

(TOOL MOTION : NUTATION)

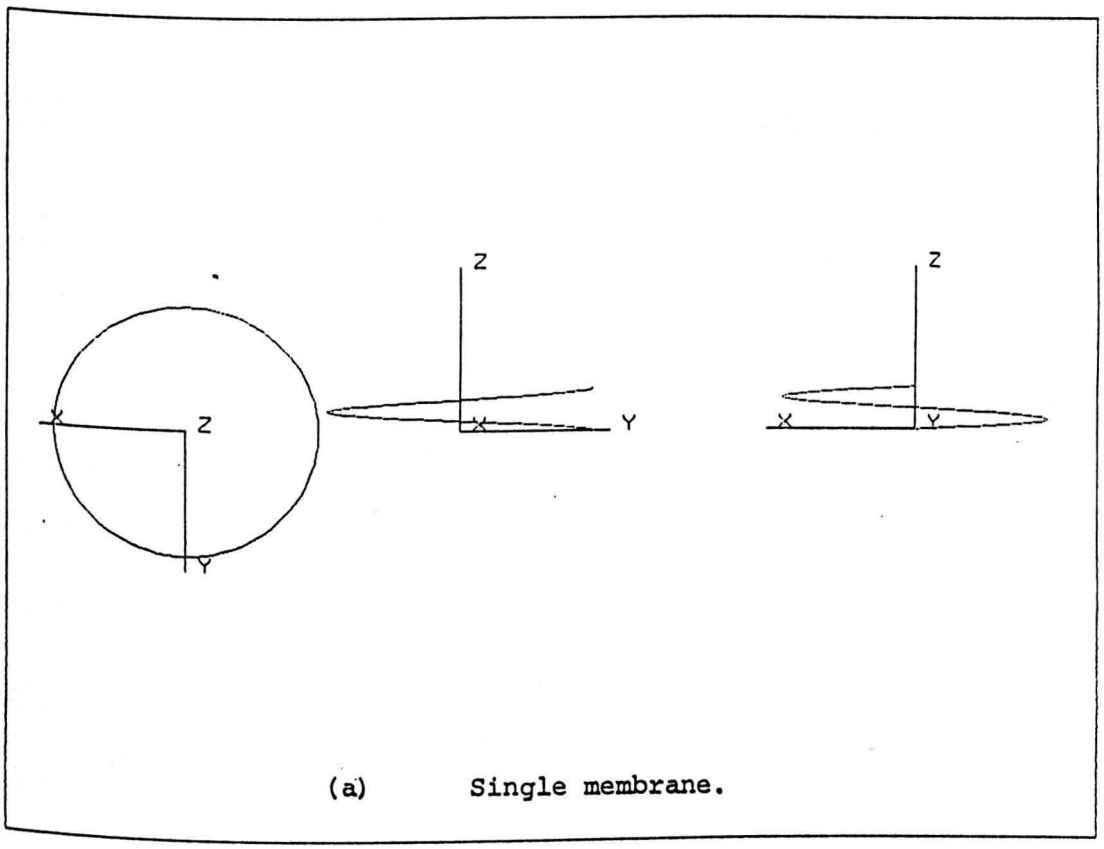

(a) Single membrane.

Fig. 4.21. A spiral surface, penetrated by a Conic Tool
$\dot{S}$ = 0.3 (Unit/sec)

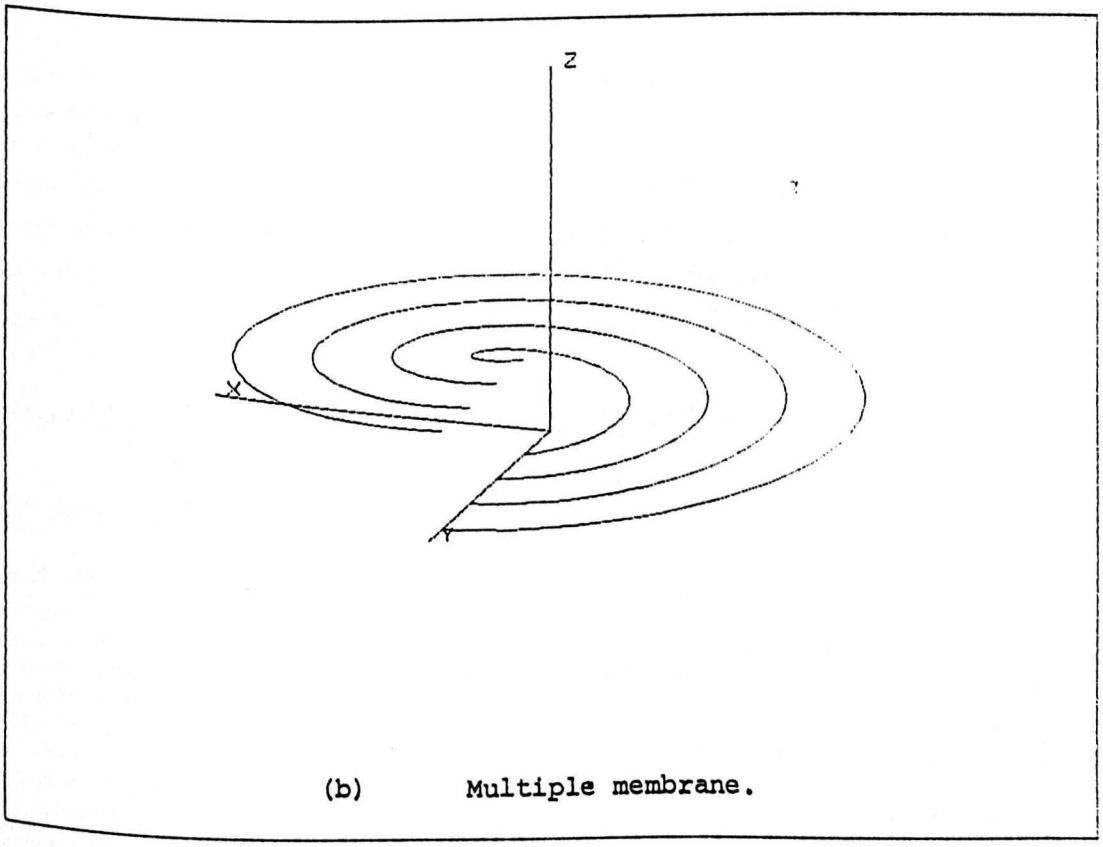

(b) Multiple membrane.

Fig. 4.22. The uni-axial compression
α = 30 (Deg), θ = 0

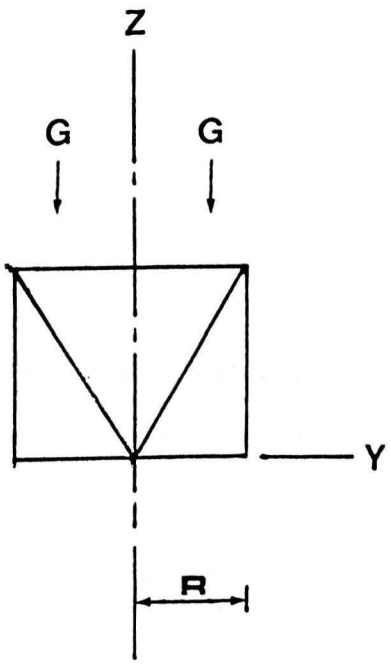

(a) View ZY

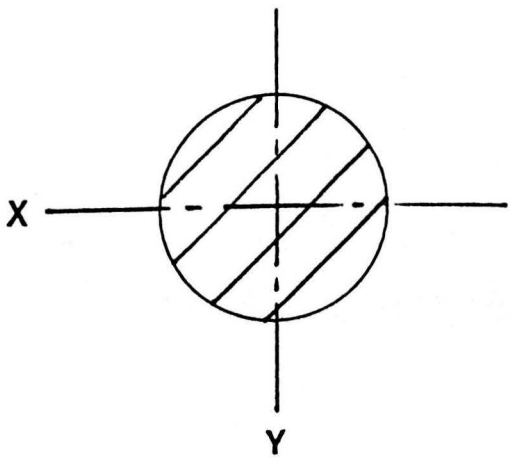

(b) View GG

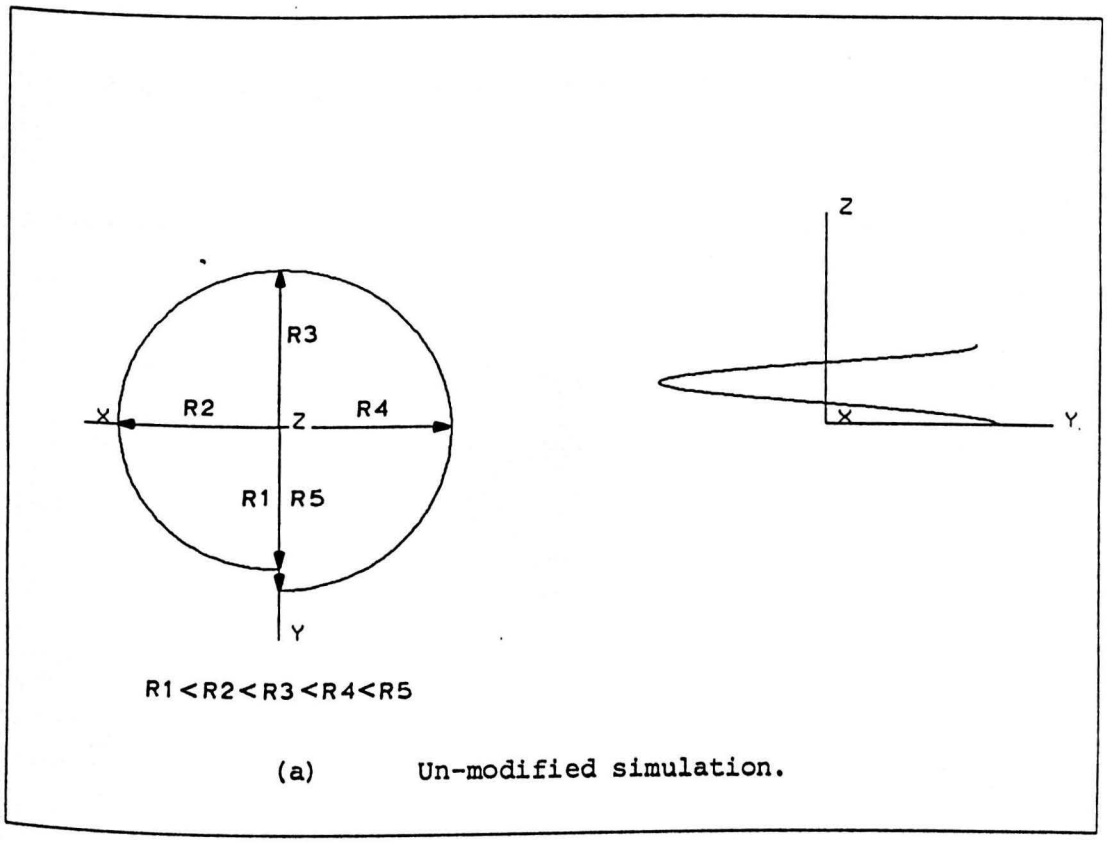

(a) Un-modified simulation.

Fig. 4.23 Spiral on a single membrane, generated by a nutating Conic Tool.

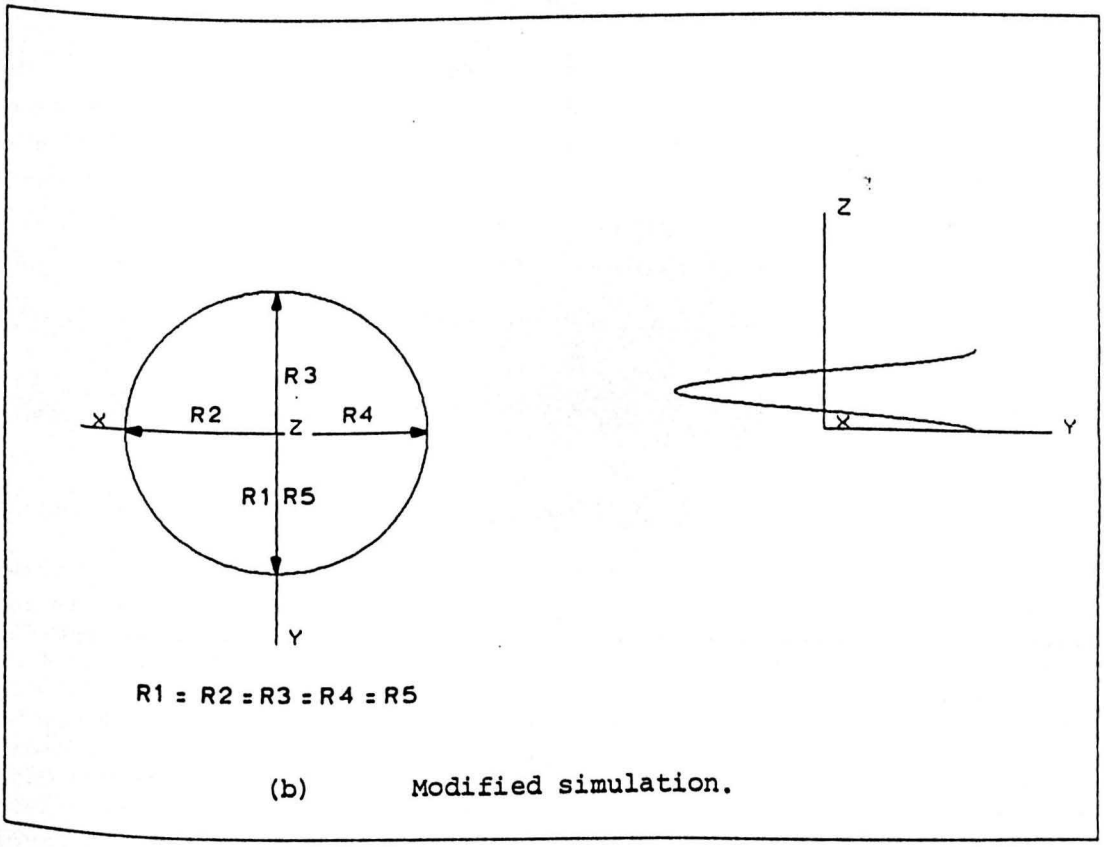

(b) Modified simulation.

Fig. 5.1. Superposition of a simulated conic tool on a spiral surface

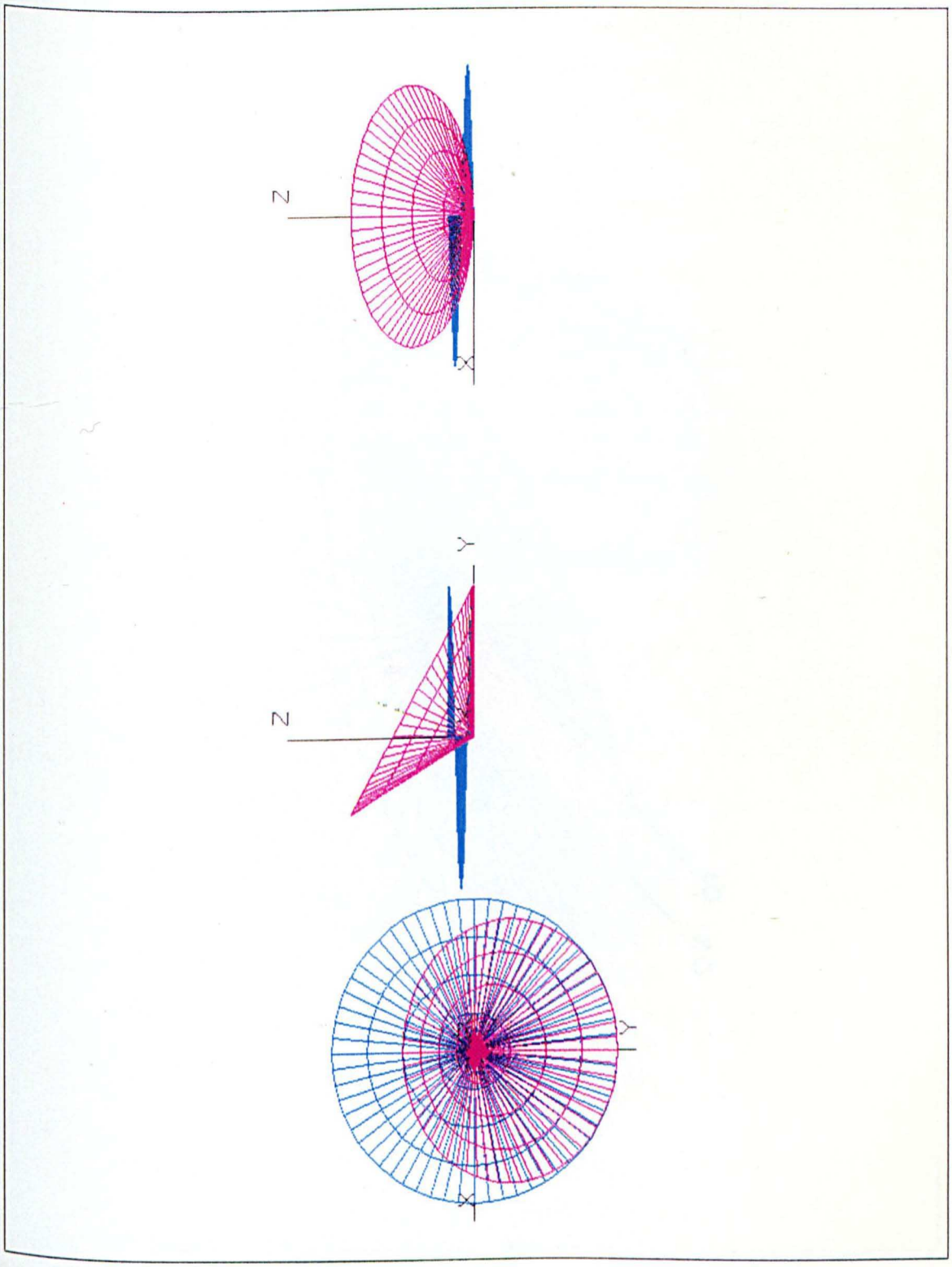

Fig. 5.2. An isometric view, showing superposition of a simulated conic tool on a spiral surface.

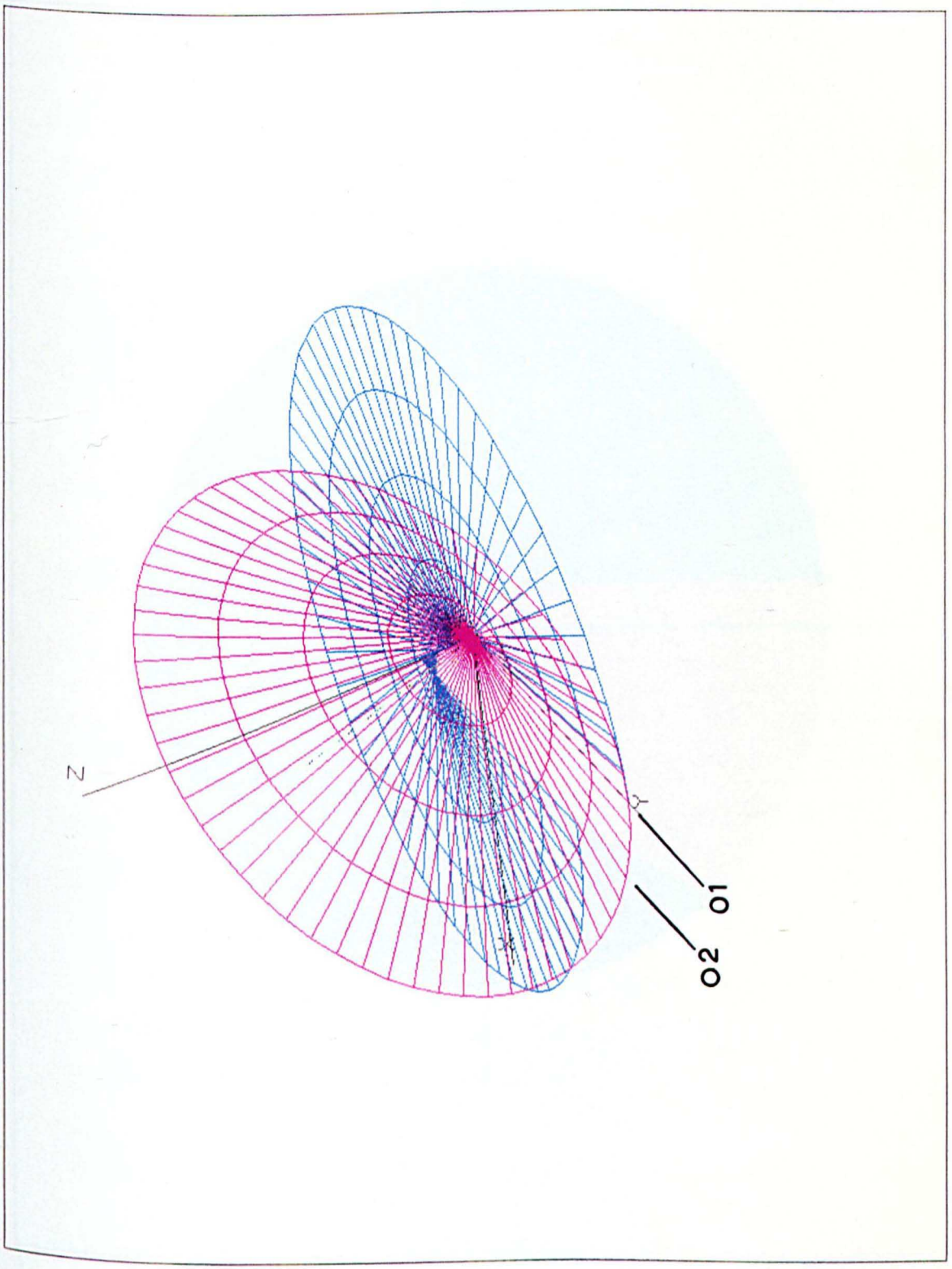

Fig. 5.3. The simulation of surface elements, formed in rotary forging (Magenta representing ICA)

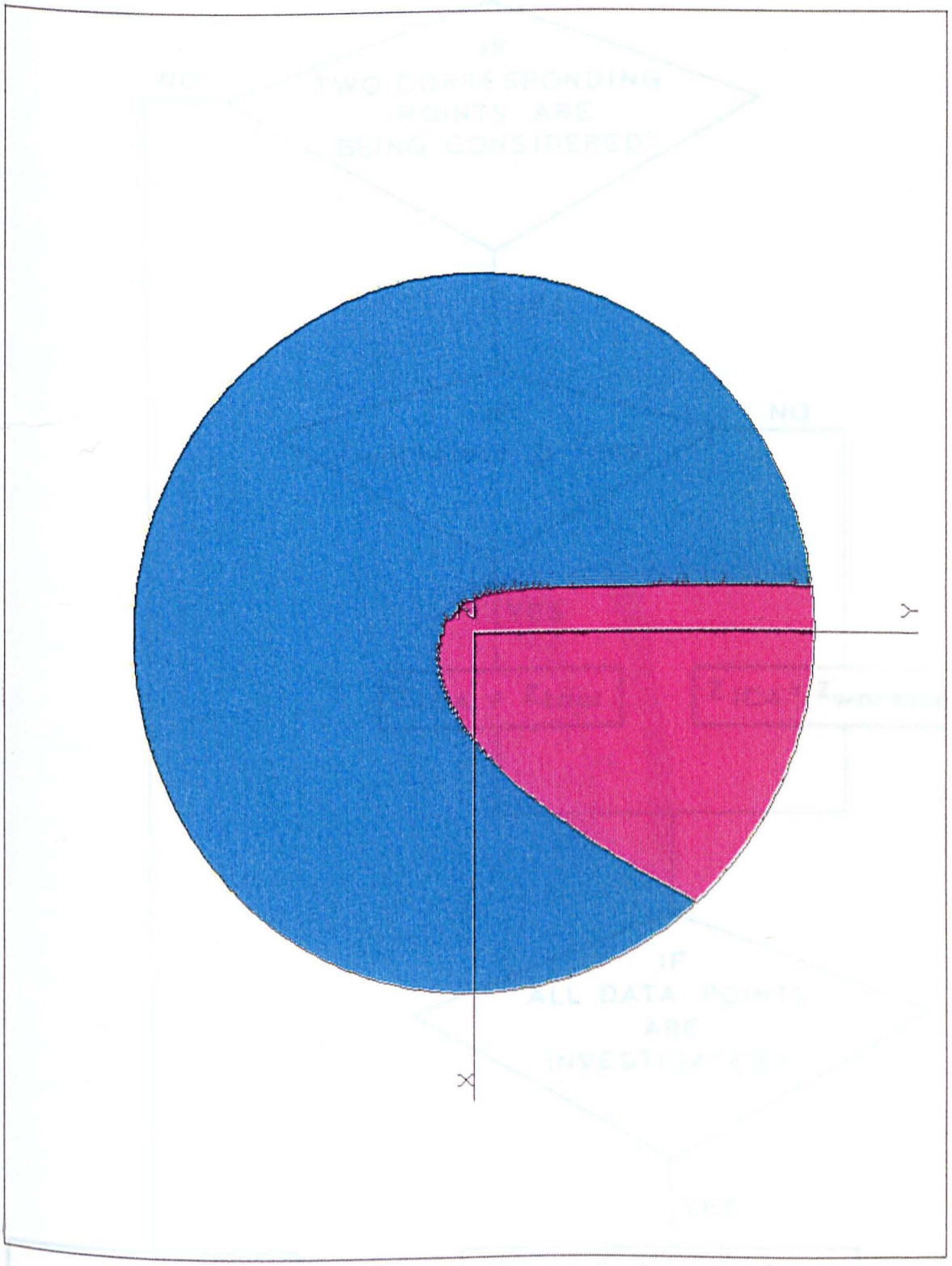

Fig. 5.4. The flow chart diagram of the subroutine which extracts the Instantaneous Area of Contact (ICA)

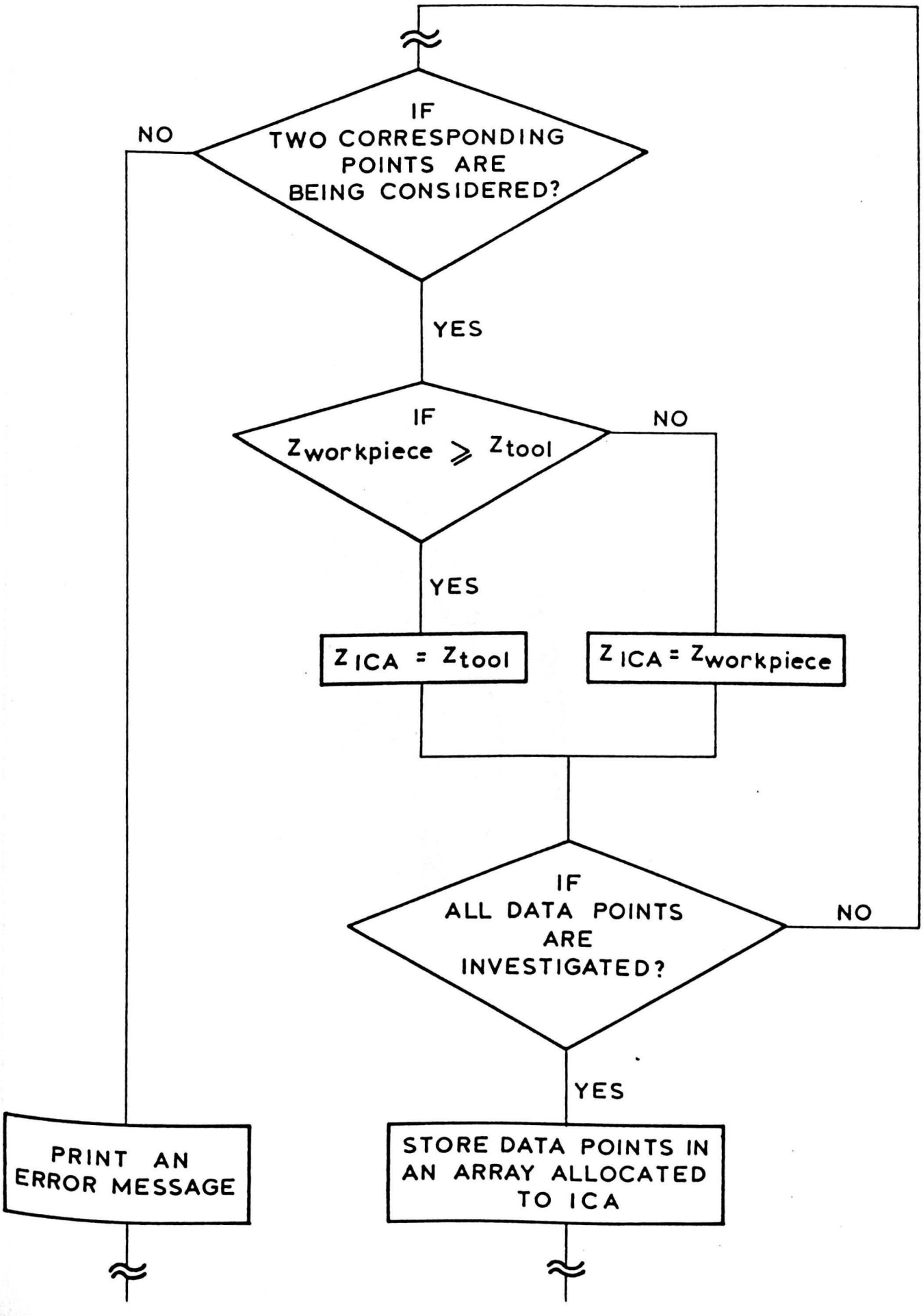

Fig. 5.5. The isometric view of a simulated billet being deformed by a conic tool

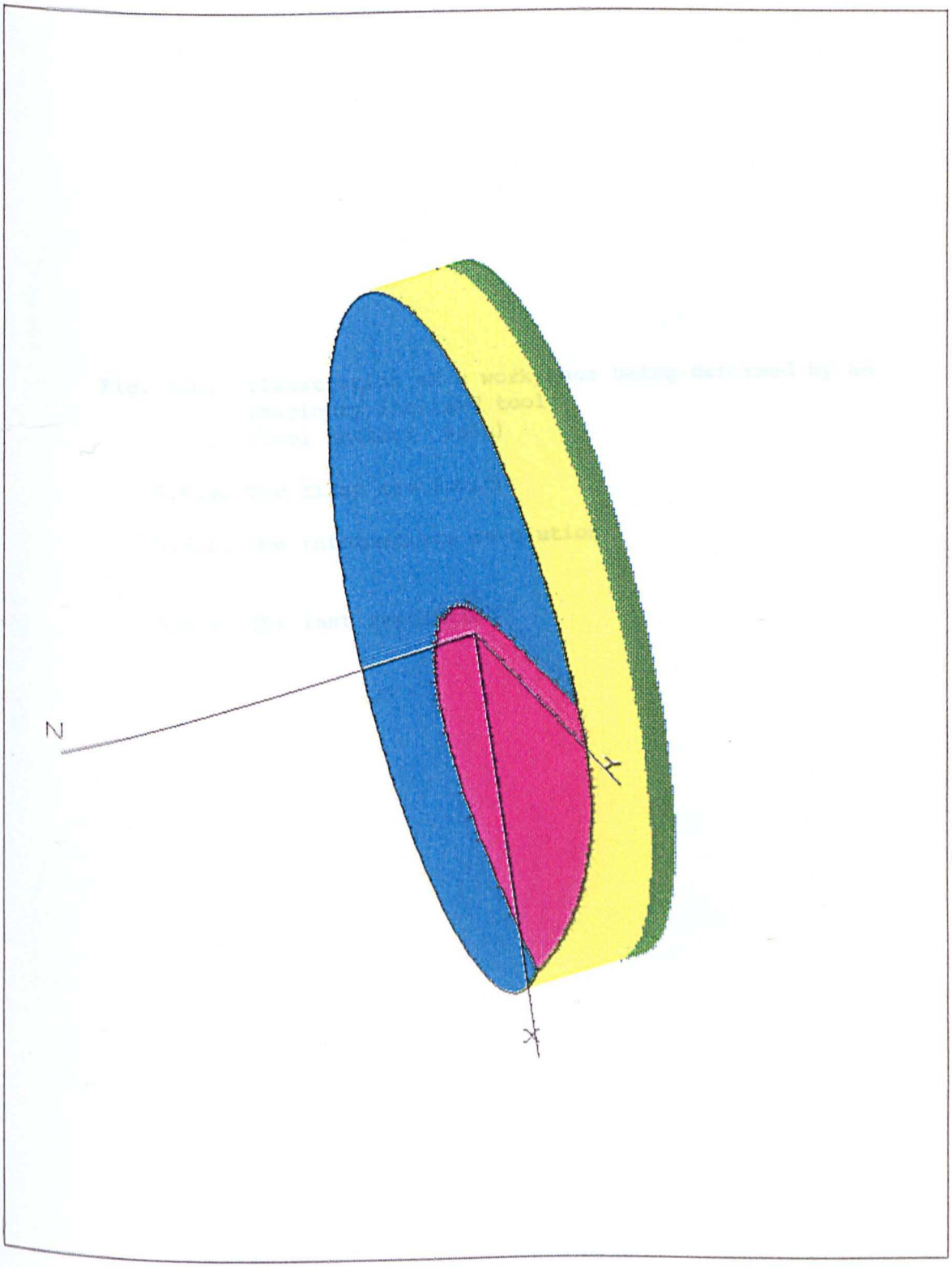

Fig. 5.6. Illustration of a workpiece being deformed by an imaginary inclined tool
(Tool motion: Spin)

5.6.a. The first revolution

5.6.b. One intermediate revolution

5.6.c. The last revolution

Fig. 5.6.a.

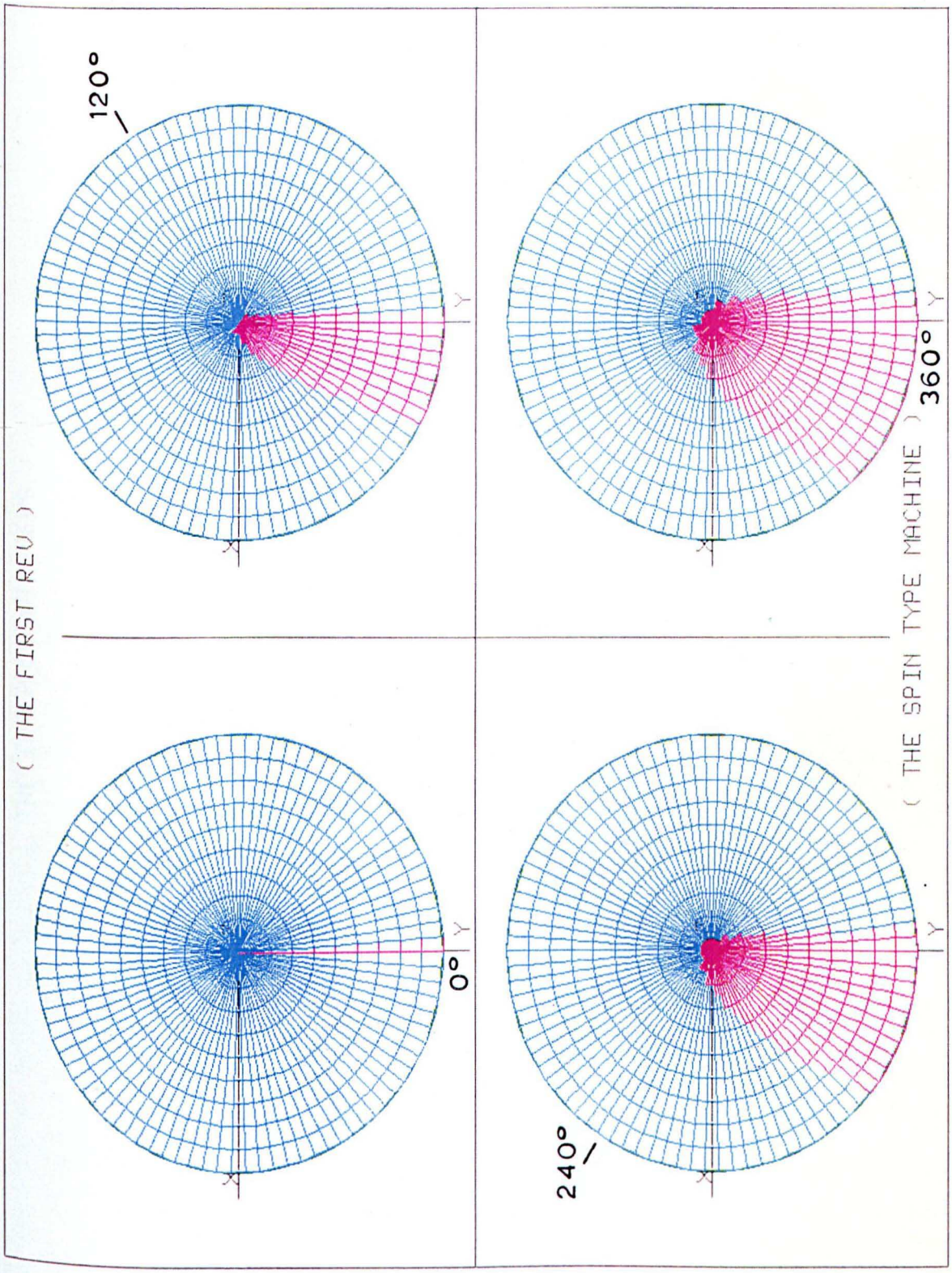

Fig. 5.6.b.

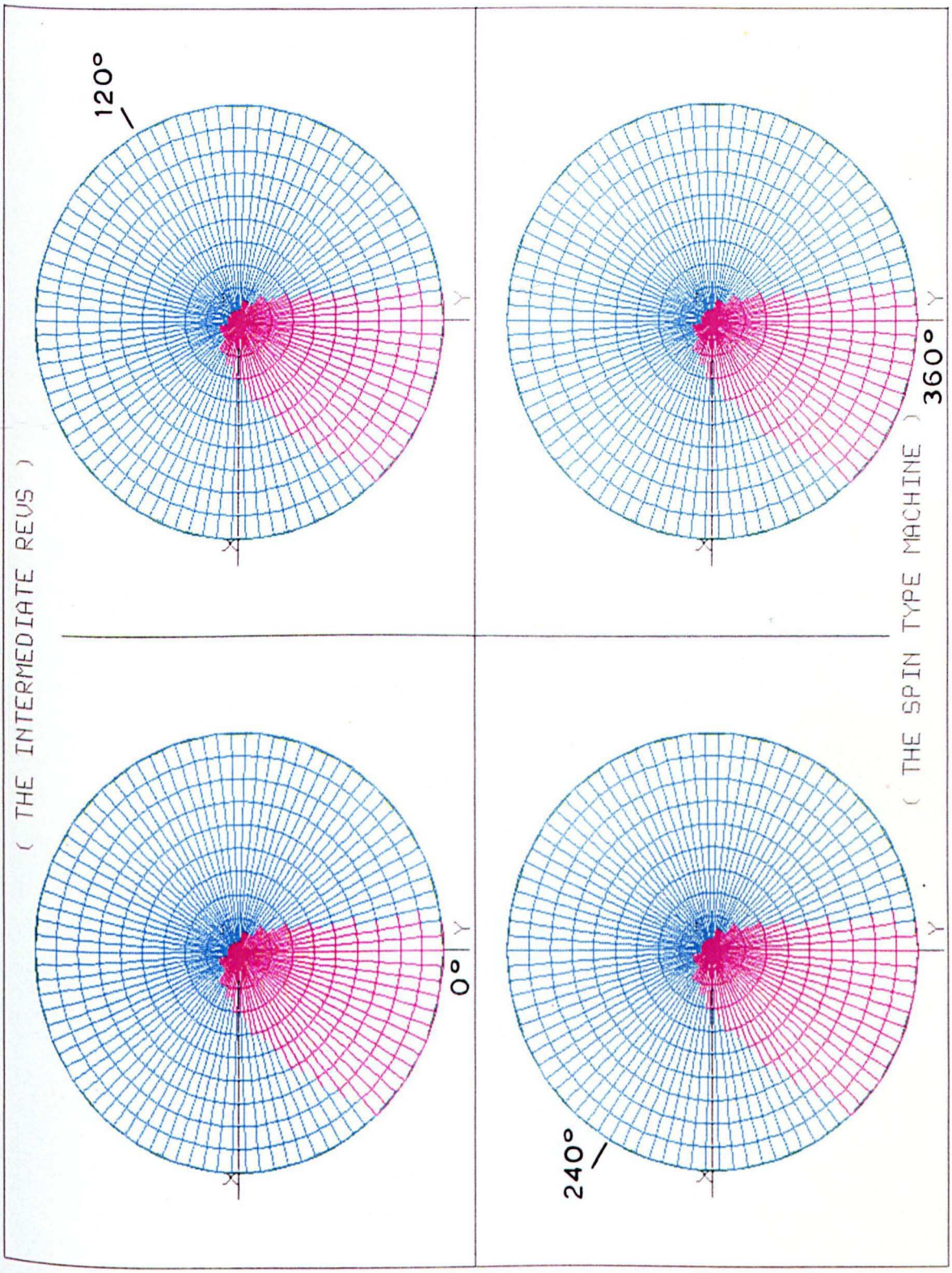

Fig. 5.6.c.

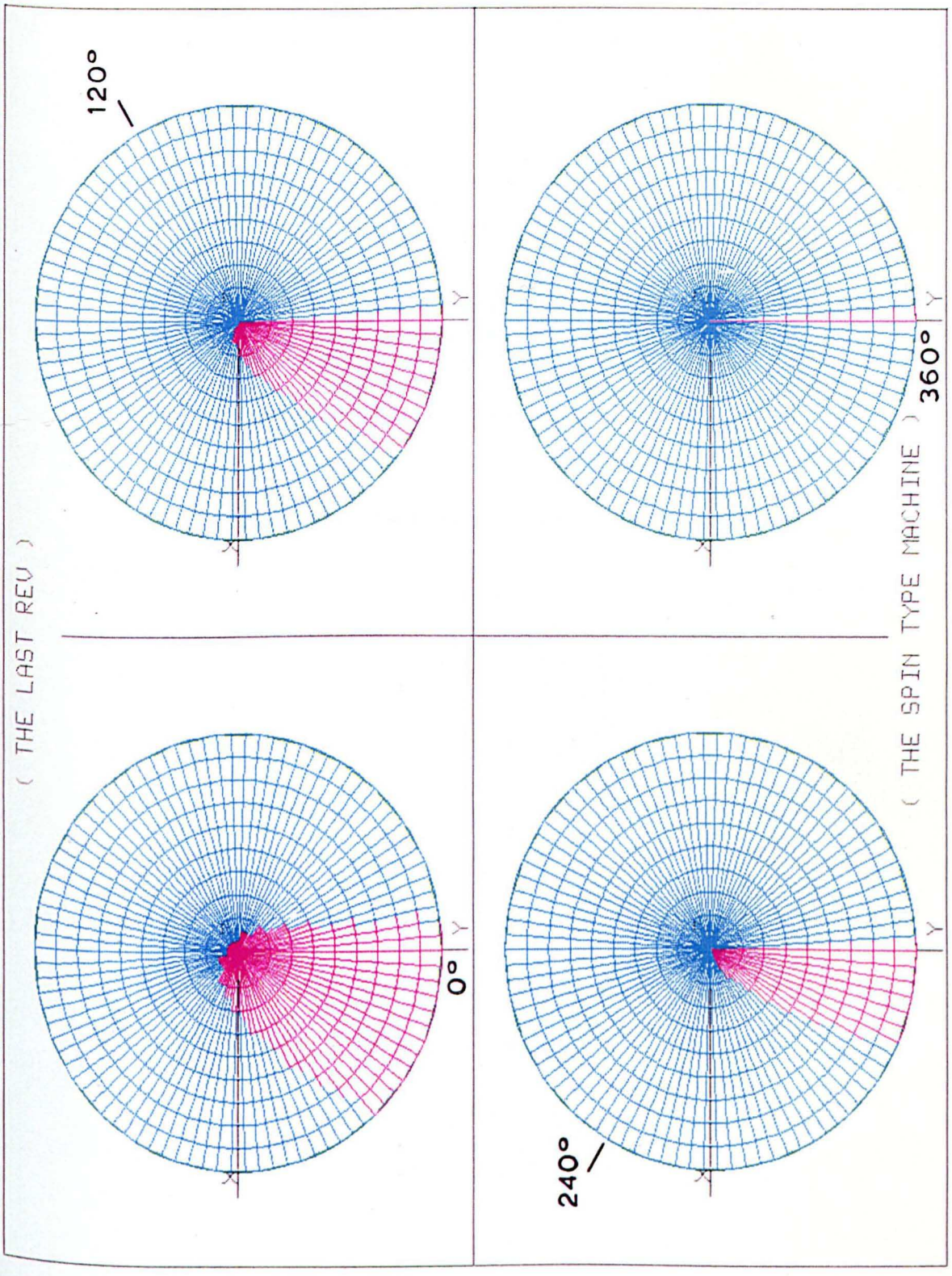

Fig. 5.7. Illustration of a workpiece being deformed by an imaginary inclined tool
(Tool motion: Spin)

5.7.a. The first revolution

5.7.b. One intermediate revolution

5.7.c. The last revolution

Fig. 5.7.a.

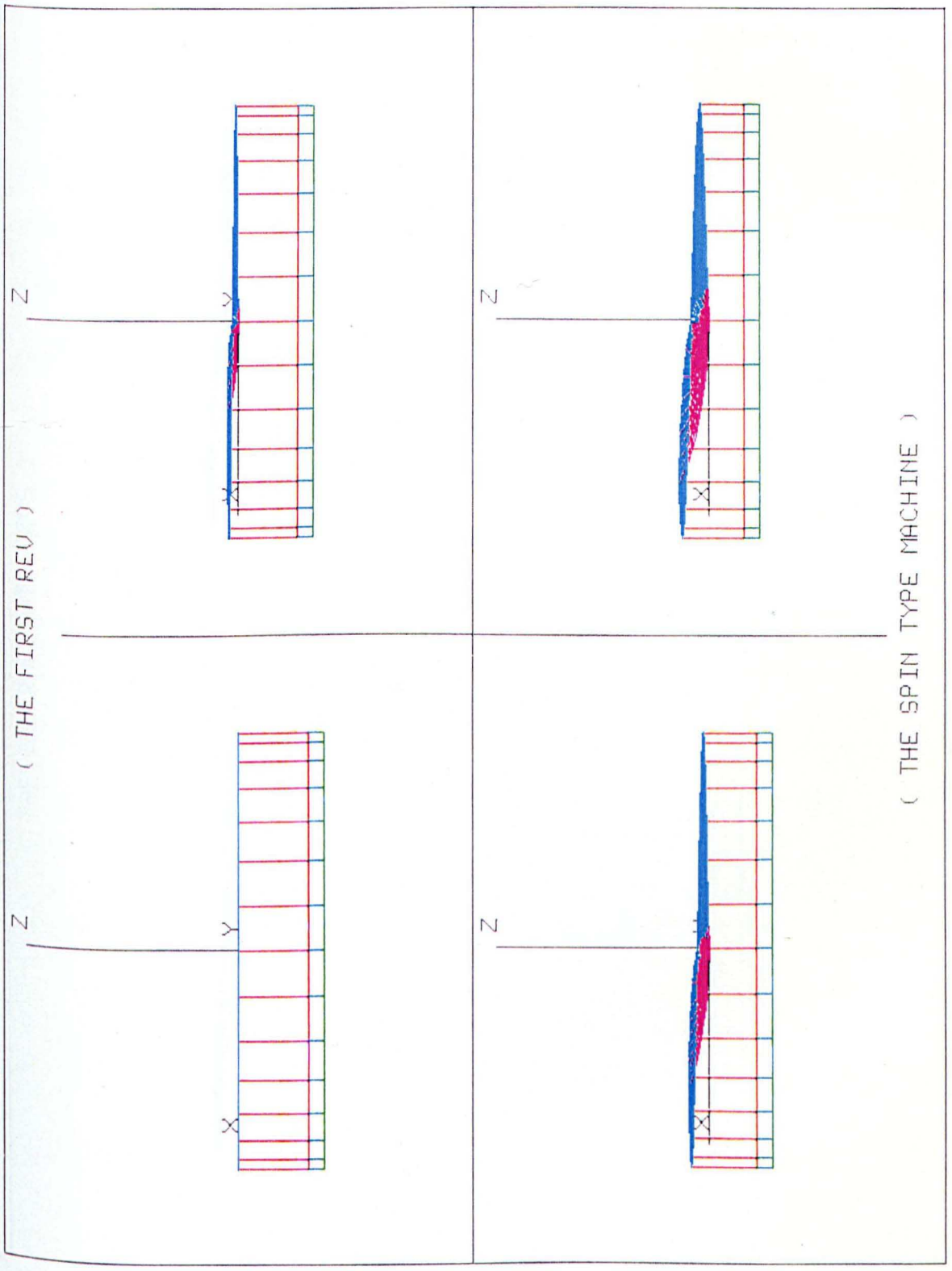

Fig. 5.7.b.

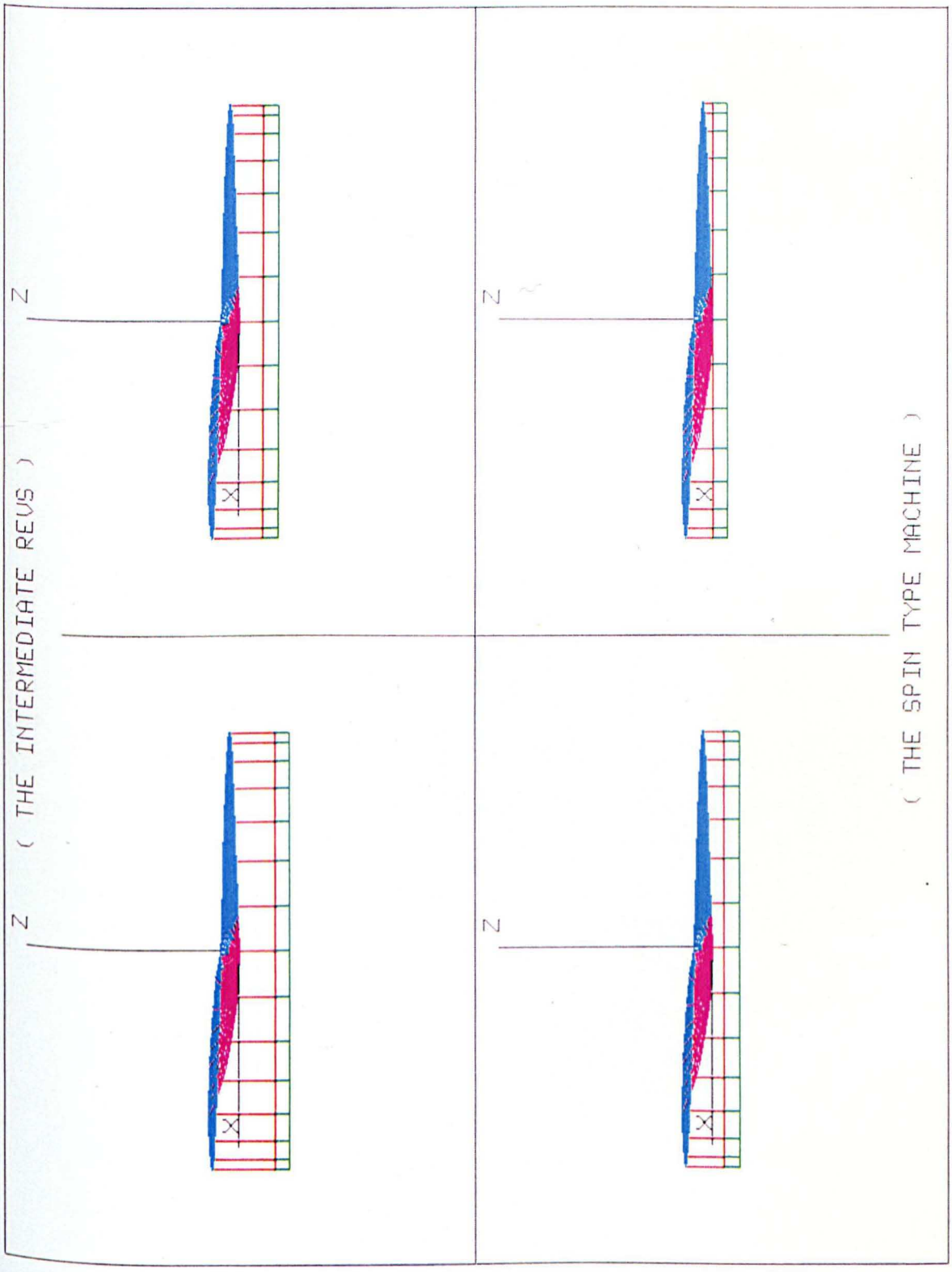

Fig. 5.7.c.

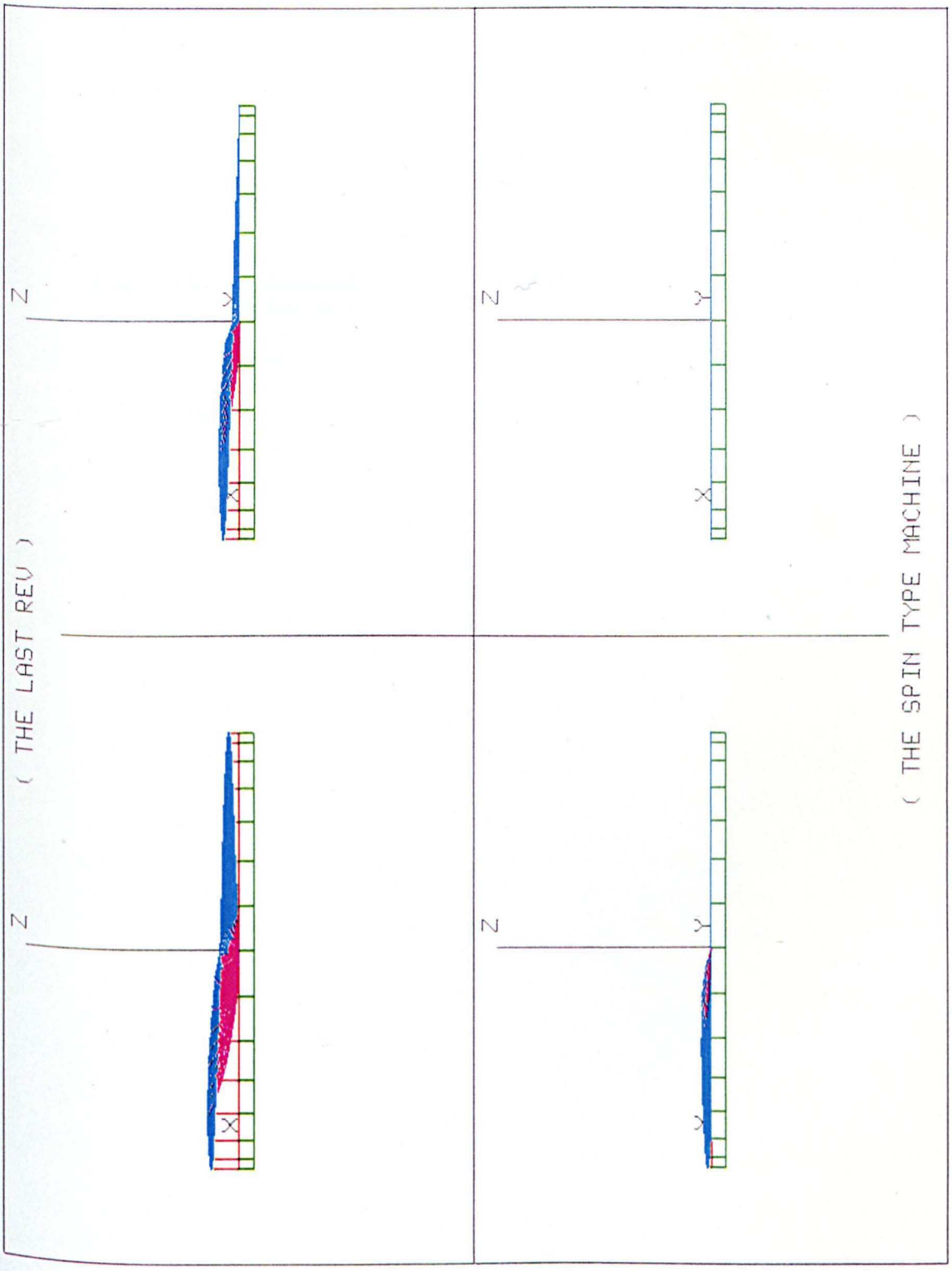

Fig. 5.8. Illustration of a workpiece being deformed by an imaginery inclined tool

(Tool motion:Spin)

5.8.a. The first revolution

5.8.b. One intermediate revolution

5.8.c. The last revolution

Fig. 5.8.a.

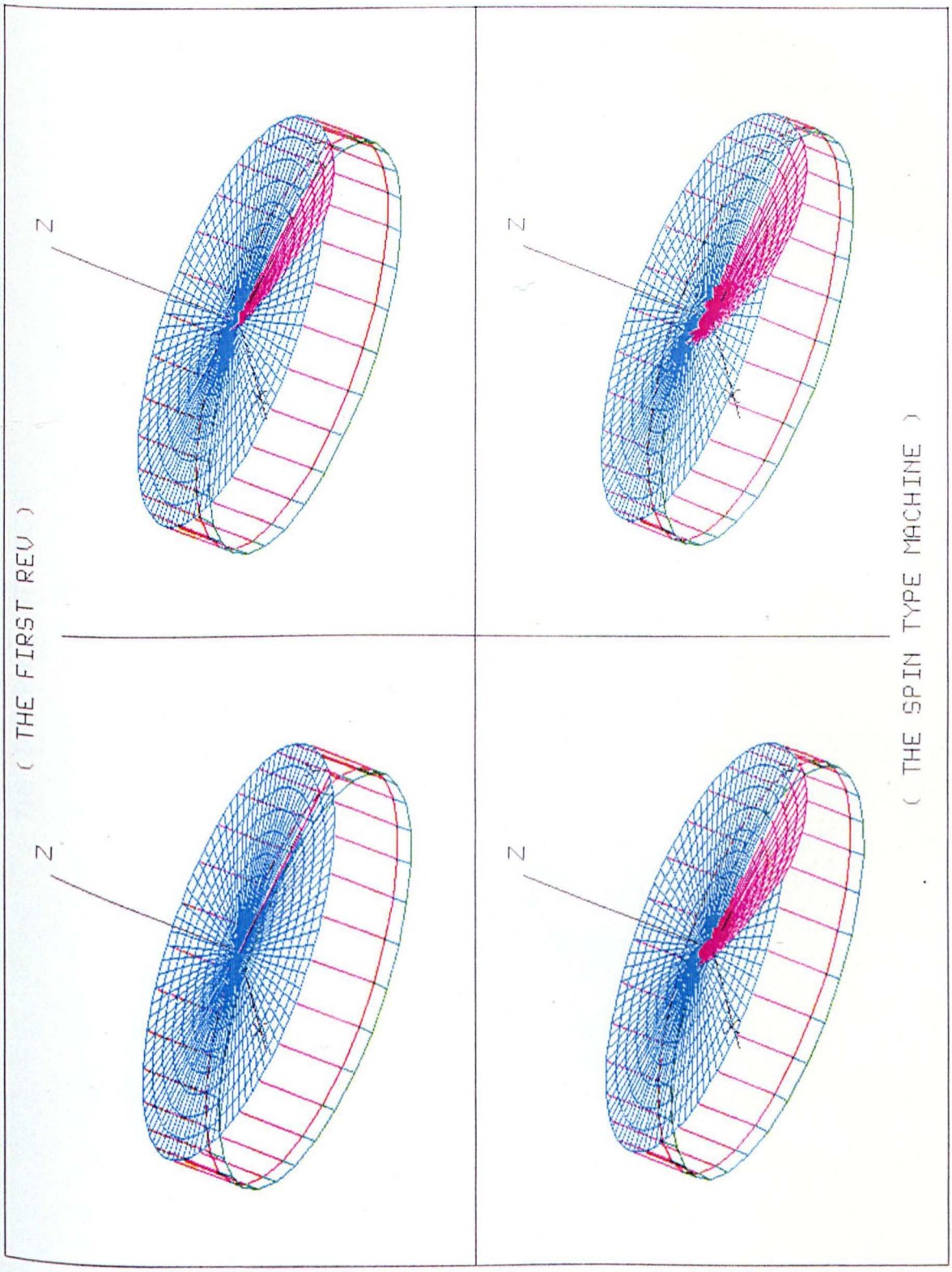

Fig. 5.8.b.

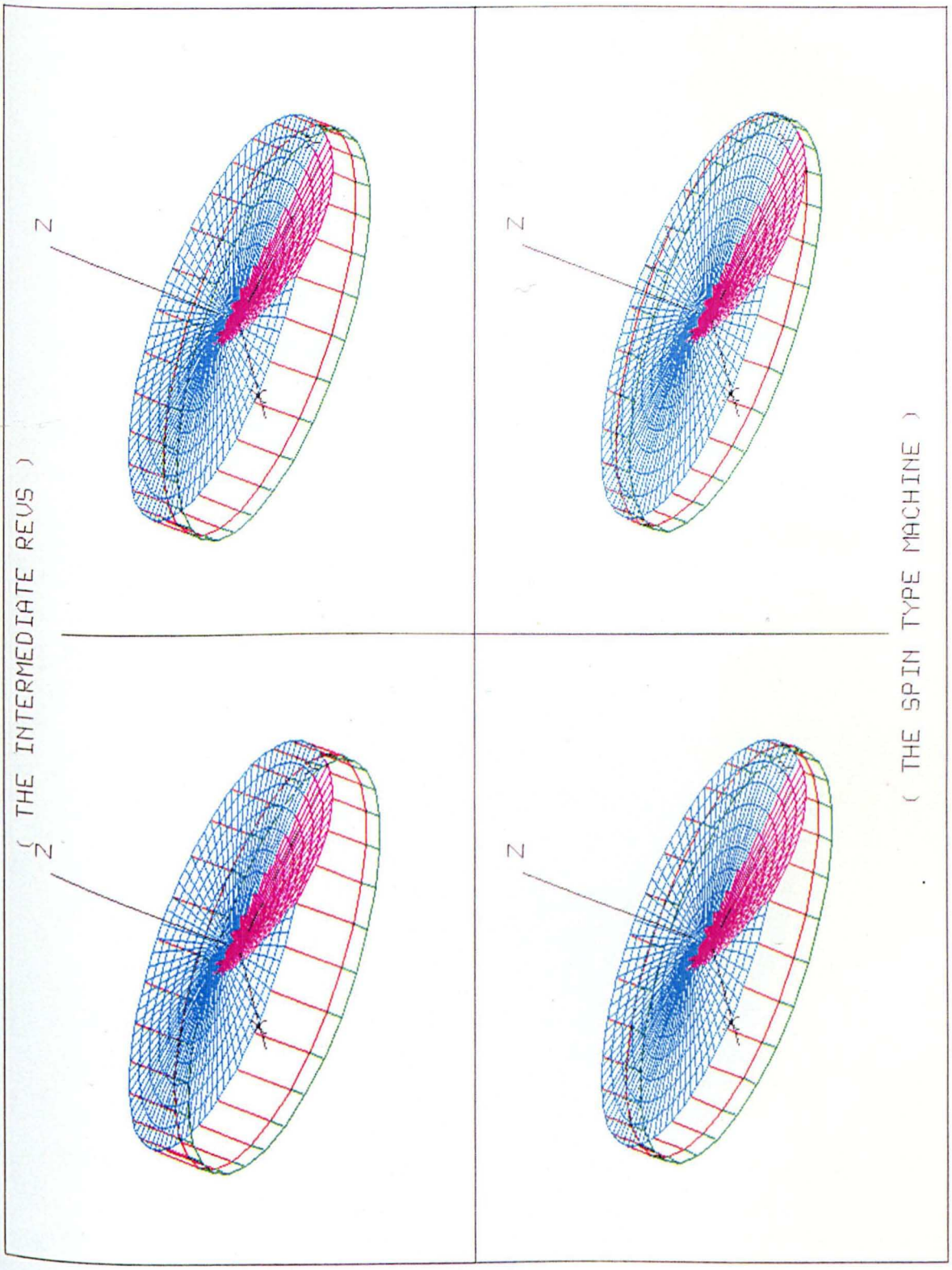

Fig. 5.8.c.

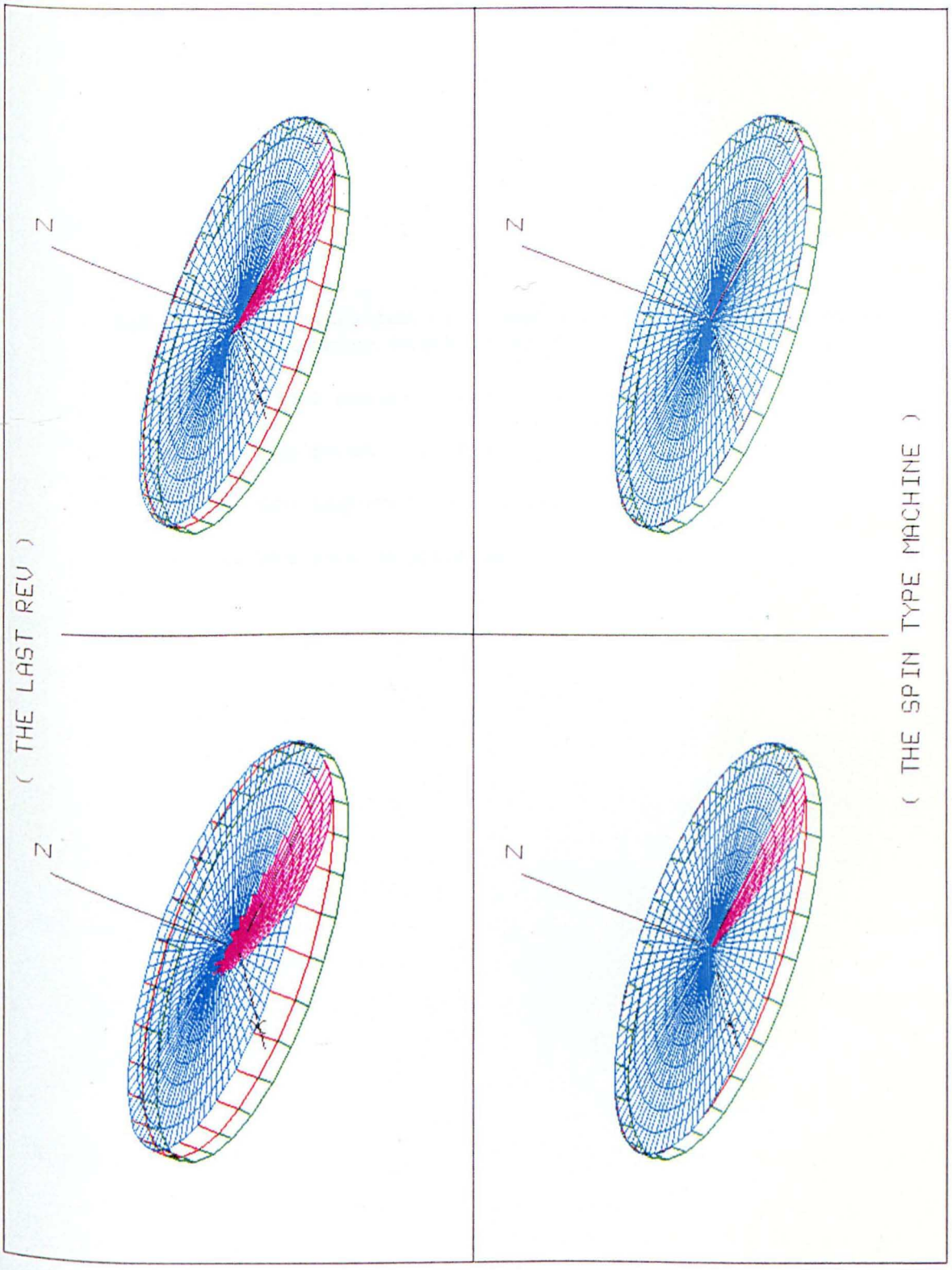

Fig. 5.9. Illustration of a workpiece being deformed by an imaginary inclined tool

(Tool motion: Precession)

5.9.a. The first revolution

5.9.b. One itnermediate revolution

5.9.c. The last revolution

Fig. 5.9.a.

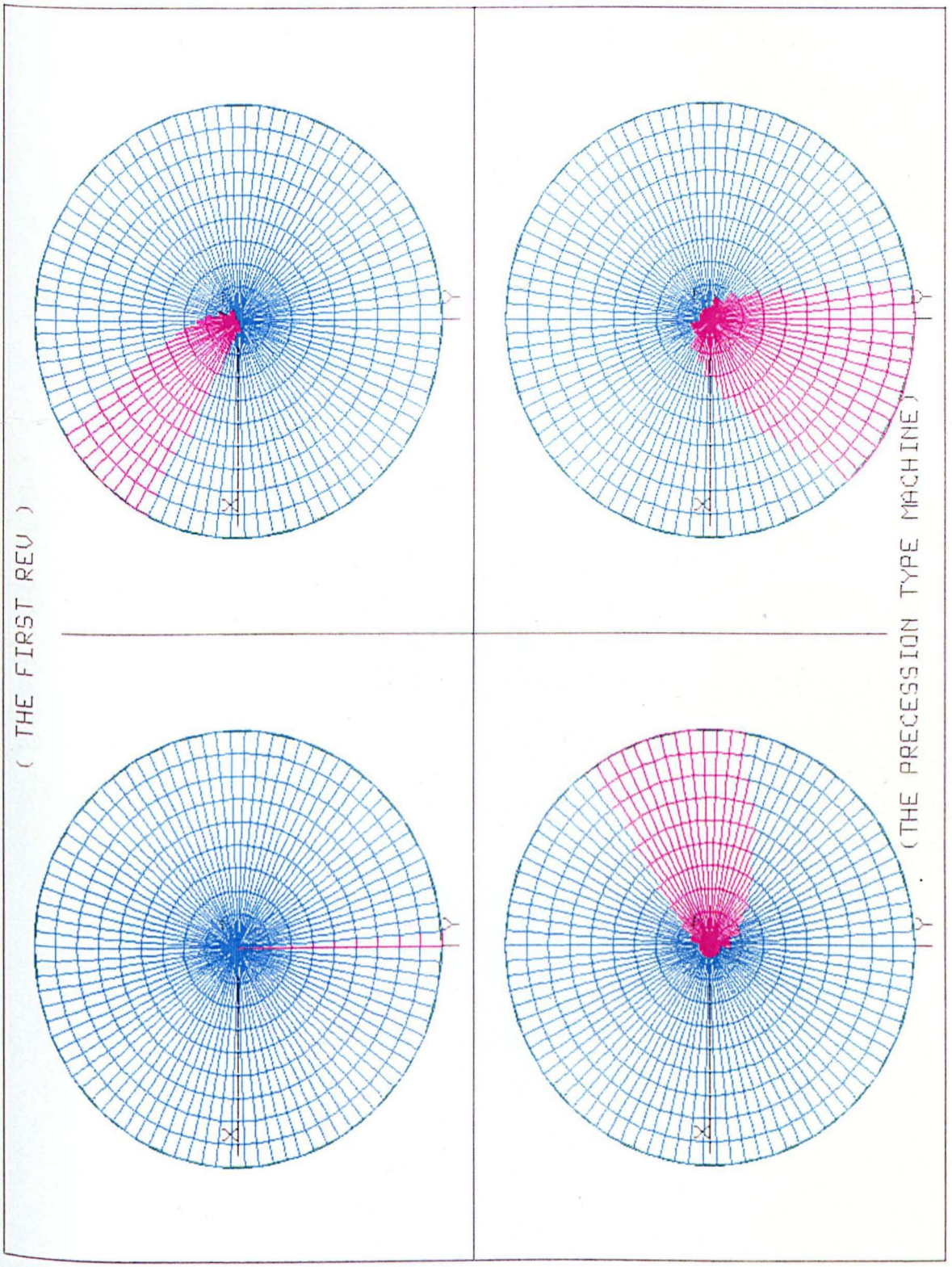

Fig. 5.9.b.

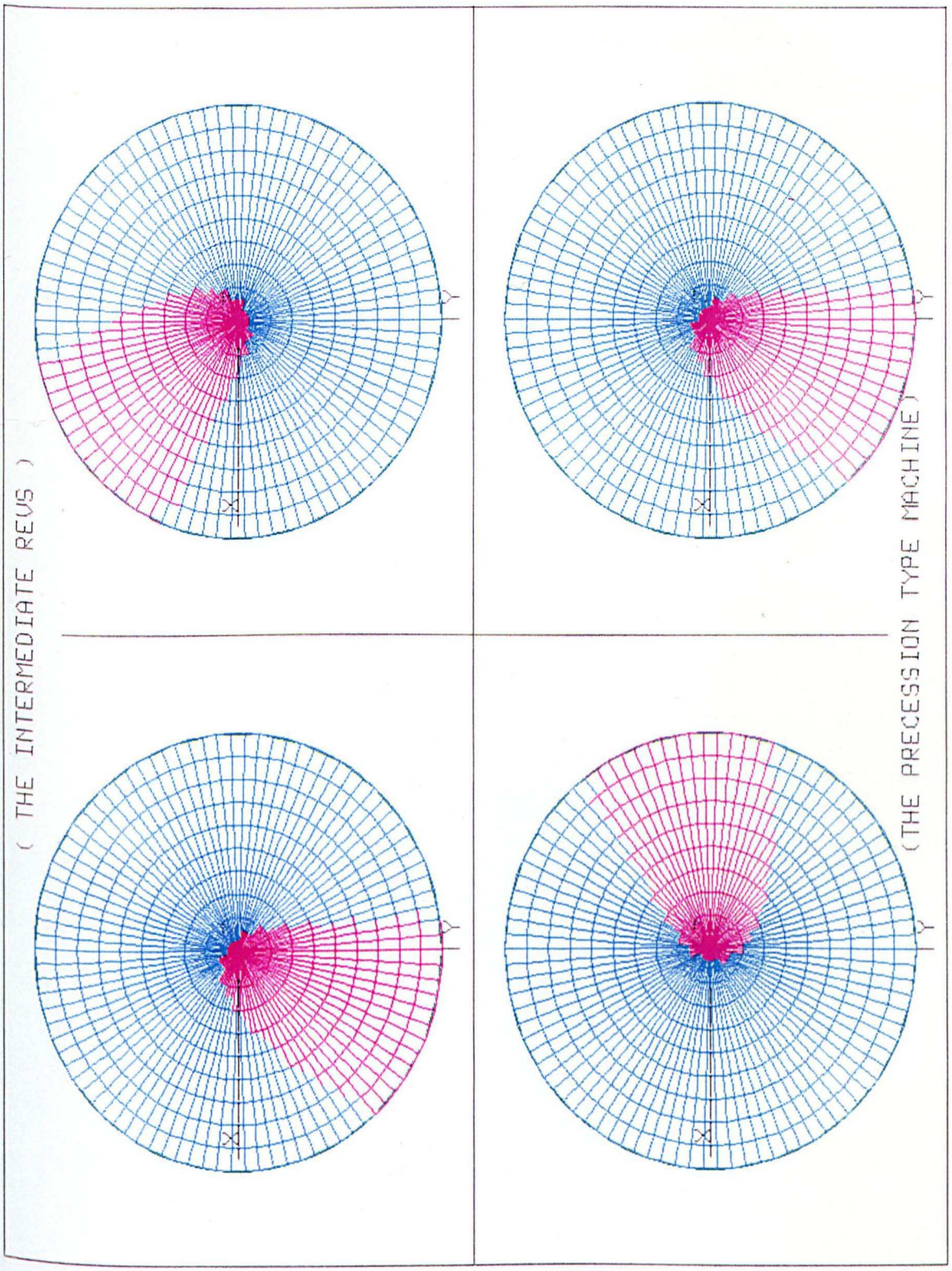

Fig. 5.9.c.

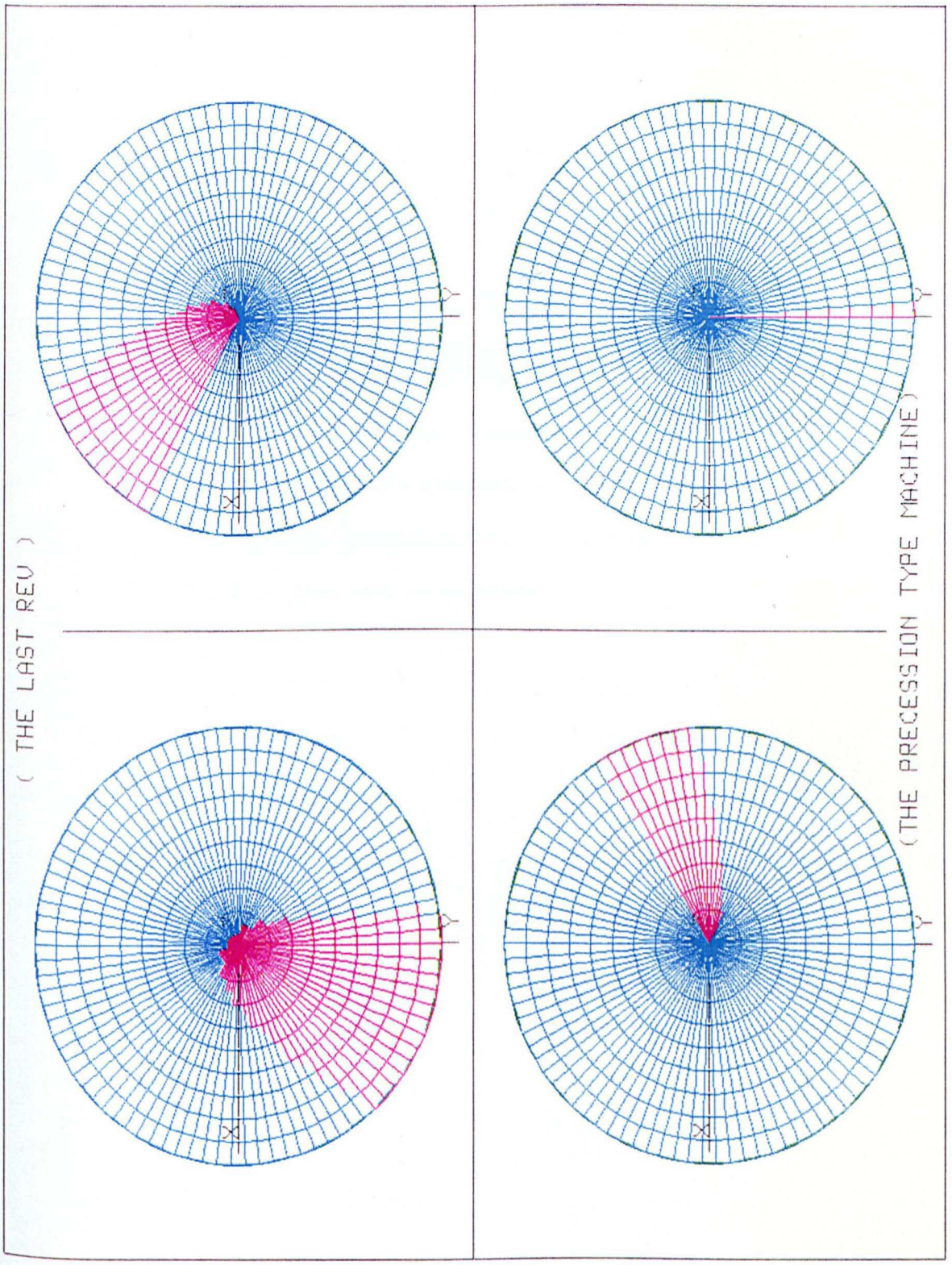

Fig. 5.10 Illustration of a workpiece being deformed by an imaginary inclined tool

(Tool motion: Precession)

5.10.a. The first revolution

5.10.b. One intermediated revolution

5.10.c. The last revolution

Fig. 5.1Q.a.

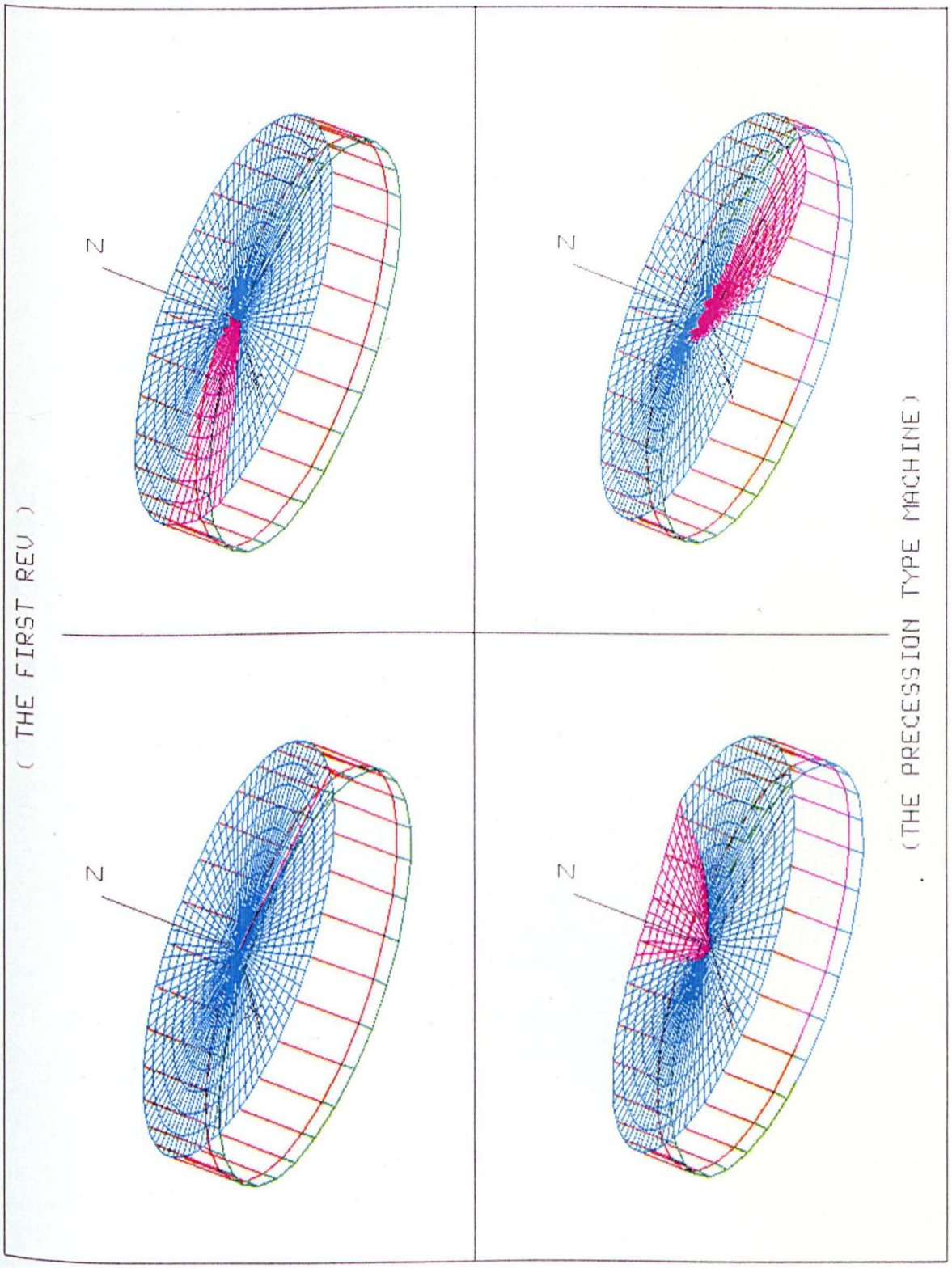

Fig. 5.10.b.

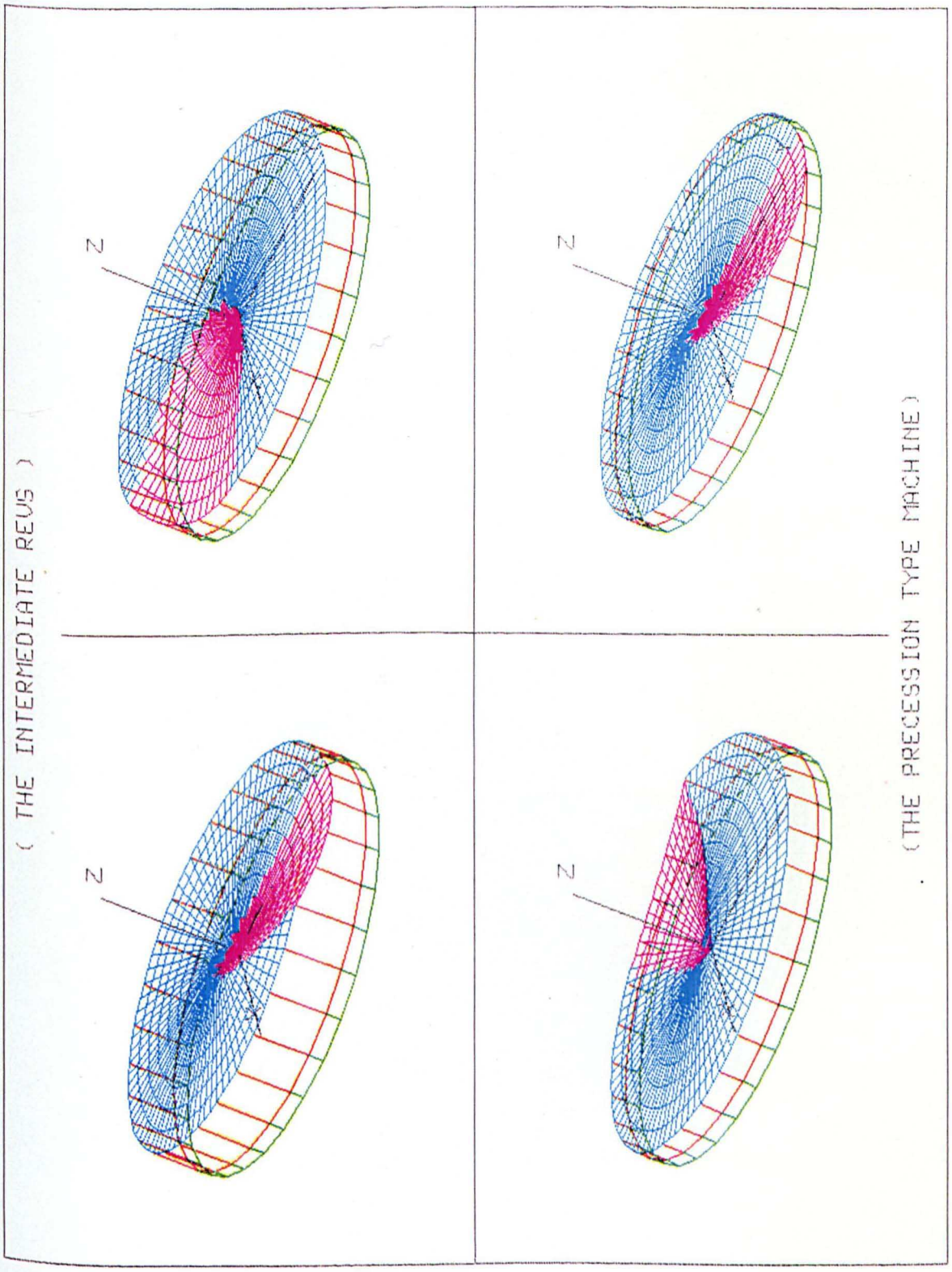

Fig. 5.10.c.

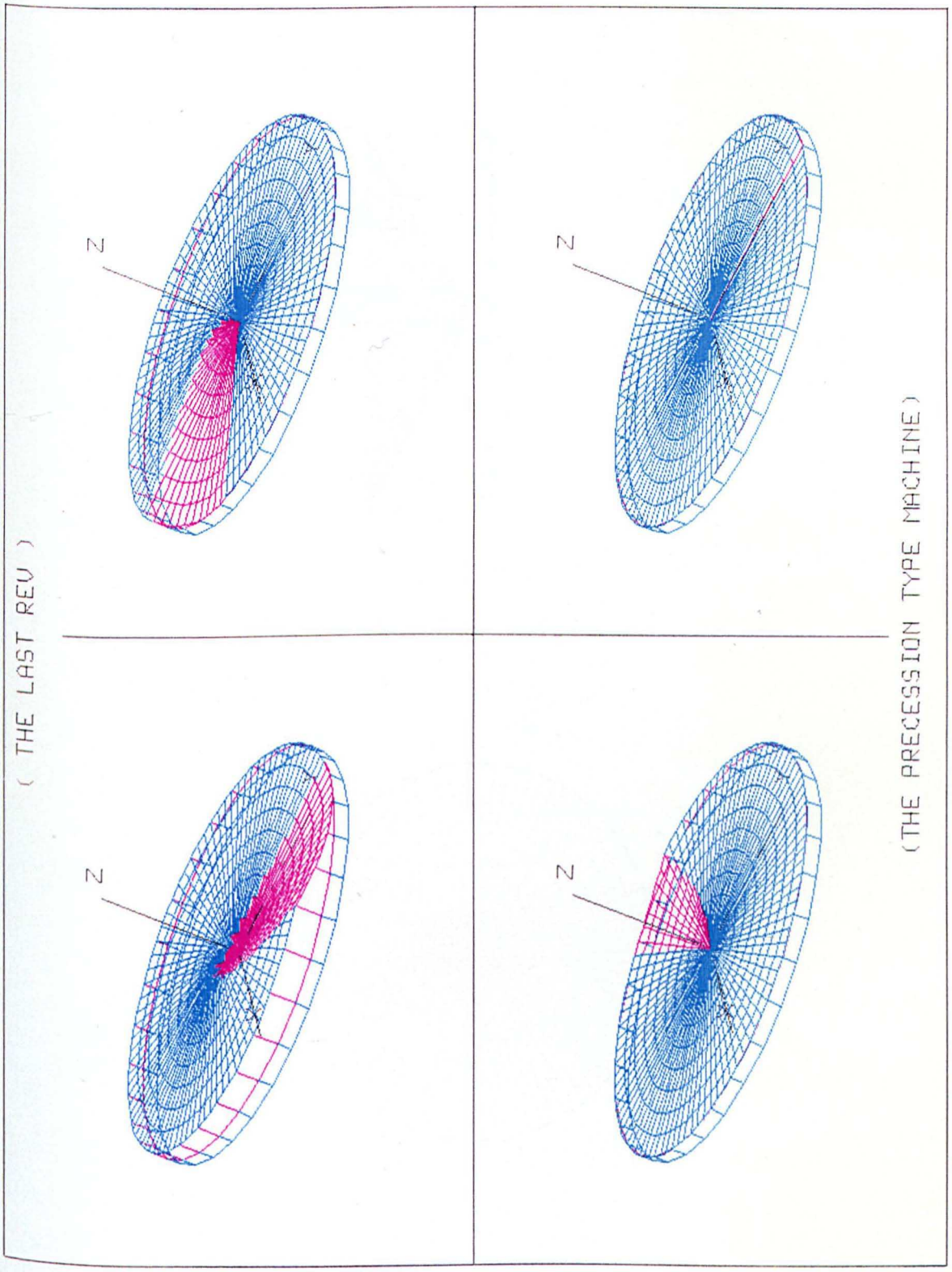

Fig. 5.11 Illustration of a non-constant volume workpiece, in a uni-axial axisymmetric compression

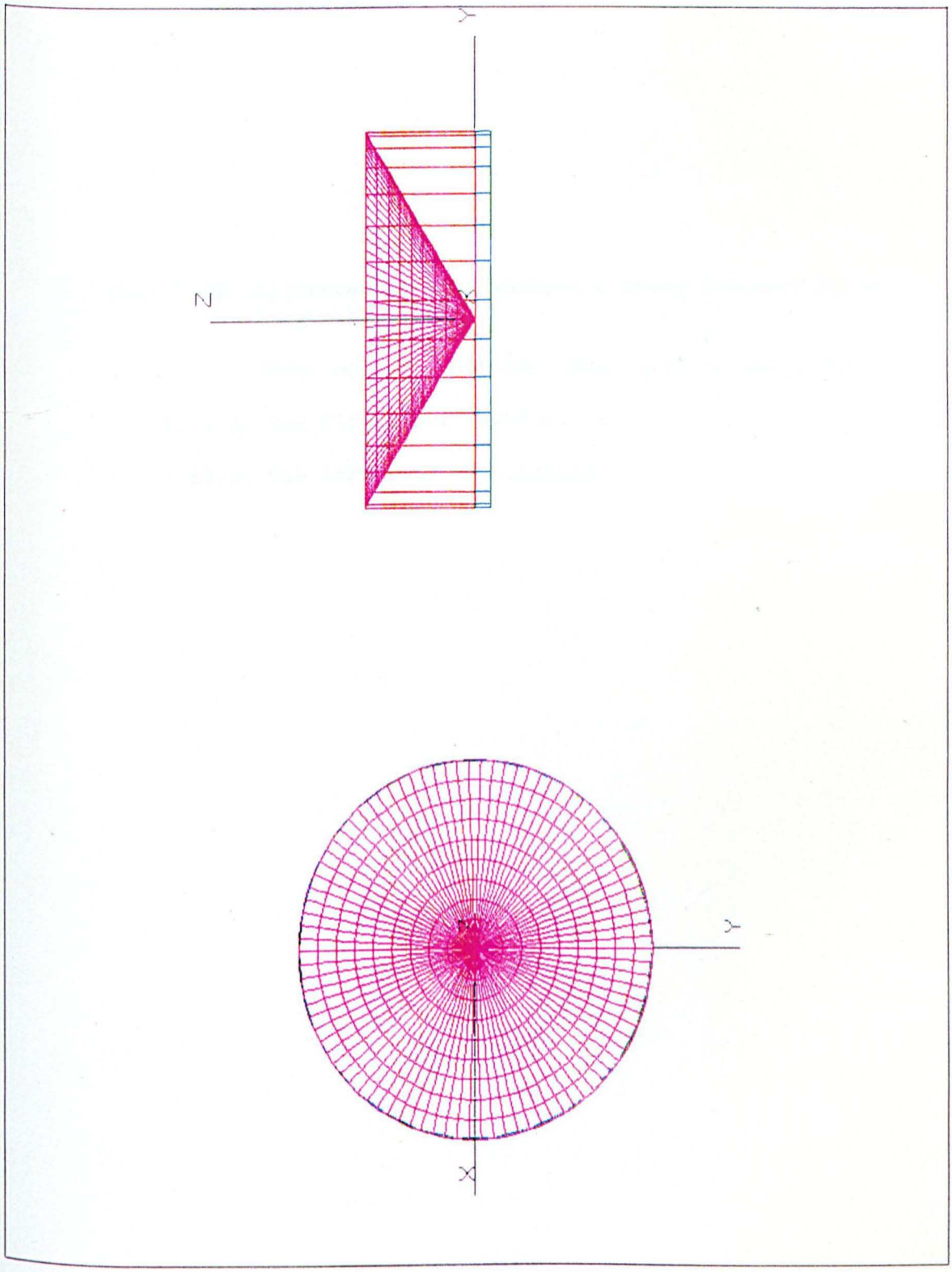

Fig. 5.12 Illustration of a workpiece being deformed by an imaginary tool

(Tool motion: Nutation-Spin with no axial feed)

5.12.a. The first four revolutions

5.12.b. The last four revolutions

Fig. 5.12.a.

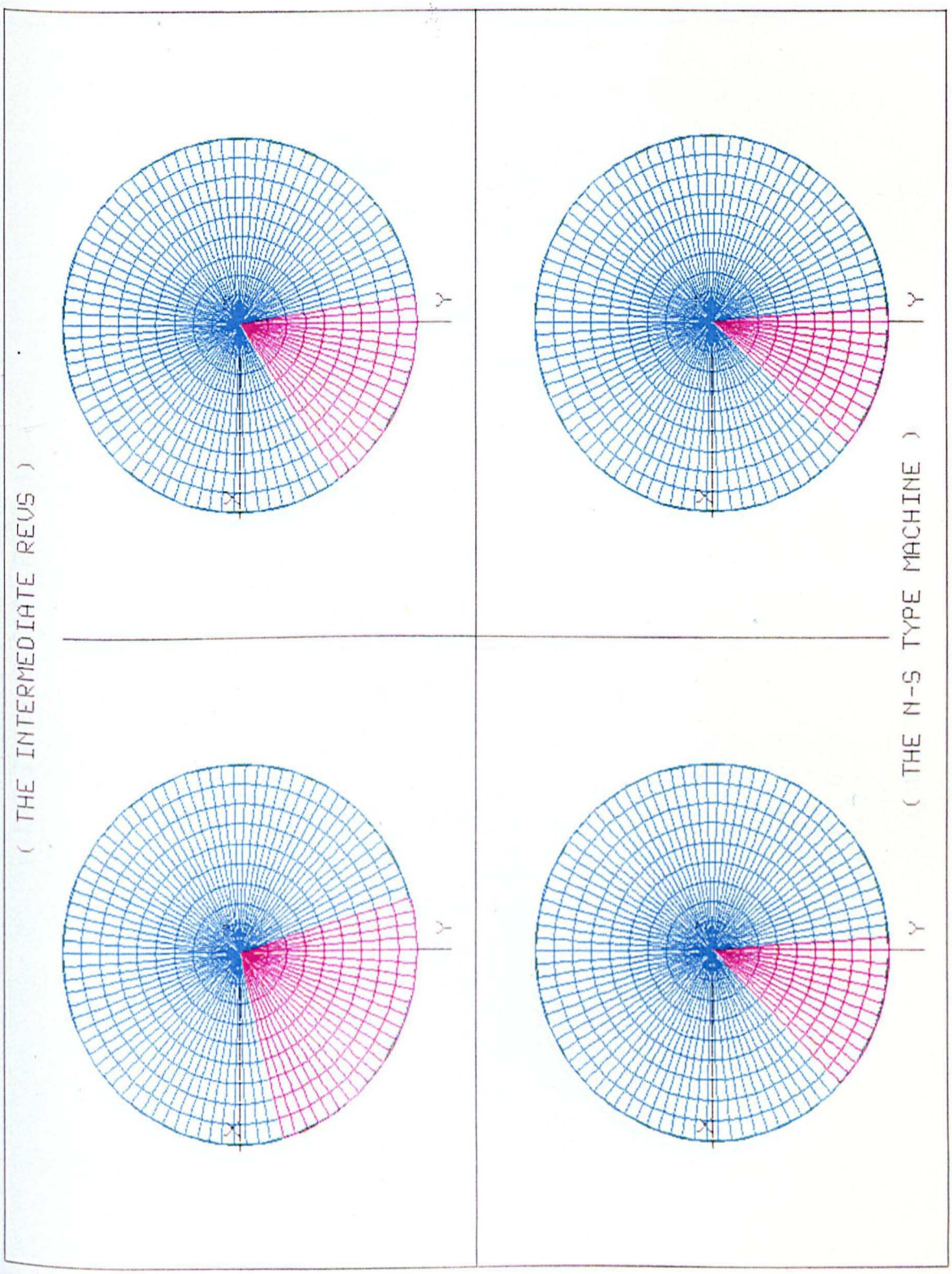

Fig. 5.12.b.

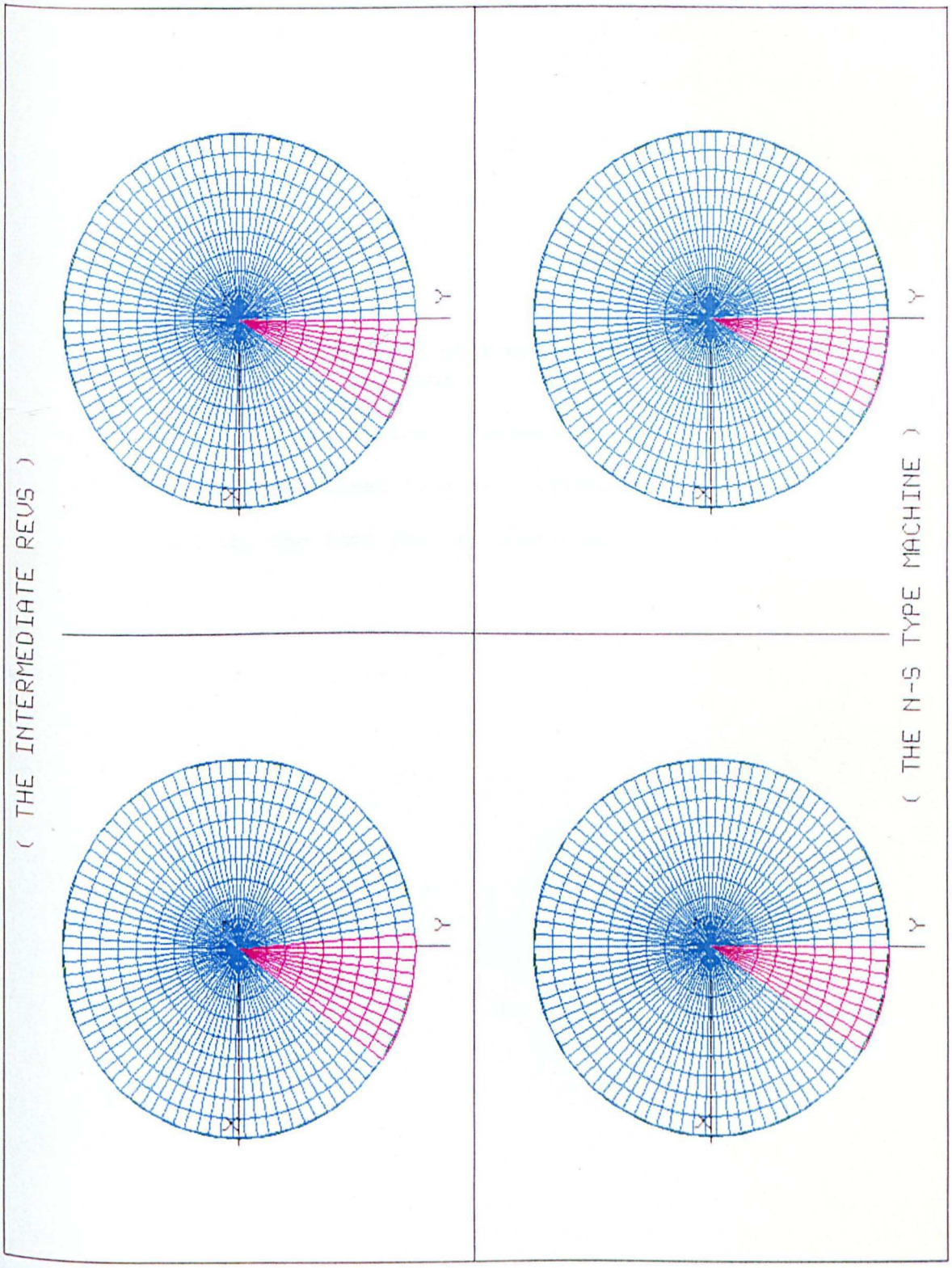

Fig. 5.13 Illustration of a workpiece being deformed by an imaginary tool

(Tool motion: Nutation-Spin with no axial feed

5.13.a. The first four revolutions

5.13.b. The last four revolutions

Fig. 5.13.a.

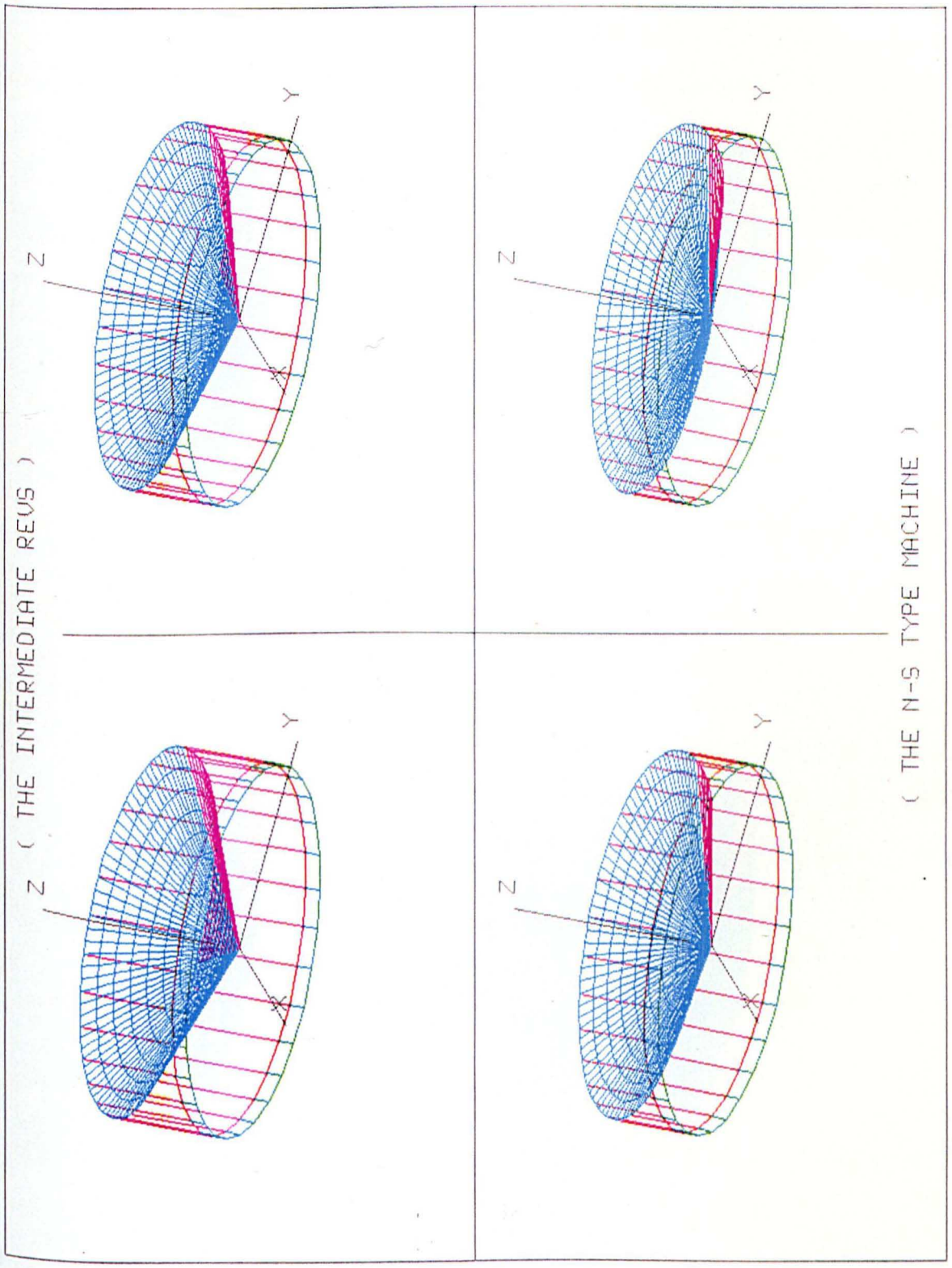

Fig. 5.13.b.

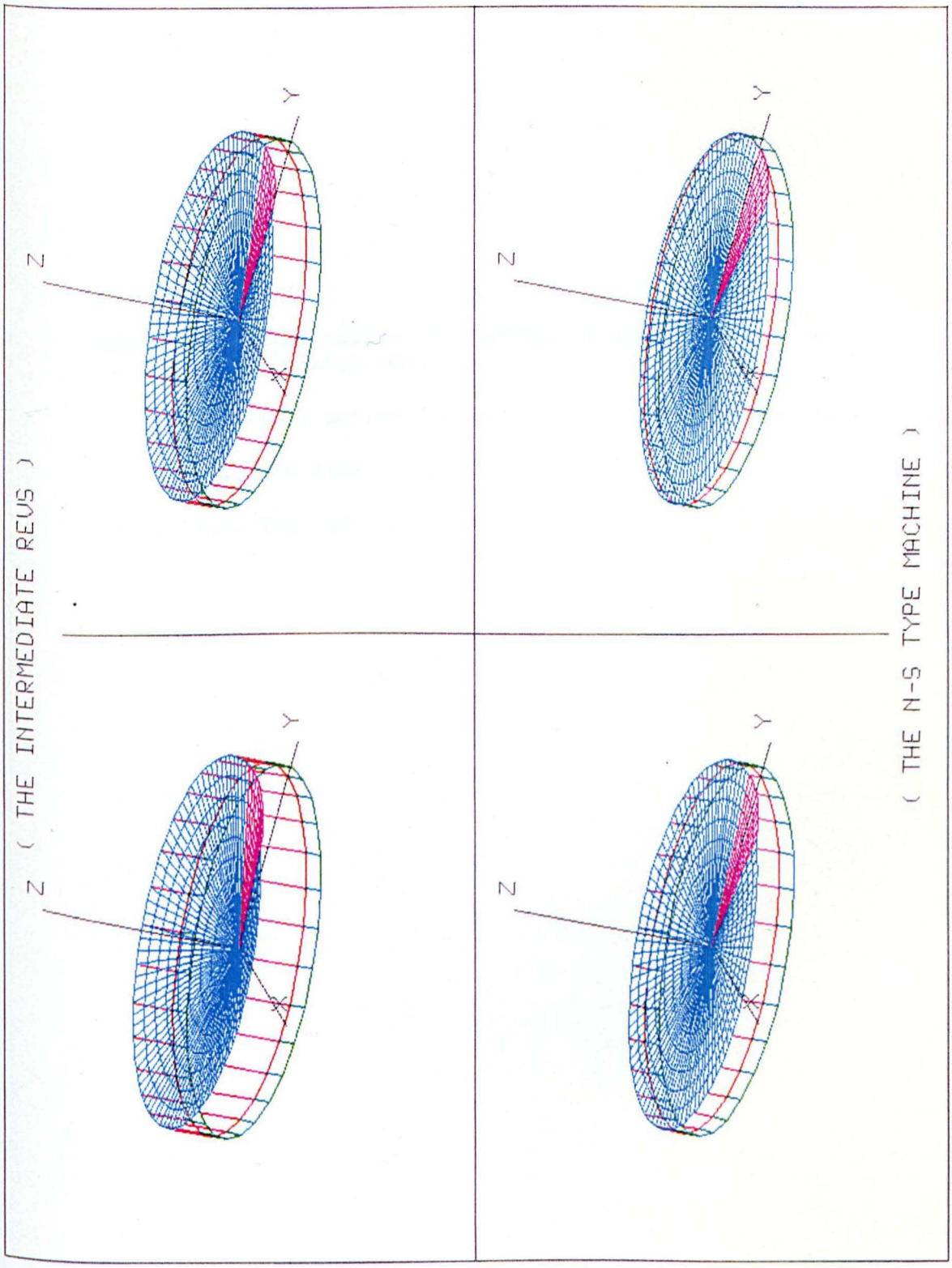

Fig. 5.14. Illustration of a workpiece being deformed by an imaginary tool

(Tool motion: Nutation-Spin with constant axial feed)

5.14.a. The first four revolutions

5.14.b. The last four revolutions

Fig. 5.14.a.

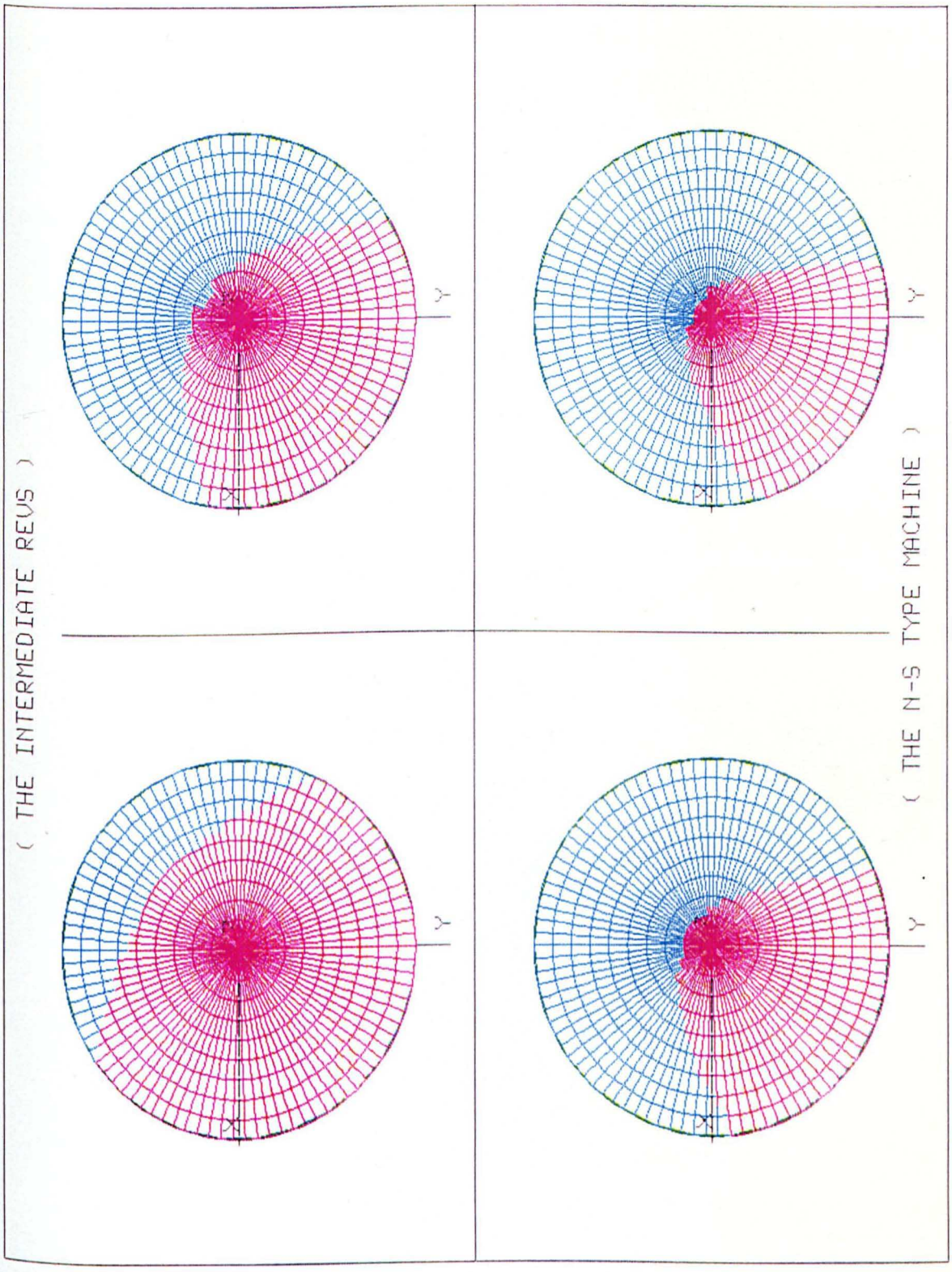

Fig. 5.14.b.

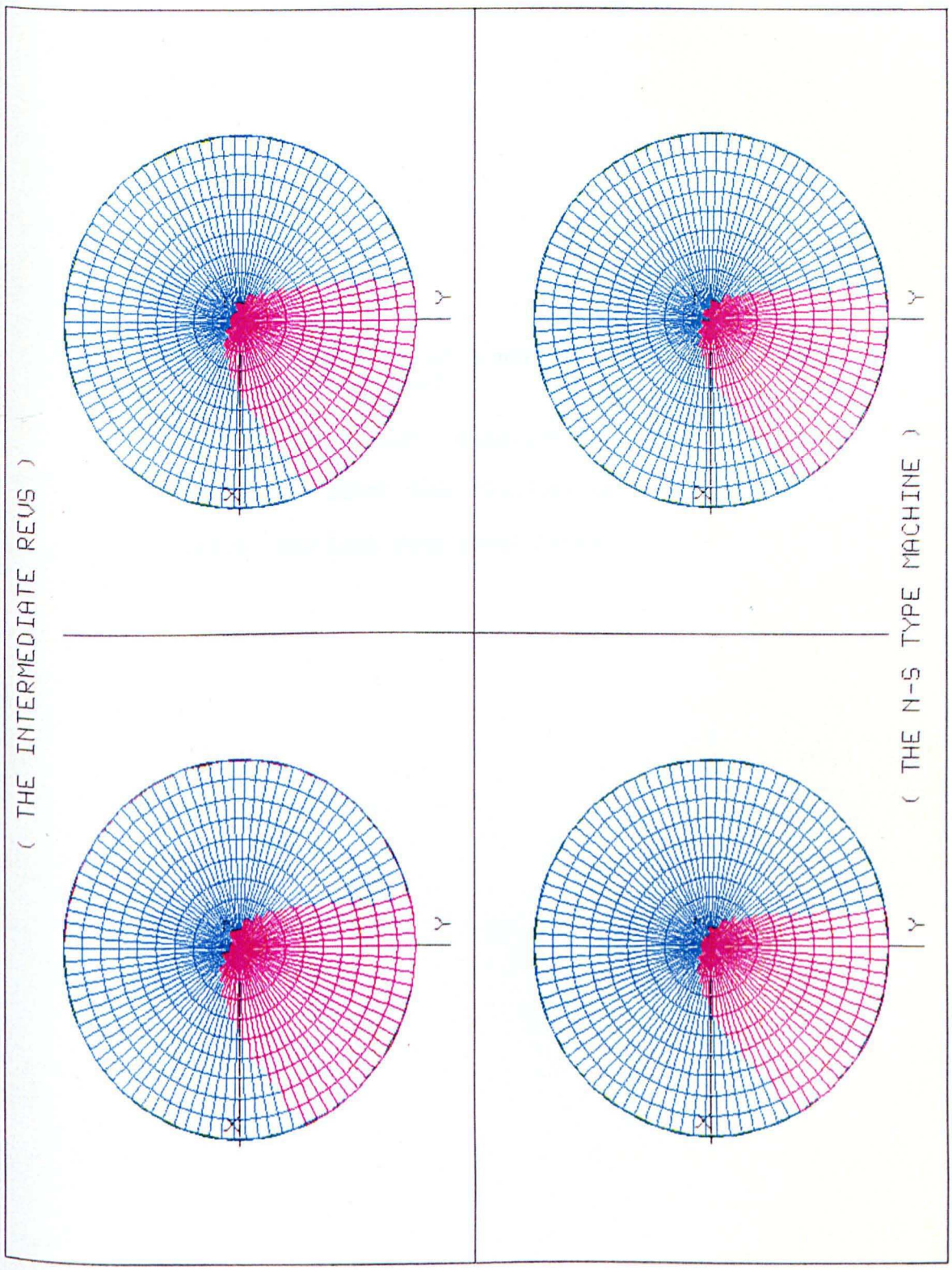

Fig. 5.15. Illustration of a workpiece being deformed by an imaginary tool

(Tool motion: Nutation-Spin with constant axial feed)

5.15.a. The first four revolutions

5.15.b. The last four revolutions

Fig. 5.15.a.

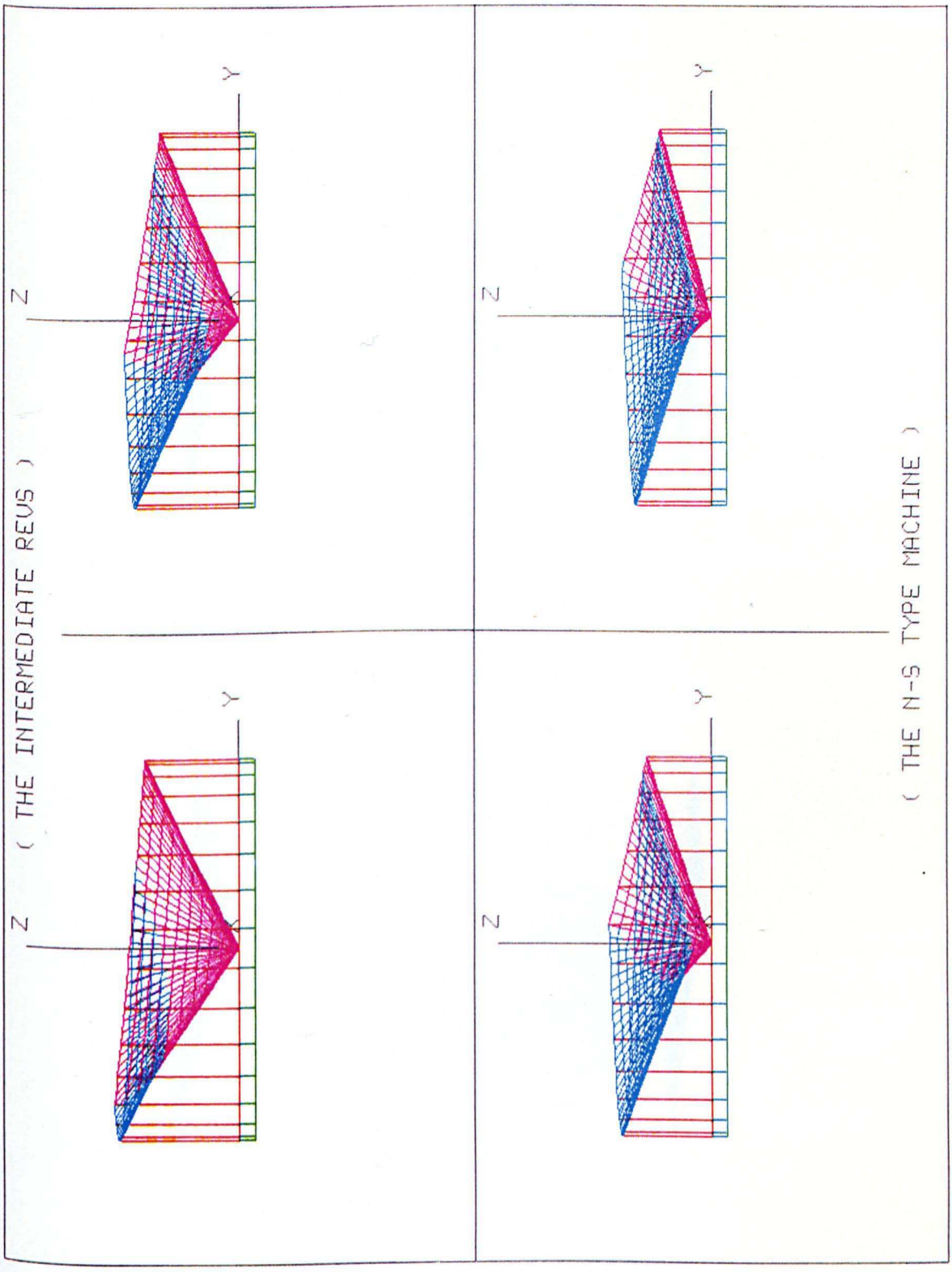

Fig. 5.15.b.

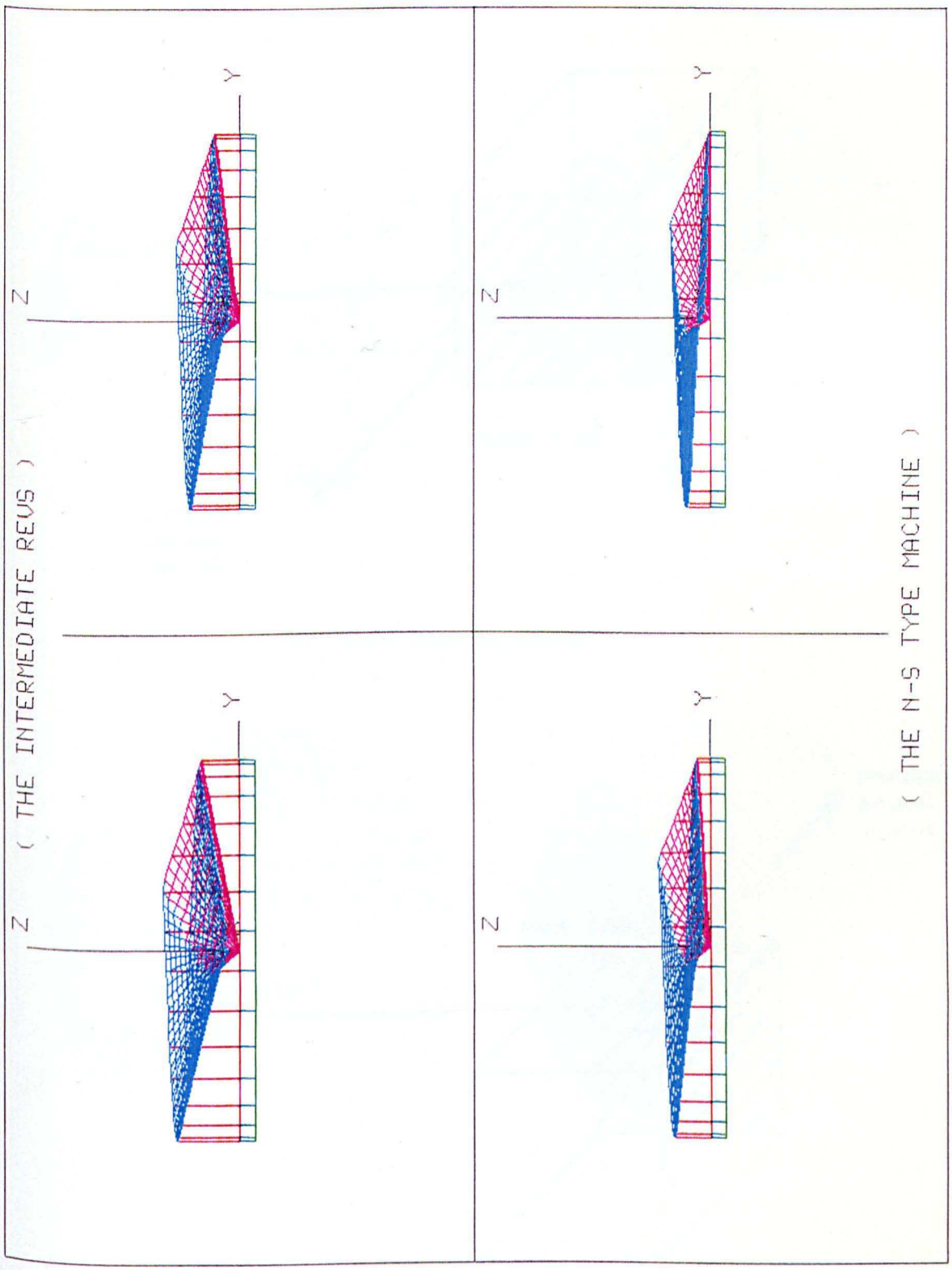

Fig. 5.16 The visibility test based on angle between line of sight and surface normal vector

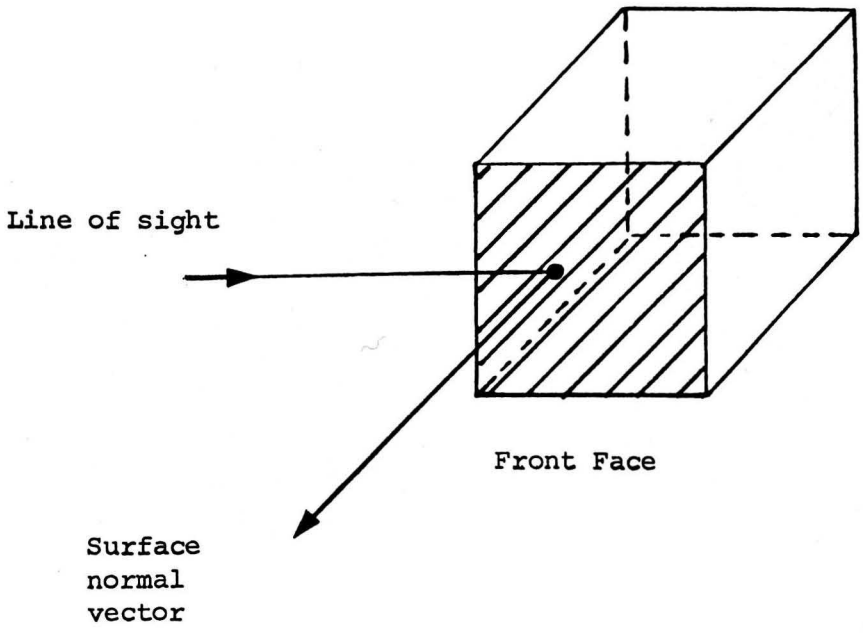

(a) Less than 90 degrees

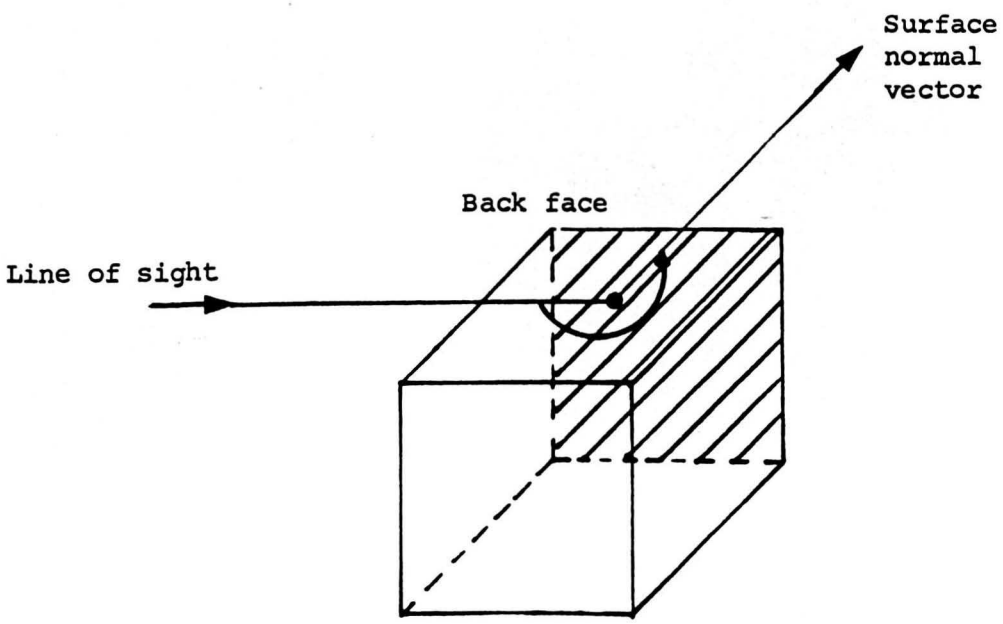

(b) Greater than 90 degrees

Fig. 5.17 Surface illustration of a workpiece being deformed by an imaginary inclined tool

(Tool motion: Precession)

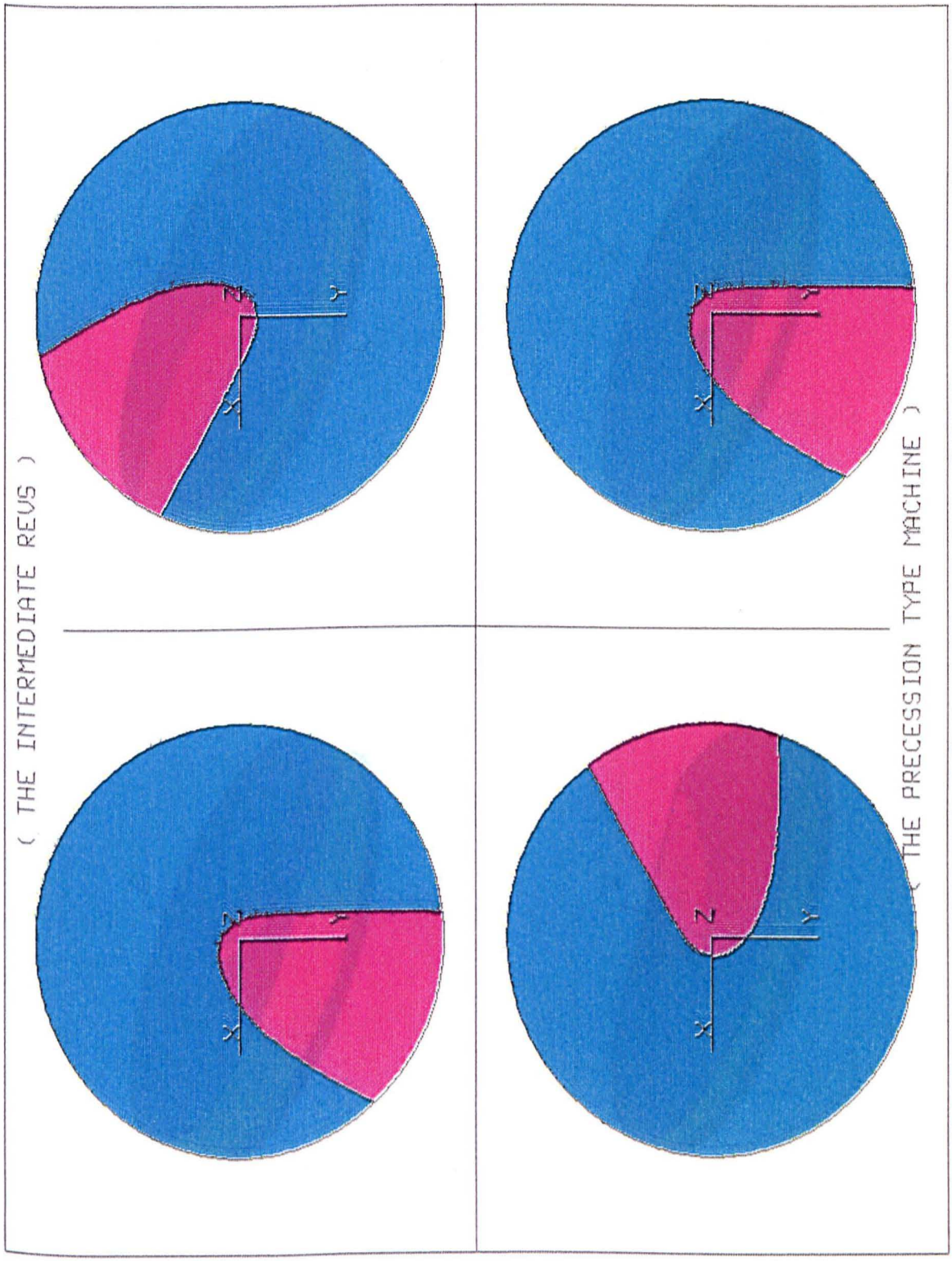

Fig. 5.18 Surface illustration of a workpiece being deformed by an imaginary inclined tool
(Tool motion: Precession)

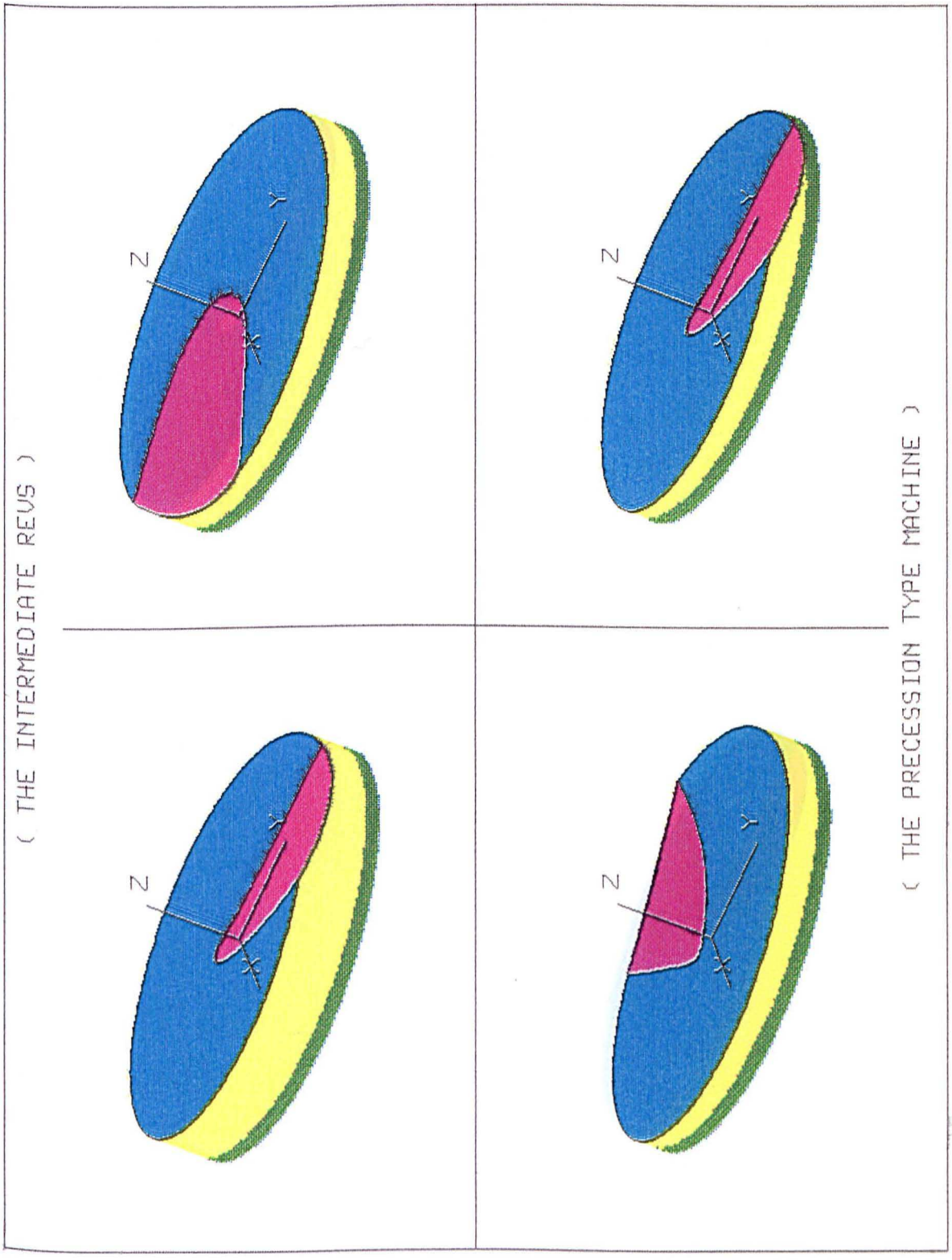

Fig. 5.19 Surface illustration of a workpiece being deformed by an imaginary inclined tool
(Tool motion: Spin)

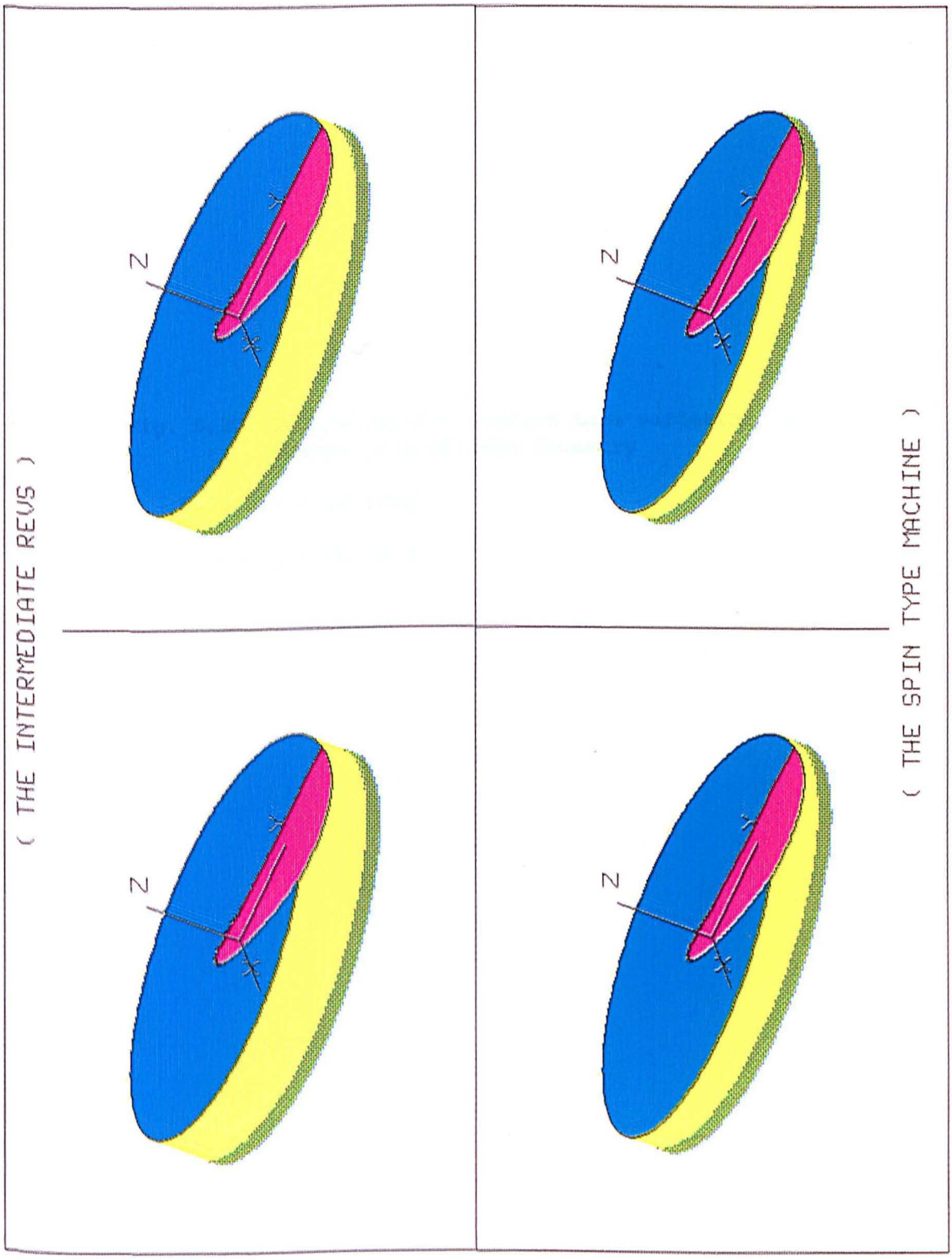

Fig. 5.20 Tool/workpiece contact zone variation, due to change in workpiece geometry

5.20.a. α = 10 (Deg)

5.20.b. α = 20 (Deg)

Fig. 5.20.a

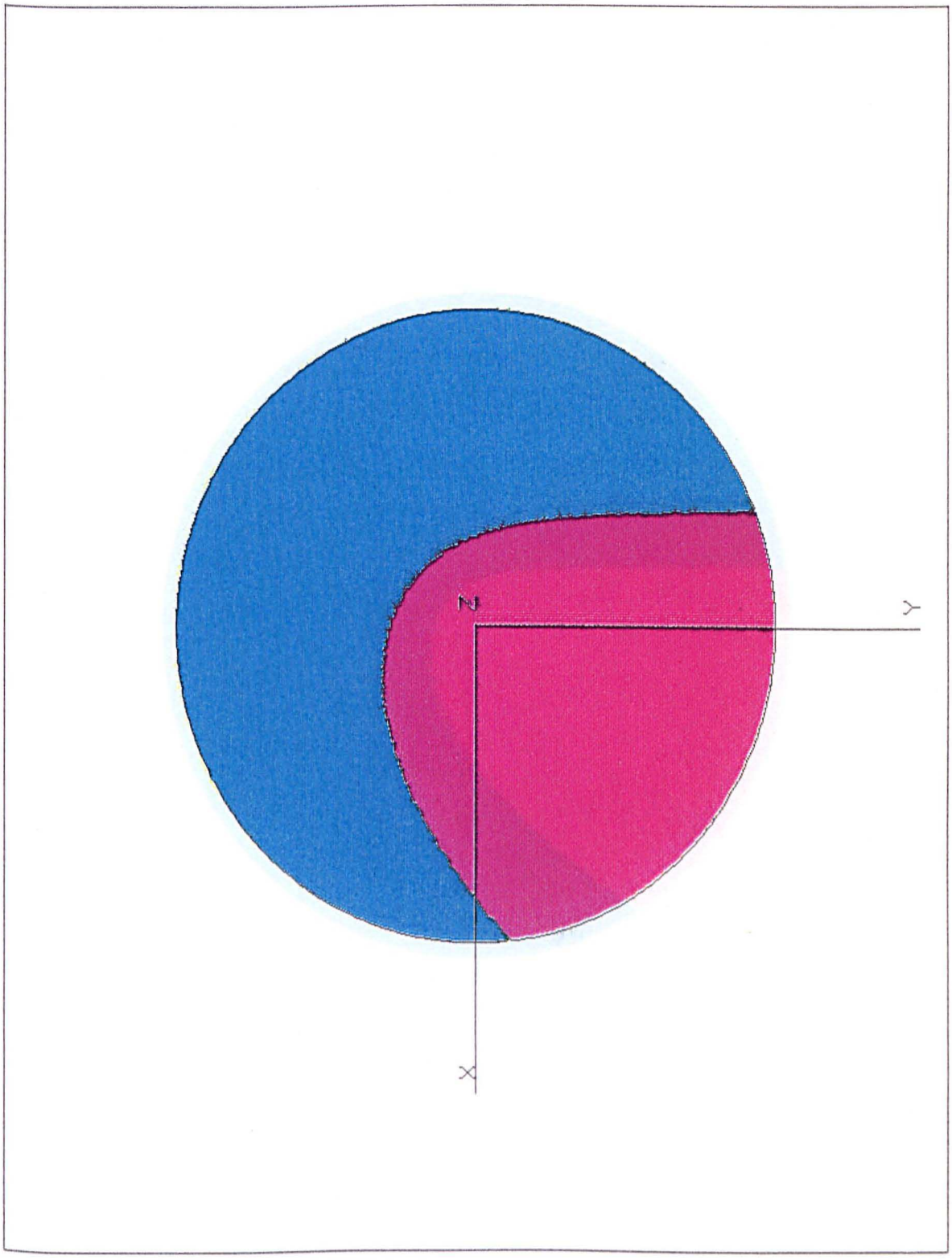

Fig. 5.20.b

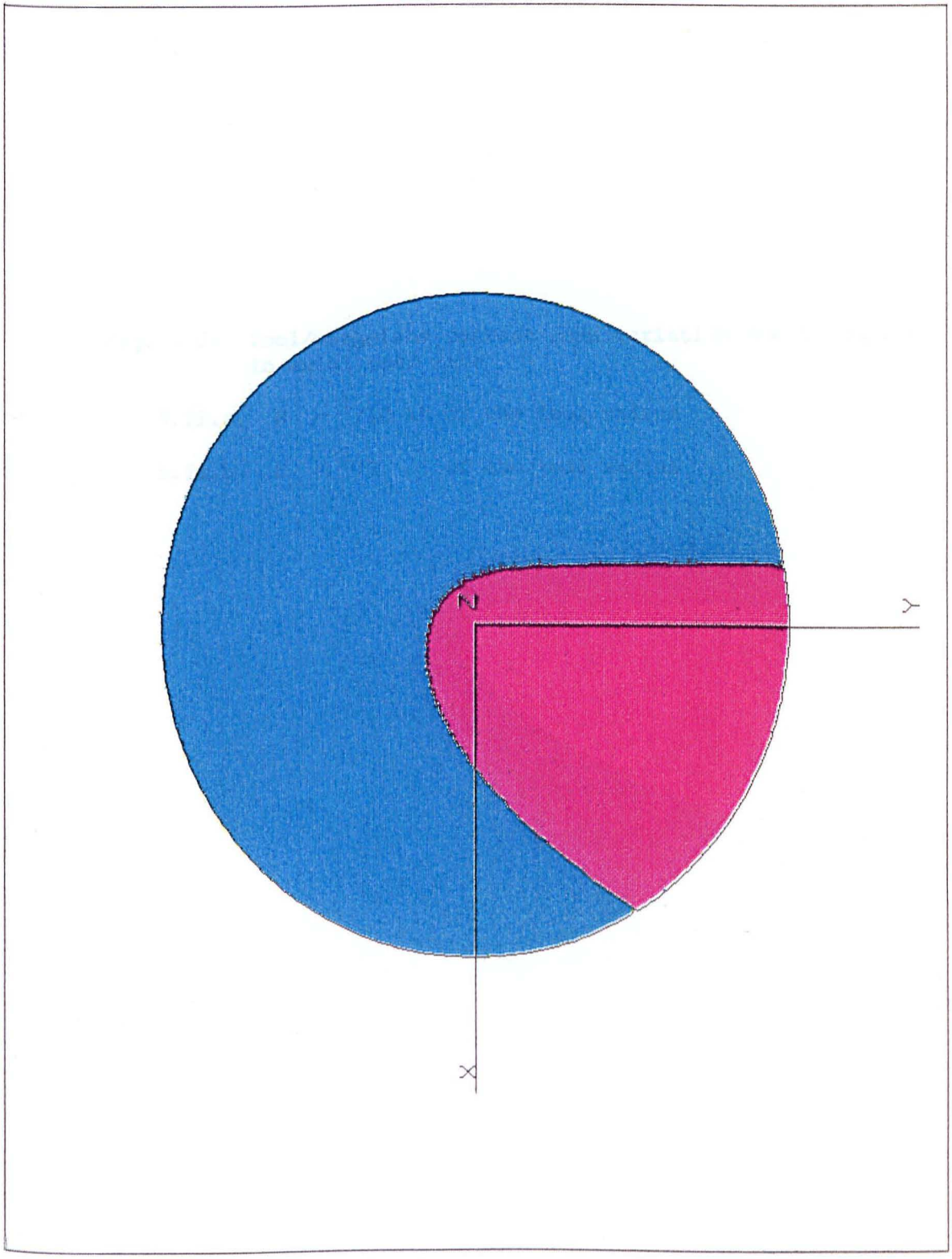

Fig. 5.21 Tool/workpiece contact zone variation due to change in axial feed rate

5.21.a. S = $^{1}/_{10}$ th of the tool radius

5.21.b. S = $^{1}/_{2}$ of the tool radius

Fig. 5.21.a

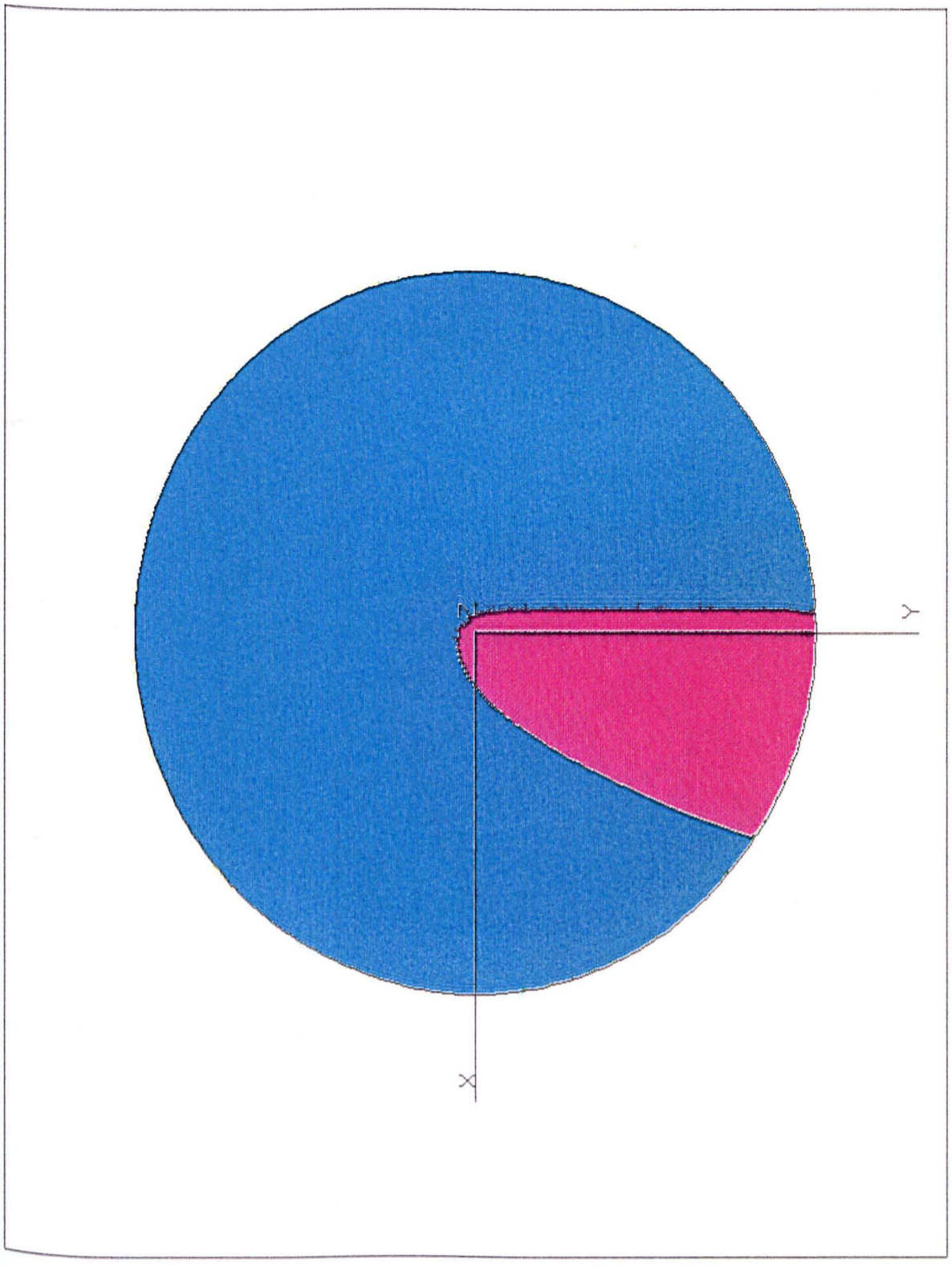

Fig. 5.21.b

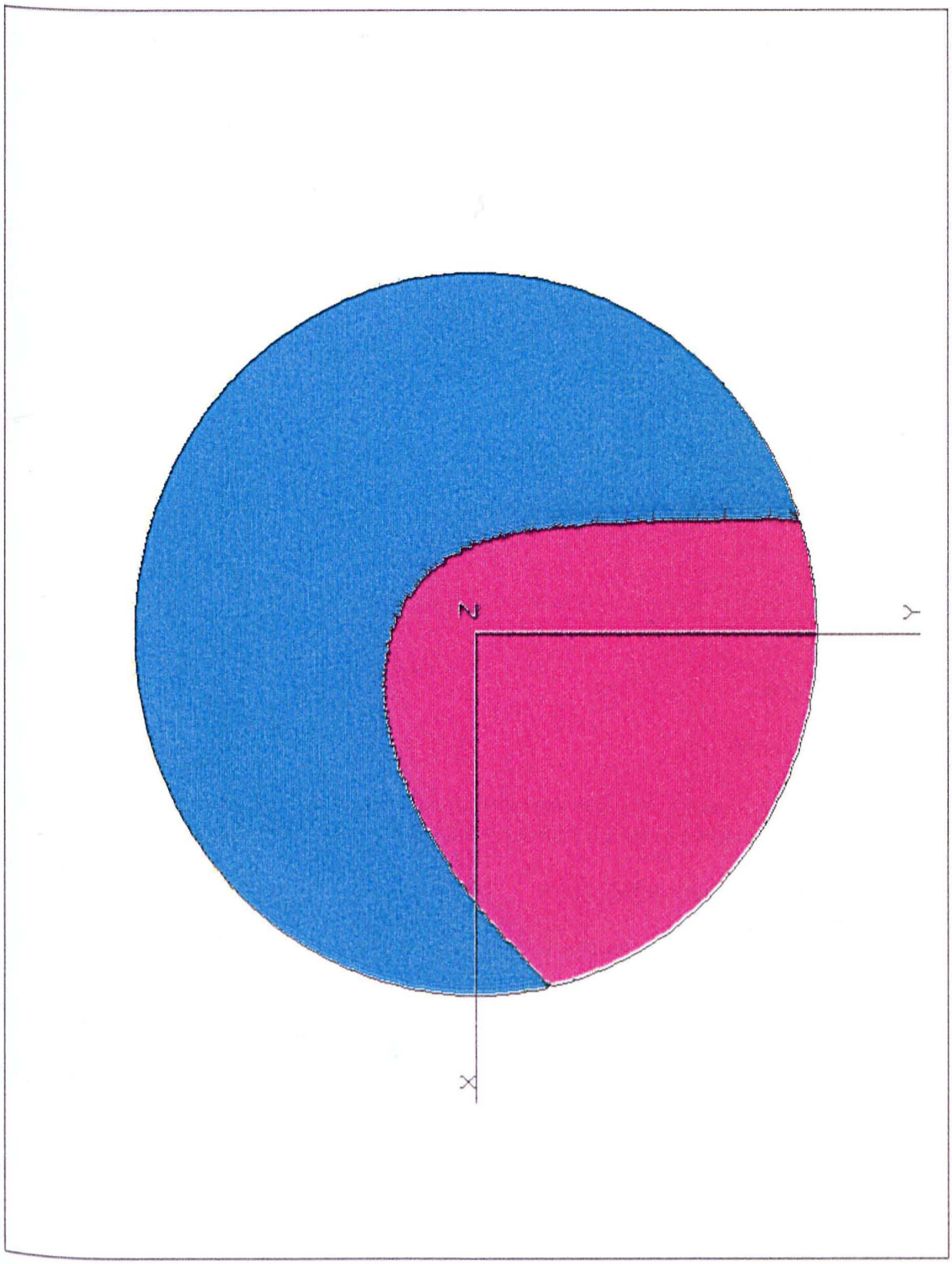

Fig. 6.1 The cross-section of a formed billet. The ICA is divided into a number of macro-blocks

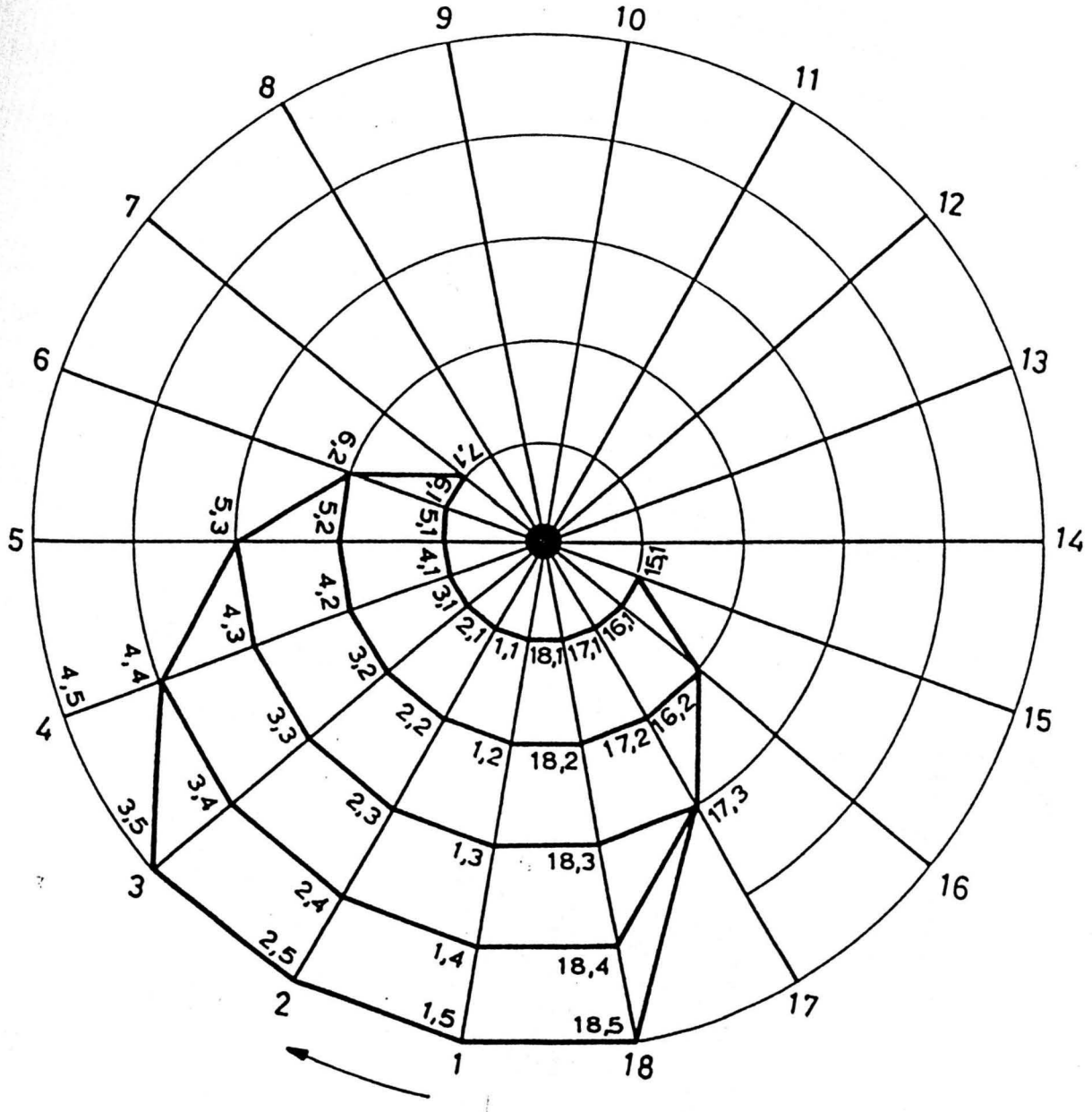

Fig. 6.2. A flow chart diagram for mesh generation within the Instantaneous Contact Area (ICA)

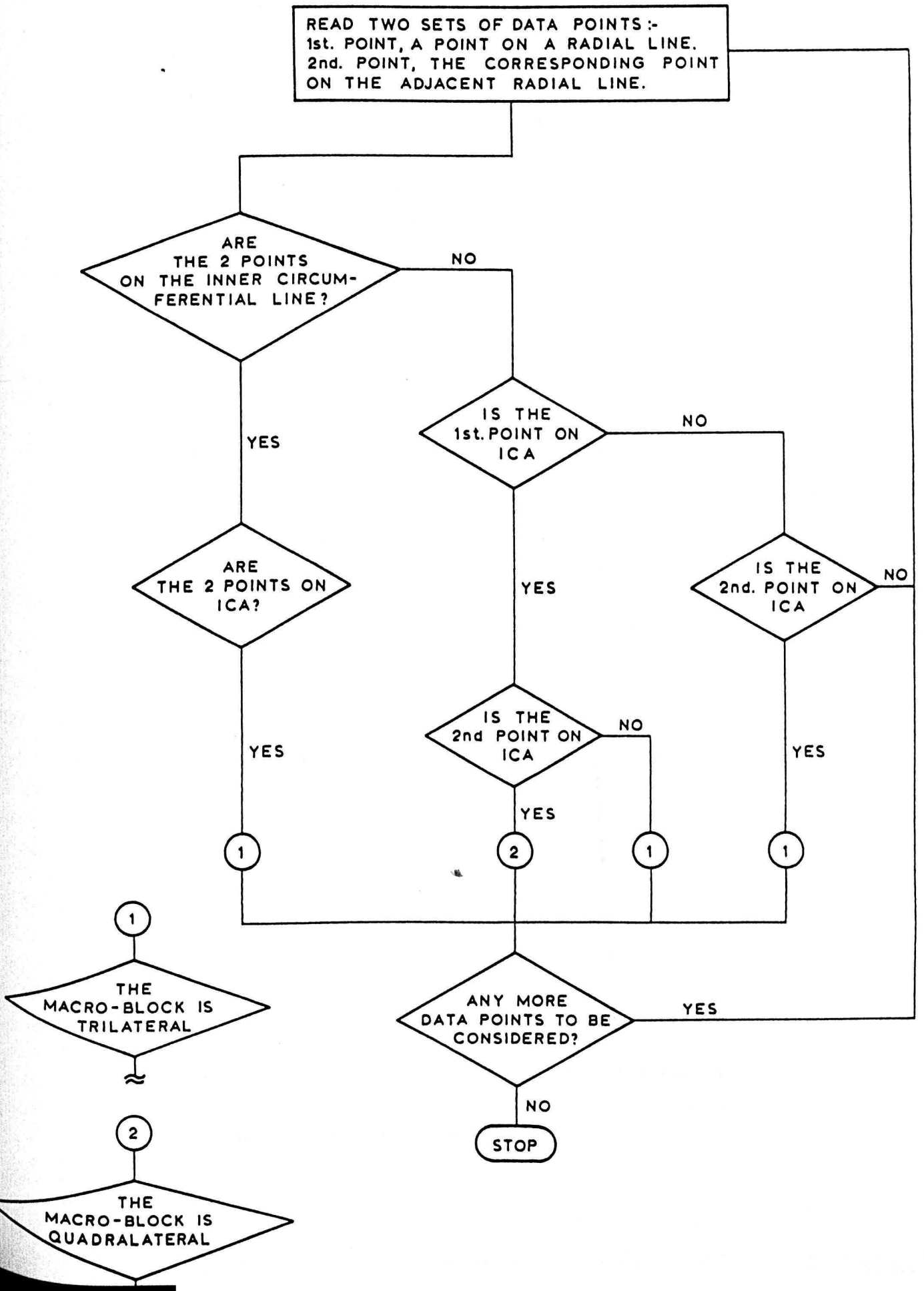

Fig. 6.3. The geometry of the macro-blocks, and the order in which data co-ordinates, are employed for surface area calculation

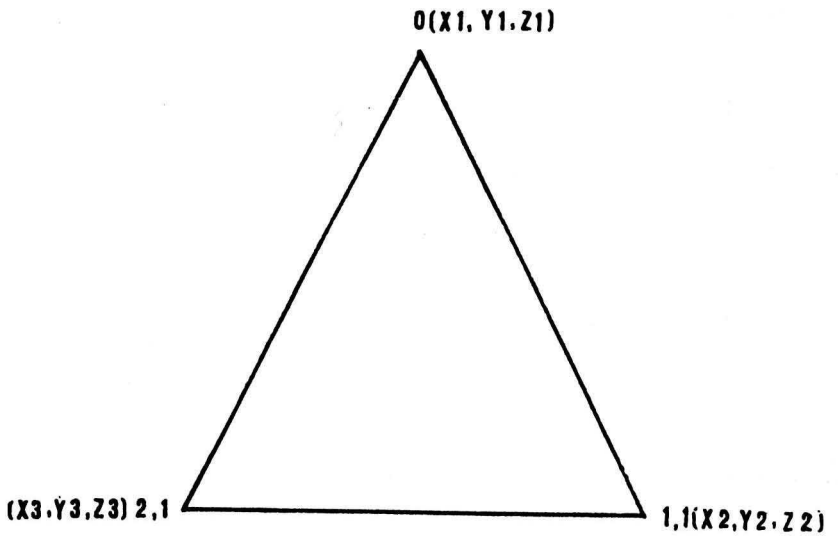

(a) Trilateral macro-block

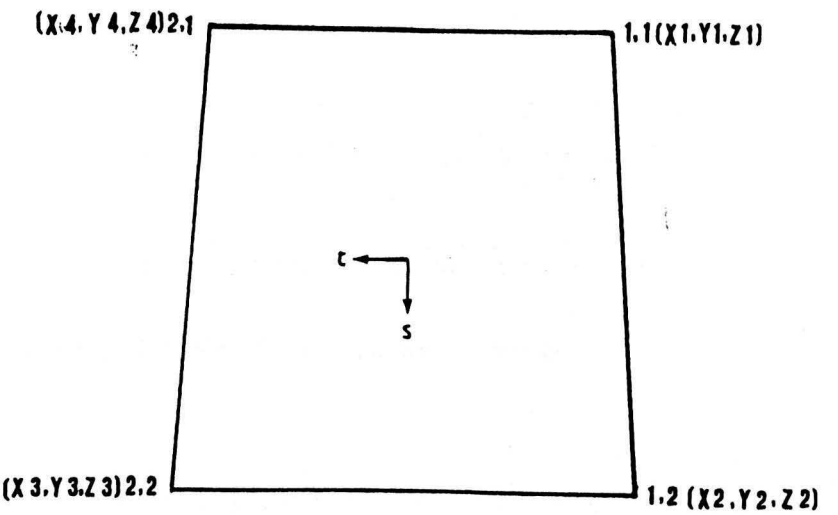

(b) Quadrilateral macro-block

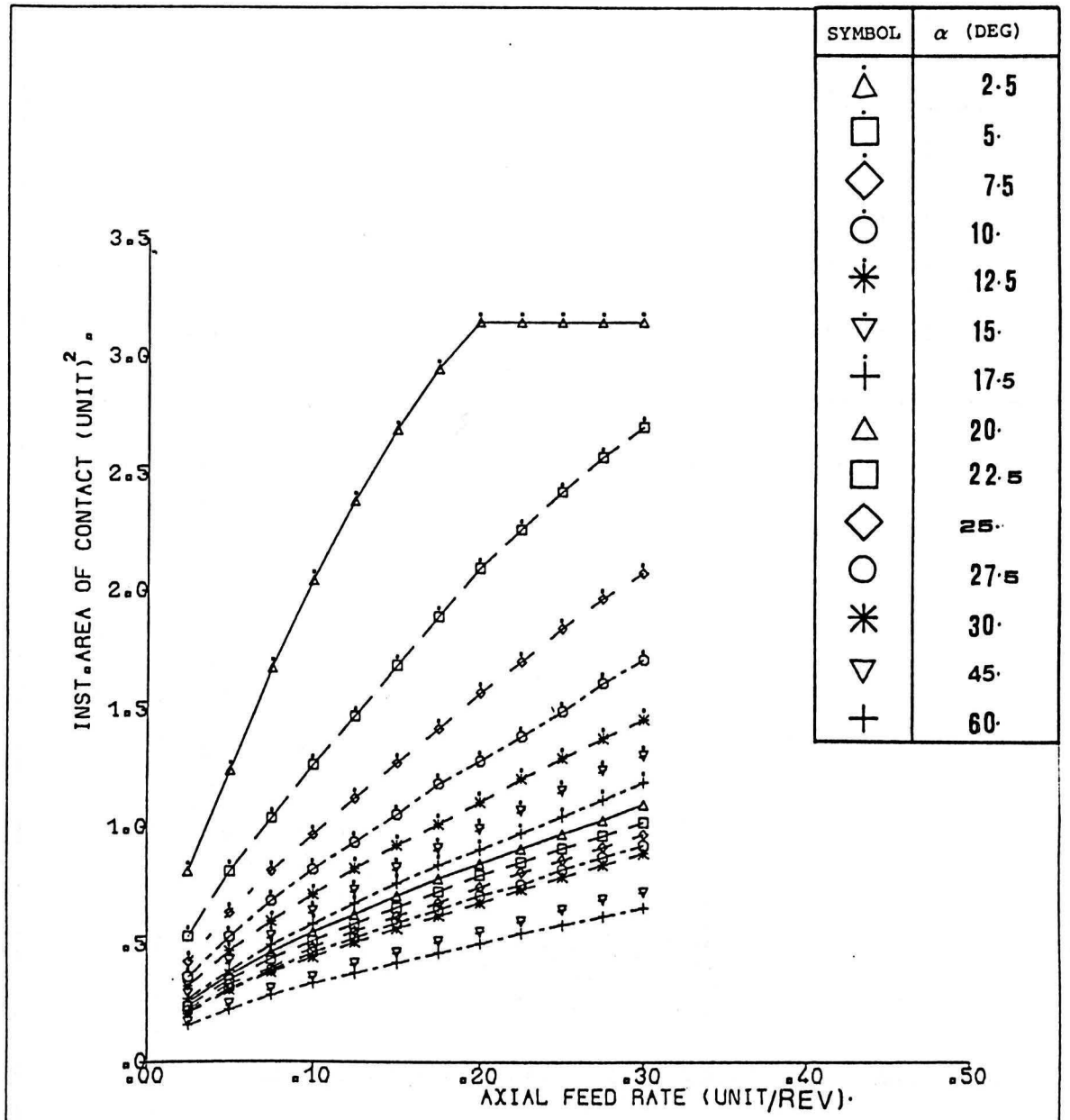

FIG.6.4.a.GRAPH OF INST.AREA OF CONTACT VS AXIAL FEED RATE FOR VARIOUS TOOL GEOMETRIES.

$'\theta = \alpha'$.

(TOOL MOTION : SPIN)

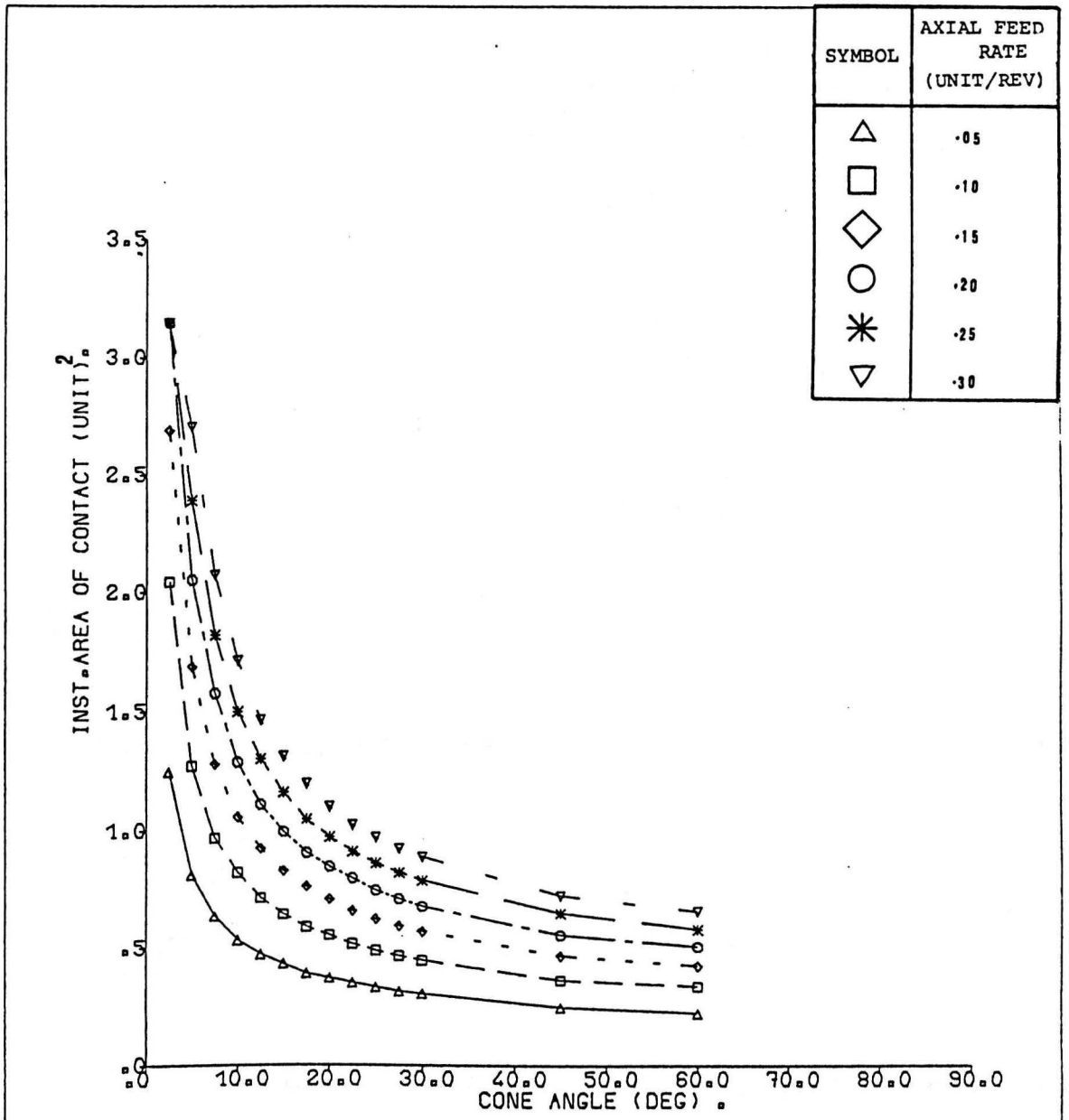

FIG.6.4.b.GRAPH OF INST.AREA OF CONTACT VS CONE ANGLE FOR VARIOUS AXIAL FEED RATES.

'$\theta = \alpha$'

(TOOL MOTION : SPIN)

DIAMETER (MM)	KUBO	FROGS
40	△	□
50	◇	○
70	✳	▽

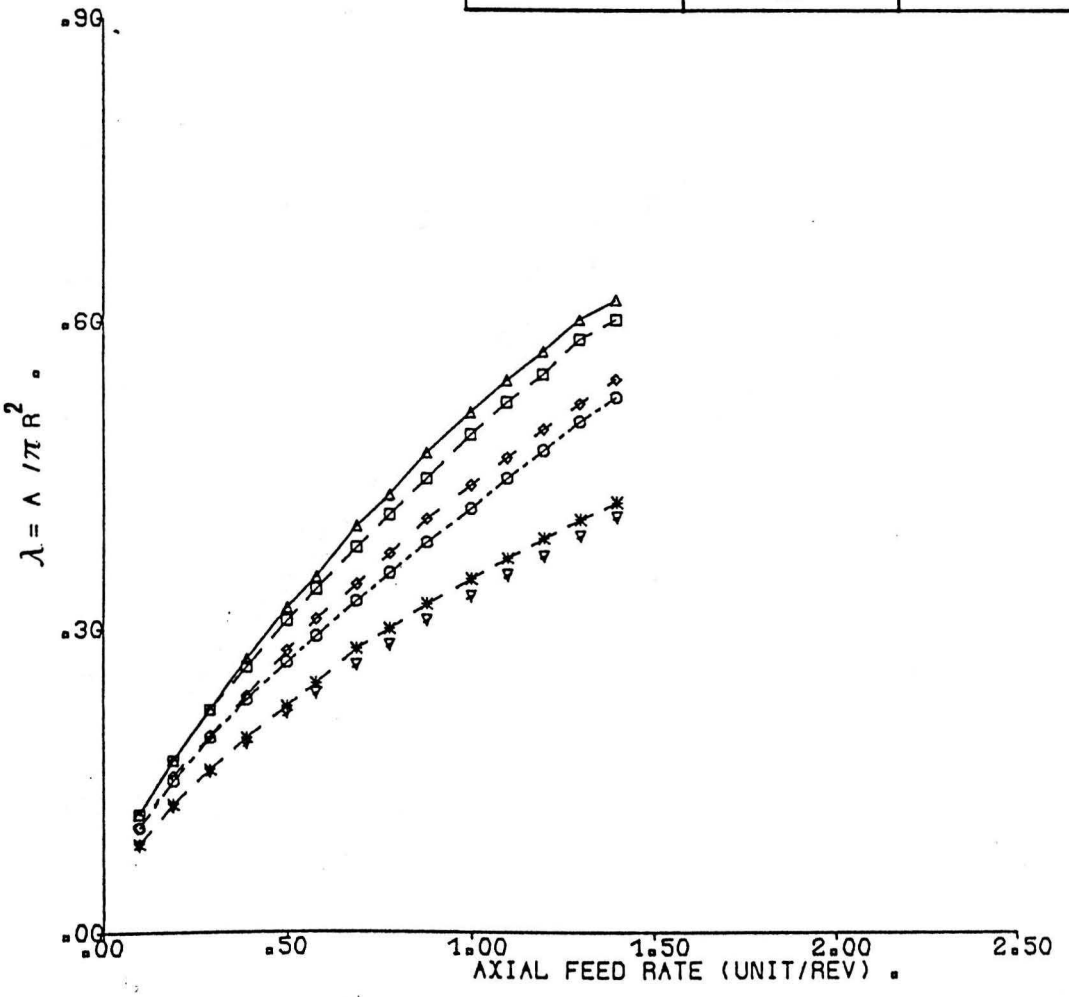

FIG.6.5.a.GRAPH OF COEFFICIENT 'λ' VS AXIAL FEED RATE FOR VARIOUS WORKPIECE DIAMETERS.

'$\theta = \alpha = 2$' (DEG) .

(TOOL MOTION : SPIN)

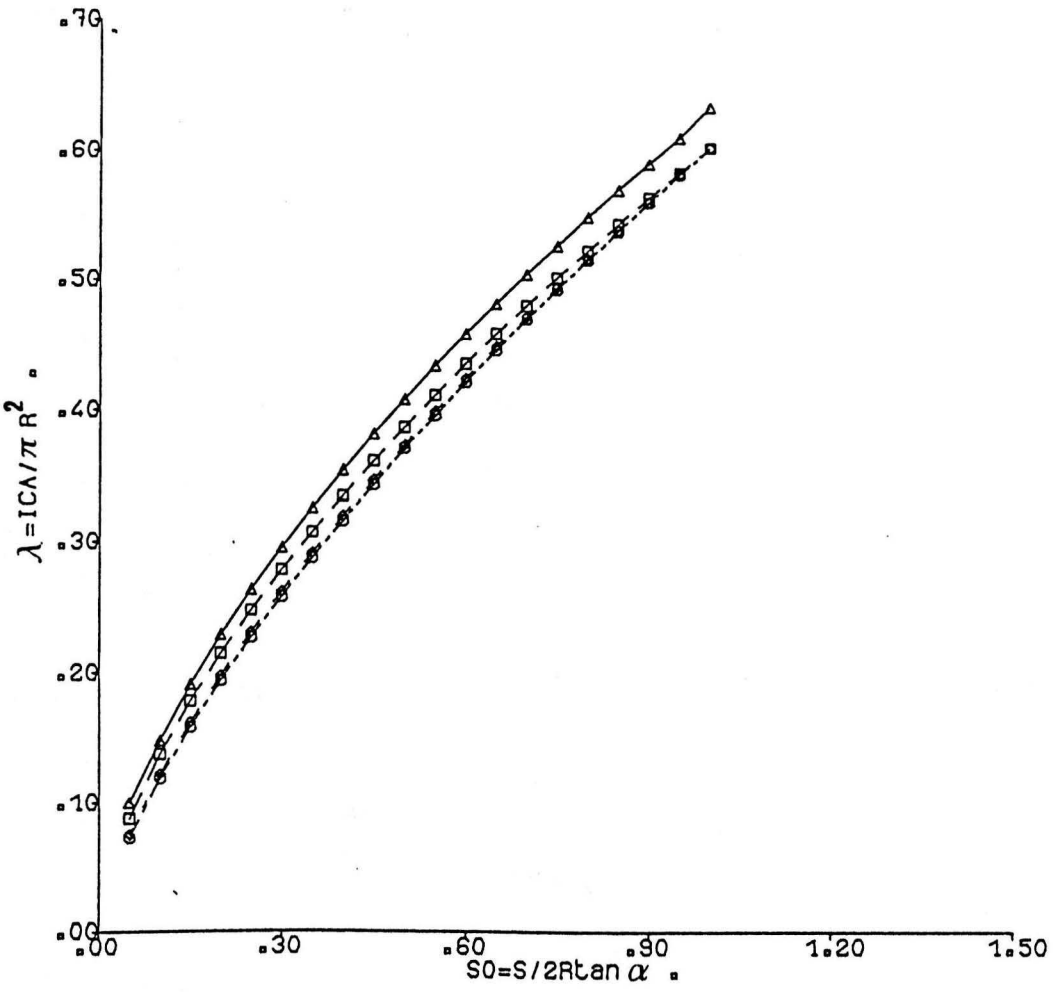

FIG.6.5.b.GRAPH OF COEFFICIENT 'λ' VS RELATIVE SPIRAL FEED FOR VARIOUS TOOL GEOMETRIES.

'$\theta=\alpha$'

(TOOL MOTION : SPIN)

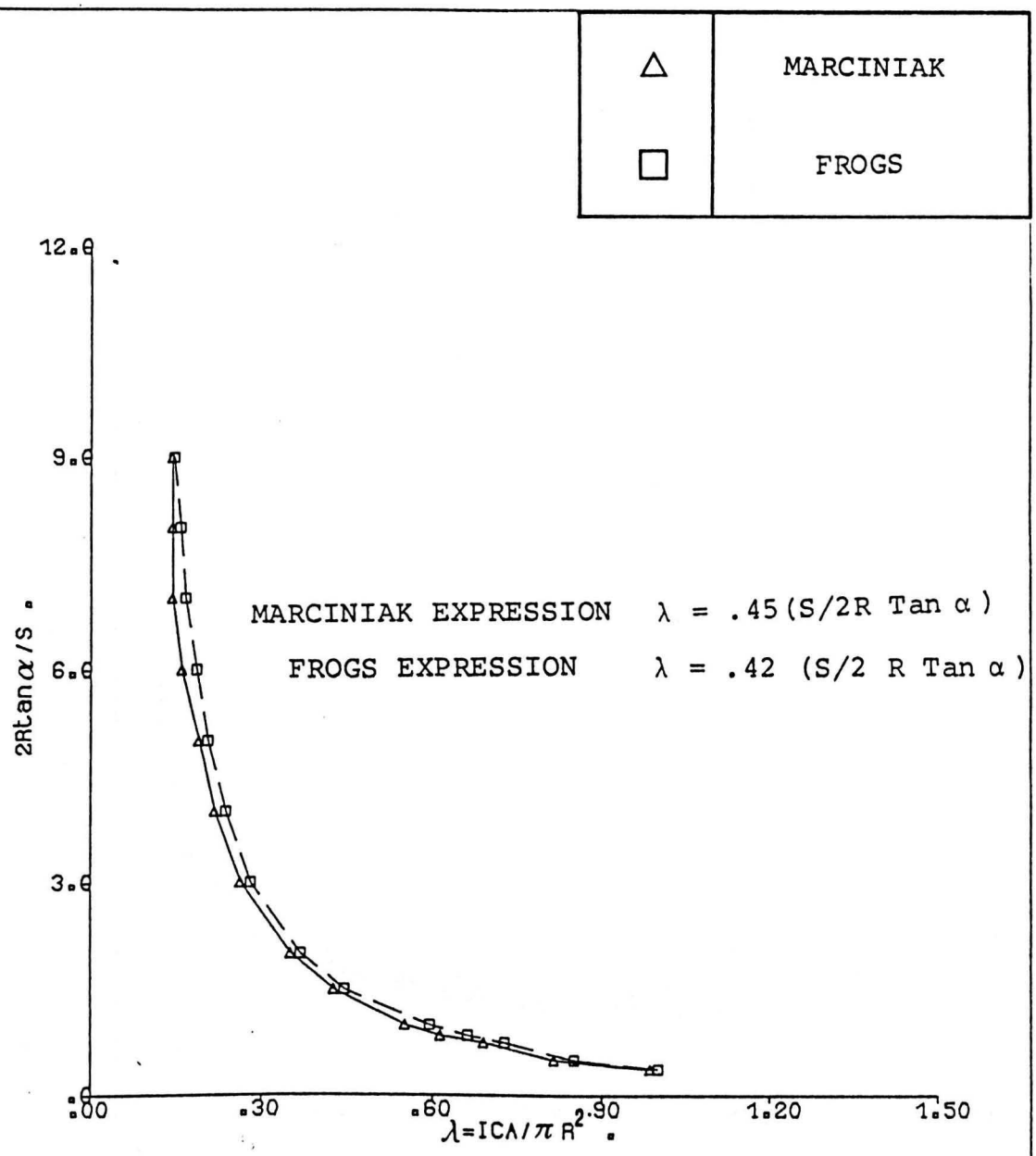

FIG.6.6.a.GRAPH OF COEFFICIENT 'λ' VS '$2R\tan\alpha/s$'

'$\theta=\alpha=2$' (DEG).

(TOOL MOTION : SPIN)

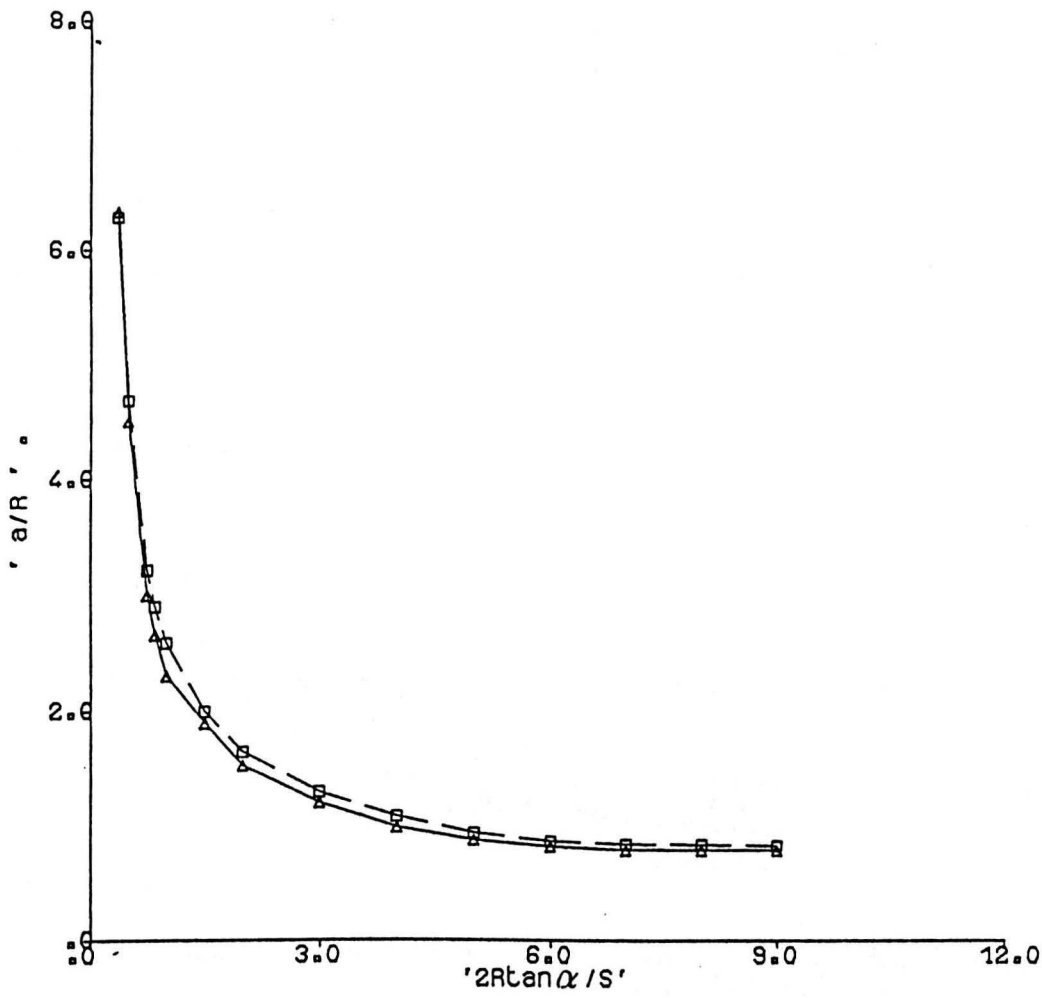

FIG.6.6.b.GRAPH OF 'a/R' VS '2Rtanα/S'.

'$\theta=\alpha=$ 2' (DEG).

(TOOL MOTION : SPIN).

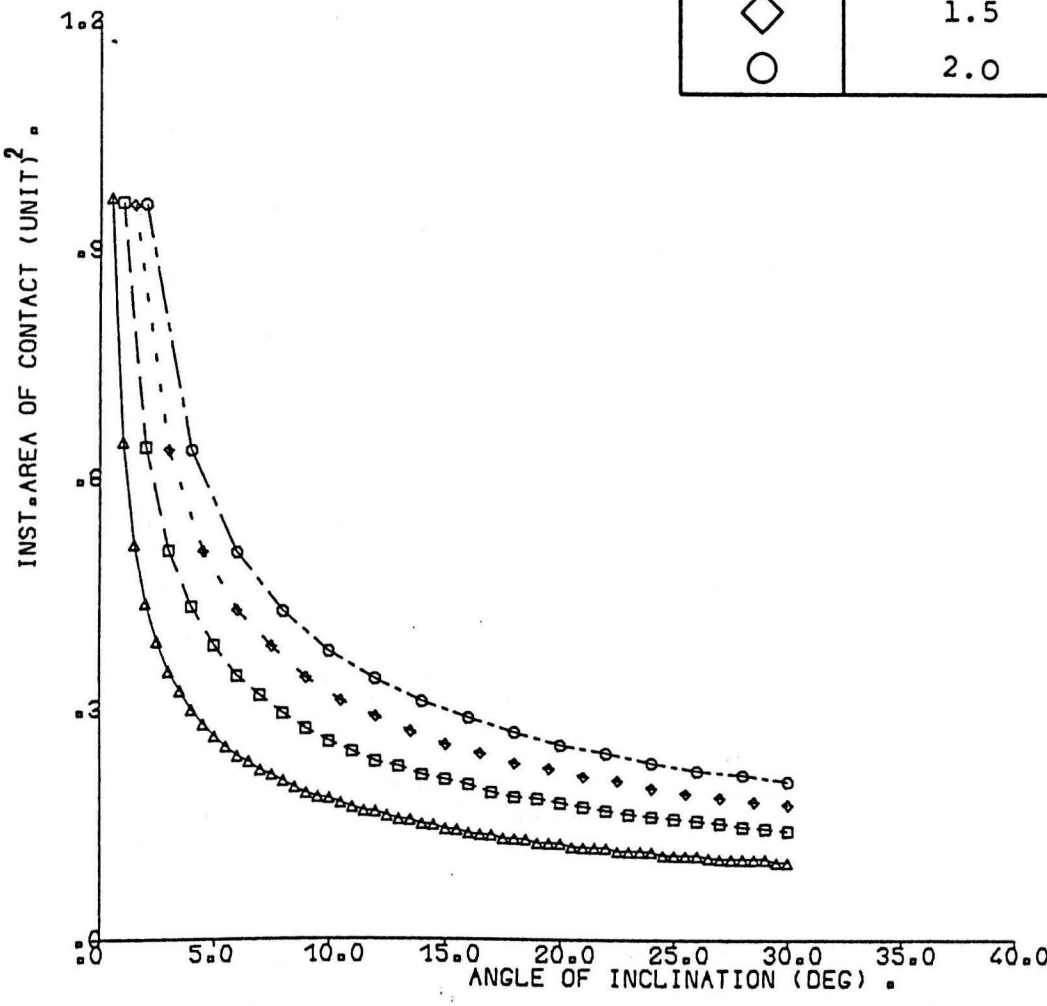

FIG.6.7.a.GRAPH OF INST.AREA OF CONTACT VS ANGLE OF INCLINATION FOR VARIOUS NUT.RATES.

AXIAL FEED RATE = 0 . α= 30 (DEG) .

(TOOL MOTION : NUTATION-SPIN)

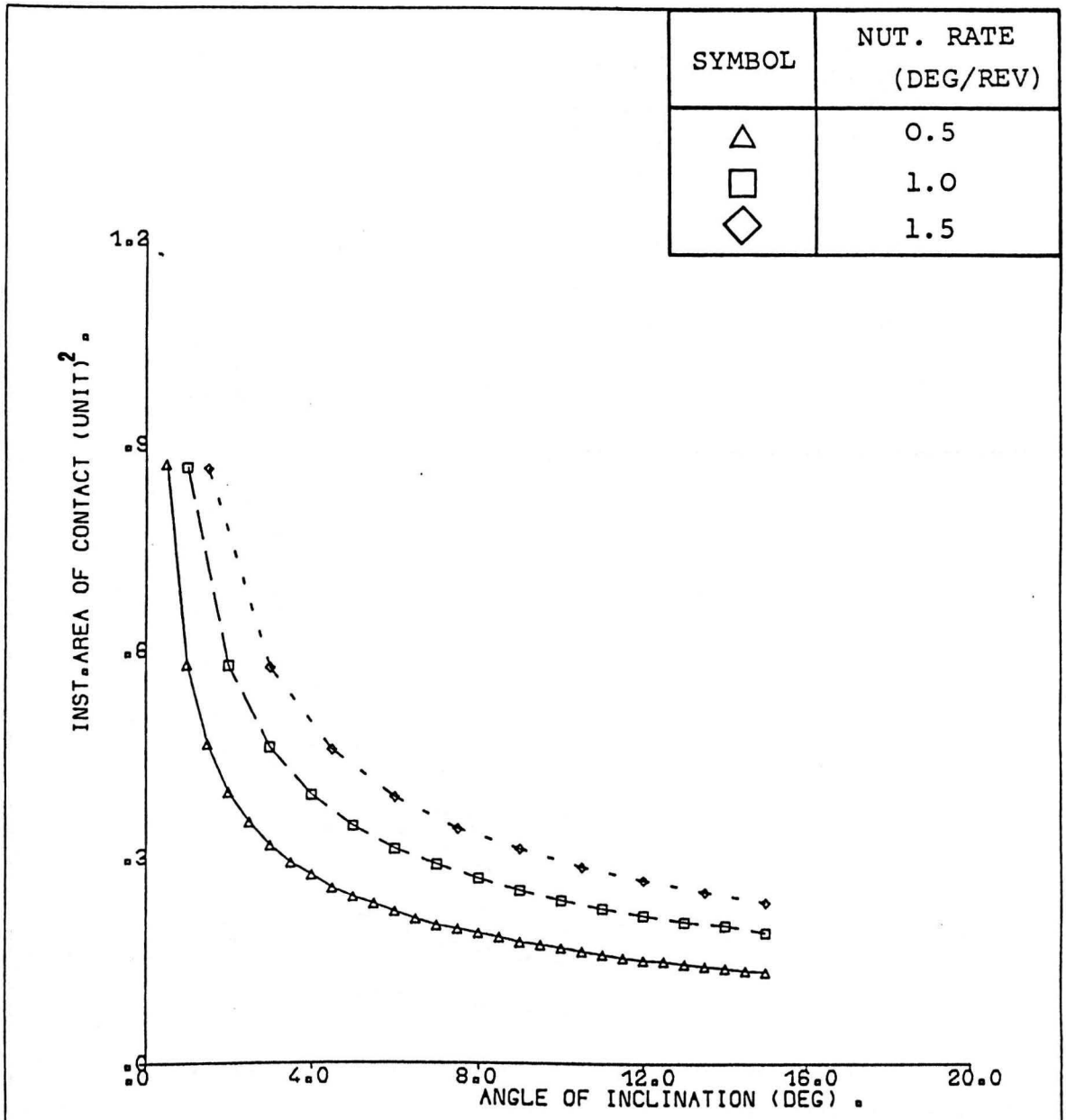

FIG.6.7.b.GRAPH OF INST.AREA OF CONTACT VS ANGLE OF INCLINATION FOR VARIOUS NUT.RATES.

AXIAL FEED RATE = 0. α= 15 (DEG).

(TOOL MOTION : NUTATION-SPIN)

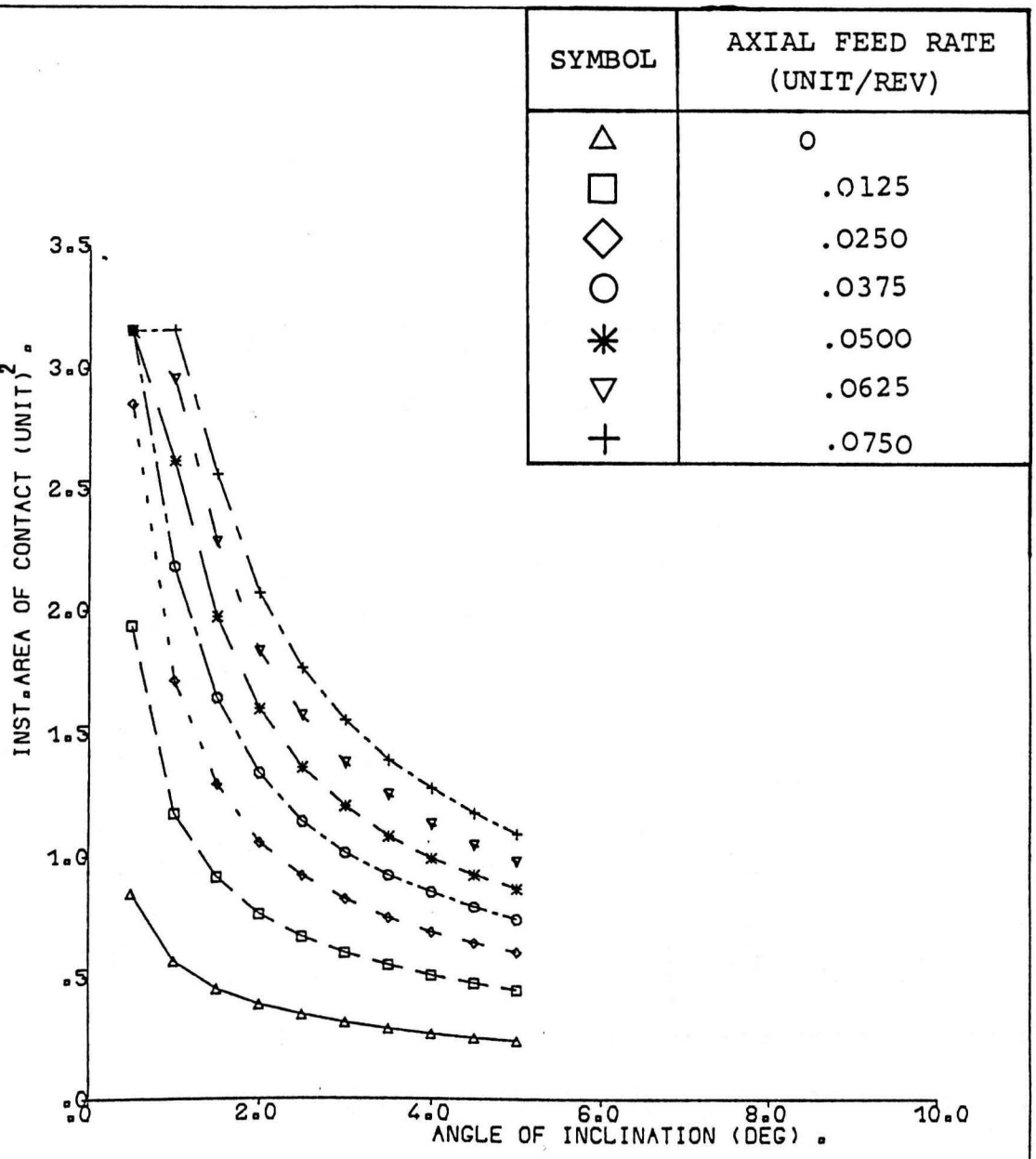

FIG.6.8.a.GRAPH OF INST.AREA OF CONTACT VS ANGLE OF INCLINATION FOR VARIOUS AXIAL FEED RATES. NUTATION RATE = .5 (DEG/REV). α= 5 (DEG). (TOOL MOTION : NUTATION-SPIN).

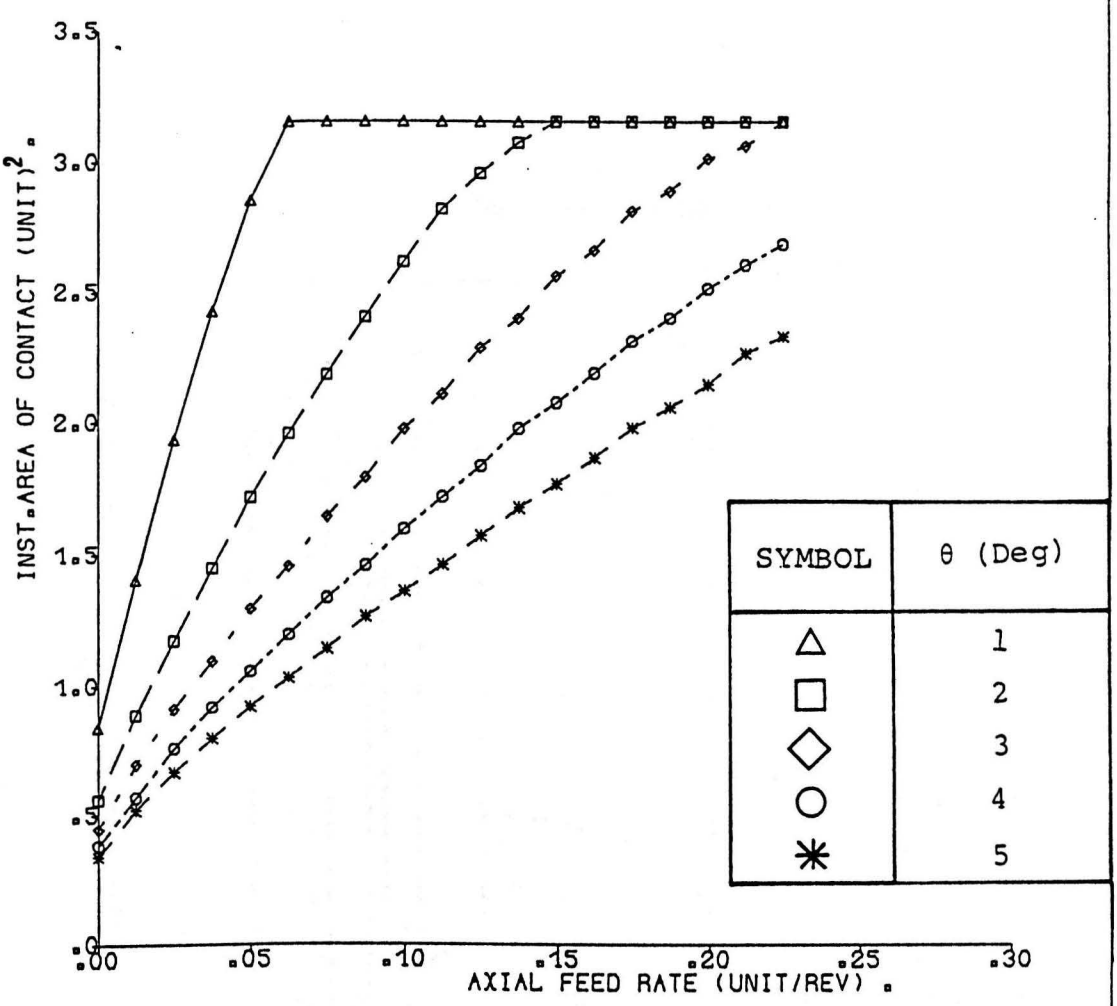

FIG.6.8.b.GRAPH OF INST.AREA OF CONTACT VS AXIAL FEED RATE FOR VARIOUS ANGLES OF INCLINATION.

NUTATION RATE = 1 (DEG/REV). α= 5 (DEG).

(TOOL MOTION : NUTATION-SPIN)

Fig. 6.9. The cylindrical workpiece of radius 'R' and height 'H'. Two elements shown within various membranes

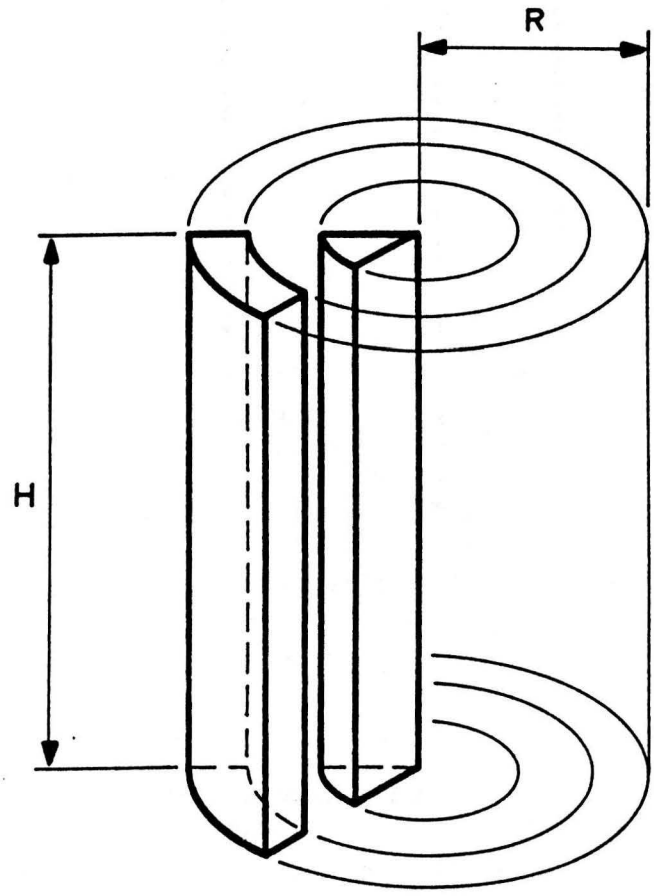

Fig. 6.10. The geometry of macro-blocks representing a billet

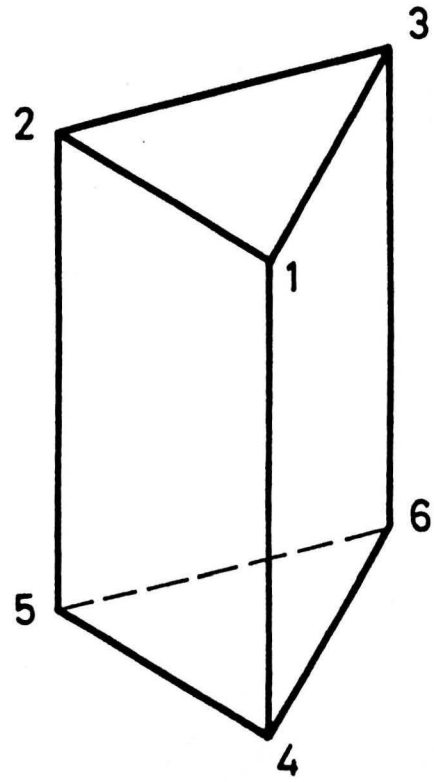

(a) Prismatic - Pentahedron.

(b) Hexahedron.

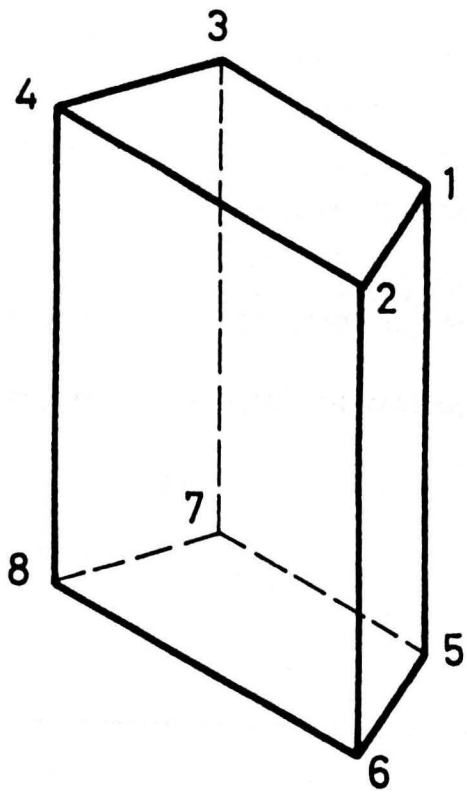

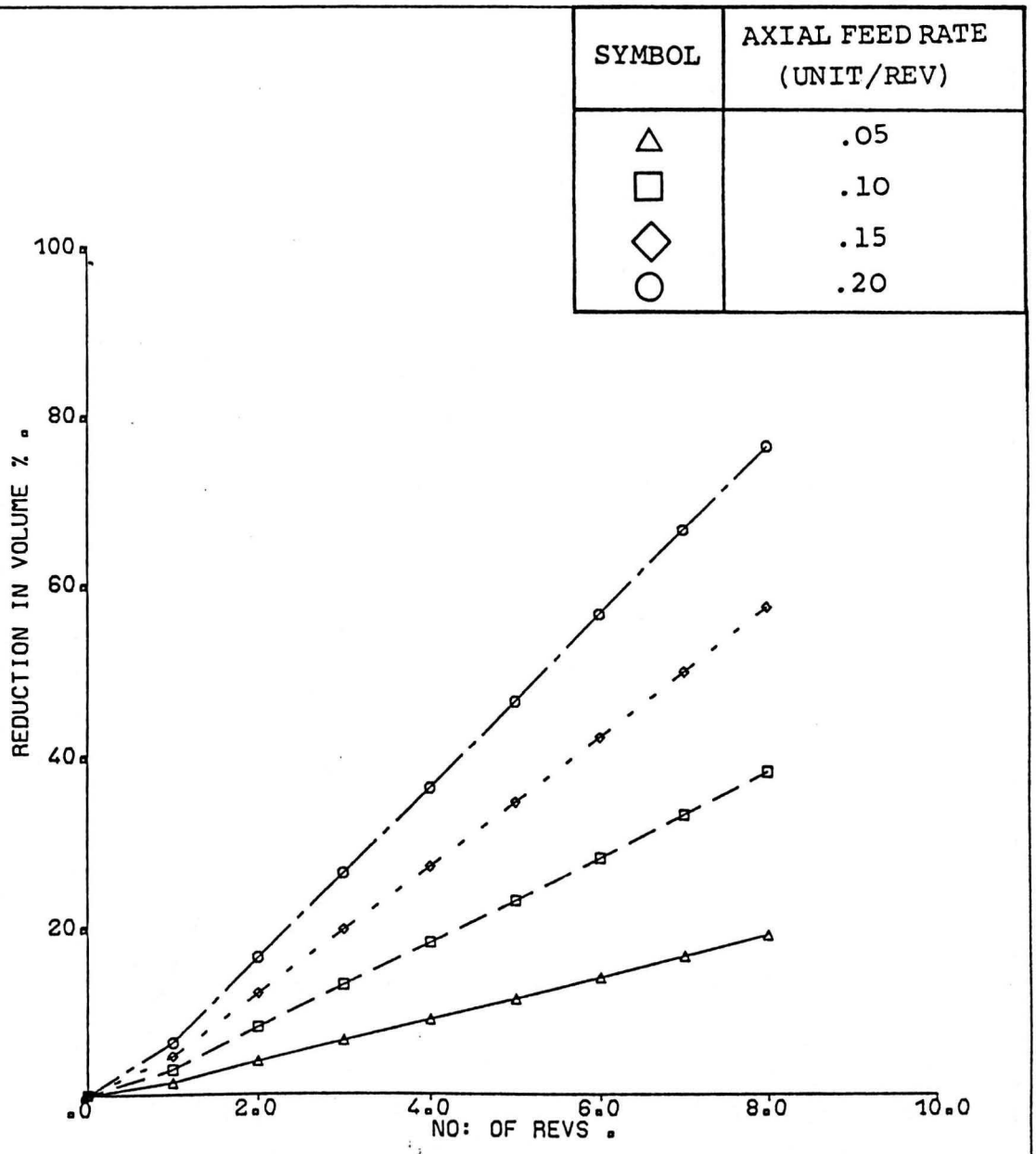

FIG.6.11.a.GRAPH OF REDUCTION IN VOLUME OF THE WORKPIECE VS NO: OF REVS FOR VARIOUS AXIAL FEED RATES. $\theta=\alpha$ = 30 (DEG). H/D = 2.

(TOOL MOTION : SPIN)

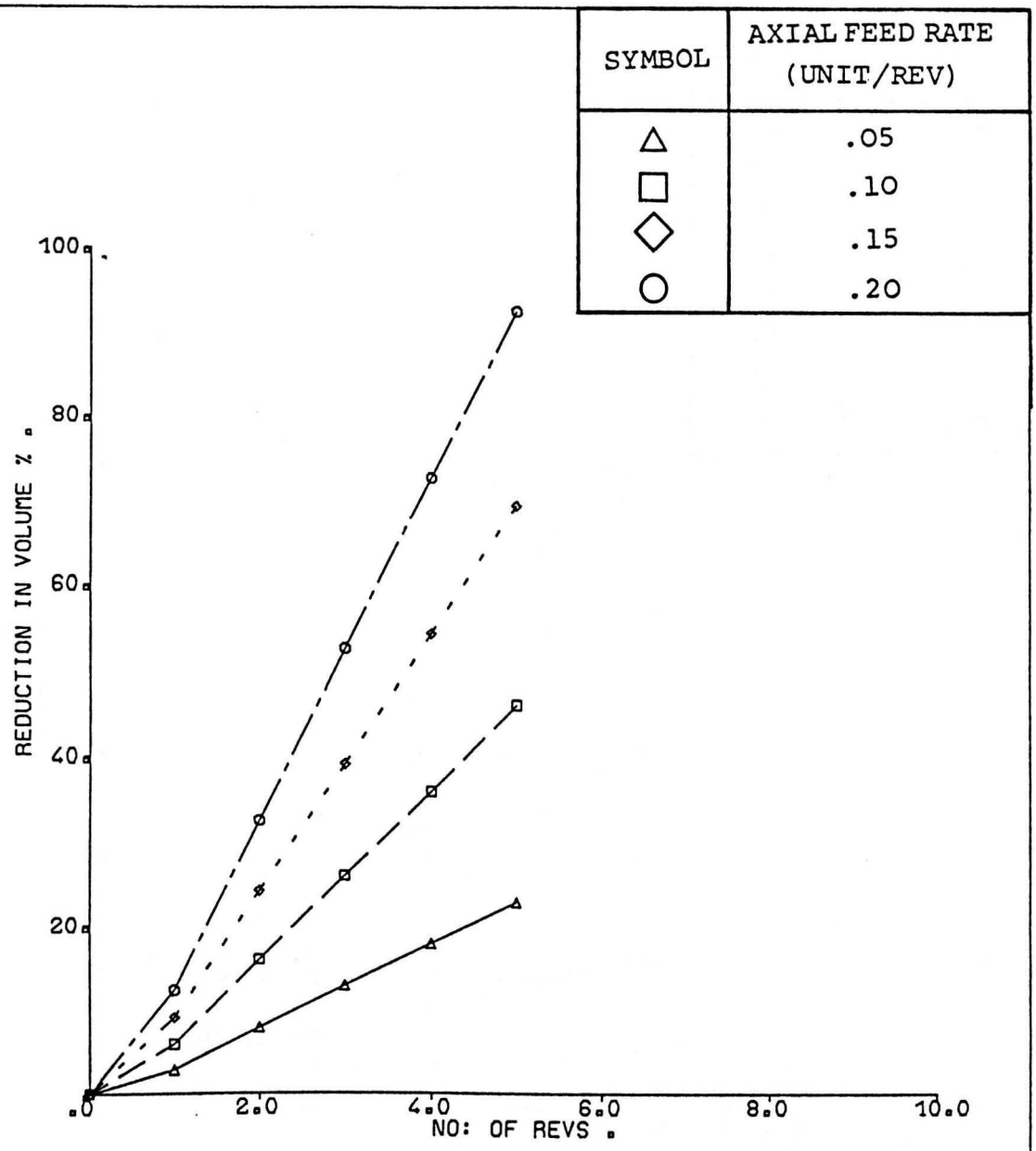

FIG.6.11.b.GRAPH OF REDUCTION IN VOLUME OF THE WORKPIECE VS NO:OF REVS FOR VARIOUS AXIAL FEED RATES. $\theta = \alpha = 30$. H/D = 1 .

(TOOL MOTION : SPIN)

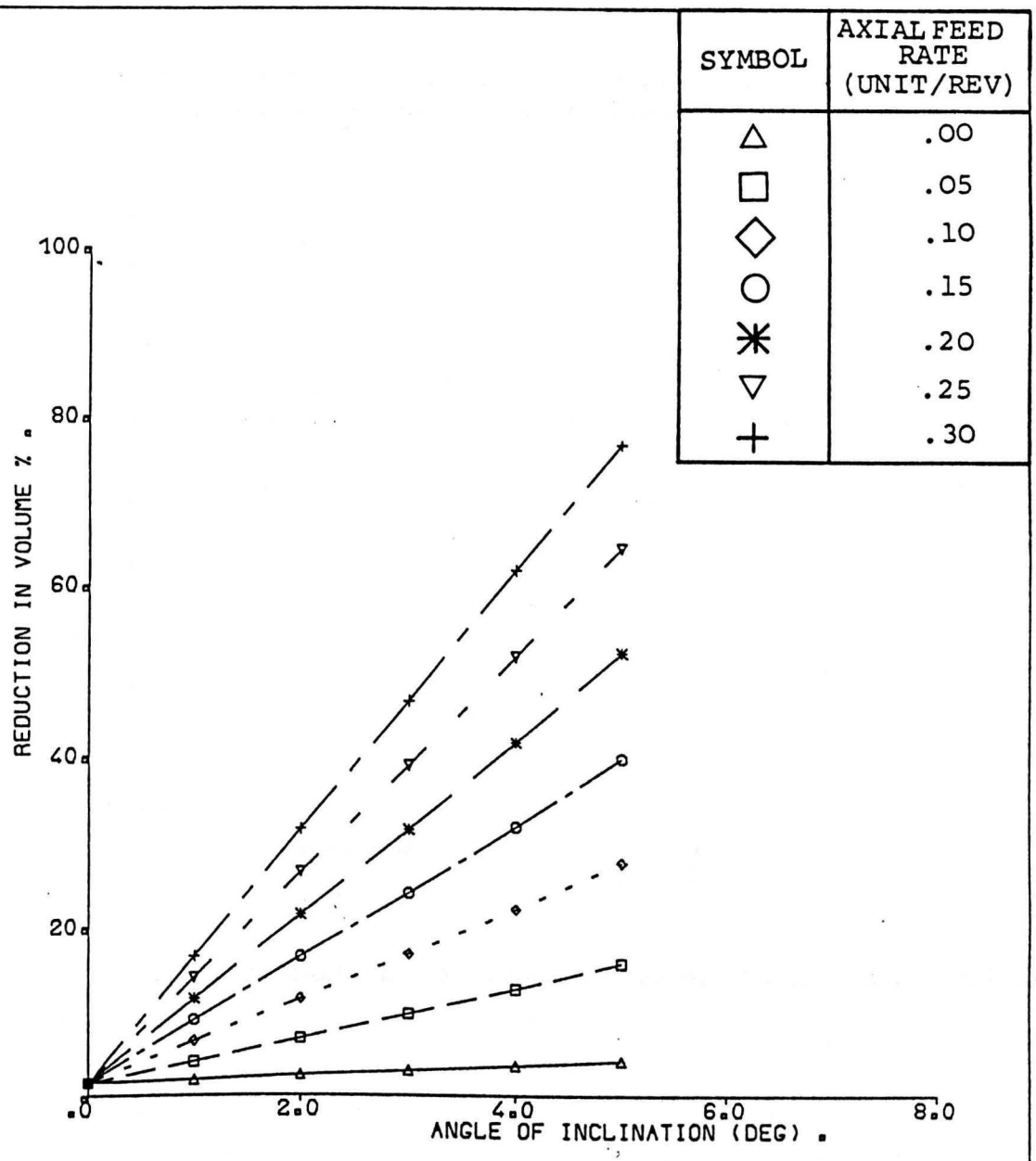

FIG.6.12.GRAPH OF REDUCTION IN VOLUME OF THE WORKPIECE VS ANGLE OF INCLINATION.

NUTATION RATE = 1 (DEG/REV). α = 5 (DEG).

(TOOL MOTION : NUTATION-SPIN)

Fig. 7.1. The necessary steps for FROGS, in order to introduce radial configuration, from a predefined data file

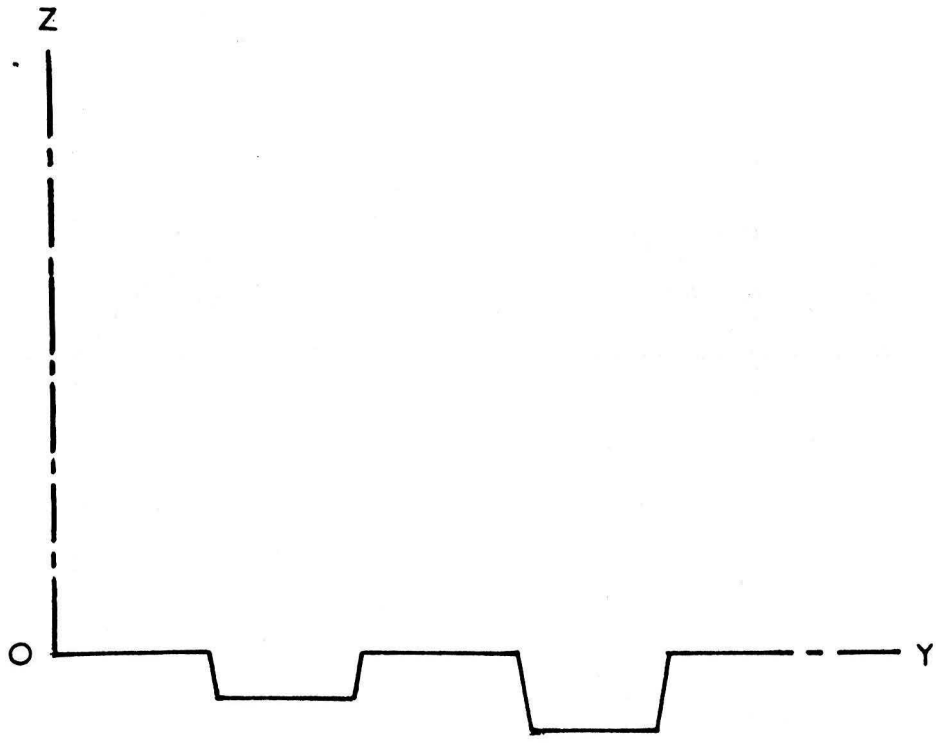

(a) A radially configurated generator, on the horizontal plane

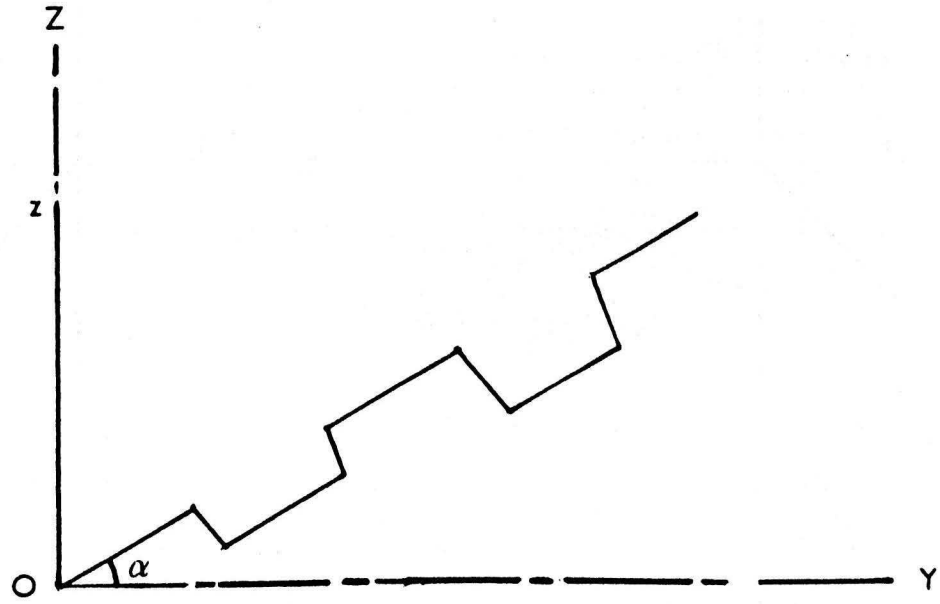

(b) A radially configurated generator, after rotation of α degrees about the pivot point

Fig. 7.2. Range of theoretically possible radial features
$o \leq \omega \leq 360^{o}$

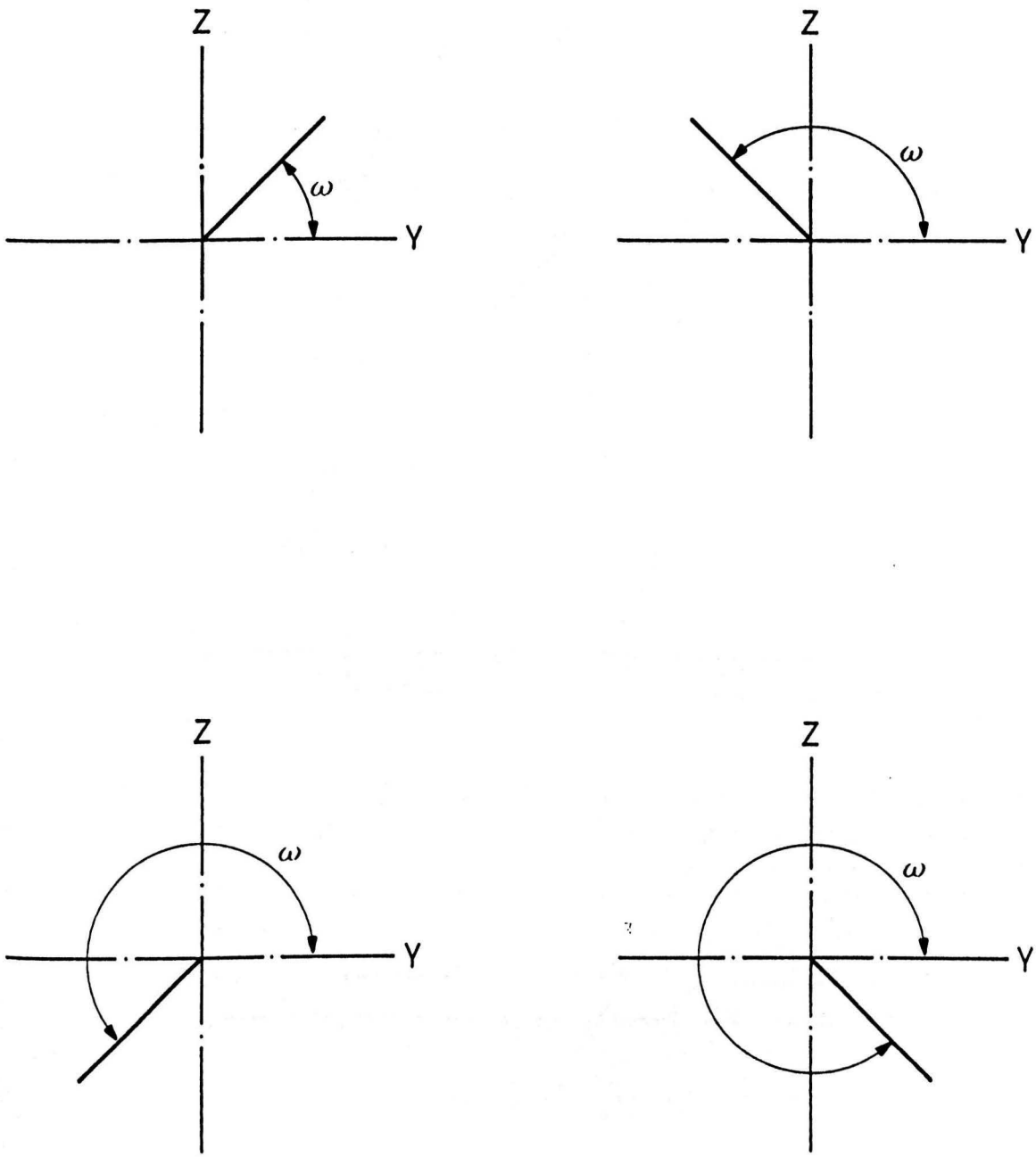

Fig. 7.3. Limitationsto be considered in designing a radially configurated conic tool

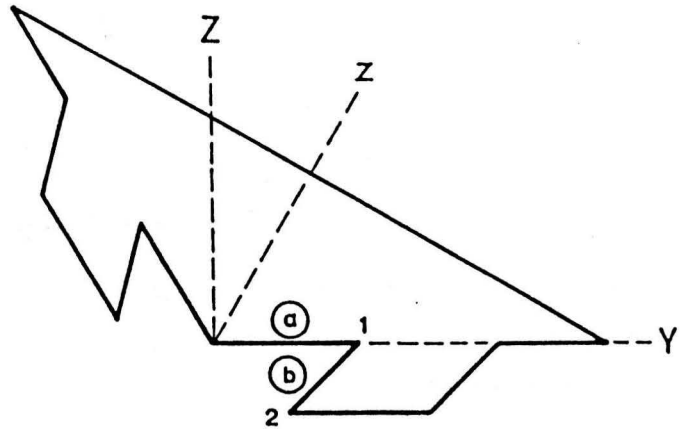

(a) Practically un-feasible radially configurated tool.

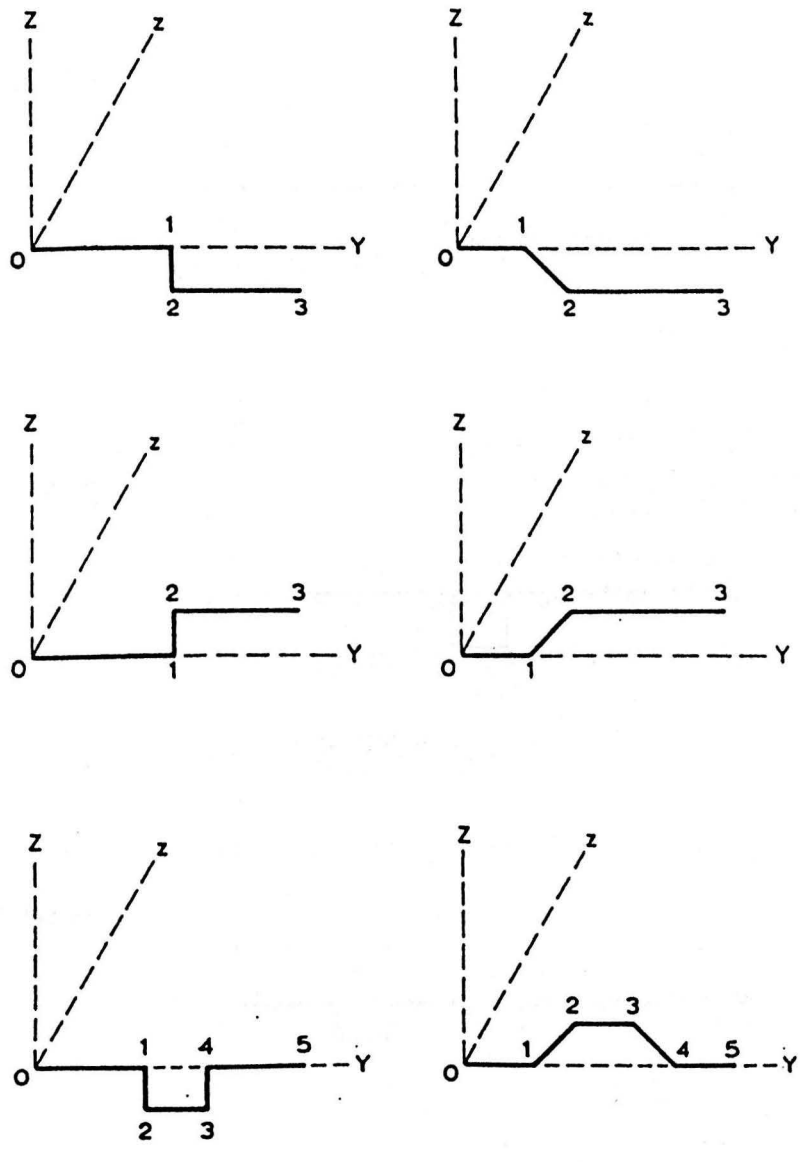

(b) Practically feasible radially configurated tools.

Fig. 7.4. The four radial configurations currently available using FROGS

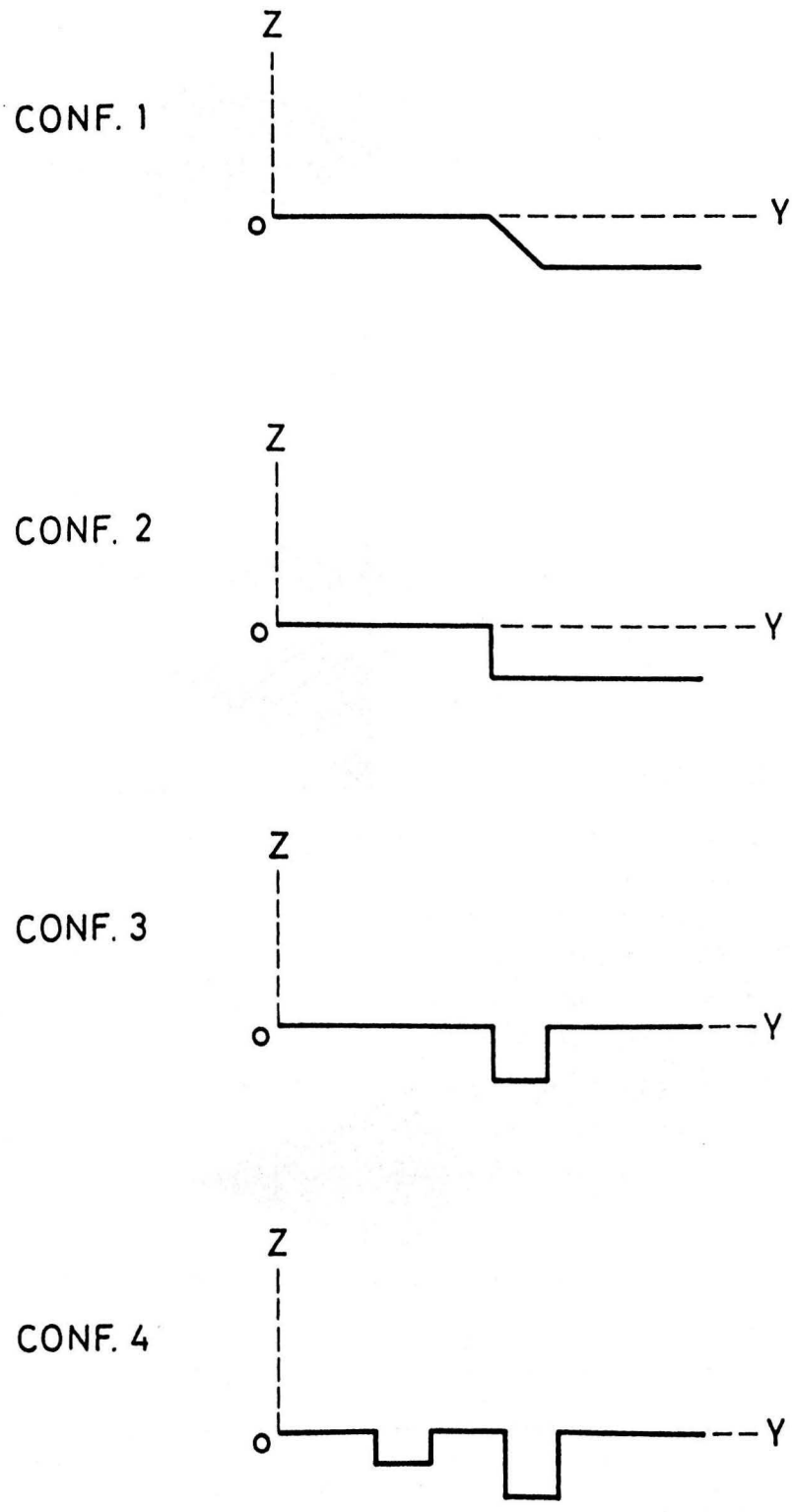

Fig. 7.5.a. Loci of the lowest generator on a radially configurated tool (CONF 3)
(Tool motion: Precession)

$\dot{\phi}$ = 360 (Deg/rev) $\theta = \alpha$ = 30 (Deg)

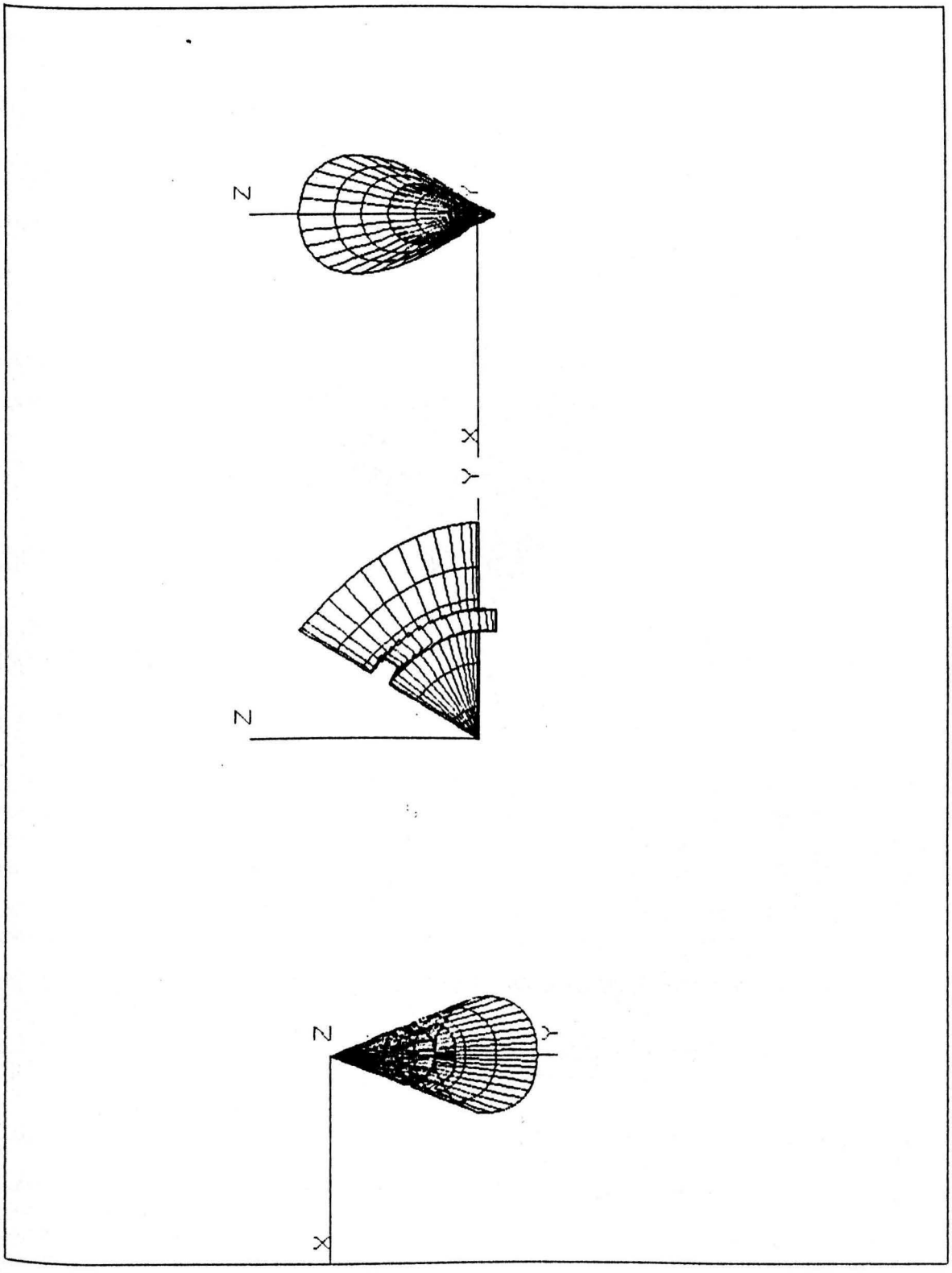

Fig. 7.5.b. Loci of the lowest generator (CONF 3)
(Tool motion: Precession)

$\dot{\phi}$ = 360 (Deg/rev) $\theta = \alpha$ = 30 (Deg)

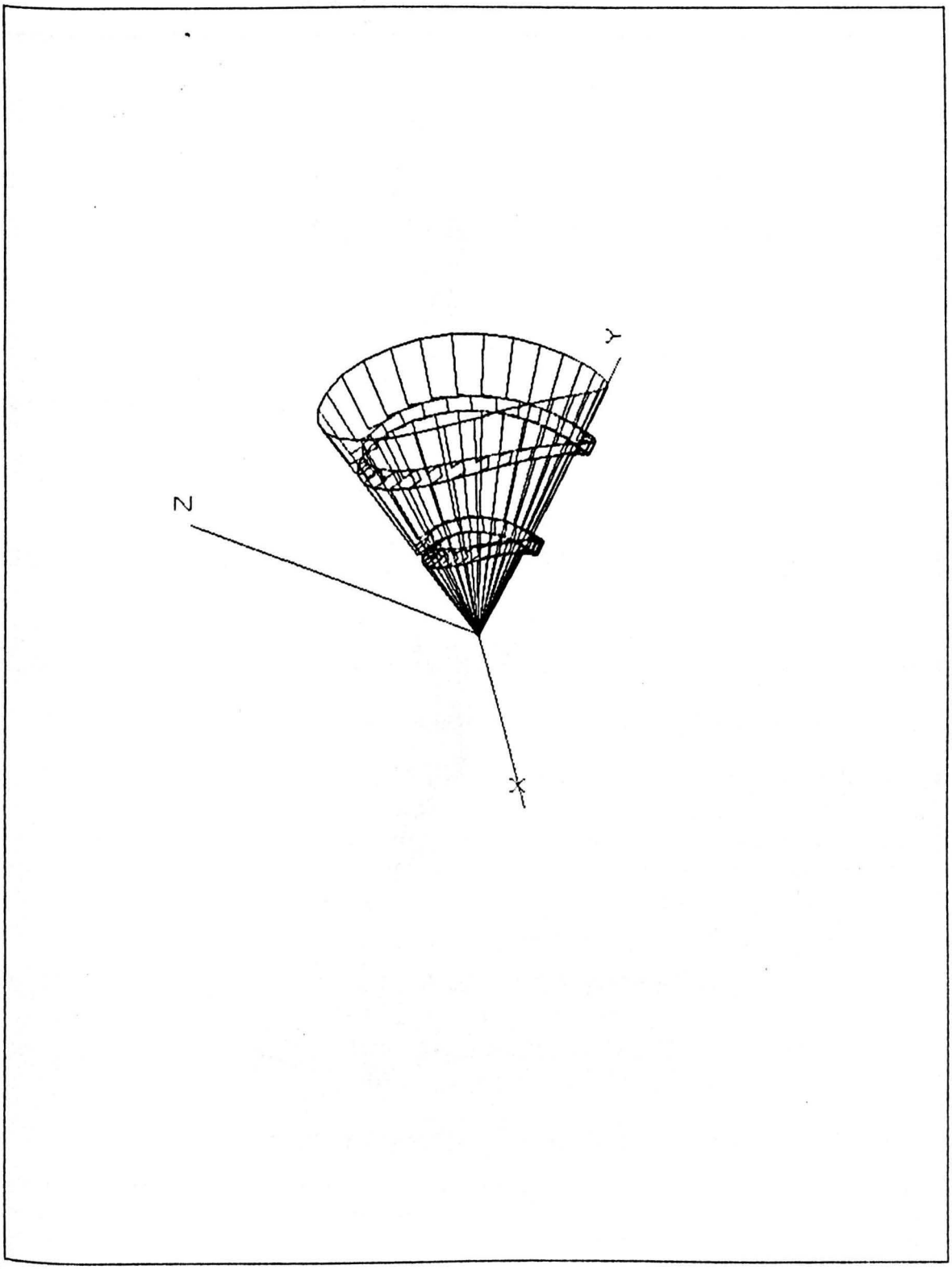

Fig. 7.6.a. Loci of the lowest generator on a radially configurated tool (CONF 1)
(Tool motion: Nutation-Spin)

$\dot{\theta}$ = 20 (Deg/rev) $\dot{\psi}$ = 360 (Deg/rev) α=30 (Deg) θ = 0

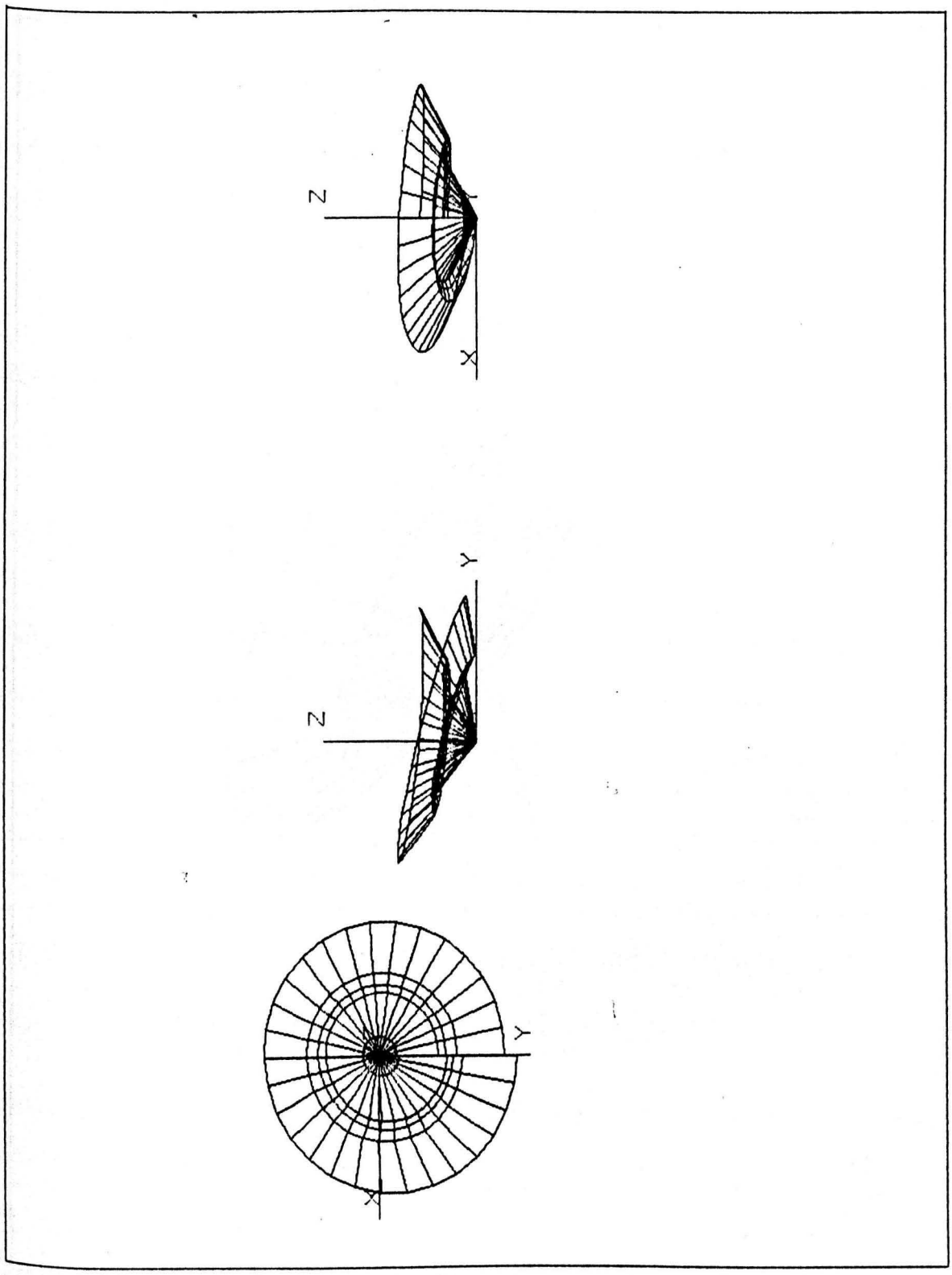

Fig. 7.6.b. Loci of the lowest generator (CONF 1)
(Tool motion: Nutation-Spin)

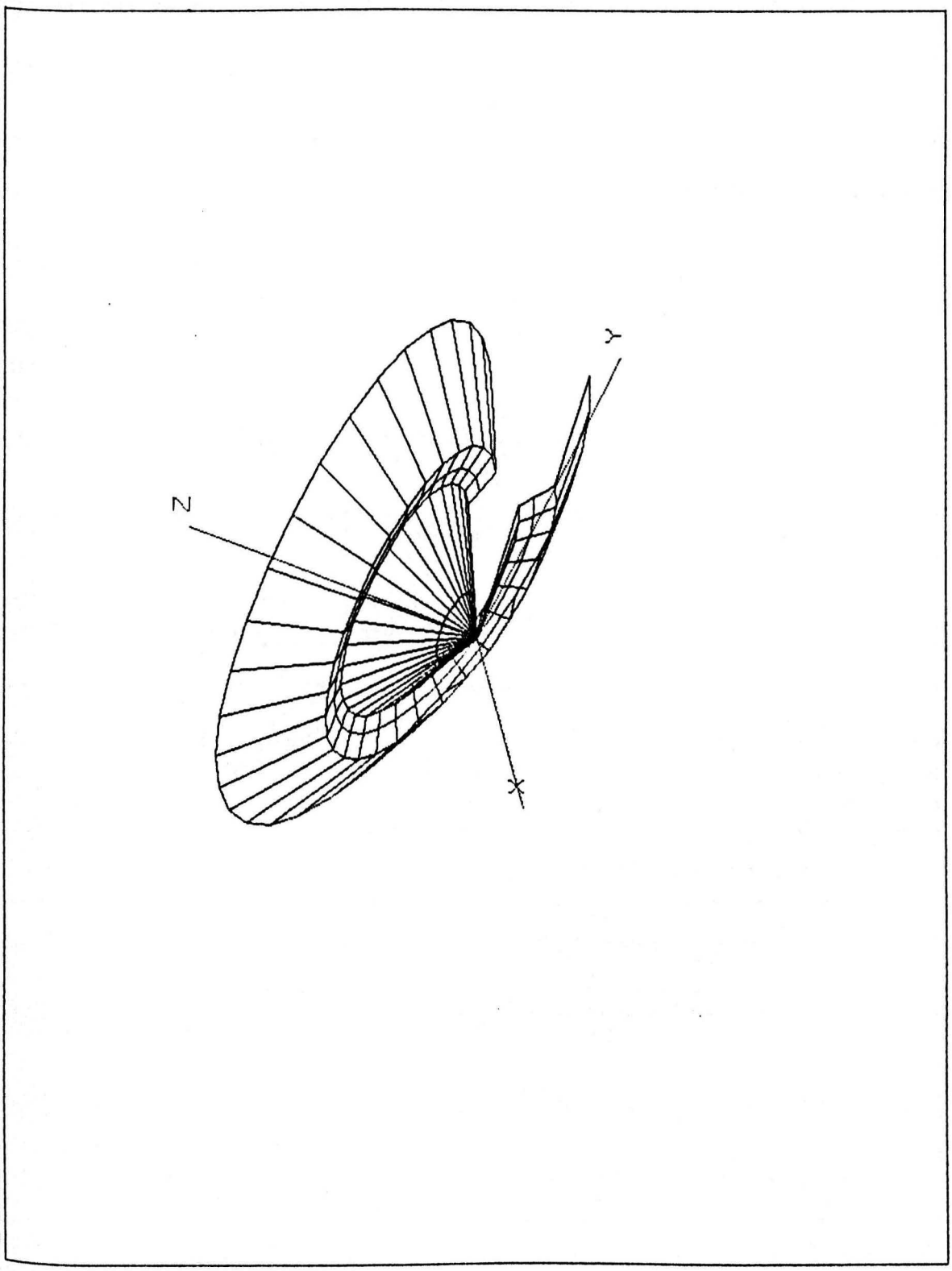

Fig. 7.7. Loci of the lowest generator on a radially configurated tool (CONF 1)
(Tool motion: Nutation-Precession-Spin)

$\dot{\theta}$ = 15 (Deg/rev) $\dot{\phi}$ = 90 (Deg/rev) $\dot{\psi}$ = 360(Deg/rev) θ = 10 (Deg).
α = 30 (Deg)

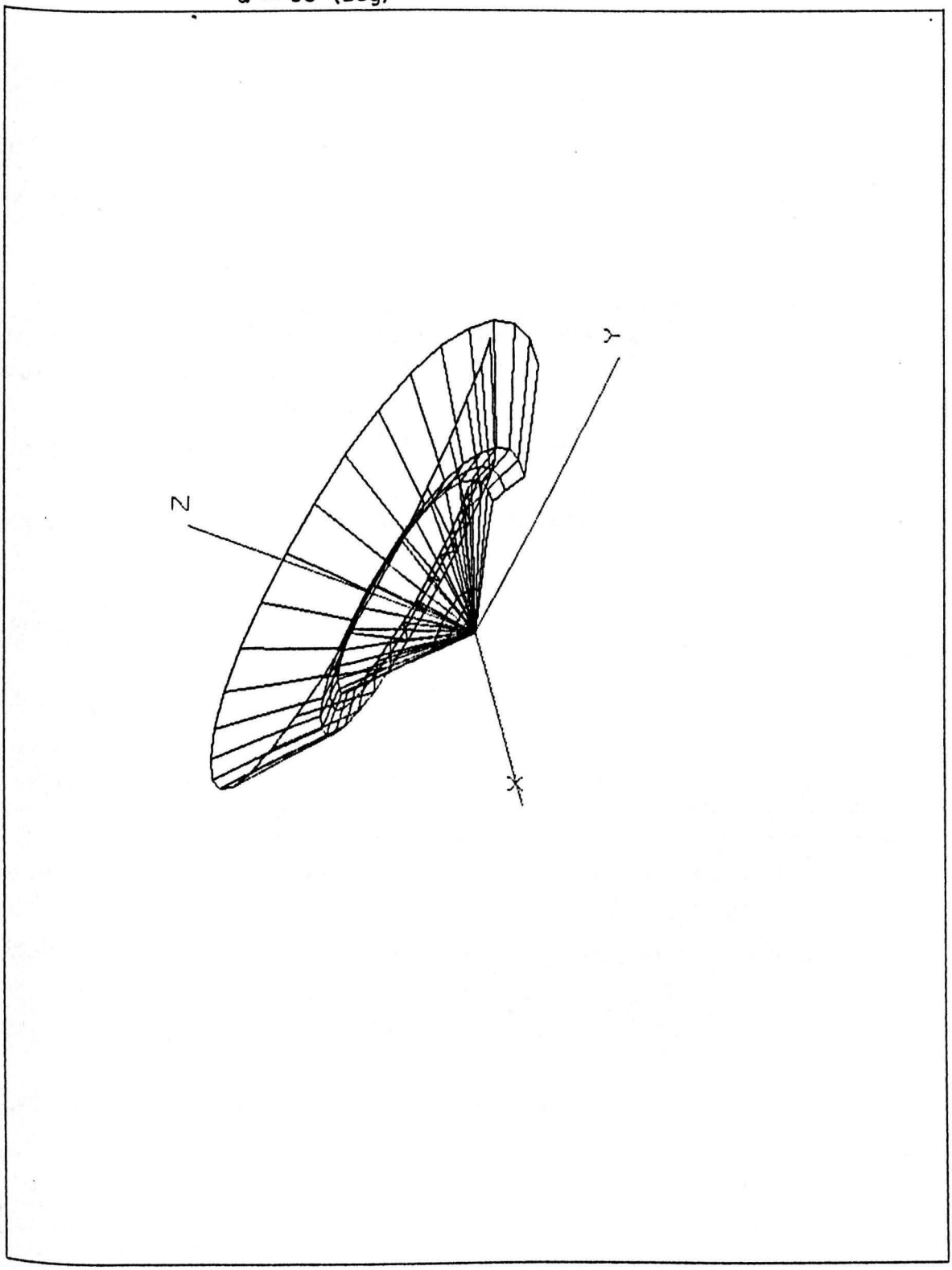

Fig. 7.8. Illustration of a workpiece being deformed by a radially configurated conic tool (Tool motion: Spin)

7.8.a. Tool Profile CONF1
$\theta = \alpha = 30$ (Deg)

7.8.b. Tool Profile CONF3
$\theta = \alpha = 5$ (Deg)

Fig. 7.8.a.

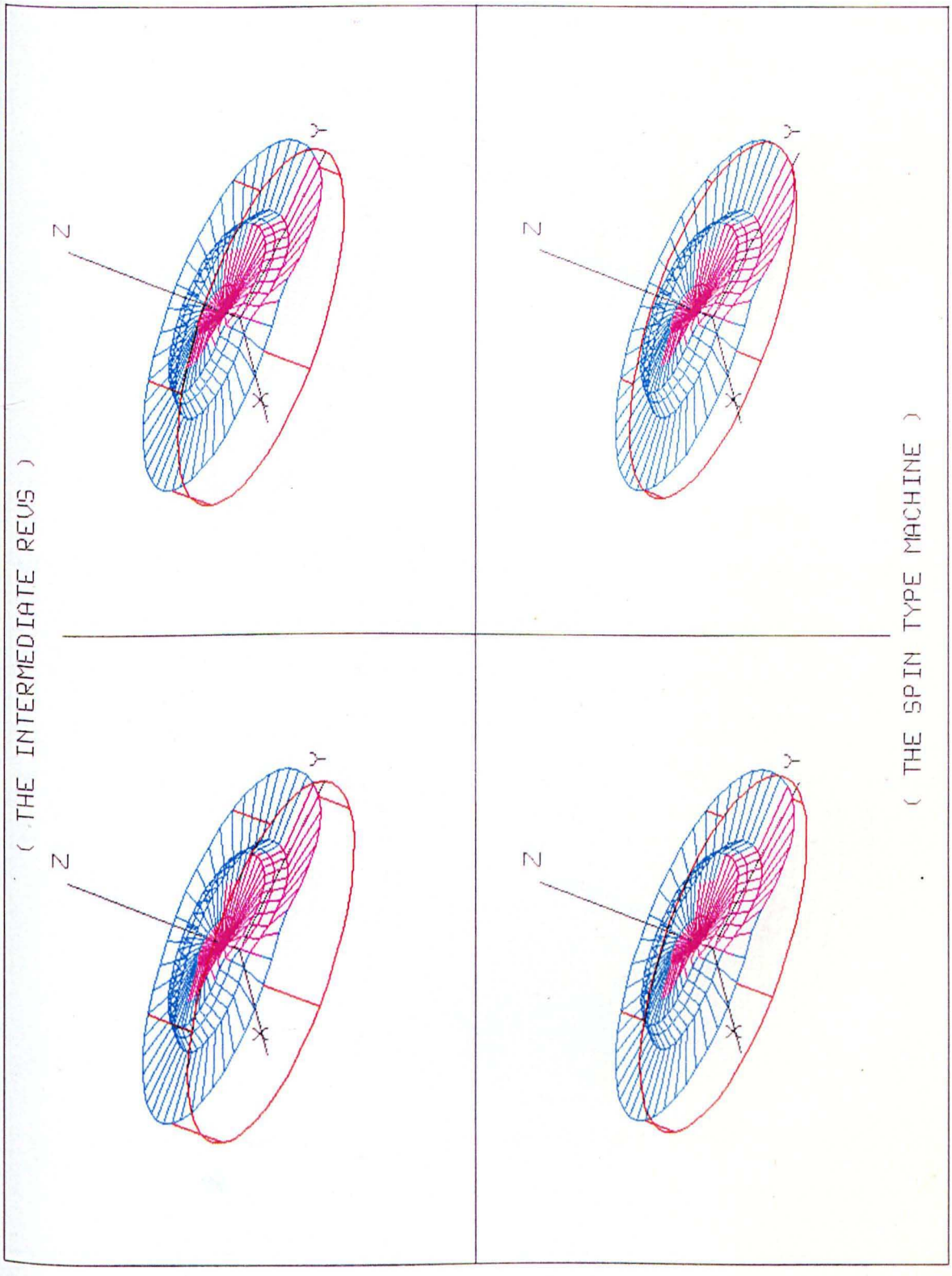

Fig. 7.8.b.

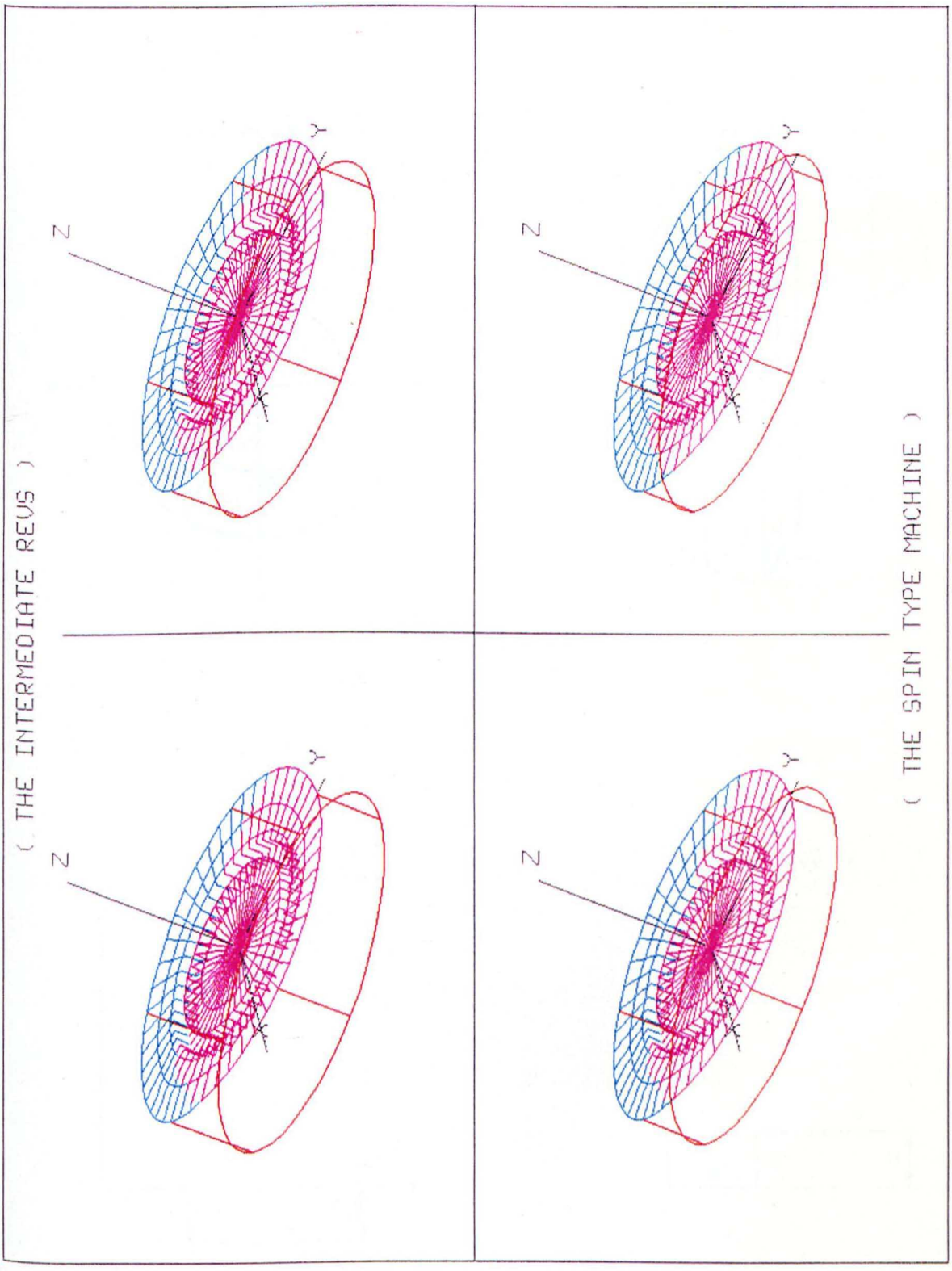

Fig. 7.9. A cylindrical workpiece, being deformed by a radially configurated tool

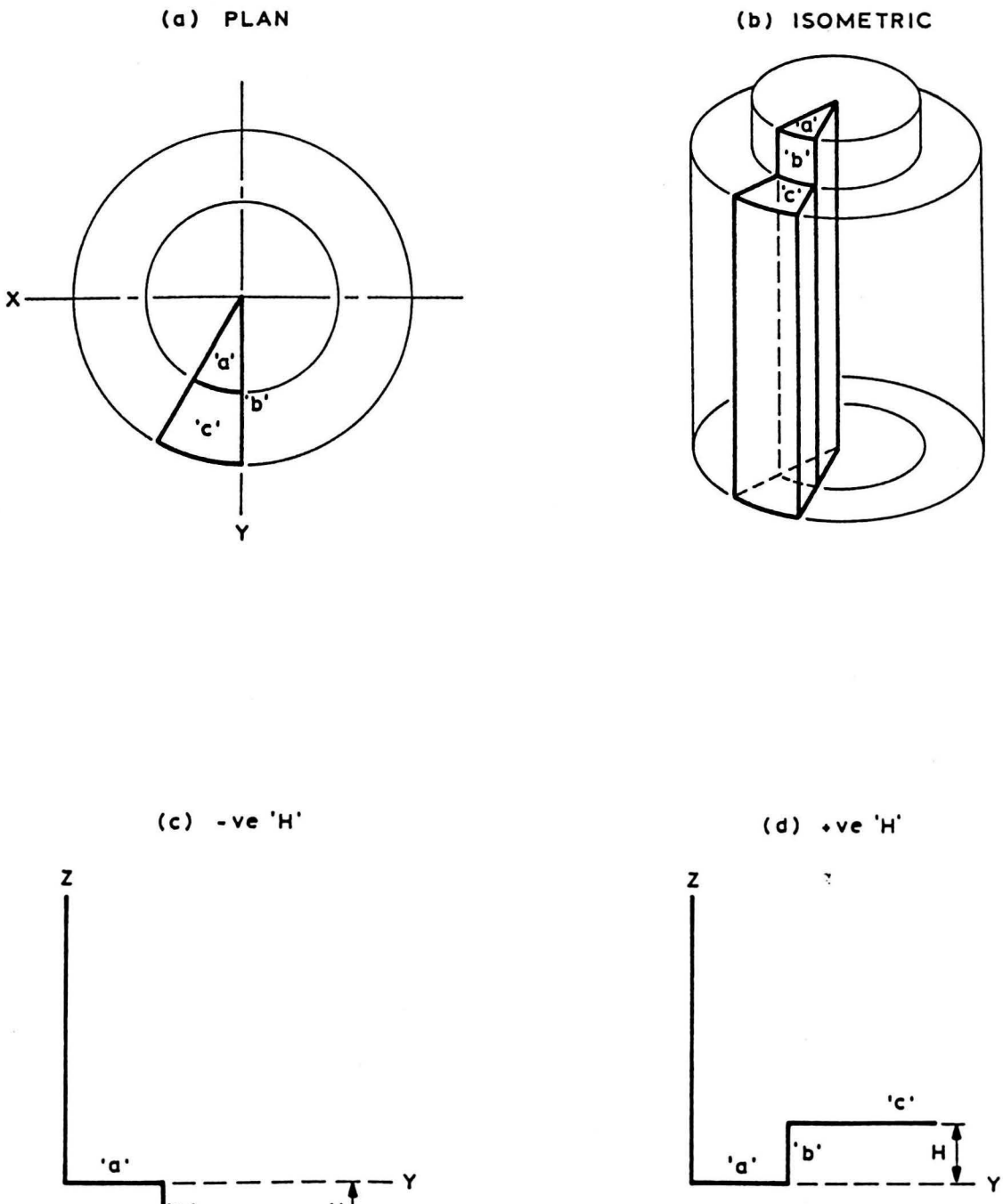

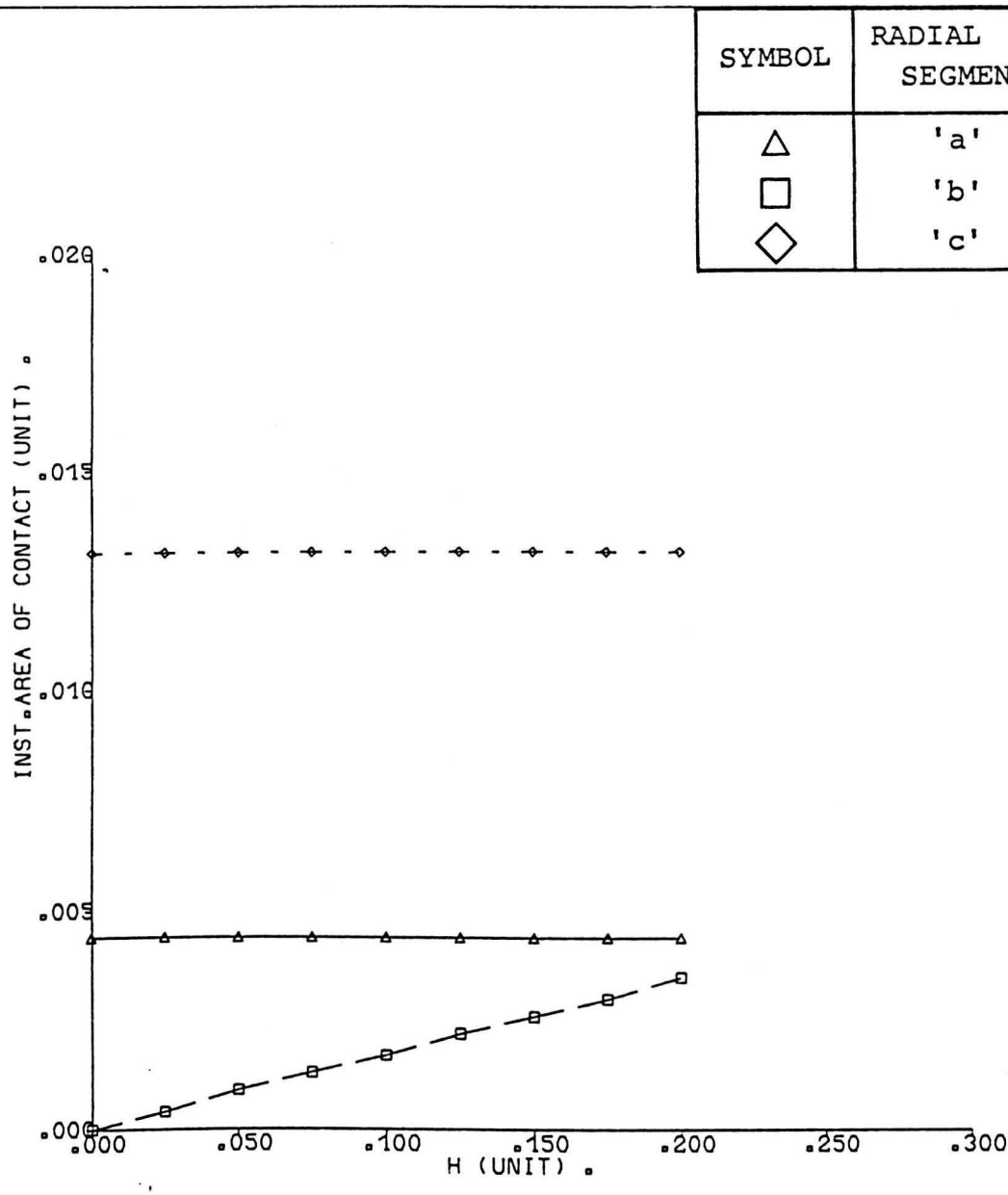

FIG.7.10.GRAPH OF INST.AREA OF CONTACT FOR ONE RADIAL SEGMENT VS H.

$\theta = \alpha =$ 30 (DEG).

(TOOL MOTION : SPIN).

Fig. 7.11. Two radially configurated tool profiles as they nutate towards the Y-axis. α = 30 (Deg) θ = 0, 15, 30 (Deg)

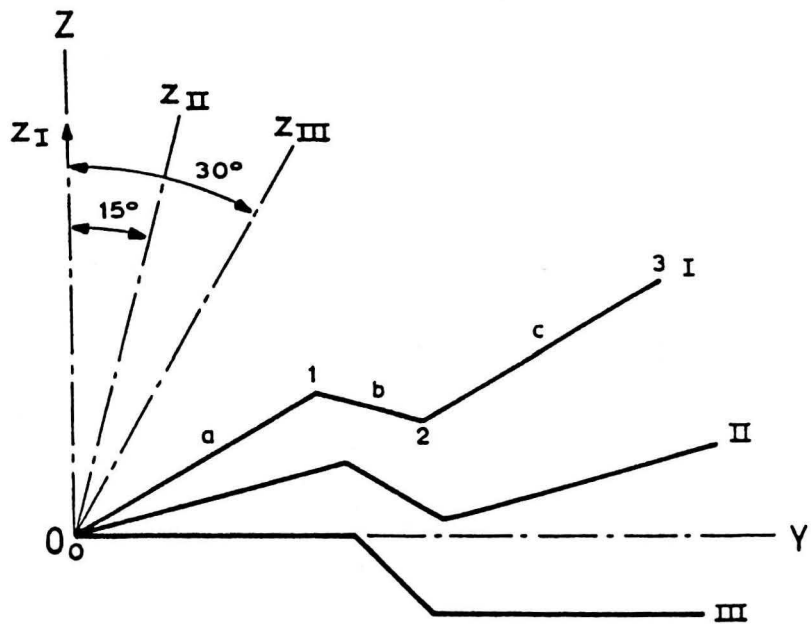

(a) A radially configurated conic tool profile (CONF. 1)

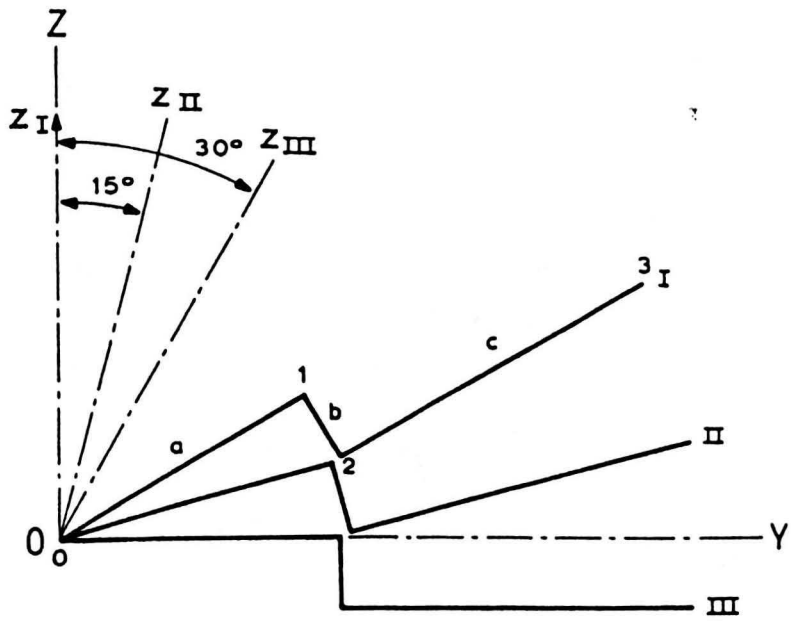

(b) A radially configurated conic tool profile (CONF. 2)

Fig. 7.12 Two radially configurated tool profiles as they nutate towards the Y-axis. α = 30 (Deg) θ = 0, 15, 30 (Deg) (Solid line representing the profile after the required modifications).

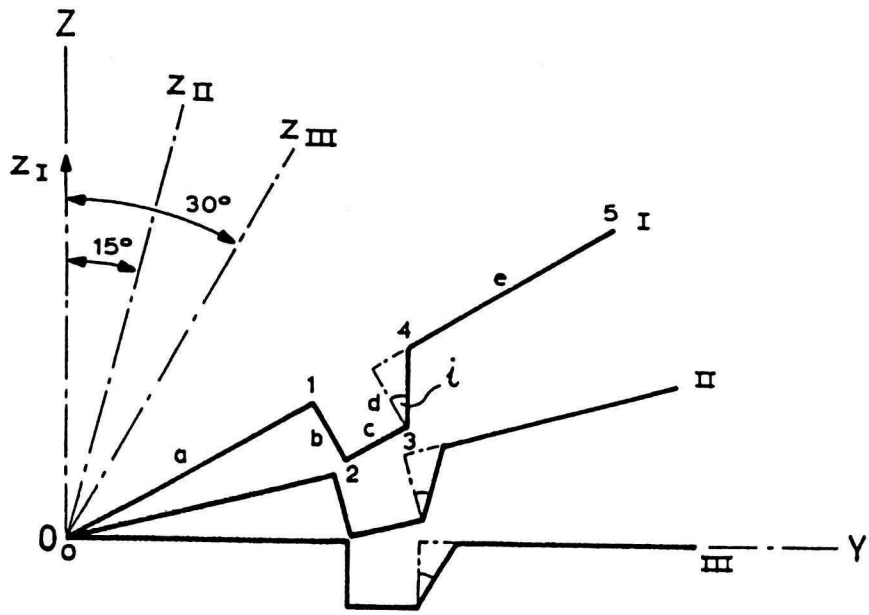

(a) A radially configurated conic tool profile (CONF. 3)

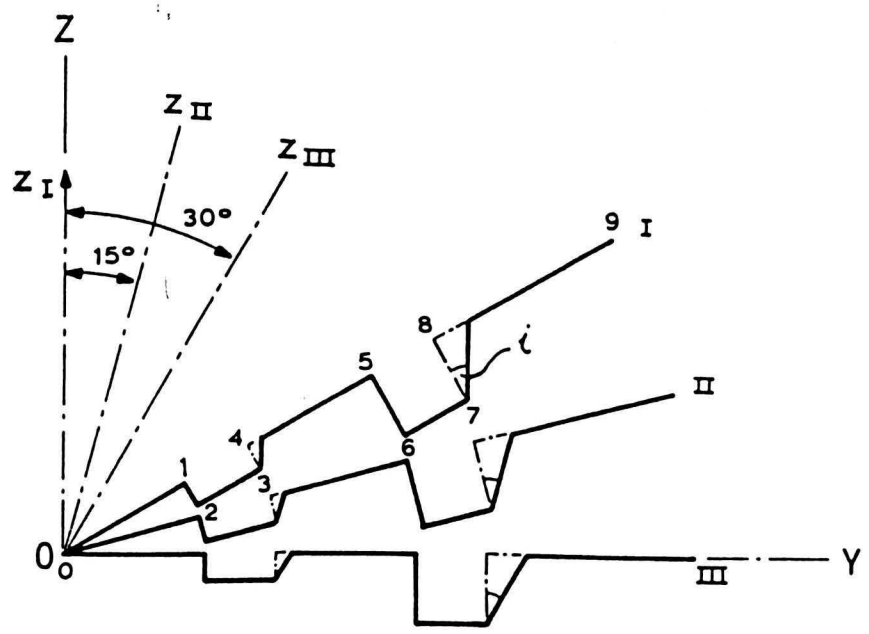

(b) A radially configurated conic tool profile (CONF. 4)

Fig. 7.13. Illustration of a workpiece being deformed by a radially configurated conic tool

Tool Profile CONF1

α = 32 (Deg), $\dot{\theta}$ = 4 (Deg/rev), $\dot{\phi}$ = 360 (Deg/rev)

(Tool motion: Nutation-Spin)

7.13.a. Plan

7.13.b. Isometric

Fig. 7.13.a.

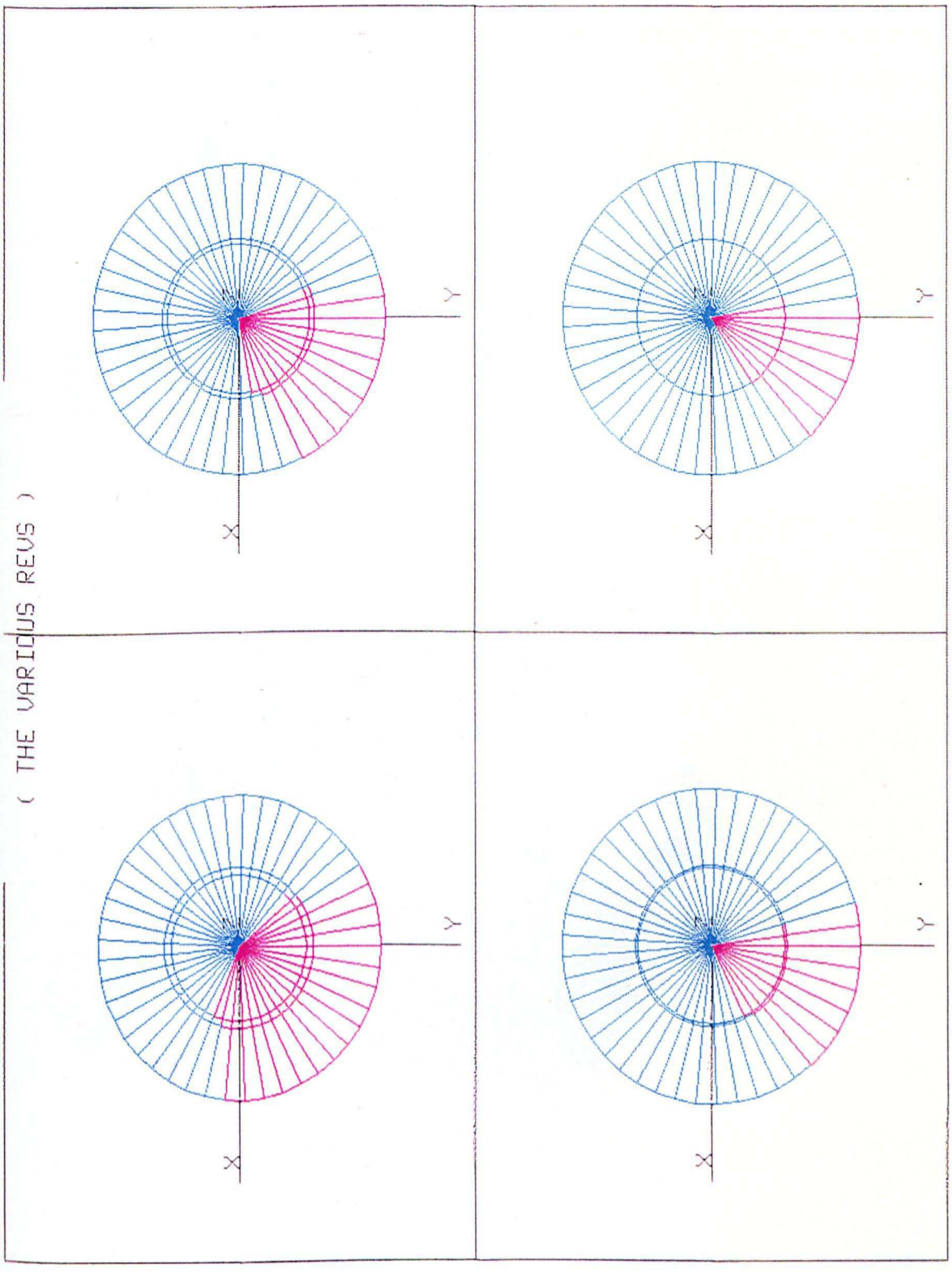

Fig. 7.13.b.

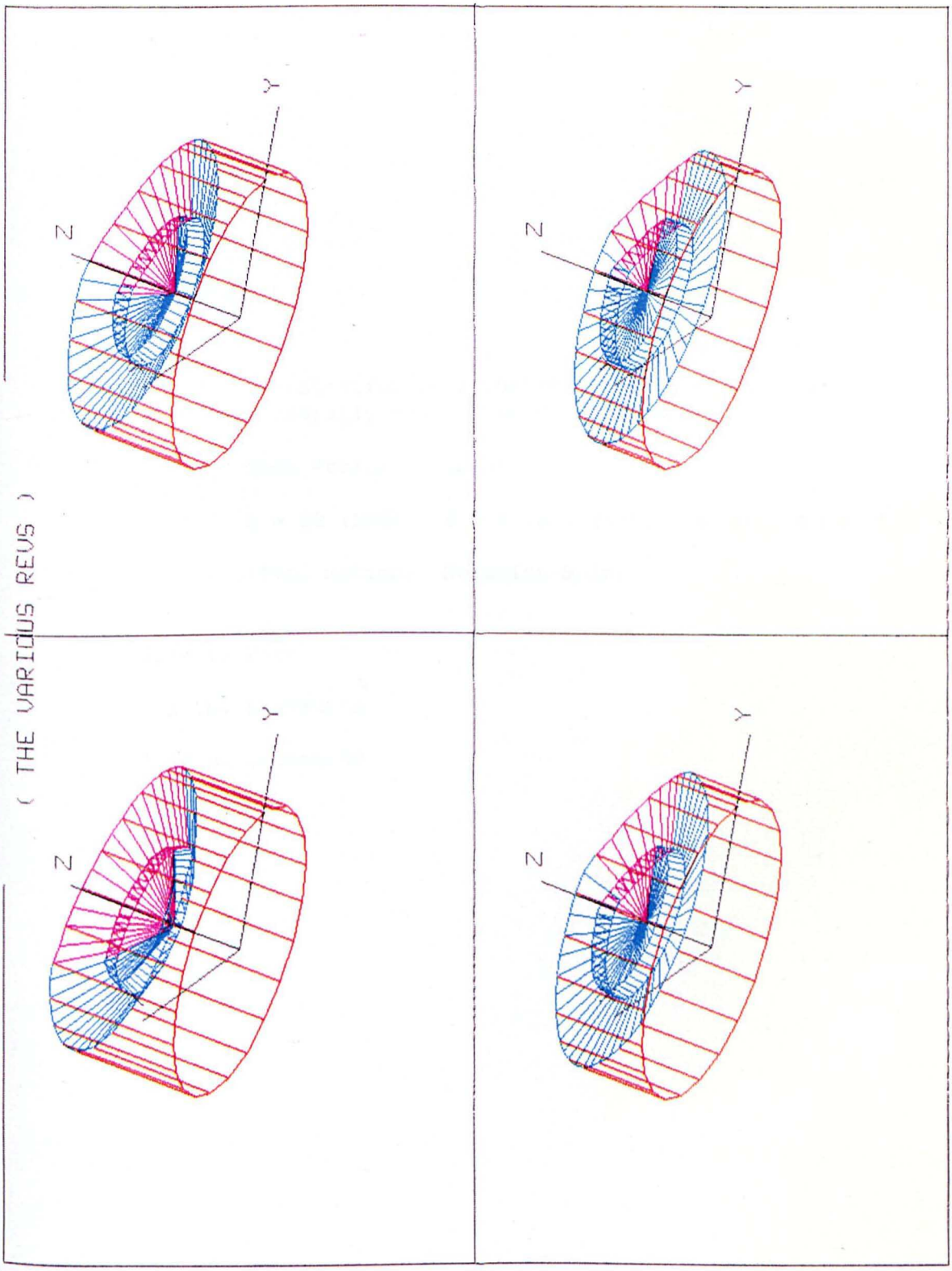

Fig. 7.14. Illustration of a workpiece being deformed by a radially configurated conic tool

Tool Profile CONF3

α = 32 (Deg), $\dot{\theta}$ = 4 (Deg/rev), $\dot{\phi}$ = 360 (Deg/rev)

(Tool motion: Nutation-Spin)

7.14.a. Plan

7.14.b. Elevation

7.14.c. Isometric

Fig. 7.14.a.

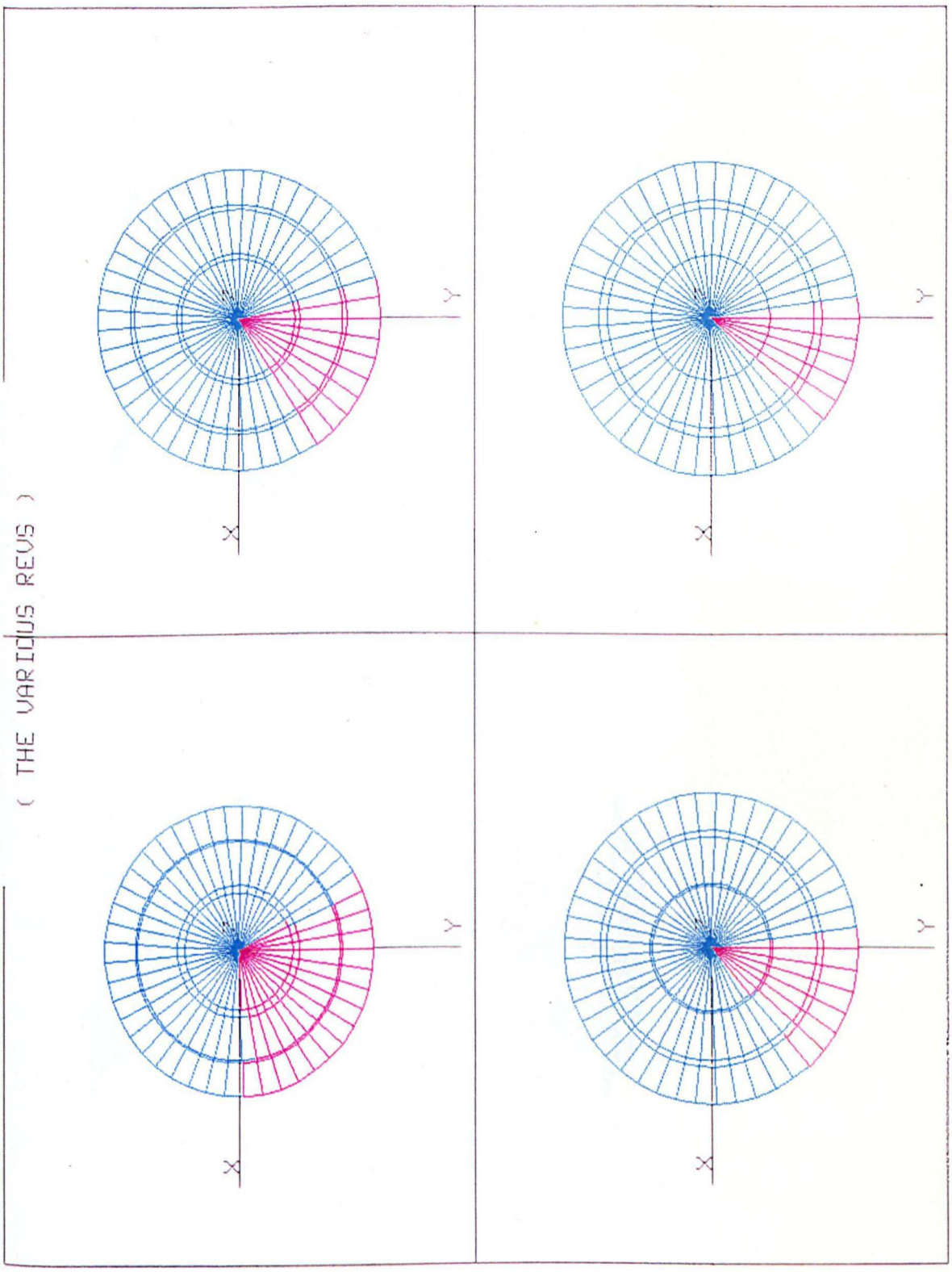

Fig. 7.14.b.

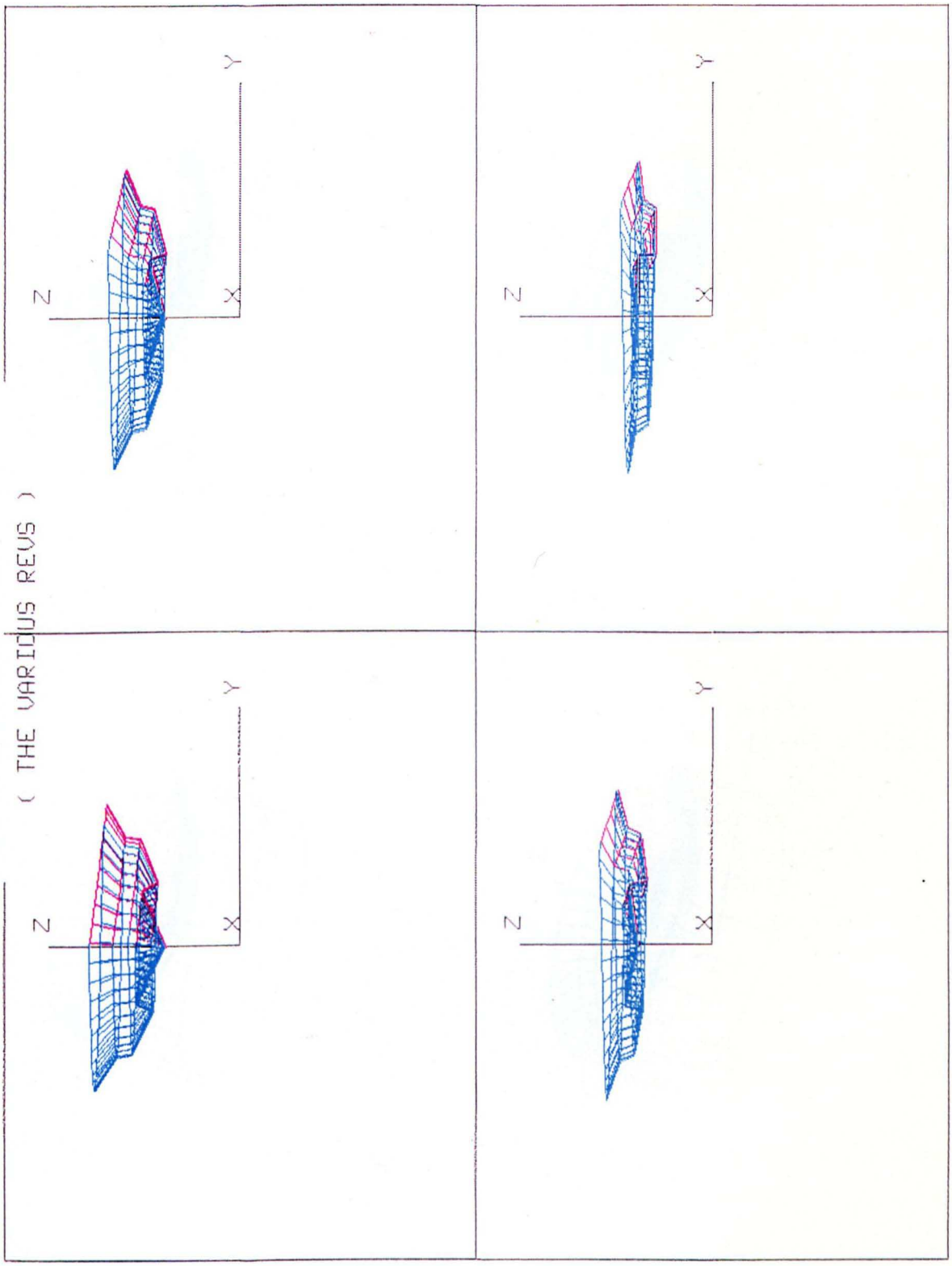

Fig. 7.14.c.

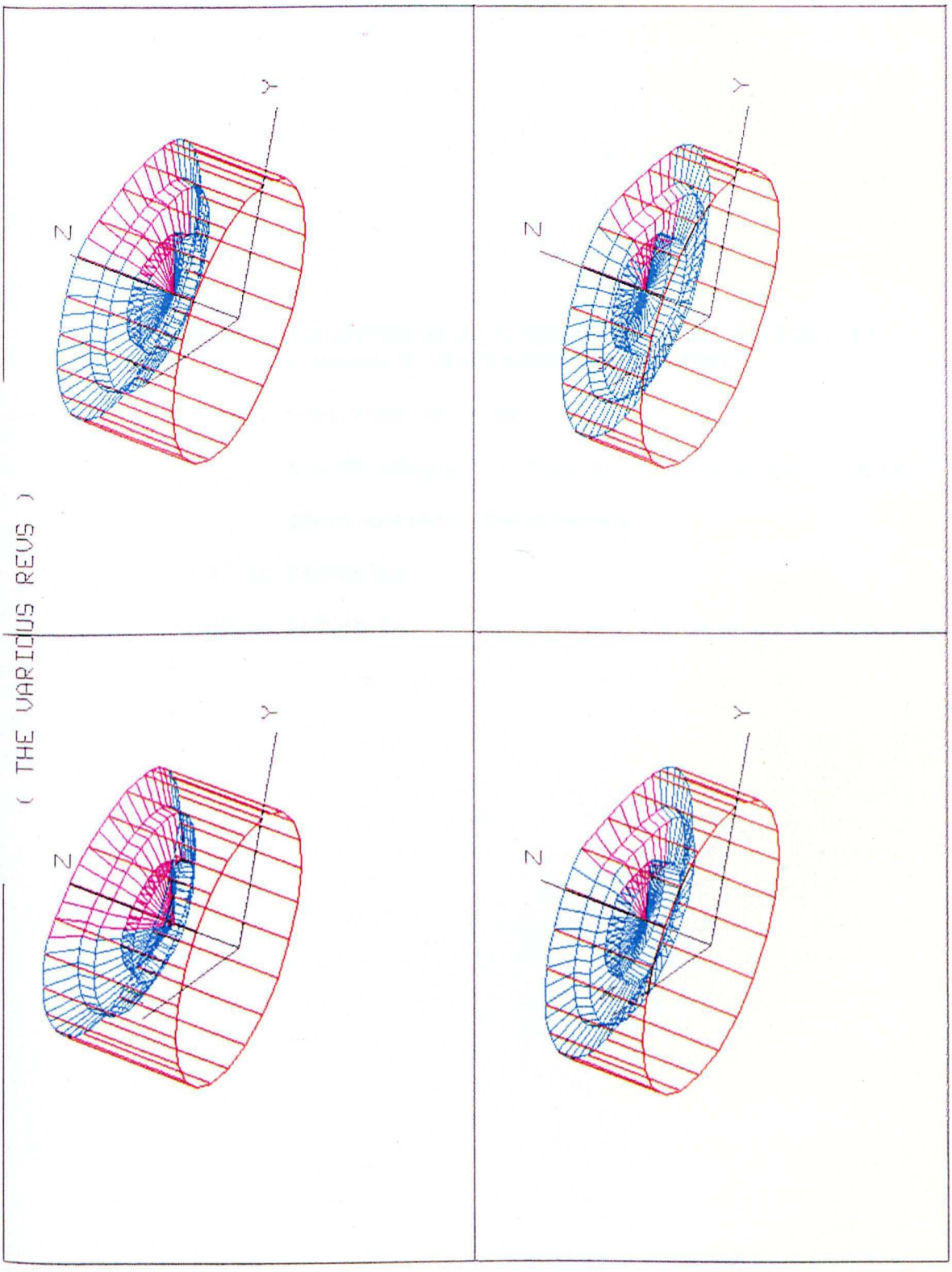

Fig. 7.15. Illustration of a workpiece being deformed by a radially configurated conic tool

Tool Profile CONF3

α = 32 (Deg), $\dot{\theta}$ = 1 (Deg/rev), $\dot{\phi}$ = 360 (Deg/rev)

(Tool motion: Nutation-Spin)

7.15.a. Elevation

7.15.b. Isometric

Fig. 7.15.a.

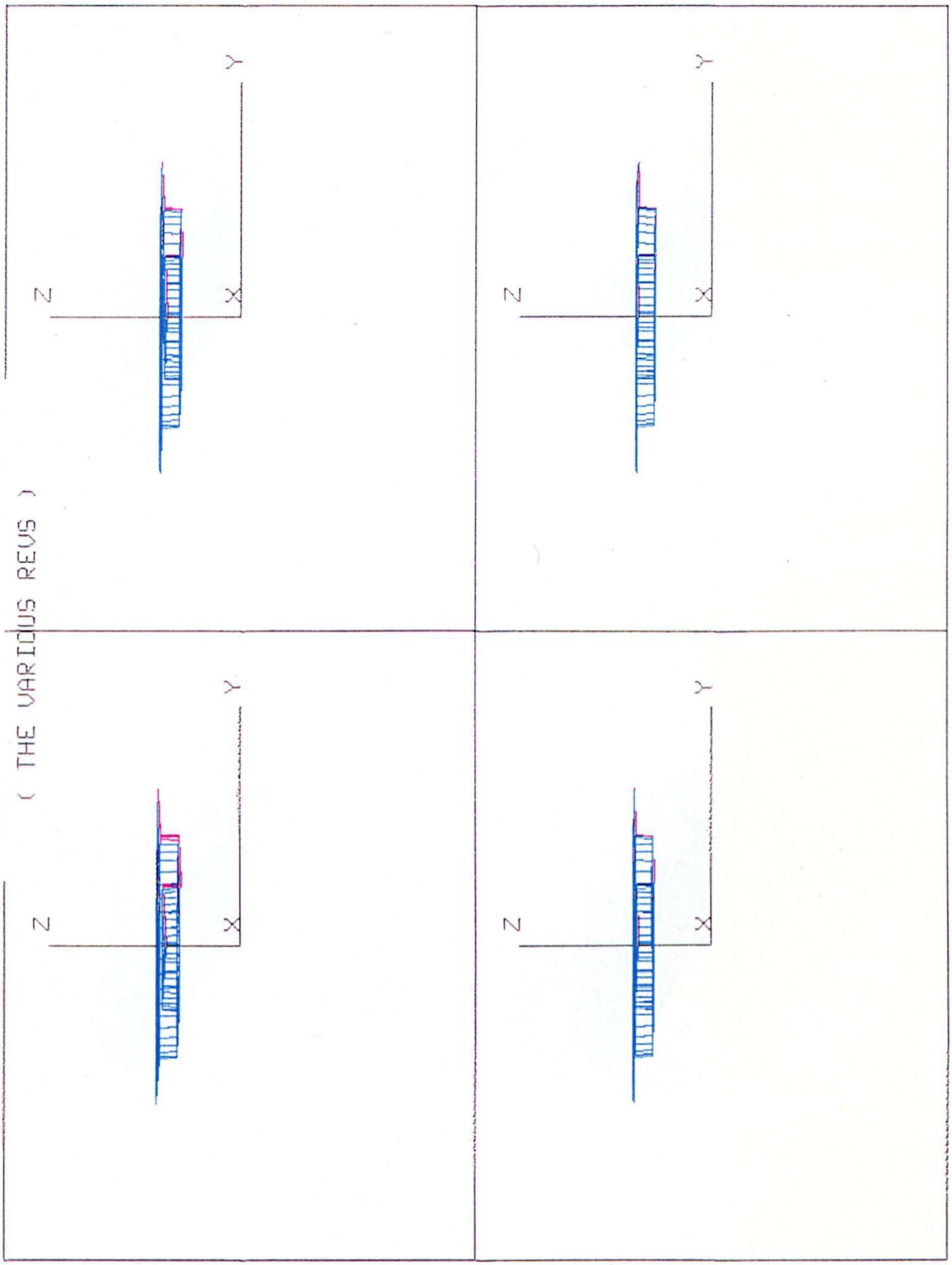

Fig. 7.15.b.